The Use of Results from Regional Climate Models for Local-scale Permafrost Modelling in Complex High-mountain Topography
–
Possibilities, Limitations and Challenges for the Future

Dissertation

zur

Erlangung der naturwissenschaftlichen Doktorwürde
(Dr. sc. nat.)

vorgelegt der

Mathematisch-naturwissenschaftlichen Fakultät

der

Universität Zürich

von

Nadine Denise Salzmann
von
Luzern LU

Promotionskomitee
Prof. Dr. Wilfried Haeberli (Vorsitz)
Dr. Martin Hölzle
PD Dr. Christoph Frei

Zürich, 2006

“Der Mensch zerstört mit der Anwendung physikalischer Gesetze
die bestehende Ordnung der Natur”

Hans Ruh

Summary

The impacts of climatic changes on the mountain cryosphere can have serious effects on a major part of the global population. Changes in the ice and snow regime can lead to shifts in peak river runoff as well as to changes in their water storage capacity. Thawing of permafrost can cause severe instabilities and provoke rockfalls, debris flows or problems with engineering structures. The assessment and modelling of such changes in mountain regions requires climate data with high spatial and temporal resolution from the past, present and future. Regional Climate Models (RCMs) are among the most promising tools for generating such climate data. However, because of their relatively coarse horizontal resolution (currently about 10–50 km for multi-decadal simulations) and the many associated uncertainties, the effective benefit of the use of their output for impact modelling in complex topographical high-mountain regions has to be investigated first. Until now, no universally applicable solutions have been developed to overcome the mentioned limitations.

The present thesis assesses the potential and benefits of RCM results for their applicability to local-scale high-mountain cryosphere models, with a focus on permafrost. In a first part, the relevant scientific background related to RCMs and mountain permafrost is provided. In a second part, the conducted research is presented which includes the following main subjects: Two matching approaches to overcoming the scale differences between RCMs and permafrost models for complex high-mountain topography are developed and discussed, approaches intended to allow for the handling of the associated uncertainties and to permit possible changes in the climate variability. A set of ten different RCM-based scenario time series is applied to a local-scale energy balance model to assess possible ranges of change in the ground surface temperature (GST) of steep rockwalls with variable topographical characteristics (elevation, slope, aspect). The applied emission scenarios, the RCMs and the choice of the matching approaches exercised a significant influence on the GST results. With the exception of aspect, the topographic effects were in general smaller. In a further step, the RCM-based GST results were compared to the GST results obtained with incremental scenarios (mainly temperature changes). It becomes evident that the application of RCM-based scenarios in mountain topography is particularly important and leads to results, which significantly differ from those of incremental scenarios. The subsurface thermal regime in complex topography is profoundly influenced by strong lateral components of subsurface heat fluxes. These fluxes were visualised by driving a transient 3-dimensional ground-heat conduction scheme. Changes have been calculated with RCM-scenario-based ground-surface thermal states for different idealized high-mountain topographies. With a view to spatially distributed GST simulations in mountain regions, the digital terrain model (DTM) becomes an important component. The corresponding influence on the sensitivity of an energy-balance model was investigated by applying six different DTMs, including five with different interpolators and a photogrammetrically derived one. It could be shown that uncertainties also arise from the DTM.

Overall, the new approach investigated in this thesis of using results from RCM simulation for local mountain-cryopshere models has proven to hold a promising potential. In order to enhance the benefit to climate and impact modellers, further investigations of the relevant processes on various spatial and temporal scales and increased interdisciplinary cooperation are strongly recommended.

Zusammenfassung

Die Folgen klimatischer Veränderungen auf die alpine Kryosphere können für einen grossen Teil der Weltbevölkerung gravierende Auswirkungen haben. Änderungen im Eis- und Schneesystem können zu Verschiebungen der Abflusspitzen von Flüssen und zu Änderungen der Wasserspeicherkapazität führen. Das Auftauen von Permafrost kann Instabilitäten verursachen und Felsstürze, Murgänge oder Probleme mit Infrastrukturen auslösen. Zur Abschätzung und Modellierung solcher Veränderungen sind Klimadaten mit hoher räumlicher und zeitlicher Auflösung für die Vergangenheit, die Gegenwart und die Zukunft erforderlich. Regionale Klimamodelle (RCMs) sind vielversprechende Hilfsmitteln, um solche Daten zu generieren. Wegen ihrer relativ groben horizontalen Auflösung (gegenwärtig ca. 10–50 km für Simulationen über mehrere Dekaden) und der vielen Unsicherheiten muss der effektive Nutzen von RCM Resultaten für die Verwendung in Impaktmodellen in komplexer Hochgebirgstopographie jedoch zuerst untersucht werden. Bis heute sind keine allgemein-gültigen Anwendungsverfahren verfügbar, um die erwähnten Defizite zu überwinden.

Die vorliegende Arbeit untersucht das Potential und den Nutzen von RCM Resultaten für die Anwendung in hochauflösenden Hochgebirgskryospherenmodellen, mit Fokus auf den Permafrost. Im ersten Teil werden die relevanten wissenschaftlichen Grundlagen betreffend RCMs und Gebirgspermafrost besprochen. Im zweiten Teil wird die durchgeführte Forschung präsentiert, mit den folgenden Schwerpunkten: Zwei Ansätze werden entwickelt und diskutiert, um die Skalenunterschiede zwischen RCMs und Gebirgspermafrostmodellen zu überwinden, um den Umgang mit den vorhandenen Unsicherheiten zu erlauben und um mögliche Veränderungen in der Klimavariabilität zu berücksichtigen. Ein Set von zehn verschiedenen RCM-basierten Szenariozeitreihen wird auf ein lokales Energiebilanzmodell angewendet, um Bandbreiten möglicher Veränderungen der Bodenoberflächentemperaturen (GST) in steilen Felswände mit unterschiedlicher topographischer Charakteristik (Höhe, Neigung, Exposition) zu untersuchen. Die angewandten Emissionsszenarien, die RCMs und die gewählte Matchingstrategie zeigten alle erheblichen Einfluss auf die GST Resultate. Mit Ausnahme der Exposition sind die topographischen Effekte allgemein geringer. Die RCM-basierten GST Resultate werden zusätzlich mit GST Resultaten verglichen, welche mit gestuften Szenarienansätzen berechnet wurden (hauptsächlich Temperaturveränderung). Dabei wird deutlich, dass die Anwendung von RCM basierten Szenarien vor allem in Gebirgstopographie wichtig ist und zu Resultaten führt, die sich wesentlich von solchen von gestuften Ansätzen unterscheiden. Das thermale Untergrundsystem in komplexer Topographie ist stark von lateralen Komponenten der Wärmeflüsse im Untergrund beeinflusst. Diese Wärmeflüsse werden mit einem transienten 3-dimensionalen Boden-wärmeleitungsmodel visualisiert. Veränderungen werden mittels RCM-Szenarien basierten thermalen Bodenoberflächenzuständen für idealisierte Topographien gerechnet. Mit Blick auf räumlich verteilte GST Simulationen im Gebirge, wird das digitale Geländemodell (DTM) zu einer wichtigen Komponente. Deshalb wird die Sensitivität eines Energiebilanzmodells auf sechs verschiedene DTMs untersucht, wobei fünf DTMs mit verschiedenen Interpolatoren und ein photogrammetrisch abgeleitetes DTM verwendet werden. Es konnte gezeigt werden, dass auch das DTM ein Unsicherheitsfaktor darstellt.

Insgesamt betrachtet ist der in dieser Arbeit untersuchte neue Ansatz der Verwendung von RCM Resultaten für die Modellierung der Hochgebirgskryosphere sehr

erfolgsversprechend und besitzt ein grosses Potential. Um den Nutzen und Gewinn für die Klima- und die Impaktmodellierung zu erhöhen, sind allerdings zusätzliche Untersuchungen der relevanten Prozesse auf unterschiedlichen zeitlichen und räumlichen Skalen, sowie vermehrte interdisziplinäre Zusammenarbeit, unerlässlich.

Contents

Part B

Paper 1:
Salzmann, N., Frei, C., Vidale, P.L., Hoelzle, M., 2006. **The application of Regional Climate Model output for the simulation of high-mountain permafrost scenarios**. Global and Planetary Change, doi: 10.1016/j.gloplacha.2006.07.006.

Paper 2:
Salzmann, N., Nötzli, J., Hauck, C., Gruber, S., Hoelzle, M., Haeberli, W., (in press). **Ground-surface temperature scenarios for complex high-mountain topographies based on Regional Climate Model results.** Journal of Geophysical Research – Earth Surface.

Paper 3:
Nötzli, J., Gruber, S., Kohl, T., Salzmann, N., Haeberli, W., (subm.). **Three-dimensional distribution and evolution of permafrost temperatures in idealized high-mountain topography**. Journal of Geophysical Research – Earth Surface.

Paper 4:
Salzmann, N., Gruber, S. Hugentobler, M., Hoelzle, M., 2006. **The influence of different Digital Terrain Models (DTMs) on Alpine permafrost modeling**. Journal of Environmental Modeling and Assessment, DOI 10.1007/s1066-006-9065-3.

List of abbreviations

BTS	Bottom Temperature of Snowpack
CHRM	Climate High-Resolution Model (IAC-ETHZ)
CRU	Climate Research Unit (University of East Anglia, UK)
CTRL	Control simulation
DTM	Digital Terrain Model
ECMWF	European Centre for Medium-range Weather Forecasts
ENSEMBLES	6th Framework EU project
ERA-40	ECMWF 40 years reanalysis
GCM	General Circulation Model (also: Global Climate Model)
GHG	Greenhouse Gas
GIS	Geographical Information System
GST	Ground Surface Temperature
IPCC	Intergovernmental Panel on Climate Change
LAM	Limited Area Model
MAAT	Mean Annual Air Temperature
MAGT	Mean Annual Ground Temperature
MAGST	Mean Annual Ground Surface Temperature
MIP	Model Intercomparison Project
NARCCAP	Northern American Regional Climate Change Assessment Program
NCAR	National Center for Atmospheric Research (USA)
NCCR Climate	National Centre of Competence in Research on Climate (Swiss)
NCEP	National Center for Environmental Prediction (USA)
NetCDF	Network Common Data Format
NWP	Numerical Weather Prediction
OPeENDAP/DODS	Open-source Project for a Network Data Access Protocol
PIRCS	Project to Intercompare Regional Climate Simulations
PRUDENCE	Prediction of Regional scenario and Uncertainties for Defining EuropeaN Climate change risks and Effects (EU Project)
RCM	Regional Climate Model
SCEN	Scenario simulation
SDS	Statistical Downscaling
SRES	Special Report on Emission Scenarios
WGMS	World Glacier Monitoring Service

PART A

CHAPTER 1

Introduction

1.1 Modelling the impact of climate change on the high-mountain cryosphere

Coping with climate change is among the greatest challenges facing mankind in the 21st century. For the coming decades, climate models predict increases in the mean values and variability of key variables, such as air temperature and precipitation, that exceed the statistical reference distribution (IPCC, 2001; Schär and Jendritzky, 2004; Schär et al., 2004). Major changes are likely to occur in the global hydrological and energy cycles. The mountain cryosphere is a key component of the hydrological cycle and additionally among the best natural indicators of ongoing climate change:

- Since 1850, glaciers have been shrinking and melting worldwide (WGMS, 2005), which is in accordance with the measured increased air temperature on a global, and for most regions, also on a regional scale (IPCC, 2001).
- A similar warming trend is measured for ground temperatures, for example in European mountain permafrost boreholes (Harris et al., 2003).
- Several studies report observed decreases in mountain snow days (e.g., Laternser and Schneebeli, 2003). Scherrer et al. (2005) showed that the recent decrease in low-altitude snow cover in the Swiss Alps can be attributed mainly to an increase in air temperature.

There are substantial consequences associated with changes in the mountain cryopshere. Shifts in the duration and amount of the seasonal snow cover and the extent of glacierization have an important impact on the function of snow and ice as a temporal form of water storage. This is because these two factors control a significant portion of the discharge rates and timing of the hydrological runoff of rivers that originate in mountain regions, thus altering the supply of fresh water for millions of people (Meybeck et al., 2001; Beniston, 2003; Diaz et al., 2003; Barnett et al., 2005). The thawing of mountain permafrost can have a severe effect on the stability of rock walls and debris slopes, as well as on engineered structures (Haeberli et al., 1997; Davies et al., 2001; Kääb et al., 2005). The melting of glaciers leads to increased formation of glacier lakes, which can burst and trigger far-reaching debris flows (e.g. Huggel, 2004).

In many regions the mountain cryopshere is particularly sensitive to climatic change due to its proximity to melting conditions (Haeberli and Beniston, 1998), and the assessment of the future development of the high-mountain cryosphere is a challenging task. Complex topography, a common and unique feature of all mountain regions, produces various regional to local climate subsystems, which determine and influence the climate of mountain regions significantly (Whitemann, 2000). Thus, the assessment of climatic

changes is particularly difficult in such regions. The dynamics of mountain cryopsheric systems are closely linked to the regional and local climate and microclimate condition. Therefore, the modelling of their spatial distribution and temporal development requires climate information on a regional to local scale. When focusing on mountain permafrost, spatial model resolution on the meso and micro scales only is appropriate (Etzelmüller et al., 2001a). Accordingly, climate information on a similar scale is necessary for impact modelling in high-mountain regions.

Regional Climate Models (RCMs) are at present the only tools able to provide quantitative estimates of future regional climate scenarios on a physically consistent and plausible basis (IPCC, 2001). Over the past few years, increased attention has been devoted to the development of RCMs and the dynamic downscaling techniques have been improved substantially. Accordingly, the availability of RCM results for impact application is increasing. RCMs are currently capable of attaining a horizontal grid resolution of 10–50 km for continuous multi-decadal time-slice simulations (e.g. Christensen et al., 1997,1998; Leung et al., 2003a,b). Due to parameterization and computational limitations, existing RCM processes cannot simply be scaled to finer resolution. Considering the spatial scales required by mountain impact models (for example, ~25 m for permafrost), a significant spatial scale gap is recognized between that which climate models are able to provide and what impact models actually require. The challenge of applying RCM results for impact modelling in complex high-mountain topography is thus, first of all, a problem of spatial scale mismatches.

This thesis aims at investigating the possibilities and benefits as well as the limitations of current RCM simulations, for application in complex high-mountain topography. The main focus is on modelling the impact of climate change on mountain permafrost.

1.2 Objectives

The increasing quality and availability of regional climate model results opens new perspectives for impact modellers. However, the spatial scale mismatch lowers the applicability of RCM output to mountain cryopshere models. Until present the development of techniques to overcome this scale mismatch has only rarely been investigated for complex mountain topography, and the effective value and potential of RCM results for application to mountain cryosphere models needs to be evaluated. This study explores the potential of this new generation of datasets and aims at developing approaches to apply RCM results in general, and RCM scenario results in particular, to mountain permafrost models.

The thesis concentrates on the following scientific questions and topics, all of which are specifically related to complex high-mountain topography:

- Providing an introduction to the state of the art of regional climate modelling;
- Assessing the effective information that RCM can provide to impact modellers;
- Identifying other shortcomings and limitations in addition to the spatial scale mismatch, relating to the applicability of RCM results for local to regional impact modelling;

- Developing approaches for applying RCM results to high-resolution permafrost models;
- Developing approaches for constructing scenarios to simulate the evolution and dynamics of mountain permafrost;
- Assessing the added value of RCM results for cryosphere impact modelling;
- Formulating recommendations for future developments according to the anticipated progress in climate modelling.

1.3 Outline

The thesis consists of two parts. Part A outlines and describes the scientific setting of the thesis and part B presents the scientific work published as part of the thesis.

Part A has five chapters.

Following the introductory Chapter 1, Chapter 2 provides information on basic aspects of regional climate modelling and primarily addresses impact modellers not yet familiar with climate models. The most important issues about RCMs, with regard to their application to impact models in mountain regions, are summarized and should provide a basis for other impact modellers intending to use RCM results.

Chapter 3 provides a background summary of mountain permafrost modelling, focusing on the issues that are central to this thesis.

In Chapter 4, the work published within the framework of this thesis is summarized and the main conclusions are given.

Finally, in Chapter 5, the overall conclusions of the thesis are provided and in Chapter 6 a discussion of the necessary direction to be taken and an outlook for the future are presented.

Part B consists of the scientific journal papers published as part of this thesis.

CHAPTER 2

Climate Modelling and Regional Application

Climate models exist in different complexities. A distinction can be made between relatively basic statistical-dynamical models and more sophisticated circulation models. This thesis focuses on the use of results from the latter climate model type. General Circulation Models (GCMs) alone represent the climate system on a mainly physical basis, and are thus the only tools that can account for the non-linearity of the climate system.

2.1 General Circulation Models (GCMs)

GCMs are comprehensive models of the earth's climate system. They are based on physical laws represented by mathematical equations that are solved using a full three-dimensional grid over the globe (Fig. 2.1). This is the only tool that can provide quantitative estimates of future climate changes on a physically consistent basis (IPCC, 2001). GCMs attempt to simulate the major and relevant processes of the climate system. Over the past few decades, models of the main components, including the atmosphere, the continents, the ocean, the cryosphere (ice sheets) and the biosphere have been developed as separate models and were then gradually integrated along with coupling procedures for the processes that go on within and between them (Fig. 2.2). The further development and enhancement of GCMs, including their coupling with other important subsystems such as the carbon cycle, is a primary and challenging topic of climate research, and currently in full progress. As a consequence, comprehensive climate models are also becoming known as 'coupled climate system models' or 'earth system models' (McGuffie and Henderson-Sellers, 2005).

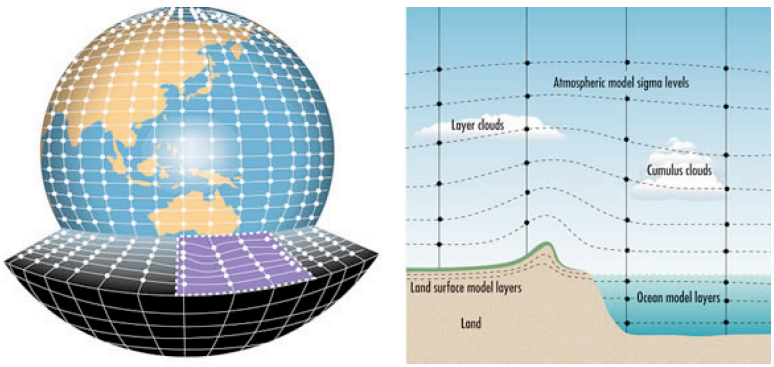

Fig. 2.1: 3-dimensional grid over the globe as represented by a GCM (left), including several coupled subsystems (right) (Source: www.bom.gov.au).

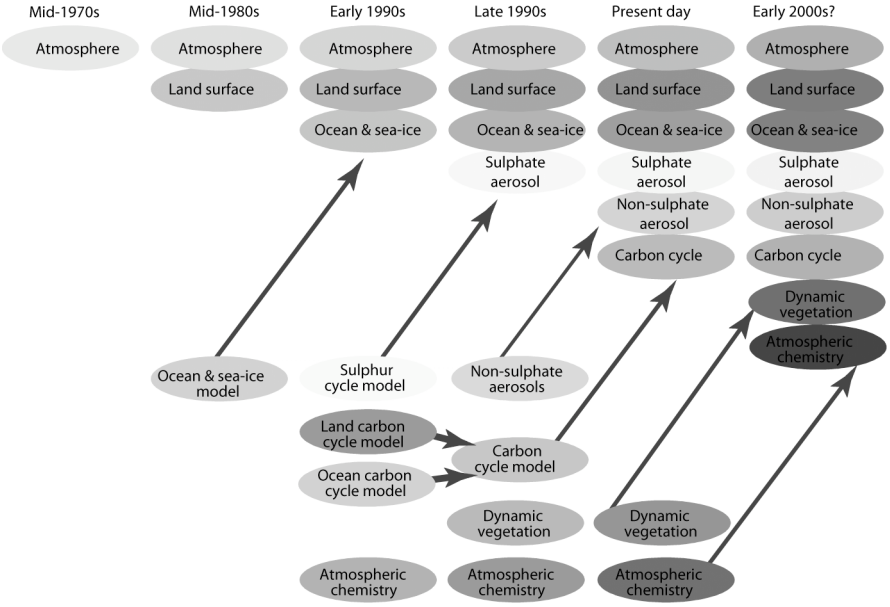

Fig. 2.2: The development of climate models over the last decades, showing how the different components were first developed separately and later coupled to produce comprehensive climate models (Source: IPCC, 2001).

The accuracy of a GCM depends partly on the spatial resolution of the grid points and the length of the time steps of a model integration. A compromise must be found between the desired resolutions, the length of integration and the computational facilities available (e.g. Schubert and Henderson-Sellers, 1997). Currently, the atmospheric grid has a horizontal resolution between 1° and 5° of latitude and longitude (~ 200 – 550 km; T106 – T42). The vertical resolution is obtained by dividing the atmosphere into several unevenly spaced levels (Fig. 2.3). These levels are more concentrated near the surface than at the top level, which is located at about 30 km height (i.e., in the middle of the stratosphere). The levels are spaced, on average about 1 km apart, resulting in a total of about 20 to 30 levels. The equations are integrated forward in steps of about half an hour through the finite interval (model integration) depending on the resolution. Furthermore, the computational constraints also lead to problems of a more theoretical nature, i.e., with the current coarse grid-spacing of GCMs, small-scale atmospheric processes (termed 'subgrid-scale processes') such as thundercloud formation cannot be modelled and therefore must be parameterized, i.e., represented in simplified equations (e.g. McGuffie and Henderson-Sellers, 2005).

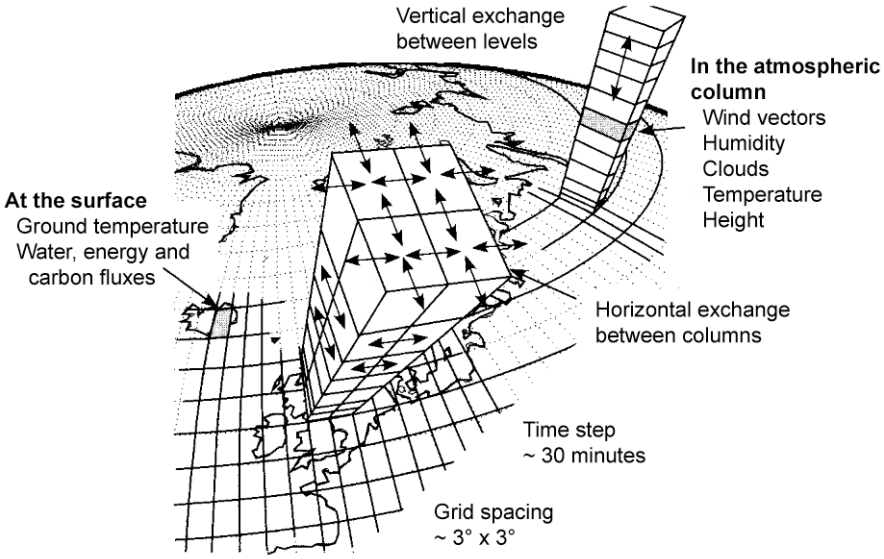

Fig. 2.3: The finite grid construction of a GCM (Source: McGuffie and Henderson-Sellers, 2005).

Focusing on climate models in terms of their application to impact models, the current relatively coarse information provided by GCMs may be sufficient when impact assessments are continental in scale or larger, or when subgrid variations are weak. However, climate information at scales smaller than the model grid resolution cannot be provided by definition and the effects of subgrid-scale processes on the larger scales can only be approximated. Nevertheless, the impact of climate change will be manifested to the greatest extent locally, via changes in the frequency and intensity of extreme events such as heavy precipitation, droughts, heat waves or wind storms (Christensen et al., 2002; Leung et al., 2003; Frei et al., 2006). These phenomena depend to a big extent on processes at small scales. Therefore, detailed spatial structure of the climate is required for regions of enhanced vulnerability and in particular when the area is significantly influenced by regional characteristic such as topography, coastal zones, narrow land masses or large lake systems (Giorgi and Mearns, 1991; Jones et al., 1995; Walsh and Gregory, 1995; Mearns et al., 2001a). Furthermore, local subgrid-scale processes that are induced by a high degree of heterogeneity of topography or of land surface, but that are not resolved by global models, are not only relevant at the regional scale, but can also feed back onto the global scale. As a consequence of the regional deficiency of current GCMs and because they cannot simply be scaled to a finer resolution due to the parameterization and computational limitation mentioned above, increased attention has been devoted to the development of different regionalization (downscaling) techniques over the past decade.

2.2 Downscaling methods

The regionalization techniques can be placed in the three categories described in the following sections. This thesis focuses primarily on the dynamical downscaling (based on Regional Climate Models) techniques (Section 2.2.1). Nevertheless, a brief summary of the other two approaches is provided for the sake of completeness. Each of the techniques has

advantages and disadvantages in terms of its application to impact models. However, in practice, the choice of method for a specific application often also depends on the requirements and availabilities of data and models.

2.2.1 Regional Climate Models (RCMs) – Dynamical Downscaling

Regional climate modelling is a physical, dynamical downscaling approach commonly referred to as nesting technique (e.g. Dickinson et al., 1989; Giorgi, 1990). This technique essentially originated from regional numerical weather prediction. The concept consists of driving a high-resolution limited-area model (LAM) with initial conditions, time-dependent lateral meteorological boundary conditions and surface boundary conditions taken from a GCM (or global reanalysis; see Section 2.3.1) for a selected time slice of the global model run (Fig. 2.4) (e.g. McGregor, 1997; Giorgi and Mearns, 1999). In this way, the GCM is used to simulate the evolution of the global climate system, while an RCM zooms into a limited subdomain of the globe solving similar equations like a GCM but at higher resolution. Most RCMs are formulated using the hydrostatic primitive equations, i.e., vertical acceleration in the atmosphere is assumed to be small in regard to hydrostatic equilibrium and hence vertical motions are diagnosed separately from the equation of state. These RCMs are capable of attaining horizontal grid resolution down to about 10–20 km for continuous multi-decadal time-slice simulations (e.g. Christensen et al., 1997; Leung et al., 2003). In theory, finer spatial resolution can be achieved by the use of non-hydrostatic formulation i.e., explicit description of vertical acceleration of air masses (Grell et al., 2000). A few RCMs such as the MM5 (Pennsylvania State University / NCAR mesoscale model) or the CRCM (Canadian Regional Climate Model) use non-hydrostatic terms. However, an improvement in the simulated climatology has yet to be demonstrated (Wang et al., 2004).

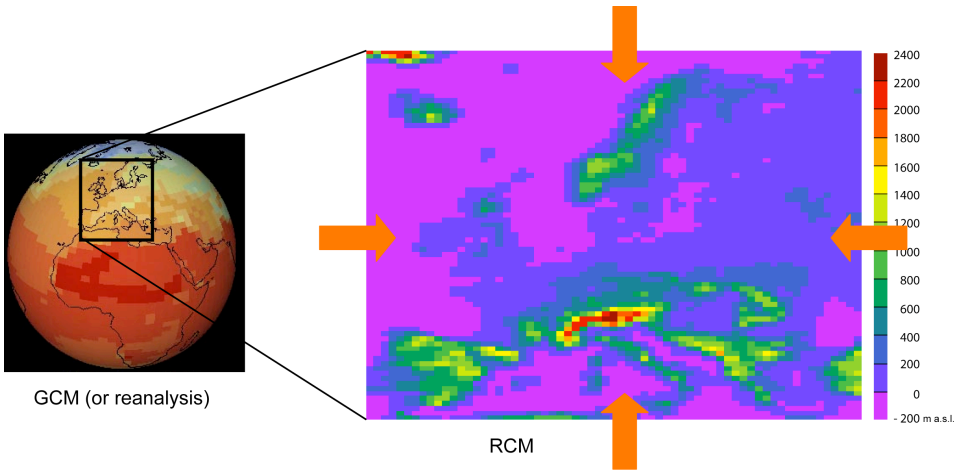

Fig. 2.4: The concept of RCMs. A limited area of a GCM is driven with boundary conditions taken from a GCM or reanalysis. In this figure, the RCM domain shows the topography as used by the CHRM RCM. Note the vertical resolution particularly over the Alps.

In order to simulate the climate conditions at the recent past, RCMs can be driven by reanalysis rather than by GCMs. In this manner, RCMs are expected to simulate the evolution of synoptic events very near to that observed in nature (see Section 2.3).

A great advantage of RCMs, in contrast to statistical downscaling methods (see next Section), is that they are in principle able to account for possible changes in the statistical relationship between large-scale and regional-scale features. This is particularly relevant for climate change impact studies that usually are carried out by impact modellers i.e., by non-climatologists. RCMs are less dependent on the stationarity assumption inherent to statistical downscaling models (Mearns et al., 2003; Wilby et al., 2004).

Furthermore, while the regional biases of the RCMs are not necessarily smaller than those of the driving GCMs (Laprise et al., 2000; Achberger et al., 2003), the spatial pattern of climate produced by an RCM is usually in better agreement with the observations than with the driving fields, i.e., the GCM. This is particularly true in regions with a heterogeneous surface, mainly because the better representation of orographic forcing and land surface conditions. Giorgi et al. (2001) and Denis et al. (2002) showed that the simulation of the spatial patterns of precipitation and temperature over complex terrain is generally improved with the increasing resolution obtained when using nesting techniques. The added value of RCMs is also particularly evident for precipitation pattern in the mountain regions (Kim et al., 2000; Denis et al., 2002; Frei et al., 2003, 2006) and other heterogeneous regions (Huntingford et al., 2003, Christensen and Christensen, 2003).

Limitations of RCMs mainly concern the fact that the nesting technique up to now has mostly been applied only in a one-way mode, i.e., no feedback effects from the RCM go back to the driving GCM. Only recently, first attempts in two-way nesting have been undertaken, by Lorenz and Jacob (2005) for example, whereby the RCM is run simultaneously with the host GCM, and regularly updates the host GCM within the RCM domain. In this manner, the RCM can provide added information compared to the global model by feeding regional processes back to the global scale, such as extreme precipitation events in the Alps and consequent impacts on the regional water cycle. Similar feedback benefits can be derived also from a variable resolution GCM (see Section 2.2.3).

A disadvantage of RCMs is that their simulations can be as computationally demanding as that of GCMs (depending on domain size and spatial and temporal resolution). Furthermore, RCMs require high-frequency time-dependent GCM fields, which are not routinely stored when running GCMs because of the implied mass storage space. Hence, good coordination between GCM and RCM modelling is needed (Giorgi and Mearns, 1991, 1999; Ji and Vernekar, 1997). A further limitation to note is that the RCM inherits the systematic errors of the GCM (see Section 2.3.2; Noguer et al., 1998). However, this is common to all downscaling methodologies using output from GCMs.

The important issue concerning the uncertainties of the RCM information as it relates to impact application is discussed in Section 2.3 and the added uncertainties when emission scenarios are included in Section 2.4.

2.2.2 Statistical Downscaling (SDS)

The concept of statistical downscaling (SDS) is based on the assumption that regional climate is conditioned by two factors: (a) the large-scale climatic state and (b) the regional/local physiographic features such as topography, land-sea distribution and land use (von Storch, 1995, 1999). Thus, SDS requires first the identification of the quantitative relationships between the observed large-scale and regional climate and, hence, the

determination of a statistical model, which relates large-scale climate variables ('predictors') to regional and local variables ('predictants'). By feeding the large-scale output of a GCM into the statistical model, the corresponding local climate characteristic is estimated.

Statistical downscaling techniques have their roots in synoptic climatology and empirical weather prediction. However, they are currently used for a wide range of climate applications, from historical reconstruction to regional climate change problems (Giorgi et al., 2001). Several review papers deal with downscaling concepts, their prospects and limitations, e.g. Hewitson and Crane (1996), Wilby and Wigley (1997), Gyalistras et al. (1998), Murphy (1999, 2000), Zorita and von Storch (1999), Schmidli et al. (2006).

In the following, the main SDS techniques are briefly described and divided into three categories similar to those used by Giorgi et al. (2001):

i) Weather classification schemes
Circulation classifications are typically defined by applying clustering techniques to atmospheric fields (Huth, 2000; Hewitson and Crane, 2002) and then define the local climate in dependence of the weather class (Cubasch et al., 1996a; Hewitson and Crane, 1996; Schubert and Henderson-Sellers, 1997).

ii) Regression Models
Here, linear or non-linear relationships between predictants and large-scale atmospheric forcing are established. Commonly applied methods include multiple regression (Kim et al., 1984; Wigley et al., 1990; Palutikof et al., 1997; Winkler et al., 1997; Murphy, 1999), artificial neural networks, which can be viewed as a form of non-linear multiple regression (Crane and Hewitson, 1998; Weichert and Bürger, 1998; Trigo and Palutikof, 1999; Zorita and von Storch, 1999), non-parametric models (Corte-Real et al., 1995) and canonical correlation analysis (CCA) (von Stroch et al., 1993).

iii) Weather generators
Weather generators replicate the statistical attributes of a local climate variable like mean or variance, but not observed sequences of events (Wilks and Wilby, 1999). Their parameters can, however, be estimated using GCM data as a guide. Typically, they are based on Markov Chain processes (Semenov and Barrow, 1997; Wilks and Wilby, 1999). Most of them focus on the daily time scales, as required by many impact models, but subdaily models are also available (e.g. Katz and Parlange, 1995). Stochastic weather generator methods can be also useful for temporal downscaling, for instance disaggregating monthly precipitation totals and rain days into daily amounts (Kilsby et al., 1998; Fowler et al., 2000).

An important advantage of SDS is that it is computationally inexpensive and can thus easily and rapidly be applied to output from different GCM experiments. From an impact modeller's point of view, another advantage is that they are able to provide site-specific information (e.g., points, catchments).

The major theoretical weakness of SDS is its basic assumption, which prescribes that the statistical relationships developed for present-day climate also hold under the different forcing conditions of possible future climates. However, this is difficult to verify and, for some simpler forms of SDS there have been indications of non-stationarity behaviour

(Murphy, 1999; 2000, Schär et al., 2004). Another limitation is that these empirically based techniques cannot account for possible systematic changes in regional forcing conditions or feedback processes. Furthermore, in particular for remote areas and/or regions of complex topography, the observational data required to develop the statistical relationships are often not available.

2.2.3 High-resolution and variable-resolution time slice GCM experiments

High-resolution (Cubasch et al., 1995, 1996a) or variable-resolution (Déqué and Piedelievre, 1995; Déqué and Gibelin, 2002) GCMs simulate selected time slices of a transient GCM simulation with increased resolution. Variable-resolution models such as the ARPEGE (see Déqué et al., 1998) vary the resolution for example from 700 km over the southern Pacific to 60 km over the Mediterranean. These model types make additional spatial details available without having to perform the whole transient simulation with high-resolution models. The main theoretical advantage is the global consistency of the simulations. However, since they use the same formulation as at coarse resolution for which these have been optimized, some processes may be represented less accurately when finer scales are resolved. Furthermore, the use of high- or variable-resolution models is very computationally demanding, which applies limits to the increase in resolution (currently about 50 km). The experience with such models is still limited. In a recent study, Déqué et al. (2005) compared global high-resolution models with RCMs and concluded that RCMs can produce similar reliable results at a more attractive computation cost than can high-resolution models. Nevertheless, high-resolution GCMs might be used to obtain forcing fields for RCMs or SDS, and thus effectively provide an intermediate step between GCMs and regional and empirical models.

2.3 RCMs - performance and uncertainties

The application of RCM results to impact models presumes knowledge of the performance and uncertainties of the RCM simulations. Therefore, in the following section a short overview of validation methods and the performance and uncertainties of the currently available RCMs is provided.

2.3.1 Validation and evaluation of RCMs

Validation

The validation of any model is an important step to be performed before applying it for simulation purposes. In climate research, the validation and improvement of (regional) climate models is a both challenging and important task (Vidale et al., 2003; Giorgi et al., 2001). Depending on the goal of the RCM simulation (e.g. providing input data for impact application, or serving as a tool for regional climate process studies), different validation methods and techniques as well as observational data are required. Until present, there have been no specific RCM validations carried out relating to the relevant processes for mountain permafrost (see Chapter 6). Therefore, in the following, only a brief overview of validation methods and the uncertainty of RCM simulations in general, and for the European Alps in particular, is provided.

In most cases, gridded data sets of observations are used for the validation of the present-day statistical mean climatology of an RCM. A widely used gridded data set is the CRU global climate data set (see New et al., 1999). It consists of a multi-parameter 0.5° resolution, mean monthly climatology (1961-1990) for global land areas and comprises a suite of surface variables such as precipitation, diurnal temperature range or cloud cover. For the CRU data set, the observational data from climate stations were interpolated as a function of latitude, longitude and elevation using the thin-plate splines technique. The accuracy of the CRU data set was assessed using cross-validation and by comparison with other climatologies. Although the accuracy varies both regionally and between variables, the overall accuracy is assumed to be suitable for wide application in climate related research (for details see New et al., 1999), however, this is probably not particularly true for mountain regions.

For the Alps, specific gridded climatology data sets exist for the precipitation climatology (Frei and Schär, 1998) and (Schwarb, 2000), and for temperatures (Böhm et al., 2001).

In addition to gridded observations, reanalysis such as the ERA-40 (see Uppala et al., 2005) from the ECMWF or the NCEP/NCAR reanalysis (see Kalnay et al., 1996) are options for presenting the current climate. Reanalyses are comprehensive and dynamically consistent three-dimensional fine resolution gridded data sets (e.g. for ERA-40 about a horizontal resolution of 120 km), which combine observations (measured data from satellites, radiosondes, buoyes, etc.) with simulated data from numerical models by a process known as data assimilation. They represent the best estimate of the state of the atmosphere at that time. Reanalysis datasets are used mostly for the evaluation of variables, which cannot or are difficult to observe, such as energy flux, evaporation, atmospheric water vapor, etc.

The performance of an RCM driven by lateral fields from a GCM for current climate condition (CTRL) cannot be tested against individual events, but needs to be evaluated in terms of its statistical properties (Giorgi et al., 2004; Lal et al., 1998). Only when an RCM is driven with so-called perfect boundary conditions, i.e., with operational atmospheric objective analyses or reanalysis, can it reproduce the observed weather evolution including variability and extremes (Christensen et al., 1997; Frei et al., 2003). In perfect boundary experiments the errors of the GCM that are induced via the boundary condition are minimized and thus the detection and quantification of biases due to the systematic errors in the model physics should be facilitated (Christensen et al., 1997; Lüthi et al., 1996). As a result, RCMs driven with perfect boundary conditions should reproduce the statistics of the driving data and in situations where the large-scale conditions have strong control over the interior solution, aspects of individual events may be reproduced. However, there are also uncertainties and errors found in the ‘perfect’ reanalysis, in particular in the lower-atmospheric circulation and water vapor flux (see Section 2.3.2).

When comparing RCM simulations to high-resolution observed data, care should be taken to use equivalent spatial scales. Furthermore, the problem of area representativity of observational and model data must be included in the analysis, particularly for variables such as precipitation (Goodrich et al., 1995; Frei et al., 2003). In earlier studies, it has been suggested that simulated grid-box precipitation can be interpreted as point values (Skelly and Henderson-Sellers, 1996). Currently, it is more generally accepted that what is being simulated are actually area-average means for each grid box (Osborn, 1997; Osborn and Hulme, 1997). Frei et al. (2003) suggest as a reasonable assumption, that the representative

area for simulated climate variables is somewhere between one and four grid boxes. Moreover, Kleinn (2002) observed horizontal shifts of precipitation pattern (at grid boxes scale) along mountain ranges, a fact that must be taken into account especially in regions of complex topography [see also *Paper 1*].

Denise et al. (2002) have experimented with an alternative approach to RCM validation, which does not compare observational data and model output in a traditional way. Their "perfect-prognosis" approach, nicknamed the Big Brother Experiment (BBE), consists in running a high-resolution large- (ideally global-) domain climate model to establish a reference climate (= Big Brother). This reference simulation is then degraded to the low resolution of operational GCM, either by filtering or smoothing, and these low-resolution fields are next used to nest a high-resolution RCM (= Little Brother) over a smaller domain. The resulting RCM climate is compared, in a final step, with the reference over the same window. The BBE technique is suitable to identify limitations in the nesting technique and domain setting but not necessarily errors in the dynamical core or physical parametrization of a model. Antic et al. (2004) have used this approach to test an RCM over complex topography.

Evaluation
The increased interoperability and network capability (see also Section 2.5.1) has led to model evaluations by the development of protocols and to organized model intercomparison projects (MIP). To this date, about 40 MIPs are ongoing or planned, including the evaluation of model components or parameterization schemes. An example for such a standardized experimental protocol for RCMs is the Project to Intercompare Regional Climate Simulation (PIRCS www.pircs.iastate.edu; see Takle et al., 1999; Ji and Vernekar, 1997). The most important outcomes of such MIPs are: (i) the estimation of the range of confidence (or uncertainty) inherent in predictions of any one of the 'reasonable' models, (ii) the identification of group outliers, and (iii) the development and dissemination of data sets for continuing model evaluation (McGuffie and Hendersen-Sellers, 2005).

Another possibility for evaluating and quantifing uncertainties of RCMs are ensemble simulations (Giorgi and Francisco, 2000; Murphy et al., 2004). Here, a standardized multitude of climate models are run by using different models (e.g. Frei et al., 2003; Vidale et al., 2006) or the same model but different parameterization schemes (e.g. Vidale et al., 2003), boundary conditions (e.g. Räisänen et al., 2004) and initializations (e.g. Yang and Arritt, 2002) or resolutions (e.g. Mearns et al., 1998, 1999, 2001b), and the results are statistically analyzed afterwards.

Based on IPCC (2001), the current performance of RCMs (driven by perfect boundary conditions) is for a horizontal resolution of about 50 km set for temperature within a 2°C bias, and for precipitation within a 50% bias of observation. In general, the model performance is weakest during summer and over continental regions due to weak large-scale forcing in the summer season, and discrepancies in the land surface models (Wang et al., 2004). The performance of RCM simulations can be improved using ensemble methods (see also Section 2.3.3).

Finally, it must be stressed that a model valid for today and for a specific region is not necessarily valid for other time periods or other regions (Zorita and Gonzales-Ruoco, 2002). To some extent stationarity is an issue not only for statistical downscaling but for

RCMs too especially regarding the parametrizations. But because RCMs are built primarily on first principals, non-stationarity is not a serious concern.

2.3.2 Sources of RCM uncertainties

There are several sources and reasons for the uncertainties of RCM simulations. The most important sources are:

- Uncertainties and errors from the lateral boundary forcing fields.
    - For reanalysis, these are uncertainties due to observational limitations, including (i) limitations of the interpolation and assimilation techniques, (ii) errors of the measured point observational data, which is particularly a problem in remote mountain regions, and (iii) the problem of a low-density observational network, especially in remote (mountain) areas. Simmons et al. (2004) found substantial differences between CRU, ERA-40 and NCEP/NCAR reanalysis.
    - For GCMs, the uncertainties are associated with imperfect knowledge and/or representation of physical processes, limitations due to the numerical approximation of the model's equations, simplifications and assumptions in the models and/or approaches, internal model variability, and inter-model or inter-method differences in the simulation of climate response to a given forcing (Ji and Vernekar, 1997; Giorgi and Mearns, 1999).

- Uncertainties from the RCM itself are similar to the limitations of GCMs and mainly subject to limitations in the internal physics such as missing or inadequate parameterizations, numerical shortcomings and internal model instabilities. There are also inconsistencies in the dynamics and physics between the RCM and the large-scale driving model. These boundary zones are usually treated with relaxation methods (e.g. Marbaix et al., 2003). Furthermore, important uncertainties result from the model configuration, e.g., size and position of the domain, spatial resolution and treatment of the boundary forcing (e.g. Murphy et al., 2004; Giorgi and Francisco, 2000).

- If an RCM is used for scenario simulation, the emission scenario forcing is another important source of uncertainties (see Section 4).

Depending on the region and the process to investigate, the relative importance of each uncertainty can vary. As a consequence, particular consideration should be taken for a specific application. In this context, the selection of the model domain, its size and the resolution are important, yet controversial issues. On the one hand, the model domain should be sufficiently small that the synoptic circulation does not depart from that of the driving GCM (Jones et al., 1995). On the other hand, the model domain should be large enough to allow the RCM to develop its mesoscale circulation feature (McGregor, 1997; Warner et al., 1997). Nonetheless, probably most important is that the domain includes all areas where forcing and processes are a dominant element for the climate of the specific region (Seth and Giorgi, 1998). Furthermore, the region of interest within the model domain should be as far away as possible from the lateral boundaries in order to minimize the influence of spurious boundary effects (McGregor, 1997). Similarly to the spatial resolution, the temporal model resolution should be sufficient to capture the high-

resolution forcing and circulations of relevance to the region (Giorgi, 2002; Mearns et al., 2001). At the same time, it must be considered that different components of the climate system (and thus of the climate model) have different time scales. In terms of spatial resolution, generally, RCMs with increased resolution produce better results to a certain degree, particularly for extreme events (Mo et al., 2000; Christensen and Christensen, 2003). However, the increase in grid resolution does not necessarily lead to improved model performance, since the RCMs become sensitive to internal/external model physical parameterization (Nobre et al., 2001). Furthermore, spatial and temporal resolution is also restricted due to the computational resources.

As mentioned before, the performance of an RCM must be specified for the regions and processes of interest. Therefore, in the following section the focus is on RCM performance in the European Alps, however, only in a general sense, since no specific analysis exists for the mountain cryopshere systems.

2.3.3 RCM accuracy in the Alps

The European Alps constitute a difficult climatic ground due to their complex topography, their arc-shape, their west-east alignment and the nearby land-sea distribution (e.g. Frei and Schär, 1998; Schär et al., 1998). Furthermore, the density of the measurement network is generally lower in the more remote mountain areas, although relatively satisfactory overall in the European Alps; and the data quality is generally lower due to difficult environmental site conditions and the arduous maintenance of the measurement facilities. As a consequence, model validation in such areas is especially challenging (e.g. Frei et al., 2003).

For these reasons, few validation studies have been conducted for the European Alps only. Some of them were undertaken within the project PRUDENCE (Prediction of Regional scenarios and Uncertainties for Defining EuropeaN Climate change risks and Effects; http://prudence.dmi.dk). This large European project aimed to address and reduce deficiencies in projecting future climate change, to quantify the uncertainties in predicting future climate and its impacts, and to interpret the results for adapting and/or mitigating climate change effects. As part of this project, ten RCMs have been driven by one GCM to produce ensemble simulation of current and future climates for Europe. The analyses of the RCM performance in PRUDENCE focused on three aspects of model validation: the ability to simulate: i) the long-term (30 or 40 years) mean climate, ii) the interannual variability of near-surface air temperature and precipitation, and iii) the representation of extreme events. The validation strategy included the comparison of simulated monthly, seasonal and annual means against observation as well as an extreme value statistic of appropriate observed and simulated data. One must note that the following summarized PRUDENCE results are based on GCM (HadAM3H**)** and not on reanalysis-driven RCMs.

In general, winter climate is determined by large-scale circulation and thus to a dominating extent by the boundary condition (i.e., GCM; here by the HadAM3H). This results in similar bias patterns for all RCMs for that time of year. In summer the intermodel spread is larger, since much of the weather is locally generated (Frei et al., 2003; Giorgi et al., 2004). However, there is generally a better agreement between observed and simulated values of interannual variability in summer. This can be explained by a more frequent breaking-down of the quasi-stable high pressure system over the Mediterranean region,

what is consistent with the reduced ability by the HadAM3H GCM to simulate long-lasting blocking events. Hence, the biases in summer depend on the regional model formulation, while in winter the boundary conditions (given by the GCM) are more important. To summarize for the PRUDENCE runs in Europe, there is a warm bias with respect to observations in the extreme seasons and a tendency to cold biases in the transition seasons.

With respect to the CRU climatology of temperature and precipitation, the areas with warm (cold) bias in winter generally exhibit positive (negative) precipitation biases, whereas the relationship is the reverse during summer, though much less clear. The well-known tendency of too little precipitation during summer in many RCMs is present in the PRUDENCE experiments as well.

A comparison of the bias of the mean sea level pressure in the ten PRUDENCE RCM runs for winter (DJF) and summer (JJA) has shown that the model mean deviation from the driving model is always small, with the largest differences over mountainous regions. The latter can be explained by different algorithms for reducing surface pressure to the mean sea level in the various models and in the driving model. This is also reflected by a relatively high intermodel standard deviation in mountain regions.

Within PRUDENCE it was also shown that the ensemble mean of all models behaves in general better than the 'best' individual model. Furthermore, the mean model is less prone to large deviations in particular areas; it tends to exhibit a similar quality for most areas.

Frei et al. (2003) have evaluated the statistics of daily precipitation as simulated by five RCMs in the Alpine region. Here, the RCMs are driven by ERA-15 and observed sea surface temperature (SST) and sea ice and the observation reference is based on 6600 rain gauge records that have been analyzed onto a regular grid with 2 km horizontal resolution. They could show that the performance for individual statistics varies considerably between the RCMs, and that this intermodel variability tends to be larger for daily statistics (wet-day frequency, intensity and high quantiles) than for mean seasonal precipitation. For mean precipitation, the models reproduced the main characteristics of the annual cycle and the seasonal variation in the subgrid-scale distribution. There are, however, underestimated summer mean conditions, which are also found in winter but with less magnitude.

The summer dryness in the Alps is most evident in August and September, where in early summer (June and July) the simulations are reasonable. An important result of the study of Frei et al. (2003) is that the RCMs reproduce the most prominent pattern of the spatial distribution of seasonal precipitation in the Alps. This provides confidence that RCMs are capable of simulating the major mesoscale precipitation processes reasonable for the subgrid-scale variations in the precipitation climate.

2.4 Scenarios

In general, a scenario is a plausible description or an alternative image of how the future might unfold. Climate scenarios are plausible representations of the future that are consistent with assumptions about future emissions of greenhouse gases (GHG) and other pollutants, and with the current understanding of the effect of increased atmospheric concentrations of these gases on the global climate. The development of scenarios for a period of 100 years is a relatively new field. Difficulties in scenario construction arise not

only from large scientific uncertainties and data inadequacies, but also because people are not trained to think in such time spans. By 2100 the world will have changed in ways that are difficult to imagine – as difficult as it would have been at the end of the 19th century to imagine the changes during the 100 years since.

The term scenario must strictly be distinguished from the terms prediction or forecast. A scenario represents a consistent evolution of the climate system into the future, but without an attached probability. In a climate scenario, only the physical relations are consistent but there are no known values driving the model and thus the uncertainties are multifold.

2.4.1 Scenarios for GCMs / RCMs

In order to simulate regional climate scenarios by climate models, GCMs are forced with GHG concentrations. In this procedure, the GHG concentrations were calculated from emission scenarios by using bio-geochemical cycle and chemistry models. Accordingly, an RCM scenario is simulated by driving the RCM at its lateral boundaries with a GCM that was forced with an emission scenario. RCM scenarios are typically simulated for the time slice of 2071-2100.

A widely used set of emission scenarios is the SRES group (Special Report on Emission Scenarios; Nakicenovic et al., 2002), which was commissioned by the IPCC. The SRES emission scenarios are based on four different narrative (qualitative) storylines (Fig. 2.5). Each storyline consistently describes the relationships and evolution between the driving forces (e.g. demographic, social, economic, technological and environmental developments) responsible for the GHG emission, and adds the context for the scenario quantification. The labelling of the storylines have been kept simple: A1, A2, B1 and B2, so as to avoid any particular order among the storylines. For each storyline several different scenarios were developed (40 in total) using six different modelling approaches to examine the range of outcomes arising from a range of models that use similar assumptions about driving forces. Thus, the set of SRES emission scenarios consists of six scenario groups drawn from the four families: one group each in A2, B1, B2, and three groups within the A1 family, featuring alternative developments of energy technologies: A1FI (fossil fuel intensive), A1B (balanced), and A1T (predominantly non-fossil fuel).

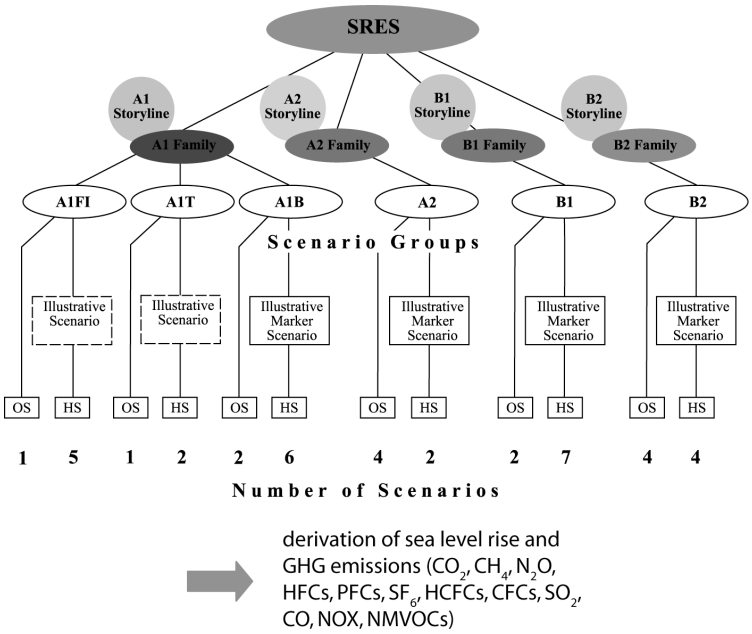

Fig. 2.5: Schematic illustration of main characteristics of the four SRES scenario storylines and scenario families (Source: Nakicenovic et al., 2002; modified).

Each scenario represents a specific quantitative interpretation of one of the four storylines. All scenarios that are based on the same storyline constitute a scenario "family", and all scenarios together encompass the current range of uncertainties of future GHG emissions. Within each family and group of scenarios, some share "harmonized" assumptions on global population, gross world product, and final energy. These are marked as "HS" for harmonized scenarios. The other scenarios (OS) denotes scenarios that explore uncertainties in driving forces beyond those of the harmonized scenarios (see Fig. 2.5).

None of the SRES scenarios represents an estimate of a central tendency and there is no single most likely, "central", or "best-guess" scenario. Probabilities or likelihood are not assigned to individual SRES scenarios and the possibility that any single emissions path will occur as described in the scenarios is highly uncertain. The scenarios cover a wide range of, but not all, possible futures. In particular, potential "surprises" are not considered and there are also no "disaster" scenarios.

An overview of the different modelled SRES scenarios of emission concentrations and the simulated changes in temperature and sea level rise is given by Figure 2.6.

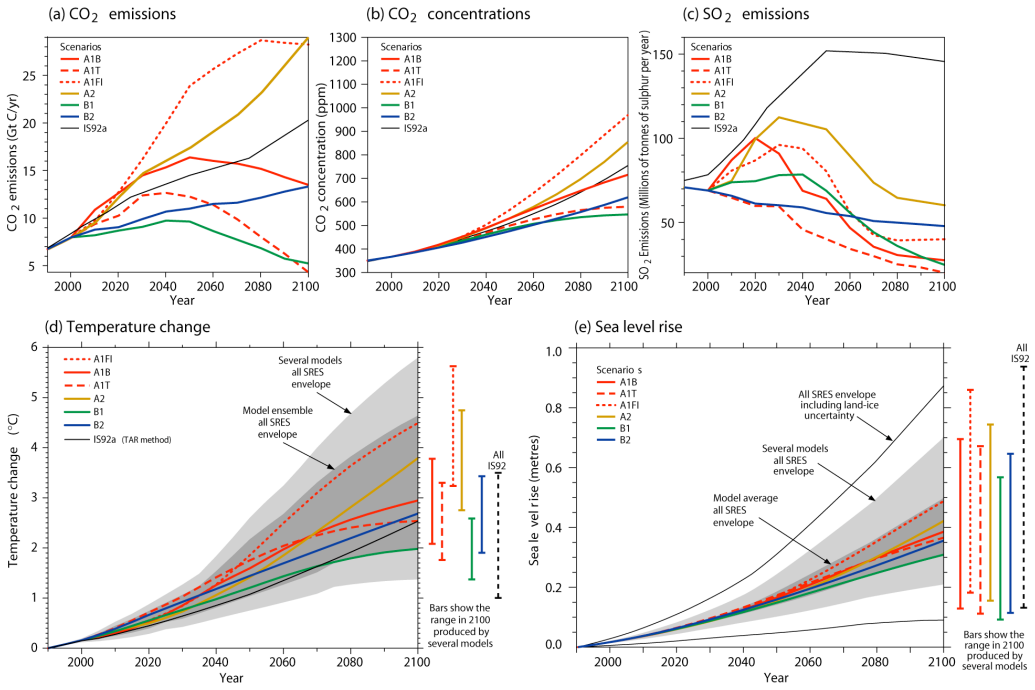

Fig. 2.6: Global climate scenarios for the 21st century (Source: IPCC, 2001).

2.4.2 Uncertainties of climate scenarios in general

With the forcing of a GCM by an emission scenario, a new dimension of uncertainty is added to the model results. The scenario uncertainties arise mainly from the uncertain nature of the emissions paths (Morita and Robinson, 2001), the uncertainties in converting emissions to GHG concentrations, the uncertainties in converting concentrations to radiative forcing, the uncertainties in modelling the climate response to a given forcing and, if applied to impact studies, the uncertainties in converting model response into inputs for impact studies (Fig. 2.7).

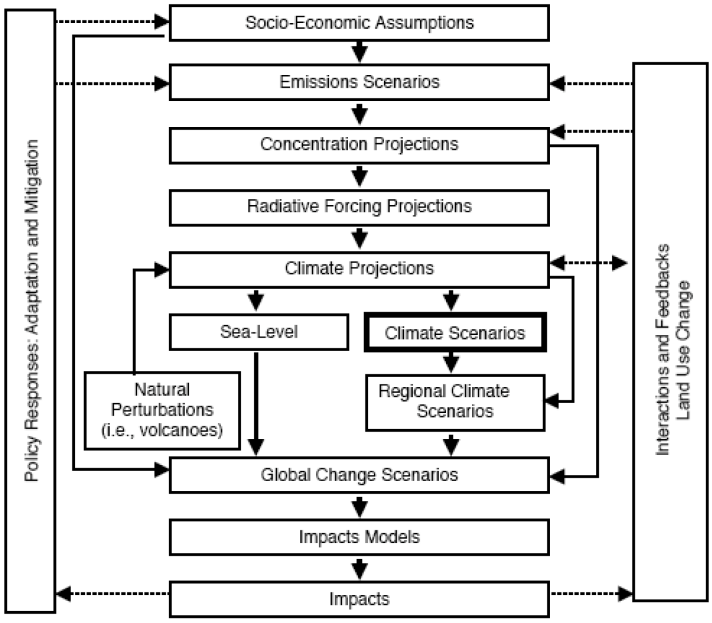

Fig. 2.7: Cascade of uncertainties (Source: Mearns et al. 2003)

A conclusion of PRUDENCE was that there is significant uncertainty in most details of climate change, e.g., the magnitude of warming, which season will warm most, and where significant changes in extreme precipitation will occur. However, although the level of uncertainty is high, it must be stressed that if any of the SRES emission scenarios come into effect in a way similar to one of the described, this will have substantial socio-economic implications.

To assess the uncertainties in climate scenarios, typically many plausible climate scenarios are combined in the form of multi-model ensembles.

2.4.3 Uncertainties of climate scenarios in the Alps

Since mountain regions are in general difficult ground for regional climate modelling, the uncertainties are accordingly higher for scenario simulations. So far, there exist only very few and recent studies that include explicitly an assessment of scenario uncertainties for the Alpine regions, e.g. Frei et al. (2006) for precipitation. However, estimates have been made for temperature and precipitation for northern and southern Switzerland by Frei (2004), based on PRUDENCE data (Fig. 2.8).

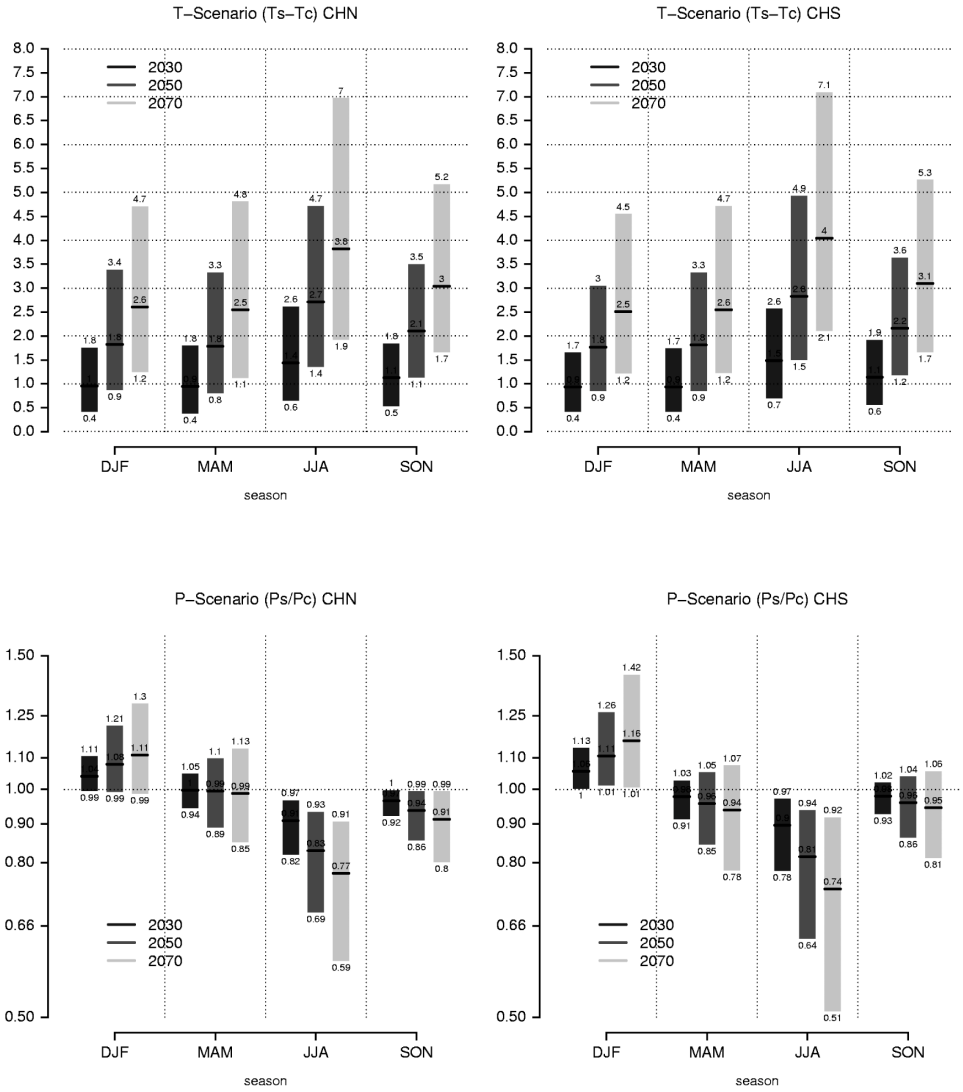

Fig. 2.8: Probabilistic scenarios for temperature (top-level) and precipitation (bottom-level) for northern (left) and southern (right) Switzerland. Vertical bars denote the 95% confidence band of the temperature and precipitation change at some time in future compared to present (1961-1990) climate (source: Frei, 2004).

According to Fig. 2.8, the changes as well as the uncertainties vary with the seasons and increase with time. Until 2050, a temperature increase in northern Switzerland in summer is estimated within 0.9 to 3.4 °C, and in winter within 1.4 to 4.7°C. There is no significant difference between north and south Switzerland. For precipitation, until 2050 an increase within 0 to 20% in winter is estimated, and a decrease in summer within 7 to 30 %, again with similar quantities in summer.

2.5 Application of RCM results for impact modelling

Only over the past few years has the use of RCM results for impact modelling gained increased attention in various scientific disciplines. Several attempts have been undertaken to benefit from the advances in regional climate modelling. The first and most numerous

studies have been conducted in the field of agriculture (e.g. Mearns et al., 1997, 1999, 2000, 2001a; Guereña et al., 2001) and hydrology (e.g. Bergström et al., 2001; Arnell et al., 2003; van der Linden and Christensen, 2003; Wood et al., 2004; Kleinn et al., 2005; Kotlarski et al., 2005). For permafrost, only very few and very recent studies exist on the use of RCM output (e.g. Christensen and Kuhry, 2000; Nan et al., 2005; Stendel et al., 2006). However, these studies included only Arctic lowland permafrost and thus, there is no topographic influence to be considered. Several studies exist for Arctic lowland permafrost, in which GCM output has been applied (e.g., Anisimov and Nelson, 1996,1997; Anisimov et al., 1997; Nelson et al., 2002; Stendel and Christensen, 2002; Lawrence and Slater, 2005). Since the distribution and occurrence of Arctic lowland permafrost is large in scale, the use of GCM output is appropriate. Furthermore, there has been some work done in glacier studies where GCM information was used (e.g., Reichert et al., 2001; van de Wal and Wild, 2001; Cook et al. 2003; Schneeberger et al., 2003).

Each region, each impact process and each specific context of an application and its aims has its specific needs of climate information regarding spatial and temporal resolution and its associated accuracy. As a consequence, in each of the studies mentioned above individual techniques and approaches with different levels of sophistication have been applied. General recommendations for the use of RCM results for impact models have been formulated by Mearns et al. (2003). However, until present, universally applicable solutions are not available and probably will not be in the foreseeable future (Synthesis Report of ENSEMBLES Workshop, Evora, 2005).

As mentioned above, the challenge of applying RCM results to an impact model varies for each study. However, there are some tasks and topics that must be considered by most impact modellers aiming at applying RCM output. This includes primarily dealing with the spatial and temporal scales which influence the exact partitioning of the different processes and their associated uncertainties, but also the technical handling [see *Paper 1*].

2.5.1 Technical issues

Model concepts and data formats (Interoperability)
Many impact models are based on model concepts and data formats that diverge from those used by climate modellers. A good example are GIS models that are often used for impact modelling. A GIS is primarily a specialized tool for managing spatial data within a coordinate reference system. GIS is not really a tool for managing temporal process data (Wilhelmi and Brunskill, 2003). Furthermore, only since very recently have first interfaces been available to convert NetCDF (Network Common Data Format; a very common data format in the climate modelling community; see below) to an ESRI (very widely used GIS-software products) point shapefile, and this is thanks to the GIS Initiative at the NCAR (Wilhelmi and Betancourt, 2005). It is planned by ESRI that the next version of ArcGIS (Version 9.2; planned for end of 2006) will be able to read NetCDF.

However, for models other than the GIS, the technical handling and conceptual understanding of the NetCDF data concept is essential if the RCM output is to be applied to impact models. Therefore, a short introduction is given in the following.
NetCDF is a data interchange format developed by Unidata (www.unidata.ucar.edu/software/netcdf/index.html) for data transfers between Unidata applications. The concept is implemented as a library of computer ‘functions’ that can be

assembled by a user to access or create NetCDF files. The files are self-describing, machine-independent data sets that can be interchanged readily between users without the need for supplementary materials. The files can contain data of different types, multiple variables and ancillary data or descriptive text. NetCDF data can be manipulated and displayed by several software packages (www.unidata.ucar.edu/software/netcdf/software.html), whereby NCO (http://nco.sourceforge.net) and Ferret (http://ferret.wrc.noaa.gov/Ferret/) are possibly worthy of note.

The exponential growth of climate model output data, as model resolution and integration times have increased, has led to the development of various distribution technologies (McGuffie and Henderson-Sellers, 2005). Instead of modellers transferring data from one machine to another, the NetCDF libraries have been extended recently to function in a distributed manner. Originally designed to deal primarily with oceanographic data, the OPeENDAP/DODS data access protocol simplifies data distribution and is a protocol for requesting and transporting data across the Internet, based on the client-server model (www.opendap.org). OPeENDAP/DODS is a community-driven project and is based on the idea that the data sets are often best distributed by their creators. Data are distributed without regard to local storage format. Anyone with a digital data archive can configure their archive as an OPeENDAP/DODS server and make it available to clients in the scientific community. Data can be accessed at remote locations and these remote data analysis and visualization systems can be modified to be OPeENDAP/DODS clients, retrieving data at the application level, instead of requiring the user to collect and store copies of the entire data set.

All of the recently completed (PRUDENCE) and ongoing (ENSEMBLES; NARCCAP) projects that produce RCM output make use of NetCDF data and are organized using OPeENDAP/DODS. To establish agreements on and development of standard protocols for transferring and applying climate model information for impact assessment was one of the key objectives of PRUDENCE.

Rotated grids

For most climate impacts, the geographic location on earth is as important as the phenomenon itself, and metadata about the coordinate reference system is particularly important. In order to avoid numerical problems at the poles of the earth, RCMs are usually calculated on rotated grids where the pole is always located outside the LAM. In this way, the reference point is the intersection between the equator and the zero meridian, in the centre of the RCM. In order to use RCM output for impact studies, the rotated grid must be re-rotated and projected to the impact modellers's needs.

2.5.2 Handling of uncertainties

A major challenge to be faced when applying RCM results to impact models is the handling of the uncertainties of the RCMs, discussed in the previous section. In this context, the relative significance of the uncertainty of a variable depends on the specific processes to be investigated and on the study region. The main process that determines permafrost occurrence is the energy balance. The RCM uncertainties related to mountain permafrost are discussed in detail in [*Paper 1*] and [*Paper 2*]. In order to overcome these

uncertainties, two approaches (termed ‘delta’ and ‘bias’) are introduced in [*Paper 1*] and applied in [*Paper 1*], [*Paper 2*] and [*Paper 3*]. For this reason, they are not discussed further here.

CHAPTER 3

Mountain Permafrost

3.1 Definition, occurrence and practical relevance related to permafrost

Permafrost is a thermal state and defined as lithospheric material that remains at temperatures below 0 °C for at least one year (Washburn, 1979). According to this definition, the occurrence of permafrost does not necessarily require the existence of ice.

The occurrence of permafrost is determined primarily by the regional climatic and the site-specific surface and subsurface properties. Worldwide, there are currently about $25*10^6$ km^2 of frozen ground in existence (Zhang et al., 2003). These areas are located mainly at high latitudes (e.g. French, 1996; Smith and Riseborough, 1996, 2002) and/or at high altitudes (e.g. Haeberli, 1975; Cheng et al., 1983; Barsch, 1992; Cheng and Dramis, 1992). The presence of permafrost is often accompagned by impressive landforms such as pingos or palsas (e.g. Sepäläa, 1986; Mackay, 1998), and on high-mountain slopes, by rock glaciers, for example (e.g. Barsch, 1971, 1992; Haeberli, 2000; Frauenfelder, 2004). In Switzerland, about 5 % of the land surface is characterized by mountain permafrost (Keller et al., 1998). In the Swiss Alps, permafrost bodies reach depths of a few decameters in debris (Vonder Mühll and Haeberli, 1990) and up to more than 1 km in the bedrock of the highest summits (Lüthi, 2000). The location of the lower boundary of the permafrost body (permafrost base) is a function of the MAGST and the geothermal heat flux (Fig. 3.1). Its position varies over very long time periods only, depending on the permafrost thickness and the ice content. The upper boundary of the permafrost body (permafrost table) is subject to the seasonal cycle of the ground surface temperature, which can thaw the uppermost layer (active layer) during the summer season.

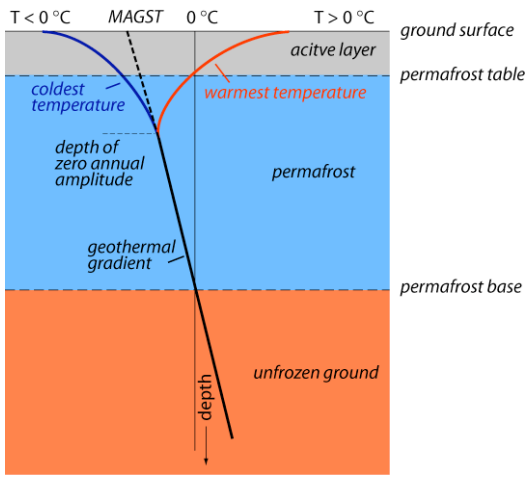

Fig. 3.1: Schematic view of the ground thermal regime (modified after J. Nötzli).

The present state of permafrost occurrence (as well as its future development) is influenced by former climatic conditions. Permafrost is a thermal system having a slow response to climatic changes. The response time of permafrost depends on the thermal conductivity, the ice content and the thickness of the frozen ground (Osterkamp, 1983; Nelson, 2003). Even relatively warm and thin discontinuous mountain permafrost has a response time which is typically measured in decades to centuries (Haeberli, 1990). In fact, the thickness and some marginal occurrences of alpine permafrost most probably still reflect maximum Holocene cooling during the Little Ice Age, which culminated in the 19th century. Temperature profiles observed in boreholes (Vonder Mühll et al., 1998; Isaksen et al., 2000; Isaksen et al., 2001; Harris et al., 2003) prove permafrost thicknesses in excess of values expected from present-day mean annual ground temperature (MAGT).

The practical relevance of changes in the ground thermal regime with current permafrost conditions is related mainly to stabilization issues (Kääb et al., 2005). The thawing of mountain permafrost can lead to destabilization of engineered infrastructure (Haeberli, 1992; Nelson et al., 2001) as well as to destabilization of debris slopes (Zimmermann and Haeberli, 1992; Zimmermann et al., 1997; Harris et al., 2001) and rockwalls (Dramis et al., 1995; Haeberli et al., 1997; Davies et al., 2001; Noetzli et al., 2003; Gruber et al., 2004). Due to the projected climate scenarios, major landslides caused by thawing of mountain permafrost cannot be excluded.

3.2 The thermal boundary conditions of mountain permafrost

In general, the thermal boundary conditions of the uppermost layers of the lithosphere are determined by the atmospheric energy fluxes and the heat flow from the earth's interior (Williams and Smith, 1989). The geothermal heat flux is relatively low and quite constant in space and time. In the context of permafrost, its variations caused by mountain topography can be neglected. As a consequence, the ground thermal regime and in particular its potential changes are determined mainly by the atmospheric net heat exchange at the surface, which is controlled by the local topography, by the surface and subsurface conditions and by the ground properties (Williams and Smith, 1989).

3.3 The energy balance at the surface

The surface energy balance Equation (1) describes the energy exchange of heat and moisture between the atmosphere and the ground surface. According to the conservation principle, the sum of all fluxes must be balanced for any time scale and every location.

$$Q^* + Q_H + Q_{LE} + Q_G + Q_M = 0 \qquad (1)$$

where Q* (net radiation) = K↓ + K↑ + L↓ + L↑ and where K↓ = incoming short-wave radiation, K↑ = reflected short-wave radiation, L↓ = incoming long-wave radiation and L↑ = outgoing long-wave radiation, Q_H = sensible heat flux, Q_{LE} = latent heat flux, Q_G = ground heat flux and Q_M = latent heat of fusion

From Equation (1) it is evident that solar radiation is the most important energy source of the surface (if geothermal heat is neglected; see above). Therefore, the surface temperature at a specific location depends significantly on the amount of incoming short-wave radiation, which varies on an annual cycle with latitude and topography. Furthermore, the partitioning of the energy balance components also varies significantly due to site-specific factors. In the following, the most important components of the energy balance are distinguished and discussed briefly for three situations in the increasing order of complexity.

3.3.1 Flat horizontal surface (without surface cover)

Assuming a flat horizontal surface without a surface cover, the term Q_M can be neglected due to the absence of a surface cover (snow). Here, the main climatic factors affecting K↓ are the latitude, the time of year and the weather conditions (cloudiness). L↓ is influenced largely by cloud conditions and atmospheric humidity. Q_H is sensitive to wind speed, temperature gradient and soil moisture, and Q_{LE} to vapour concentration gradient. The main site-specific surface factors are (i) the albedo, which significantly influences K↑ and dominates Q*, (ii) the infrared emissivity, which influences L↑, (however, it is less variable than the albedo), and (iii) the thermal conductivity of the ground, which depends on moisture and porosity (soil, air and water content) and affects Q_H, Q_{LE} and Q_G.

3.3.2 Complex topographical surface (without surface cover)

In addition to the factors mentioned above, in complex topography the amount of short-wave radiation reaching the ground is influenced to a significant extent by the slope angle and aspect. Furthermore, topography generates and modifies airflow (Oke, 1987). Though they are important, these topographical effects of airflow are not discussed further here.

In general, the total K↓ received at the surface is,

$$K\downarrow = S + D \qquad (2)$$

where, S = direct-beam short-wave radiation, D = diffuse short-wave radiation.
Only S is dependent upon the angle at which it strikes the receiving surface.

The relationship between *the slope angle* and S can be derived from the cosinus law of illumination and be written as

$$S\hat{} = S_i \cos \Theta\hat{} \qquad (3)$$

where, S^= the radiant flux density incident on the slope surface, S_i = the radiant flux density perpendicular to the incident beam (i.e., on the imaginary surface CD), and Θ^ = the angle between the direct beam and a normal to the slope surface (Fig. 3.2)

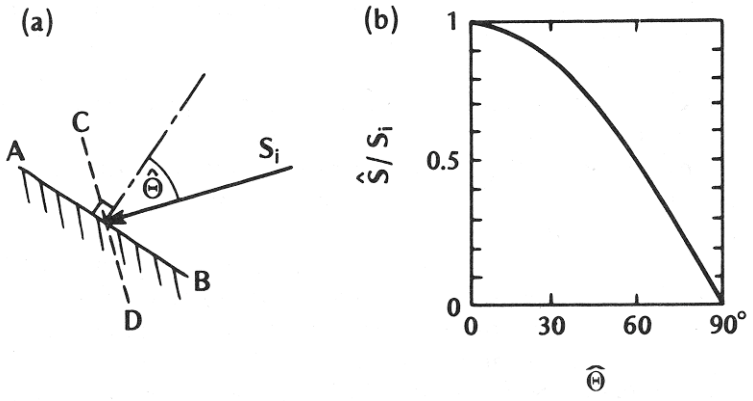

Fig. 3.2: (a) Diagrammatic representation of the angle Θ^ between the surface and the incident direct-beam short-wave radiation, S^. (b) The form of the cosinus law of illumiation (Source: Oke, 1987).

Due to the Equation (3) and Fig. 3.2b, the direct-beam solar input value is almost uniformly high for angles of Θ^ less than 30°, but above this it drops at an increasing rate.

The aspect is an important variable in determining the total amount of potential energy income. In the northern hemisphere, south-facing slopes receive substantially more direct beam solar input than north-facing slopes and vice versa on the southern hemisphere (e.g. Oke, 1987). Fig. 3.3 gives an example of the total daily direct-beam solar radiation S^ incident upon slopes of differing angles and aspects at latitude 45°N at the times of the equinoxes. Marked differences can be seen for slopes and different aspect. It is notable that the maximum load would be on a south 45° slope (Θ^ = 0°), whereas no direct-beam reaches north-facing slopes with an angle greater than 45°.

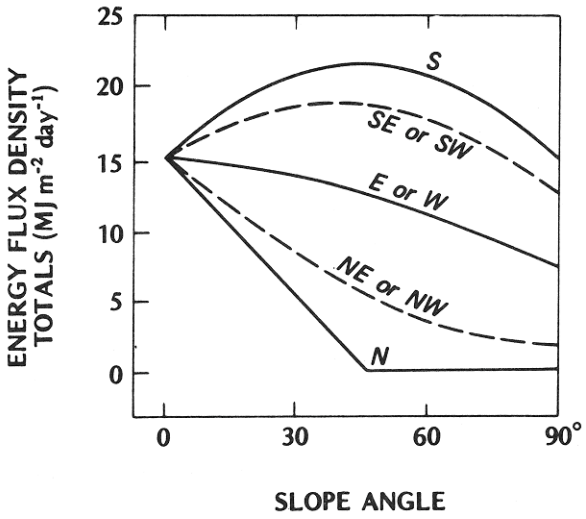

Fig: 3.3: Total daily direct-beam solar radiation incident upon slopes of differing angles and aspects at latitude 45°N at the time of the equinoxes (Source: Oke, 1987).

Furthermore, in complex high-mountain topography, the ground surface temperature can be influenced additionally by 3D effects, where the conducting ground energy flux is received from opposing slopes (e.g., Nötzli et al., subm.) [*Paper 3*].

3.3.3 Surface with buffer layer between the ground surface and the atmosphere

In high-mountain areas, the most common and important buffer layers are snow (seasonal), ice (perenniel) and different classes of rock material. Each of these buffer layers can occur separately or in a combination. As discussed in the following, they significantly influence the surface energy balance and thus the ground thermal regime.

For snow cover, one of the most important characteristics is its high albedo and thus its influence on K↓ - K↑. In addition, the surface energy balance is influenced by Q_m, by the emissivity (snow has a higher emissivity than bare ground) and the roughness length. Snow cover also complicates the surface energy balance since it allows penetration of short-wave radiation, in general with exponential attenuation with depth up to about 1 m (see Oke, 1987). The general attenuation is, however, disturbed by the snow pack internal water movements and phase changes. The seasonal snow cover is one of the primary factors influencing the ground thermal regime, in particular in regions where the MAGT is generally close to 0°C (Keller and Gubler, 1993; Zhang et al., 2001; Stieglitz et al., 2003). Since heat exchange takes place at the snow surface rather than at the ground surface, the range of annual ground surface variation is reduced and ground temperatures are higher in winter as well as on an annual basis (Williams and Smith, 1989).

The influence of a seasonal snow pack on the ground thermal regime and thus on the occurrences of permafrost may be summarized as follow: The low thermal conductivity of snow makes it a good insulator (Zhang et al., 1996; Zhang et al., 2001; Ling and Zhang, 2004, Zhang, 2005). An early establishment of a deep winter snow cover enhances the insulation impact and thus restricts heat loss from the ground over the entire cold season. In contrast, a thin autumn snow cover effectively conducts heat out of the ground. In

spring, a long-lasting snow cover prevents the ground from heating up and enhanced surface cooling is indicated due to the consumption of latent heat of snowmelt (Zhang et al., 2001). In general, the timing of snow cover onset has less influence on the solar radiation balance than the end of it, since the solar elevation is lower at that time of the year (Zhang et al., 2001). This is, however, more important in high latitudes and in regions where no or only low topography is present. In high-mountain areas, the complex topography can locally relativise the solar elevation effect. Furthermore, the duration and thickness of the snow cover distribution depends also on redistribution by wind (direction and speed) and in high-mountain environments additionally by the steep slope angles of the topography, as a local factor of snow redistribution for avalanches.

A surface cover layer of perenniel ice affects the surface energy balance in a similar way as snow. From a temporal point of view, the most important impact of an ice cover on the ground thermal regime are probably the large changes in the albedo, and the missing uptake of summer heating due to icemelt. The current rapid retreat of glacier cover as a response to climate change (Paul et al., 2004) will alter the thermal regime of the new ice-free ground in short-term stretches (Haeberli et al., 1997; Wegmann et al., 1998).

The type and size of rock material lying on the ground has significant effects on the ground thermal regime. Effects of such buffer layers on the surface energy balance are indicated by different roughness lengths, emissivity and albedo. Furthermore, significant differences in the thermal regimes of slopes are found between layers of coarse blocky material and fine-grained soil (Harris and Pedersen, 1998, Gorbunov et al., 2004). In coarse blocky material, the influence of complex non-conductive heat transfer processes (Goering and Kumar, 1996; Wakonigg, 1996; Humlum, 1998; Hoelzle et al., 1999; Hanson and Hoelzle, 2004, 2005), convection both within the matrix (vertical and horizontal) and across the surface boundary (vertical), and ice formation between the blocky material can lead to colder MAGT than in fine material under the same climatic and topographical conditions (Harris and Pedersen, 1998, Sawada et al., 2003). As a consequence, permafrost may even form under a positive MAAT and MAGST in the presence of such a surface cover (Gorbunov et al., 2004), and in alpine environments the lower limit of discontinuous permafrost is often found along areas with very coarse-grained or blocky surface cover. The physical processes that lead to thermal differences between MAGT and MAGST are termed ‘thermal offset’ (Goodrich, 1982), an object of ongoing research (Hanson and Hoelzle, 2004; Delaloye and Lambiel, 2005). In addition, the processes within the blocky layers are complicated by a seasonal snow cover and steep slope angles (Hoelzle et al., 1999; Mittaz et al., 2002) as discussed above.

Organic layers such as peat or grass are also important for the ground thermal regime in particular due to the albedo and moisture supply. However, organic layers are much more common in high latitudes than in the high altitudes of lower latitudes. For this reason, these influences are not further discussed here.

3.4 The subsurface ground thermal regime

The propagation of the ground surface temperature into the ground depends on the ground thermal properties for heat transfer (Williams and Smith, 1998).

$$Q_G = -k(\Delta T / \Delta z) \qquad (4)$$

From Equation (4) it is evident that the rate of the specific heat transfer is a function of the thermal conductivity k [$Wm^{-1}K^{-1}$]. The thermal change in the medium depends, in the end, on the volumetric heat capacity C [$Jm^{-3}\ K^{-1}$]. The thermal diffusivity κ is defined with the coefficient of heat diffusion [m^2s^{-1}]

$$\kappa = \frac{k}{C} \qquad (5).$$

The final heat conduction equation for a simple, homogenous ground is:

$$\frac{\partial T}{\partial t} = \kappa \frac{\partial^2 T}{\partial z^2} \qquad (6).$$

This is only a very brief summary of the heat transfer processes into the ground and of course it does not cover the complexity of the thermal flow in the ground. The natural variability of the ground thermal properties (thermal conductivity, heat capacity, thermal diffusivity), are important factors to account for. Furthermore, in order to assess current subsurface ground temperatures, the non-stationary conditions mentioned in Section 3.1, due to the slow temporal response of permafrost, must be considered, as well as 3D effects of the mountain topography (Gruber et al., 2004b; Noetzli et al., subm. [*Paper 3*]). However, atmospheric changes affect only the ground surface in a direct manner via the energy balance at the surface, and thus the properties of the ground thermal regime and the propagation of the thermal flow in the ground can in principle be analysed without further reference to climate. Therefore, the heat transfer processes are not further discussed here, since the focus of this thesis is mainly on changes in the energy balance at the surface, caused by changes in the atmosphere.

3.5 Progress and current state of mountain permafrost models

A first *empirical model* to assess the occurrence of mountain permafrost was developed by Haeberli (1975). The so-called 'rules of thumb' are based on proxies such as measured Bottom Temperature of Snowpack (BTS; Haeberli, 1973), temperature measurements within the active layer and applications of geophysical methods (e.g. Hauck, 2001; Vonder Mühll et al., 2001). They enable the assessment of probabilities for permafrost occurrence as a function of topographical parameters, i.e., elevation, aspect and slope, which primarily influence the energy balance and its modification by snow and its redistribution through snowdrift and avalanching. Keller (1992) implemented these 'rules of thumb' in a GIS-based program code, called PERMAKART.

These developments were extended towards *empirical-statistical models* first introduced by Hoelzle (1996) with the GIS-based model PERMAMAP. Hoelzle (1996) used statistical relations between potential direct solar radiation and mean annual air temperature (MAAT). Similar GIS approaches as the two mentioned, followed for application to various mountain regions, for example, by Delaloye and Morand (1998), King and Kalisch (1998), Li et al. (1998), Etzelmüller et al. (1998, 2001b), Frauenfelder et al. (1998), Jensen (1999) and Lewkowicz and Ednie (2004).

In a next generation, *process-oriented models* with a focus on a detailed understanding of the energy fluxes between the atmosphere and the permafrost began to be developed. Mittaz (2002) and Mittaz et al. (2002) have taken a first step in this direction with the model PERMEBAL. Gruber (2005) has continued and extended this research with the model TEBAL. They explicitly parameterize the energy balance at the surface and require a correspondingly large amount of measured or computed data.

The spatial scale required to operate the models mentioned above must decrease from empirical to process-based model types. Etzelmüller et al. (2001a) and Hoelzle et al. (2001) have proposed distinguishing three spatial scales for empirical-statistical mountain permafrost modelling: (i) micro-scale < 25 m, (ii) meso-scale 25 m to 250 m and (iii) macro-scale > 250 m. In topographically complex mountain areas, only micro- and meso-scales are appropriate (Etzelmüller et al. 2001b) and macro-scale should only be used for overview maps. For process-based models, only the micro-scale is appropriate since they need to solve the local surface characteristics, which vary usually within very short distances in complex mountain topography.

Empirical and empirical-statistical models are able to simulate only approximate probability classes for the existence of permafrost. They neglect, for example, the influence of different surface covers. They assume steady-state conditions and are calibrated to a specific region and its current climatic conditions. Therefore, they are not well suited for extrapolation in time and space (Hoelzle et al., 2001). Nevertheless, if a model for a region is calibrated and available, it is easy to apply, has a limited need of input variables and thus can provide an overview of the probable permafrost occurrence for a greater region such as the Alps within a reasonable time. In this manner, Alpine permafrost distribution maps for Switzerland have been produced (Keller et al., 1998; Krummenacher et al., 2005).

The advantage of *process-based* energy balance models is their ability to be extrapolated in a spatial-temporal way and to describe model internal feedback mechanisms. Therefore, they are suited for simulations of the impact of changes in the atmospheric conditions based on climate models. Their potential is large, since they allow for computing ground surface temperature and the propagation of thermal fluxes in the ground. However, more effort is needed to develop and validate such models. This includes mainly measurements at high-mountain sites (which are usually not easy accessible) such as the energy fluxes (Mittaz, 2002), ground surface temperatures (Hoelzle et al., 2003; Gruber, 2004b) and borehole temperatures (Vonder Mühll et al., 1998). Furthermore, parametrisation schemes for many variables must be applied and relatively advanced computing resources are required. The development of process-based energy balance models in complex topography is subject to ongoing research.

3.6 Modelling permafrost scenarios

The common approach used so far for permafrost scenario modelling is the application of incremental scenarios. They describe techniques in which particular climatic (or related) elements are changed incrementally by plausible though arbitrary amounts (e.g. +1, +2, +3 °C change in air temperature or +/- 10, 20, 30 % change in precipitation) (IPCC, 1994). Such scenario approaches have, for example, been used by Hoelzle and Haeberli (1995), Stocker-Mittaz et al. (2002) or Zemp et al. (2006). Incremental scenarios provide

information on an ordered range of climate change and can readily be applied in a consistent and replicable way in different studies and regions. However, such scenarios do not necessarily present a realistic set of changes that is physically plausible. They actually simulate sensitivities and not scenarios in an intrinsic sense. Thus, incremental 'scenarios' should be adopted and intended as system sensitivity studies, prior to the application of more credible, climate model-based scenarios (e.g., Rosenzweig and Iglesias, 1994; Smith and Hulme, 1998).

CHAPTER 4

Summary of Research Papers

Paper 1

Salzmann, N., Frei, C., Vidale, P.L., Hoelzle, M., 2006. **The application of Regional Climate Model output for the simulation of high-mountain permafrost scenarios**. Global and Planetary Change. doi: 10.1016/j.gloplacha.2006.07.006.

The study investigates the possibilities and limitations of the application of RCM output for local high-mountain permafrost scenario simulations. Two possible application strategies (termed as delta and bias approach) are introduced and discussed. Both approaches take into account the special challenges that arise in topographical complex high-mountain environments. Intended as an initial example rather than to make an assessment of the potential future changes in the permafrost occurrence, the two approaches are applied to the energy balance model TEBAL for the Corvatsch region (Upper Engadine, Switzerland) by considering the following variables from the CHRM RCM; temperature, precipitation, global radiation, air pressure, vapour pressure and wind speed. In doing this, three different CHRM RCM experiments were used, each driven with different boundary conditions; these are: CTRL and SCEN run and reanalysis (ERA-40). The observed meteorological data (OBS) from the Corvatsch location were used as site-specific references and in this manner used to evaluate the performance of the CHRM simulation at the Corvatsch site, as the basis for the daily scenario time series for the delta approach, and to determine the 'best' grid box for the location of interest.

In the study, the most important challenges associated with the application of RCM output to an impact model in complex high-mountain topography were identified and include:

- the spatial scale mismatch between the two model types (RCM 50 km, alpine permafrost model 25 m);
- the low vertical resolution of an RCM that cannot represent high mountains adequately;
- the horizontal shifts of precipitation pattern (at grid boxes scale) that are observed along mountain ranges;
- the high spatial variability of the climate variables;
- the reduced availability of observation data in remote mountain areas; and
- the question of what a grid point of an RCM (scenario) effectively represents, particularly in mountain regions.

The attempt is made to overcome these challenges by applying the delta and the bias approach. *The delta approach* obtains a scenario time series by adjusting the local baseline

observation by the difference (for variables like temperature) or the ratio (for variables like precipitation) between the SCEN and the CTRL time slice. *The bias approach* uses the debiased daily time series output of the SCEN simulation. Of the two approaches, the delta approach is the simpler and faster one; however, it only includes a quantitative change (e.g., increase in temperature) but not a qualitative one (e.g., increase in variability) as the bias approach does.

The main findings, conclusions and recommendations of the study are as follows:

- A direct use of RCM output is not recommended, particularly in complex high-mountain regions where the output of an RCM generally contains more uncertainties than over landscapes with low spatial variability. Furthermore, a lapse rate correction alone does not reduce the overall model bias.
- The grid box which represents best the climate condition at the location of interest, is not necessarily the grid box at which the site of interest is situated in terms of latitude and longitude.
- The choice must be made between using the average of the surrounding grid boxes or only the grid box that fits best with the climatology of the specific site. The decision depends on the applied approach and also on the specific application and sensitivities of the considered processes. The determination of a 'best' grid box is more important for the bias than for the delta approach. For the delta approach, the average approach can be considered appropriate and is may be even more robust than the use of one single grid box. For the bias approach, such a 'grid box average approach' is not suitable, since simulated regional extremes, probably represented by only one grid box, would be cut when averaging several grid boxes.
- In this study the delta approach did not show a high sensitivity regarding the number of grid boxes (one 'best' or average) included.
- The delta and the bias approach must be adapted for different climate variables.
- The application of several different skill measures is indicated to measure the performance of model output and to determine the 'best' grid box.
- Since a CHRM model year consists of only 360 days, but the TEBAL model requires 'real' years, the missing days must be added by interpolation technique.
- The additional benefit of the extra effort for a 'new' and more complex ratio bias should be evaluated first by sensitivity studies of the TEBAL model and the natural system it represents.
- A limitation of the proposed procedures is imposed by the fact that for many remote mountain areas, observational data at the required spatial and temporal resolution are lacking and/or difficult to obtain.
- Despite the many uncertainties associated with RCM output, the study showed that the application of RCM results offers new and promising perspectives for the simulation of high-mountain permafrost scenarios.

Paper 2

Salzmann, N., Nötzli, J., Hauck, C., Gruber, S., Hoelzle, M., Haeberli, W., (in press). **Ground-surface temperature scenarios for complex high-mountain topographies based on Regional Climate Model results.** Journal of Geophysical Research – Earth Surface.

This study investigates the impact of climate change scenarios on the local scale ground-surface temperature (GST), which determines an important part of the ground thermal regime. Possible ranges of changes in the GST (ΔGST) are assessed for steep rockwalls, which exclude a seasonal snow cover and/or strongly heterogeneous surface layers – two factors that significantly modify the GST. In order to account for the uncertainties associated with RCM output, a set of 12 different scenario climate time series (including ten RCM-based scenarios from three different RCMs driven with the same GCM as forced by two different SRES emission scenarios and two incremental scenarios) was applied to the energy balance model TEBAL using two different approaches (delta and bias) to simulate the average ΔGST for 36 different topographical situations (including three elevation levels (2500, 3500, 4500 m a.s.l.), three aspect slopes (N, E/W, S) and four slope angles (50°, 60°, 70°, 80°)).

The results and conclusion of this study can be summarised as follows:

- The variability of the simulated ΔGST is quite high, on average about 3.5 °C in this study, and mainly related to the emission scenario, the RCM and the approach used to apply the RCM results to the TEBAL model.
- The relative distribution of the individually simulated ΔGST points within the calculated variability ranges is relatively constant throughout all topographic situations.
- In terms of topography, aspect is more important than slope and elevation, to be explained mainly by the fact that the aspect significantly modifies the amount of solar radiation received at the surface.
- N-facing slopes compared to the S-facing slopes showed a higher sensitivity (with a difference of about 1°C) to the applied climate scenarios in this study, and the uncertainties and variability were higher for S-facing slopes. These results are probably caused by the different solar radiation received at the surface of N- and S-facing slopes.
- Assuming that a higher sensitivity of N-facing slopes is valid for the entire Swiss Alps, the observed differences in rockwall GST would decrease under the future scenario climate condition as the GST at N-facing slopes would increase to a greater amount than at S-facing slopes. Such aspect-dependent warming of the surface will affect the qualitative changes of the ground thermal regime [see *Paper 3*].
- The use of RCM-based scenarios instead of incremental scenarios for impact studies is to be preferred particularly in complex mountain topography, when a study aims at assessing the possible impact of climate change scenarios in an intrinsic manner and not when studying sensitivities of a process or a model.
- Generally, the highest ΔGST is achieved by applying the A2, and the lowest by applying the B2 emission scenario, in both cases independent of the RCM type.
- However, the choice of the approach used in combination with a potentially higher

amount of received solar radiation (e.g., due to south slope) can result in a higher ΔGST with the B2 than with the A2 emission scenario, although the same RCM is used.

- If the variability is allowed to change between OBS and SCEN (bias approach), the increase in ΔGST is reduced in our study.
- The use of multi-model approaches such as the inclusion of different emission scenarios and GCMs/RCMs is required in order to assess possible ranges of future ground surface temperature changes and in this way to cover a main part of the uncertainty range associated with the models. The range of uncertainties in complex topography can, however, be assessed only by using physically plausible RCM-based scenarios, which take into account qualitative and quantitative changes of different atmospheric variables.
- The influence of the topography on ΔGST is generally weaker than the influence of the different emission scenarios, RCMs and matching approaches (delta/bias).

Paper 3

Nötzli, J., Gruber, S., Kohl, T., Salzmann, N., Haeberli, W., (subm.). **Three-dimensional distribution and evolution of permafrost temperatures in idealized high-mountain topography**. Journal of Geophysical Research – Earth Surface.

This study concentrates on the strong lateral components of subsurface heat fluxes that exist in complex mountain topography and profoundly influence the subsurface thermal field. In order to investigate such 3-dimensional effects, numerical experimentation is conducted using typical idealized test cases of high mountain topography, such as ridges, peaks or spurs. As part of the experimentation, the results of surface energy balance model simulations are applied to a 3-dimensional ground heat conduction scheme to systematically investigate ground temperatures and permafrost occurrence under the influence of high mountain topography. Furthermore, time-dependent RCM-based scenario simulations were applied to calculate changes of the ground surface temperature.

The experiments of this study led to the following results and conclusions:

- The steady state temperature field below complex high-mountain topography is controlled mainly by varying surface temperatures of different mountain sides and is virtually untainted by the influence of the geothermal heat flux in the higher parts. Isotherms are nearly vertical and a strong heat flux is directed from the warmer to the colder side of a mountain.
- Permafrost may occur in the underground at locations where surface temperatures do not indicate it even in steady state conditions. Thus, traditional 2D-maps do not provide sufficient information to assess the permafrost distribution at depth in complex high-mountain topography.
- Irregularities on the surface such as spurs may additionally modify the ground temperatures and can induce local permafrost occurrence.
- Permafrost degradation in steep topography takes places from different sides affecting both the permafrost table and the permafrost base. This leads to an increase in the pace of permafrost degradation as compared to permafrost in flat terrain, where warming typically penetrates vertically into the ground.
- Owing to the long time needed for a temperature signal to penetrate to greater depth, permafrost can remain inside mountains over centuries. At locations where the surface temperatures rise clearly above 0 °C, substantial permafrost occurrence can be found. Time scales involved in permafrost degradation are in the order of millennia even without the retarding effect of latent heat. The influence from past cold periods such as the last ice age is likely to still be found in the interior of mountain peaks.
- With rising surface temperatures, heat fluxes strongly increase near the surface. On the northern side of a ridge, a zone develops toward which heat flows from both sides and, toward which unfrozen water migrates.
- In complex topography, permafrost occurrence must be assessed while taking into account the 3-dimensional situation as well as transient effects requiring physics-based models that simulate actual ground temperatures.

Paper 4

Salzmann, N., Gruber, S. Hugentobler, M., Hoelzle, M., 2006. **The influence of different digital terrain models (DTMs) on alpine permafrost modeling**. Journal of Environmental Modeling and Assessment, DOI 10.1007/s1066-006-9065-3.

The distribution and change of ground surface temperatures (GST) and thus permafrost in complex high mountain regions depends greatly on the topography. A digital terrain model (DTM) is thus an important component for the simulation of current and future distributed permafrost occurrence. This study investigates the influence of the DTM on the modeling of the GST. For this purpose, the energy balance model PERMEBAL was run with six different DTMs having 10 m spatial resolution. Five of the six DTMs are based on the same base data, but were generated using different interpolators, the sixth DTM is photogrammetrically derived. To ensure that only the topographical effect on the GST is calculated, seasonal snow cover was neglected in this study and uniform ground conditions were assumed for the whole test area.

The analyses were done by comparing the topographical parameters elevation, slope and aspect of the different DTMs and by analyzing the modeled average GST using image subtraction and a transect method.

The main results and conclusions can be summarized as follows:

- There are only marginal differences in elevation between the DTMs, which do not significantly influence the resulting GST. The differences for slope and aspect are greater, both in frequency variations and in pixel-to-pixel variation.
- The mean average GST over the entire test area varies within ±0.6 Kelvin [K] and the patterns of the surface parameters elevation, slope and aspect are well reflected in the pattern of the modeled average GST.
- The use of different interpolators for the generation of a DTM can result in significant deviations of the model output. These deviations were mainly found at topographical complex locations such as ridges and foot of slopes.
- The majority of the deviations between the different model outputs related to a reference DTM, however, showed only slight differences of up to 1 K, and only a few pixels deviated more than 1 K.
- South-facing slopes seem to be slightly more sensitive to topographical variations, what can be explained by the higher amount and importance of solar radiation for the energy balance of such slopes. The influence of the slope degree seems to play a less dominant role than aspect [see also *Paper 2*].
- The average GSTs modeled with the photogrammetrically derived DTM differ significantly from those modeled with the other DTMs.
- The use of a photogrammetrically derived DTM is mainly critical over snow-covered areas.
- The uncertainties associated with the DTM must be taken into account as another uncertainty factor for distributed modeling of mountain permafrost scenarios.

CHAPTER 5

Conclusion and a Critical Review

The intention of the present thesis was to assess the potential of regional climate model results for application to local high-mountain permafrost models. The specific conclusions are given in the summaries of the published research articles (Chapter 4). The overall conclusion can be summarised as follows:

- The potential of RCM results is high for applications to high-mountain permafrost models and also to other cryopshere models in complex topography.

- The application of RCM results (driven with a GCM or reanalysis) is likely to bring the mountain cryopshere (impact) modelling a crucial step forward in terms of simulations for the present, the future and the past and for remote mountain regions of the world.

- The performance of RCMs in relation to the relevant processes in complex high-mountain cryopsheric systems, i.e., the energy balance, has not yet been investigated in detail. For example, the local convection in mountain regions is a significant factor that determines the effective received short-wave solar radiation at the surface. However, local convection is a subscale process in current RCMs and thus not simulated adequately.

- The application of RCM results to impact models requires knowledge-based matching approaches, particularly in complex high-mountain areas. One must be aware of:
    - the uncertainties associated with RCM simulations,
    - the performance of an RCM by considering the specific region and the spatial and temporal resolution of the processes focused on,
    - the significance of a (coarse) grid point result of an RCM simulation,
    - the information scenarios effectively provide.

- RCM-based scenarios allow for physically plausible scenario assessment of changes in the ground thermal regime. Changes in the variability of climate variables are likely to occur. However, such changes can only be accounted for by RCM-based approaches, pherhaps in combination with weather generators.

- Although the uncertainties of current RCM scenario simulations are high, a knowledge-based application of RCM-based scenarios brings benefits by providing sound insights into changes in the high-mountain cryosphere relating to the

application of the current knowledge and assumptions about the evolution of the climate.

- Due to the many uncertainties, multi-model approaches are proposed for simulating possible ranges of change, i.e., the results of different RCMs, driven with different GCMs as forced by different emission scenarios, should be applied.

- Incremental scenarios might be used only prior to RCM-based scenario application in order to assess sensitivities, but not in the sense of a scenario in an intrinsic manner.

- Empirical and empirical-statistical impact models, which are calibrated for a specific region and the current climate condition, fall short of dealing adequately with RCM-based scenarios, i.e., with changed qualitative and quantitative climate conditions. Due to such changes, earth systems may change in a way that is not expected based on empirical knowledge. As a consequence, for climate impact studies only physically based impact models are appropriate and empirical models should be used only prior to sensitivity studies. However, it is important to note, that so-called physically based models also treat many processes using parametrisation schemes and thus are often far from being fully physically based.

- In topographical complex environments, possible changes in global radiation must be included in climate change impact analysis. As a consequence, the use of RCM-based scenarios is particularly indicated in complex mountain topography, although associated with special challenges. However, one must be aware that cloud convection, which modifies the received solar radiation at the ground surface, is one of the most critical subgrid processes not yet simulated adequately in RCMs.

- The model and data concept of GIS and thus GIS-based impact models are currently not appropriate for RCM-based impact application in the way as used in this thesis. The technical as well as the conceptual interoperability is not given, e.g., GIS are not (yet) able to read the data format used by climate models and GIS are not optimised to account for the temporal evolution of processes.

- The potential of RCM results is not yet recognized by an important part of the mountain cryosphere community.

- The effort required by an impact modeller to prepare RCM simulation results for application to an impact model is considerable. A constructive cooperation between the scientific disciplines is thus needed in order to get the most out of RCM results.

The potential of RCM simulation results for application to high-mountain cryosphere models is great. The approach, which involves applying RCM results to impact models, opens new and promising possibilities and perspectives and adds a new dimension to climate impact assessment on the high-mountain cryosphere.

In order to cope with the associated challenges and to derive maximum benefits from the interdisciplinary potential, constructive communication and cooperation within the scientific disciplines involved is fundamental. The ‘impact community’ is generally treated as one group and as the end-user of climate model results. However, in fact, the impact

community is a highly heterogeneous group, including policymakers, social scientists and natural scientists. Although these members of the impact community are all dealing with the assessment of climate change impacts, their demands on climate model results are vastly different. Moreover, the requirements within each of these impact subgroups are different, since they are dependent on the specific process being focused upon and on the model concepts being used. As a consequence, the overall discussions about what impact modellers need (e.g., concerning spatial resolution) and what climate modellers can provide often ends in diffuse and thus unsatisfactory conclusions, which inhibit progress.

A current main focus of RCM performance analysis is on the simulations of extreme events, such as heavy precipitation, draughts or heat waves, since these are the greatest and most direct threats to society on a regional scale. In this context, it is assumed that changes in variability are more important than changes in mean relating to extreme events (Katz and Brown, 1992). However, with a focus on permafrost, it is not clear whether extreme events and the related atmospheric processes are the most significant changes for the mountain cryosphere (see also Chapter 6).

CHAPTER 6

Perspectives - Further Needs and Challenges

The present thesis is a first step into an interdisciplinary field with promising perspectives. The expected interdisciplinary synergies gain benefits for the high-mountain cryopshere (including permafrost, glacier and snow) and the climate community, as well as for policymakers.

The necessary next steps with focus on the mountain cryosphere include:

- **Analysis of the performance of RCMs to simulate the relevant processes in high-mountain cryosphere environments, i.e., the processes that determine the energy balance in complex mountain topography. These include:**
  - short-wave radiation
  - dynamics of the duration and thickness of the seasonal snow cover
  - air temperature at the time of the initial snow cover
  - air temperature during the snow-free time of the year

  Here, it must also be taken into account that, in fact, the different cryosphere systems of permafrost, glacier and snow have very varying response times and thus differing demands on the performance of an RCM at a specific spatial scale.

- **Sensitivity analyses of the mountain cryosphere (subsurface thermal regime, glaciers, snow) with respect to changes in mean values and variability of the key climate variables, for different spatial and temporal scales and for different seasons.**
  The response of the cryosphere to changes in the dynamics of atmospheric processes is so far not clear in every detail. In terms of extreme events such as heavy precipitation or heat waves for example, it is assumed, based on the extreme value theory, that an increase in climate variability is more important than changes in mean. Since extreme events are very direct threats to humanity with significant impacts on a regional scale, a main focus in regional climate modelling is the identification and modelling of such events. However, the influence of changes in climate variability on mountain cryosphere systems has not yet been investigated in detail. With regard to permafrost, for example changes in climate variability during winter will not have an influence on the ground thermal regime as long as an insulating snow cover separates the ground from the atmospheric dynamics. Thus permafrost dynamics depend more on the atmospheric conditions during the snow free-season, which include the season (summer) that, however, is more difficult to model for RCM due to increased local and regional influences. Moreover, for surfaces with a coarse blocky surface layer, which is a characteristic of rock

glacier, for example, autumn is the most critical season (Vonder Mühll et al., 1998; Hoelzle et al., 2003). Furthermore, in addition to air temperature and precipitation, the direct short-wave radiation, which is influenced by local convection, is important for cryopshere processes in complex high-mountain areas.

- **Continued research on how to bridge the gap between spatial scales of RCMs and impact models with focus on mountain regions and also on distributed modelling.**
  The pragmatic research question at the moment concerns not only how to increase the horizontal resolution of the RCM or how to adjust the different scales, but also scales on which the best compromise is found for a specific process based on its sensitivities and by taking into account the several predetermined limitations.

- **Application of probabilistic regional scenario.**
  In order to deal adequately with the uncertainties of climate models and emission scenarios, applications to impact models must be directed towards probabilistic approaches (e.g. Wigley and Raper, 2001; Giorgi and Mearns, 2003; Tebaldi et al., 2004, 2005).

- **If GIS are aimed at being used for process impact studies, GIS concepts must be developed that allow for improved temporal process applications.**

- **Cooperative improvement of cryosphere models.**
  Physically based cryosphere models must be developed further. To this end, besides conducting individual research, it is suggested that models be compared, exchanged, discussed and enhanced within the framework of intercomparison projects, as is similarly being done by the climate modelling community.

- **Reanalysis as a substitute for observational data.**
  The nesting technique of RCMs is also used for a dynamical downscaling of reanalysis (e.g. ERA-40). In this manner, such data provide best estimates of regional climate variables for the past and present in remote mountain areas where observations are sparse or lacking. Together with widely available satellite data, such combined data sets open new possibilities for research, for example on the impacts of climate change and natural hazards in remote high-mountain regions that are unexplored so far, also due to a lack of data. This is not meant to displace measurement and monitoring systems; on the contrary, reanalysis can support such observational network systems, while the measurement themselves are incorporated for reanalysis into the data assimilation processes.

- **Temporal interpolation.**
  Regional scenario simulations are typically achieved by time slice experiments (usually 1961-1990 and 2071-2100). However, in particular for processes with a slow response time such as permafrost, continuous time series are required for modelling the qualitative and quantitative evolution of permafrost. Thus temporal interpolation techniques must be applied, as long as continuous RCM simulations are not available.

- **Intensification of the cooperation between the mountain cryosphere and climate modelling communities.**

The climate modelling community is well organized, for example, in projects on an international level (e.g., PRUDENCE, ENSEMBLES or NARCCAP). The related projects do include a (heterogeneous) group of impact modellers, and the mountain cryosphere community should participate on an increased level in the future.

For further steps to be taken in mountain cryosphere modelling, the anticipated developments in climate modelling should also be taken into account:

- **Towards coupled earth system models.**
  The developments and improvements in GCMs and RCMs will continue, probably at an increasing rate. In this connection, an increase in performance, spatial and temporal resolutions as well as integration lengths is to be expected. The development of RCMs and GCMs will include improvements due to enhanced knowledge of the processes and better numerical solutions and parametrisations. Furthermore, improvements are expected through the inclusion and coupling of new subsystems and the feedback mechanisms incorporated. First attempts in this direction relating to mountain glaciers are currently being undertaken by Kotlarski and Jacob (2005). A critical point in integrative subsystem coupling is the spatial and temporal resolution compatibilities of the different subsystems, which can attain new high levels of computational efficiency. Nevertheless, at a certain level of performance and resolution, it will no longer be necessary to use knowledge-based matching approaches when applying climate model results to impact models. Moreover, at a certain level of performance and resolution of coupled GCMs, which are evolving into 'Earth System Models' due to the many subsystems involved, the RCM downscaling step will not be necessary anymore and some of the impact models used at present will be incorporated in the Earth System Model. However, for processes in complex high-mountain topography, separate impact models will still be required for quite a long time. Nevertheless, the knowledge about high-mountain processes such as subsurface systems or glacier dynamics can be included in coupled earth system models; thereby improving high-resolution earth system models, which will then be able to provide improved information that is useful to cryospere scientists.

Beside the scientific challenges, climate change has a highly serious and existential dimension in reality of importance of the current and the next generations:

- **Challenges for the society of the 21st century.**
  Although there are many uncertainties associated with climate model scenarios, and the possibility of abrupt climate change is not taken into account, the general tendency of projected climate evolution is not in question (IPCC, 2001). The projected quantitative and qualitative changes exceed any known event in the past 1000 years (IPCC, 2001). In other words, the dynamics of the changes enter a new and greater dimension. The global and regional impacts will thus require actions and strategies that must also enter a new dimension. Mountain regions are among those most vulnerable, with local to far-reaching impacts that will affect, for example, the water supply of a major sector of the global population (e.g. Barnett et al. 2005). Climate change, by its nature, is a global challenge, with very wide, but as yet unknown regional variations.

In order to understand the ongoing changes in the natural systems, many scientific questions are still to be answered and intensive research is required. However, due to the observed and projected climatic changes that dramatically exceed the statistical reference distribution and will have serious impacts for a major part of the society and the environment, the most important task right now is to act, i.e., in a first step to decrease drastically the GHG emission.

CHAPTER 7

References

Achberger, C., Linderson, M.-L., Chen, D., 2003. Performance of the Rossby Center regional atmospheric model in southern Sweden: Comparison of simulated and observed precipitation. Theor. Appl. Climatol., 76: 219 – 234.

Anisimov, O.A. and Nelson, F.E., 1996. Permafrost distribution in the Northern Hemisphere under scenario of climate change. Global Planet. Change, 14(1): 59 – 72.

Anisimov, O.A. and Nelson, F.E., 1997. Permafrost zonation and climate change in the Northern Hemisphere: results form transient general circulation models. Clim. Change, 35: 241 – 258.

Anisimov, O.A., Shiklomanov, N.I, Nelson, F.E., 1997. Global warming and the active-layer thickness: results from transient general circulation models. Global Planet. Change, 15: 61 – 77.

Antic, S., Laprise, R., Denis, B., de Elía, R., 2004. Testing the downscaling ability of a one-way nested regional climate model in regions of complex topography. Clim. Dyn., 23(5): 473 – 493.

Arnell, N.W., Hudson, D.A., Jones, R.G., 2003. Climate change scenarios from a regional climate model: estimating change in runoff in southern Africa. J. Geophys. Res., 108(D16): 4519 – 4528.

Barnett, T.P., Adam, J.C., Lettenmaier, D.P., 2005. Potential impacts of a warming climate on water availability in snow-dominated regions. Nature, 438: 303 – 309; doi: 10.1038.

Barsch, D., 1971. Rockglacier and ice-cored morains. Geogr. Annal., 53(3 – 4): 203 – 206.

Barsch, D., 1992. Permafrost creep and rockglaciers. Permafrost Periglac. Process., 3: 175 – 188.

Beniston, M., 2003. Climate change in mountain regions: A review of possible impacts. Clim. Change, 59: 5 – 31.

Bergström, S., Carlson, B., Gardelin, M., Lindström, G., Petterson, A., Rummukainen, M., 2001. Climate change impacts on runoff in Sweden – assessments by global climate models, dynamical downscaling and hydrological modeling. Clim. Res., 16: 101 – 112.

Böhm, R., Auer, I., Brunetti, M., Maugeri, M., Nanni, T., Schöner, W., 2001. Regional temperature variability in the European Alps 1760–1998 from homogenised instrumental time series, Int. J. Climatol., 21: 1779 – 1801.

Caplan, P.J., 1993. Lifting a ton of features. A woman's guide to surviving in the academic world. University of Toronto Press.

Cheng, G., 1983. Vertical and horizontal zonation of high-altitude permafrost. In: 4th International Conference on Permafrost. Proceedings, edited by T.L. Péwé, National Academy Press, Washington D.C., Fairbanks, Alaska, pp. 136-141.

Cheng, G. and Dramis, F., 1992. Distribution of mountain permafrost. Permafrost Periglac. Process., 3: 83 – 91.

Christensen, J.H. and Kuhry, P., 2000. High-resolution regional climate model validation and permafrost simulation for the East European Russian Arctic. J. Geophys. Res, 105(D24): 29647 – 29658.

Christensen, J.H. and Christensen, O.B., 2003. Climate Modeling: Severe summertime flooding in Europe. Nature, 421: 805 – 806.

Christensen, J.H., Machenhauer, B., Jones, R.G., Schär, C., Ruti, P.M., Castro, M., Visconti, G., 1997. Validation of present-day climate simulations over Europe: LAM simulations with observed boundary conditions. Clim. Dyn., 13: 489 – 506.

Christensen, O.B., Christensen, J.H., Machenhauer, B., Botzet, M., 1998. Very high-resolution regional climate simulations over Scandinavia – Present climate. J. Clim., 11: 3204 – 3229.

Christensen, J.H., Carter, T.R., Giorgi, F., 2002. PRUDENCE employs new methods to assess European climate change. EOS Trans., 83: 147.

Cook, K.H., Yang, X., Carter, C.M., Belcher, B.N., 2003. A modelling system for studying climate controls on mountain glaciers with application to the Patagonian icefields. Clim. Change, 56: 339–367.

Corte Real, J., Zhang, X., Wang, X., 1995. Large-scale circulation regimes and surface climatic anomalies over the Mediterranean. Int. J. Climatol., 15: 1135 – 1150.

Crane, R.G. and Hewitson, B.C., 1998. Doubled CO2 precipitation changes for the Susquehanna Basin: Downscaling from the GENESIS general circulation model. Int. J. Clim., 18: 65 – 76.

Cubasch, U, Waszkewitz, J., Hegerl, G., Perlwitz, J., 1995. Regional climate changes as simulated in time-slice experiments. Clim. Change, 31: 273 – 300.

Cubasch, U., von Storch, H., Waszkewitz, J., Zorita, E., 1996. Estimates of climate change in Southern Europe derived from dynamical climate model output. Clim. Res., 7(2): 129 – 149.

Davies, M.C.R., Hamza, O., Harris, C., 2001. The effect of rise in mean annual temperature on the stability of rock slopes containing ice-filled discontinuities. Permafrost Periglac. Process., 12(1): 137 – 144.

Delaloye, R. and Morand, S., 1998. Les glaciers rocheux de la région d'Entremont (Alpes Valaisannes): inventaire et analyse spatiale à l'aide d'un SIG. In: Beiträge aus der Gebirgs-Geomorphologie. Mitteilungen der Versuchsanstalt für Wasserbau, Hydrologie und Glaziologie, ETH – Zürich, 158: 75 – 86.

Delaloye, R. and Lambiel, C., 2005. Evidence of winter ascending air circulation through talus slopes and rock glaciers situated in the lower belt of alpine discontinuos permafrost (Swiss Alps). Norw. J. Geogr., 59: 194 – 203.

Denis, B., Laprise, R., Caya, D., Côté, J., 2002. Downscaling ability of one-way nested regional climate models: the Big-Brother experiment. Clim. Dyn., 18: 627 – 646.

Déqué, M. and Piedelievre, J.P., 1995. High resolution climate simulation over Europe. Clim. Dyn., 11: 321 – 339.

Déqué, M. and Gibelin, A.L., 2002. High versus variable resolution in climate modelling. Res. Activ. Atmos. Oc. Model., 32: 704 – 705.

Déqué, M., Marquet, P., Jones, R.G., 1998. Simulation of climate change over Europe using a global variable resolution general circulation model. Clim. Dyn., 14(3): 173 – 189.

Déqué, M., Jones, R.G., Wild, M., Giorgi, F., Christensen, J.H., Hassell, D.C., Vidale, P.L., Röckel, B., Jacob, D., Kjellström, E., de Castro, M., Kucharski, F., van den Hurk, B., 2005. Global high resolution versus limited area model climate change projections over Europe: quantifying confidence level from PRUDENCE results. Cim. Dyn., 25(6): 653 – 670.

Diaz, H.F., Grosjean, M., Graumlich, L., 2003. Climate variability and change in high elevation regions: past, present and future. Clim. Change, 59: 1 – 4.

Dickinson, R.E., Enrico, R.M., Giorgi, F., Bates, G.T., 1989. A regional climate model for the western United States. Clim. Change, 15: 383 – 422.

Dramis, F., Govi, M., Guglielmin, M., Mortara, G., 1995. Mountain permafrost and slope instability in the Italian Alps: the Val Pola landslide. Permafrost Periglac. Process., 6: 73 – 82.

Etzelmüller, B., Berthling, I., Sollid, J.L., 1998. The distribution of permafrost in southern Norway – a GIS approach. In: Proceedings of the 7th International Conference on Permafrost, Yellowknife, Canada. Nordicana, 57: 251 – 257.

Etzelmüller, B., Hoelzle, M., Heggem, E.S.F., Isaksen, K., Mittaz, C., Vonder Mühll, D., Ødegård, R.S., Haeberli, W., Sollid, J.L., 2001a. Mapping and modelling the occurrence and distribution of mountain permafrost. Norw. J. Geogr., 55(4): 186 – 194.

Etzelmüller, B., Ødegård, R.S., Berthling, I., Sollid, J.L., 2001b. Terrain parameters and remote sensing data in the analysis of permafrost distribution and periglacial processes: principles and examples from Southern Norway. Permafrost Periglac. Process., 12: 79 – 92.

Fowler, H.J., Kilsby, C.G., O'Connell, P.E., 2000. Nonlinear responses of soil eroison to climate change: a modelling study of the UK South Downs, Catena, 25: 365 – 387.

Frauenfelder, R., Allgöwer, B., Haeberli, W., Hoelzle, M., 1998. Permafrost investigations with GIS – a case study in the Fletschhorn area, Wallis, Swiss Alps. In: Proceedings of the 7th International Conference on Permafrost, Yellowknife, Canada. Nordicana, 57: 291 – 295.

Frauenfelder, 2004. Regional-scale modelling of the occurrence and dynamics of rockglaciers and the distribution of paleaopermafrost. PhD-thesis. University of Zurich. pp.70.

Frei, C. 2004. Die Klimazukunft der Schweiz – Eine probabilistische Projektion. In: OcCC 2005 "Die Schweiz im Jahr 2050".

Frei, C. and Schär, C. 1998. A precipitation climatology of the Alps from high-resolution rain-gauge observations. Int. J. Climatol. 18: 873 – 900.

Frei, C., Christensen, J.H., Déqué, M., Jacob, D., Jones, R.G., Vidale, P.L., 2003. Daily precipitation statistics in Regional Climate Models: Evalution and intercomparison for the European Alps. J. Geophys. Res. 108(D3), ACL 9 – 1 – 9 – 19.

Frei, C., Schöll, R., Fukutome, S., Schmidli, J., Vidale, P.L., 2006. Future change of precipitation extremes in Europe: An intercomparison of scenarios from regional climate models. J. Geophys. Res., 111: D06105, doi:10.1029/2005JD005965.

French, H.M., 1996. The periglacial environment. Longman, Essex, 341pp.

Giorgi, F., 1990. Simulation of regional climate using a limited area model nested in a general circulation model. J. Clim. 3: 941 – 963.

Giorgi, F. 2002. Dependence of surface climate interannual variability of spatial scale. Geophys. Res. Lett., 29(23): 2101, doi:10.1029/2002GL016175

Giorgi, F. and Mearns, L.O., 1991. Approaches to the simulation of regional climate change: a review. Rev. Geophys., 29: 191 – 216.

Giorgi, F. and Mearns, L.O., 1999. Introduction to special section: regional climate modeling revisted. J. Geophys. Res., 104: 6335 – 6352.

Giorgi, F. and Francisco, R., 2000. Evaluating uncertainties in the prediction of regional climate change, Geophys. Res. Lett., 27(9): 1295 – 1298.

Giorgi, F. and Mearns, L.O., 2003. Probability of regional climate change based on the reliability ensemble averaging (REA) method. Geophys. Res. Lett., 30(12), 1629, doi:10.1029/2003GL017130.

Giorgi, F., Bi, X., Pal, J.S., 2004. Mean, interannual variability and trends in a regional climate experiment over Europe. I. Present-day climate (1961 – 1990). Clim. Dyn., 22: 733 – 756.

Giorgi, F., Hewitson, B., Christensen, J., Hulme, M., Von Stroch, H., Whetton, P., Jones, R., Mearns, L., Fu, C., 2001. Regional Climate Information – Evaluation and Projections. In: Climate Change 2001: The scientific basis. Contribution of working group I to the third assessment report of the intergovernmental panel of climate change (Houghton, J.T., Ding, Y., Griggs, D.J., Noguer, M., van der Linden, P.J., Dai, X., Maskell, K., Johnson, C.A. (eds.). Cambrige University Press, Cambrige, UK and NY, USA, pp. 881.

Goering, D.J. and Kumar P., 1996. Winter-time convection in open-graded embankments. Cold Reg, Scien. Technol., 24 (1): 57 – 74.

Goodrich, L.E., 1982. The influence of snow cover on the ground thermal regime. Can. Geotech. J., 19: 421 – 432.

Goodrich, D.C., Faures, M., Woolhiser, D.A., Lane, L.J., Sorooshian, S., 1995. Measurement and analysis of small-scale convective storm rainfall variability. J. Hydrology, 173: 283 – 308.

Gorbunov, A.P., Marchenko, S.S., Seversky, E., 2004. The thermal environment of blocky materials in the mountain of central Asia. Permafrost Periglac. Process., 15: 95 – 98.

Grell, G.A., Schade, L., Knoche, R., Pfeiffer, A., Egger, J., 2000. Nonhydrostatic climate simulations of precipitation over complex terrain. J. Geophys. Res., 105(D24), 29595 – 29608.

Gruber, S., 2005. Mountain permafrost: Transient spatial modeling, model verification and the use of remote sensing. PhD thesis. University of Zurich.

Gruber, S., Hoelzle, M., Haeberli, W., 2004a. Permafrost thaw and destabilization of Alpine rock walls in the hot summer of 2003. Geophys. Res. Lett., 31: L13504, doi:10.1029/2004GL020051.

Gruber, S., Hoelzle, M., Haeberli, W., 2004b. Rock-wall temperatures in the Alps: modelling their topographic distribution and regional differences. Permafrost Periglac. Process., 15(3): 299 – 307.

Guereña, A., Ruiz-Ramon, M., Diaz-Ambrona, C., Conde, J., Minguez, M., 2001. Assessment of climate change and agriculture in Spain using climate models. Agron. J., 93: 237 – 349.

Gyalistras, D., Schär, C., Davies, H.C., Wanner, H., 1998: Future Alpine climate. In: Cebon, P., Dahinden, U., Davies, H.C., Imboden, D., Jaeger, C.C. (eds.). Views from the Alps. Regional Perspectives on Climate Change. Cambridge, Massachusetts: MIT Press, 171 – 223.

Haeberli, W., 1973. Die Basistemperatur der winterlichen Schneedecke als möglicher Indikator für die Verbreitung von Permafrost in den Alpen. Zeitschr. Gletscherk. Glazialgeol. ETHZ, 17, pp. 221.

Haeberli, W., 1975. Untersuchungen zur Verbreitung von Permafrost zwischen Flüelapass und Piz Grialetsch (Graubünden). Mitteilungen der Versuchsanstalt für Wasserbau, Hydrologie und Glaziologie, 17, ETH Zürich.

Haeberli, W., 1990. Glacier and permafrost signals of 20th-century warming. Annal. Glaciol., 14: 99 – 101.

Haeberli, W. 1992. Construction, environmental problems and natural hazards in periglacial mountain belts. Permafrost Periglac. Process., 3(2): 111 – 124.

Haeberli, W., 2000. Modern research perspectives relating to permafrost creep and rock glaciers. Permafrost Periglac. Process., 11: 290 – 293.

Haeberli, W. and Beniston, M., 1998. Climate change and its impact on glaciers and permafrost in the Alps. Ambio, 27(4): 258 – 265.

Haeberli, W., Wegmann, M., Vonder Mühll, D. 1997. Slope stability problems related to glacier shrinkage and permafrost degradation in the Alps. Eclogae Geol. Helv., 90(3): 407 – 414.

Hanson, S. and Hoelzle, M., 2004. The thermal regime of the active layer at the Murtèl rock glacier based on data from 2002. Permafrost Periglac. Process., 15: 273 – 282.

Hanson, S. and Hoelzle, M., 2005. Installation of a shallow borehole network and monitoring of the ground thermal regime of a high alpine discontinuous permafrost environment, Eastern Swiss Alps. Norw. J. Geogr., 59(2): 84 – 93.

Harris, S.A. and Pedersen D.E., 1998. Thermal regimes beneath coarse blocky materials. Permafrost Periglac. Process., 9: 107 – 120.

Harris, C., Rea, B., Davies, M., 2001. Scaled physical modeling of mass movement processes on thawing slopes. Permafrost Periglac. Process., 12(1): 125 – 135.

Harris, C., Vonder Muehll, D., Isaksen, K., Haeberli, W., Sollid, J.L., King, L., Holmlund, P., Dramis, F., Guglielmin, M., Palacios, D., 2003. Warming permafrost in European mountains. Global Planet. Change, 39: 215 – 225.

Hauck, C. 2001. Geophysical methods for detecting permafrost in high mountains. PhD. thesis, VAW – ETH Zurich. Mitteilungen Nr. 171, pp. 204.

Hauck, C., Guglielmin, M., Isaksen, K. Vonder Mühll, D., 2001. Applicability of frequency- and time-domain electromagnetic methods for mountain permafrost studies. Permafrost Periglac.

Process., 12(1). 39 – 52.

Hewitson, B.C. and Crane, R.G., 1996. Climate downscaling: techniques and application. Clim. Res., 7: 85 – 95.

Hewitson, B.C. and Crane, R.G. 2002. Self-organizing maps: application to synoptic climatology. Clim. Res., 22: 13 – 26.

Hoelzle, M., 1996. Mapping and modelling of mountain permafrost distribution in the Alps. Norw. J. Geogr, 50: 11 – 15.

Hoelzle, M. and Haeberli, W., 1995. Simulating the effects of mean annual air temperature changes on permafrost distribution and glacier size. An example from the Upper Engadin, Swiss Alps. Ann. Glaciol., 21: 400 – 405.

Hoelzle, M., Wegmann, M., Krummenacher, B., 1999. Miniature temperature data loggers for mapping and monitoring of permafrost in high mountain areas: First experience from the Swiss Alps. Permafrost Periglac. Process., 10(2): 113 – 124.

Hoelzle, M., Mittaz, C., Etzelmüler, B., Haeberli, W., 2001. Surface energy fluxes and distribution models of permafrost in European mountain areas: an overview of current developments. Permafrost Periglac. Process., 12: 53 – 68.

Hoelzle, M., Haeberli, W., Stocker-Mittaz, C., 2003. Miniature ground temperature data logger measurements 2000 – 2002 in the Murtèl – Corvatsch area. In: Proceedings of the 8th International Conference on Permafrost, Zurich, Switzerland, 419 – 424.

Huggel, C., 2004. Assessment of glacial hazards based on remote sensing and GIS modelling. PhD thesis, University of Zurich.

Humlum, O., 1998. Active layer thermal regime 1991–1996 at Qeqertarsuaq, Disko Island, Central West Greenland. Arctic Alp. Res., 30(3): 295 – 305.

Huth, R., 2000. A circulation classification scheme applicable in GCM studies. Theor. Appl. Climatol., 67: 1 – 18.

Hutingford, C., Jones, R.G., Prudhomme, C., Lamb, R., Gash, J.H.C., Jones, D.A., 2003. Regional climate-model predictions of extreme rainfall for a changing climate. Quart. J. Roy. Meteo. Soc., 129(590): 1607 – 1621.

IPCC, 1994. Climate Change 1994: Radiative Forcing of Climate Change and an Evaluation of the IPCC IS92 Emission Scenarios [Houghton, J.T., L.G. Meira Filho, J.P. Bruce, Hoesung Lee, B.T. Callander, E.F. Haites, N. Harris, and K. Maskell (eds.)]. Cambridge University Press, Cambridge and New York, pp. 339.

IPCC, 2001. Climate Change 2001: The scientific basis. Contribution of working group 1 to the third assessment report of the intergovernmental panel on climate change. [Houghton, J.T., Ding, Y., Griggs, D.J., Noguer, M., van der Linden, P.J., Dai, X., Maskell, K., Johnson, C.A. (eds.)]. Cambrige University Press, Cambrige, UK and NY, USA, pp. 881.

Isaksen, K., Vonder Mühll, D., Gubler, H., Kohl, T., Sollid, J.L., 2000. Ground surface temperature reconstruction based on data from a deep borehole in permafrost at Janssonhaugen, Svalbard. Annl. Glaciol., 31: 287 – 294.

Isaksen, K., Holmlund, P., Sollid, J.L., Harris, C., 2001. Three deep alpine-permafrost boreholes in Svalbard and Scandinavia. Permafrost Periglac. Process., 12(1): 13 – 25.

Jensen, J., 1999. An analysis of permafrost distribution on Plateau Mountain, Alberta using the Geographic Information System ARC/INFO. Calgary, University of Calgary.

Ji, Y. and Vernekar, A.D., 1997. Simulation of the Asian Summer Monsoons of 1987 and 1988 with a regional model nested in a global GCM. J. Clim., 10: 1965 – 1979.

Jones, R.G., Murrphy, J.M., Noguer, M., 1995. Simulation of climate change over Europe using a nested regional-climate model. Part I: Assessment of control climate, including sensitivity to location of lateral boundaries. Quart. J. Roy. Meteor. Soc., 123: 265 – 292.

Kääb, A., Reynolds, J.M., Haeberli, W., 2005. Glacier and permafrost hazards in high mountains. In: Huber, U.M., Bugmann, H.K.M., Reasoner, M.A. (eds.), Global Change and Mountain Regions (A State of Knowledge Overview). Springer, Dordrecht. pp. 225 – 234.

Kalnay, E., Kanamitsu, M., Kistler, R., Collins, W., Deaven, D., Gandin, L., Iredell, M., Saha, S., White, G., Woollen, J., Zhu, Y., Leetmaa, A., Reynolds, B., 1996. The NCEP/NCAR 40-year reanalysis project. Bull. Amer. Meteor. Soc., 77: 437 – 471.

Katz, R.W. and Parlange, M.B., 1995. Overdispersion phenomenon in stochastic modeling of precipitation. J. Clim., 11(4): 591 – 601.

Katz, R.W. and Brown, B.G., 1992. Extreme Events in a changing climate – variability is more important than averages. Clim. Change, 21: 289 – 302.

Keller, F., 1992. Automated mapping of mountain permafrost using the program PERMAKART within the geographical information system ARC/INFO. Permafrost Periglac. Process., 3: 133 – 38.

Keller, F. and Gubler, H., 1993. Interaction between snow cover and high mountain permafrost, Murtèl–Corvatsch, Swiss Alps. In: Proceedings of 6th International Conference on Permafrost, July 5 – 9, 1993, Beijing, China, Vol. 1: 332–337.

Keller, F., Frauenfelder, R., Gardaz, J.M., Hoelzle, M., Kneisel, C., Lugon, R., Philips, M., Reynard, E., Wenker, L., 1998. Permafrost map of Switzerland. In: Proceedings of 7th International Conference on Permafrost, Yellowknife, Canada. Nordicana, 57: 557 – 562.

Kilsby, C.G., Cowpertwait, P.S.P., O'Connell, P.E., Jones, P.D. 1998. Predicting rainfall statistics in England and Wales using atmospheric circulation variables. Int. J. Climatol., 18: 523 – 539.

Kim, J.W., Chang, J.T., Baker, N.L., Wilks, D.S., Gates, W.L., 1984. The statistical problem of climate inversion: Determination of the relationship between local and large-scale climate. Month. Weath. Rev., 112: 2069 – 2077.

Kim, J., Miller, N.L., Farrara, J.D., Hong, S.-Y., 2000. A seasonal precipitation and stream flow hindcast and prediction study in the Western United States during 1997/8 winter season using a dynamic downscaling system. J. Hydrometeor., 1(4): 311 – 329.

King, L. and Kalisch, A., 1998. Permafrost distribution and implications for construction in the Zermatt area, Swiss Alps. In: Proceedings of 7th International Conference on Permafrost, Yellowknife, Canada. Nordicana, 57: 569 – 574.

Kleinn, J. 2002. Climate change and runoff statistics in the Rhine basin: A process study with a coupled climate-runoff model. PhD thesis, Swiss Federal Institute of Technology (ETHZ), pp.114.

Kleinn, J., Frei, C., Gurtz, J., Lüthi, D., Vidale, P.L., Schär, C., 2005. Hydrologic simulations in the Rhine basin driven by a regional climate model, J. Geophys. Res., 110: D04102, doi:10.1029/2004JD005143.

Kotlarski, S. and Jacob, D., 2005. Development of a subgrid scale parametrization of mountain glaciers for use in regional climate modelling. WGNE Blue Book, WMO, 4 – 133.

Kotlarski, S., Block, A., Böhm, U., Jacob, D., Keuler, K., Knoche, R., Rechid, D., Walter, A., 2005. Regional climate model simulations as input for hydrological applications: evaluation of uncertainties. Adv. Geoscien., 5: 119-125.

Krummenacher, B., Hunziker, G., Keller, F., 2005. Hinweiskarte der potentiellen Permafrost-verbreitung in der Schweiz. Bundesamt für Umwelt, 9 pp.

Lal, M., Bhaskaran, B. Singh, S.K., 1998. Indian summer monsoon variability as simulated by a regional model nested in a global model. Chinese J. Atm. Sc., 22: 93 – 102.

Laprise, R., Varma, M.R., Denis, B., Caya, D., Zawadzki, I. 2000. Predictability of a nested limited-area model. Mon. Weath. Rev., 128: 4149 – 4154.

Laternser, M. and Schneebeli, M., 2003. Long-term snow climate trends of the Swiss Alps (1931 – 99). Int. J. Climatol., 23: 245 – 261.

Lawrence, D.M. and Slater, A.G., 2005. A projection of severe near-surface permafrost degradation during the 21st century. Geophys. Res. Lett., 32: L24401, doi:10.1029/2005GL025080.

Leung, L.R., and Qian, Y., 2003. The sensitivity of precipitation and snowpack simulations to model resolution via nesting in regions of complex terrain. J. Hydrometeorol., 4: 1025 – 1043.

Leung, L.R., Mearns, L.O., Girogi, F., Wilby, R.L. 2003. Regional climate research – needs and opportunities. Bull. Amer. Meteor. Soc., 84: 89 – 95.

Leung, L.R., Qian, Y., Bian, X., Hunt, A., 2003a. Hydroclimate of the western United States based on observations and regional climate simulation of 1981 – 2000. Part I: Seasonal statistics. J. Clim., 16: 1892 – 1911.

Leung, L.R., Qian, Y., Bian, X., Hunt, A., 2003b. Hydroclimate of the western United States based on observations and regional climate simulation of 1981 – 2000. Part II: Mesoscale ENSO anomalies. J. Clim., 16:1912 – 1928.

Lewkowicz, A.G. and Ednie, M., 2004. Probability mapping of mountain permafrost using the BTS method, wolf Creek, Yukon Territory, Canada. Permafrost Periglac. Process., 15(1): 67 – 80.

Li, X., Cheng, G., Chen, X., 1998. Response of permafrost to global change on the Qinghai-Xizang plateau – a GIS aided model. In: Proceedings of 7th International Conference on Permafrost, Yellowknife, Canada. Nordicana, 57: 657 – 661.

Ling, F. and Zhang, T., 2004. A numerical model for surface energy balance and thermal regime of the active layer and permafrost containing unfrozen water. Cold Reg. Sci. Technol., 38(1): 1 – 15.

Lorenz, P. and Jacob, D., 2005. Influence of regional scale information on the global circulation: A two-way nesting climate simulation. Geophys. Res. Lett., 32(18), L18706, doi:10.1029/2005GL023351.

Lüthi, D., Cress, A., Frei, C., Schär, C., 1996. Interannual variability and regional simulations. Theor. Appl. Climatol., 53: 185 – 209.

Lüthi, M., 2000. Rheology of cold firn and dynamics of a polythermal ice stream: Studies on Colle Gnifetti and Jakobshavns Isbrae. In Vischer, D., (ed.), Mitteilungen der Versuchsanstalt für Wasserbau, Hydrology and Glaziologie, 165. ETH Zürich. 212p.

Mackay, J.R., 1998. Pingo growth and collapse, Tuktoyaktuk Peninsula Area, Western Arctic Coast, Canada: a long-term field study, Géogr. Phys. Quatern., 52: 271 – 323.

Marbaix, P., Gallee, H., Brasseur, O., van Ypersele, J.P., 2003. Lateral boundary conditions in regional climate models: a detailed study of the relaxation procedure. Monthl. Weath. Rev., 131(3): 461 – 479.

McGregor, J.L., 1997: Regional climate modelling. Meteorol. Atmos. Phys., 63: 105 – 117.

McGuffie, K. and Henderson – Sellers, A., 2005. A climate modelling primer. John Wiley & Sons, Chichester, England.

Mearns, L.O., 2000. The importance of spatial scale of climate scenarios for regional climate change impacts analysis: Implications for regional climate modelling activities. In: Preprints of the tenth PSU/NCAR Mesoscale User's Workshop, 21–22 June 2000, Boulder CO. Mesoscale and Microscale Division, National Center for Atmospheric Research: Boulder, pp. 127 – 130.

Mearns, L.O., Rosenzweig, C., Goldberg, R., 1997. Mean and variance change in climate scenarios: Methods, agricultural applications, and measures of uncertainty. Clim. Change, 35: 367 – 396.

Mearns, L.O., Easterling, W., Hays, C., 1998. The effect of spatial scale of climate change scenarios on the determination of impacts: An example of agricultural impacts on the great plains. In: Proceedings of the International Workshop on Regional Modelling of the General Monsoon System in Asia, Beijing, October 20-23, START Regional Center for Temperate East Asia. TEACOM Report No. 4: 70 – 73.

Mearns, L.O., Mavromatis, T., Tsvetsinskaya, E., Hays, Easterling, W., 1999. Comparative responses of EPIC and CERES crop models to high and low resolution climate change scenarios. J. Geophys. Res., 104(D6): 6623 – 6646.

Mearns, L.O., Easterling, W., Hays, C., Marx, D., 2001a. Comparison of agricultural impacts of climate change calculated from high and low resolution climate model scenarios: Part I. The uncertainty due to spatial scale. Clim. Change, 51: 131 – 172.

Mearns, L.O., Hulme, M., Carter, T.R., Leemans, R., Lal, M., Whetton, P., 2001b. Climate scenario development. In: Climate Change 2001: The scientific basis. Contribution of working group I to the third assessment report of the intergovernmental panel of climate change (Houghton, J.T., Ding, Y., Griggs, D.J., Noguer, M., van der Linden, P.J., Dai, X., Maskell, K., Johnson, C.A. (eds.). Cambrige University Press, Cambrige, UK and NY, USA, pp. 881.

Mearns, L.O., Giorgi, F., Whetton, P. Pabon, D., Hulme, M., Lal, M., 2003. Guidelines for use of climate scenario developed from regional climate model experiments. Guidance material of DDC of IPCC TGCIA.

Meybeck, M., Green, P., Vörösmarty, C., 2001. A new typology for mountains and other relief classes: An application to global continental water resources and population distribution, Mountain Res. Dev., 21: 34 – 45.

Mittaz, C. 2002. Permafrost distribution modeling based on energy balance data. PhD-thesis, University of Zurich. pp. 122.

Mittaz, C., Imhof, M., Hoelzle, M., Haeberli, W., 2002. Snowmelt evolution mapping using an energy balance approach over an alpine terrain. Arctic Alp. Res., 34(3): 274 – 281.

Mo, K.M., Kanamitsu, H.-M., Juang, H., Hong, S.Y., 2000. Ensemble regional and global climate prediction for the 1997/1998 winter. J. Geophys. Res., 105(D24): 29 609 – 29 624.

Morita, T. and Robinson, J., 2001. Greenhouse gas emission mitigation scenarios and implications. In Climate Change 2001: Mitigation. Contribution of Working Group III to the IPCC Third Assessment Report.

Murphy, J.M., 1999. An evaluation of statistical and dynamical techniques for downscaling local climate. J. Climate, 12: 2256 – 2284.

Murphy, J.M., 2000. Predictions of climate change over Europe using statistical and dynamical downscaling techniques. Int. J. Climatology, 20: 489 – 501.

Murphy, J.M., Sexton, D., Barnett, D., Jones, D., Webb, M., Collins, M., Stainfroth, D., 2004. Quantification in a large ensembles of climate change simulation. Nature, 430, 768 – 772.

Nakicenovic, N. and Swart, R., (Eds.) 2000. Emissions Scenarios. 2000, Special Report of the Intergovernmental Panel on Climate Change Cambridge University Press, UK. pp. 570.

Nan, Z.T., Li, S.X., Cheng, G.D., 2005. Prediction of permafrost distribution on the Qinghai-Tibet Plateau in the next 50 and 100 years. Sci. China Series, 48(6): 797 – 804.

Nelson, F.E., 2003. (Un)frozen in time. Science, 299: 1673 – 1675.

Nelson, F.E., Anisimov, O.A. Shiklomanov, N.I., 2001. Subsidence risk from thawing permafrost. Nature, 410(6831): 889 – 890.

Nelson, F.E., Anisimov, O.A. Shiklomanov, N.I. 2002. Climate change and hazard zonation in the circum-Arctic permafrost regions. Nat. Haz.,, 26(3): 203 – 225.

New, M., Hulme, M., Jones, P.D., 1999. Representing twentieth century space-time climate variability. Part 1: development of a 1961 – 1990 mean monthly terrestrial climatology. J. Clim., 12: 829 – 856.

Nobre, P., Moura, A.D., Sun, L. 2001. Dynamical downscaling of seasonal climate prediction over Nordeste Brazil with ECHAM3 and NCEP's regional spectral models at IRI. Bull., Amer. Meteor. Soc., 82, 2787 – 2769.

Noetzli, J., Hoelzle, M., Haeberli, W., 2003. Mountain permafrost and recent Alpine rockfall events: A GIS-based approach to determine critical factors. Proceedings of the 8th International Conference on Permafrost 2003, Zurich, Switzerland (2): 827 – 832.

Noguer, M., Jones, R.G., Murphy, J.M., 1998. Sources of systematic errors in the climatology of a regional climate model over Europe. Clim. Dyn., 14: 691 – 712.

Oke, T.R., 1987. Boundary layer climates. Routledge, London/New York, 2nd edition. 435p.

Osborn, T.J., 1997. Areal and point precipitation intensity changes: Implications for the application of climate models. Geophys. Res. Lett., 24, 2829 – 2832.

Osborn, T.J. and Hulme, M., 1998. Development of a relationship between stations and grid-box rainday frequency for climate model evaluation. J. Climate, 10: 1885 – 1908.

Osterkamp, T.E., 1983. Response of Alaskan permafrost to climate. In: Final Int. Conf. Permafrost, Fairbanks, Alaska. NAS, Washington, DC: 145 – 152.

Palutikof, J.P., Winkler, J.A., Goodess, C.M., Andresen, J.A., 1997. The simulation of daily time series from GCM output. Part 1: Comparison of model data with observations. J. Clim., 10: 2514 – 2532.

Paul, F., Kääb, A., Maisch, M., Kellenberger, T.W., Haeberli, W., 2004. Rapid disintegration of Alpine glaciers observed with satellite data. Geophys. Res. Lett., 31: L21402, doi:10.1029/2004GL020816.

Räisänen, J., Hansson, U., Ullerstig, A., Döscher, R., Graham, L.P., Jones, C.H., Meier, E.M., Samuelsson, P., Willén, U., 2004. European climate in the late twenty-first century: regional simulations with two driving global models and two forcing scenarios. Clim., Dyn., 22(1): 13 – 31.

Reichert, B.K., Bengtson, L., Oerlemans, J., 2001. Midlatitude forcing mechanisms for glacier mass balance investigated using general circulation models. J. Clim., 14(17), 3767 – 3784.

Rosenzweig, C., Iglesias, A., 1998. The use of cropmodels for international climate change impact assessment. In: Tsuji, G.Y., Hoogenboom, G., Thornton, P.K. (Eds.), Understanding Options for Agricultural Production. Kluwer Academic Publishers, Dordrecht, pp. 267–292.

Sawada, Y., Ishikawa, M., Ono, Y., 2003. Thermal regime of sporadic permafrost in a block slope on Mt. Nishi-Nupukaushinupuri, Hokkaido Island, Northern Japan. Geomorphology, 52: 121 – 130.

Schär, C. and Jendritzky, G., 2004. Hot news from summer 2003. Nature, 432: 559 – 560.

Schär C., Davies, T.D., Frei, C., Wanner, H., Widmann, M., Wild, M., Davies, H.C., 1998. Current Alpine climate. In: A view from the Alps: Regional perspectives on climate change (eds: Cebon, P., Dahinden, U., Davies H.C., Jaeger, C.). MITPress, Boston.

Schär, C., Vidale, P.L., Lüthi, D., Frei, C., Häberli, C., Liniger, M., Appenzeller, C., 2004. The role of increasing temperature variability for European summer heat waves. Nature, 427: 332 – 336.

Schubert, S. and Henderson-Sellers, A., 1997. A statistical model to downscale local daily temperature extremes from synoptic-scale atmospheric circulation patterns in Australian region. Clim. Dyn., 13: 223 – 234.

Semenov, A.M. and Barrow, M.E., 1997. Use of a stochastic weather generator in the development of climate change scenarios. Clim. Change, 35(4): 397 – 414.

Seppälä, M., 1986. The origin of palsas, Geogr. Annal., Series A, 68: 141 – 147.
Scherrer, S., Appenzeller, C., Laternser, M., 2005. Trends in Swiss alpine snow days: The role of local- and large-scale climate variability. Geophys. Res. Lett., (31): L13215, doi:10.1029/2004GL020255.

Schmidli, J., Frei, C., Vidale, P.L., 2005. Downscaling from GCM precipitation: A benchmark for dynamical and statistical downscaling methods. Int. J. Climatol., 26(5): 679 – 689.

Schneeberger, C., Blatter, H., Abe-Ouchi, A., Wild, M., 2003. Modelling changes in the mass balance of glaciers of the northern hemisphere for a transient 2 x CO2 scenario. J. Hydrol., 282: 145 – 163.

Schwarb, M., 2000. The Alpine precipitation climate – Evaluation of a high-resolution analysis scheme using comprehensive rain-gauge data. Diss ETH No. 13911.

Seth, A. and Giorgi, F., 1998. The effects of domain choice on summer precipitation simulation and sensitivity in a regional climate model. J. Climate, 11: 2698–2712.

Simmons, A.J., Jones, P.D., da Costa Bechtold, V., Beljaars, A.C.M., Kallberg, P.W., Saarinen, S., Uppala, S.M., Viterbo, P., Wedi, N. 2004. Comparison of trends and variability in CRU, ERA-40 and NCEP7NCAR analyses of monthly-mean surface air temperature. ERA-40 Project Report Series. ECMWF, Reading, England.

Skelly, W.C. and Henderson-Sellers, A., 1996. Grid box or grid point: what types of data do GCMs deliver to climate impacts researchers? Int. J. Climatology, 16: 1079 – 1086.

Smith, J.B. and Hulme, M., 1998. Climate change scenarios. In: UNEP Handbook on Methods for Climate Change Impact Assessment and Adaptation Studies [Burton, I., J.F. Feenstra, J.B. Smith, and R.S.J. Tol (eds.)]. Version 2.0, United Nations Environment Programme and Institute for Environmental Studies, Vrije Universiteit, Amsterdam, pp. 3-1 to 3-40. Available online at http://www.vu.nl/english/o_o/instituten/IVM/research/climatechange/Handbook.htm

Smith, M.W. and Riseborough, D.W., 1996. Ground temperature monitoring and detection of climate change. Permafrost Periglac. Process., 16: 313 – 335.

Smith, M.W. and Riseborough, D.W., 2002. Climate and the limits of permafrost: A zonal analysis. Permafrost Periglac. Process., 13 (1): 1 – 15.

Stendel, M., Christensen, J.H., 2002. Impact of global warming on permafrost conditions in a coupled GCM. Geophys. Res. Lett. 29(13), GL014345.

Stendel, M., Romanovsky, V.E., Christensen, J.H., Sazonova, T., 2006. Using dynamical downscaling to close the gap between global change scenarios and local permafrost dynamics. Global Planet. Change, doi:10.1016/j.gloplacha.2006.07.014.

Stieglitz, M., Dery, S.J., Romanovsky, V.E., Osterkamp, T.E., 2003. The role of snow cover in the warming of arctic permafrost. Geophys. Res. Lett., 30(13), 1721, doi:10.1029/2003GL017337.

Stocker-Mittaz, C., Hoelzle, M., Haeberli, W., 2002. Modelling alpine permafrost distribution based on energy-balance data: a first step. Permafrost Periglac. Process., 13: 271 – 282.

Takle, E.S., Gutowski Jr., W.J., Arritt, R.W., Pan, Z., Anderson, C.J., Silva, R., Caya, D., Chen, S.-C., Christensen, J.H., Hong, S.-Y., Juang, H.-M.H. Katzfey, J.J. Lapenta, W.M., Laprise, R., Lopez, P., McGregor, J., Roads, J.O., 1999. Project to Intercompare Regional Climate Simulations (PIRCS): Description and initial results. J. Geophys. Res., 104: 19443 – 19462.

Tebaldi, C., Mearns, L.O., Nychka, D., Smith, R.L., 2004. Regional probabilities of precipitation change: A Bayesian analysis of multimodel simulations. Geophys. Res. Lett., 31: L24213.

Tebaldi, C., Smith, R., Nychka, D., Mearns, L.O., 2005. Quantifying uncertainty in projections of regional climate change: a Bayesian approach to the analysis of multimodel ensembles. J. Clim., 18(10): 1524 – 1540.

Trigo R.M. and Palutikof J.P., 1999. Simulation of daily temperatures for climate change scenarios over Portugal: a neural network model approach. Clim. Res., 13, 45 – 59.

Uppala, S.M., Kallberg, P.W., Simmons, A.J., Andrae, U., da Costa Bechtold, V., Fiorino, M., Gibson, J.K., Haseler, J. Hernandez, A., Kelly, G.A., Li, X., 2005. The ERA-40 Reanalysis. Quart. J. Roy. Meteor. Soc., 131(612): 2961 – 3012.

Van der Linden, S. and Christensen, J.H., 2003. Improved hydrololgical modeling for remote regions using a combination of observed and simulated precipitation data. J. Geophys. Res., 108(D2), 4072, doi:10.1029/2001JD001420.

Van de Wal, R.S.W. and Wild, M., 2001. Modelling the response of glaciers to climate change by applying volume-area scaling in combination with high resolution GCM. Clim. Dyn. 18: 356 – 366.

Vidale, P.L., Lüthi, D., Frei, C., Seneviratne, S.I., Schär, C., 2003. Predictability and uncertainty in a regional climate model. J. Geophys. Res. Atmos., 108 (D18), 4586, doi: 10.1029/2002JD002810.

Vidale, P.L., Lüthi, D., Wegmann, R., Schär, C., 2006. European summer climate variability in a heterogeneous multi-model ensemble. Clim. Change, (in press).

Vonder Mühll, D. and Haeberli, W., 1990. Thermal characteristics of the permafrost within an active rock glacier (Murtèl/Corvatsch, Grisons, Swiss Alps). J. Glaciol., 36(123): 151 – 158.

Vonder Mühll, D., Stucki, T., Haeberli, W., 1998. Borehole temperatures in Alpine permafrost: a ten years series. In: 7th International Conference on Permafrost (Yellowknife. 23 – 27 June 1998). Collection Nordicana 57. 1089 – 1095. Centre d'études nordiques, Université Lavai, Québec.

Vonder Mühll, D., Hauck, C., Gubler, H., McDonald, R., Russill, N., 2001. New geophysical methods of investigating the nature and distribution of mountain permafrost. Permafrost Periglac. Process., 12 (1): 27 – 38.

Von Storch, H., 1995. Inconsistencies at the interface of climate impact studies and global climate research. Meteorol. Zeitschrift, 4: 72 – 80.

Von Stroch, H. 1999. On the use of “inflation” in statistical downscaling. J. Clim., 12: 3505 – 3506.

Von Storch, H., Zorita, E., Cubasch, U., 1993. Downscaling of global climate-change estimates to regional scale – an application to Iberian rainfall in wintertime. J. Clim., 6 (6): 1161 – 1171.

Wakonigg, H. 1996. Unterkühlte Schutthalden. Arbeiten aus dem Geographischen Institut der Universität Graz (AGIUG), 33: 209 – 223.

Walsh, K. and McGregory, J.L., 1995. January and July climate simulations over Australian region using limited-area model. J. Clim., 8: 2387 – 3673.

WangY., Leung, L.R., McGregor, J.L., Lee, D.-K.., Wang, W.-C., Ding, Y., Kimura, F. 2004. Regional climate modeling: Progress, challenges and prospects. J. Meteorol. Soc. Jap., 82(6): 1599 – 1628.

Warner, T.T., Peterson, R.A., Treadon, R.E., 1997. A tutorial on lateral conditions as a basic and potentially serious limitation to regional numerical weather prediction. Bull. Am. Met.. Soc., 78: 2599 – 2617.

Washburn, A.L., 1979. Geocryology: A survey of periglacial processes and environments. Ed. Arnold Ltd, London. 406p.

Wegmann, M., Gudmundsson, H., Haeberli, W., 1998. Permafrost changes in rock walls and the retreat of alpine glaciers: a thermal modelling approach, Permafrost Periglac. Process., 9: 23 – 33.

Weichert, A. and Bürger, G., 1998. Linear versus nonlinear techniques in downscaling. Clim. Res., 10: 83 – 93.

WGMS, 2005. Fluctuations of glaciers 1995-2000. Haeberli, W., Zemp, M., Frauenfelder, R., Hoelzle, M., Kääb, A. (eds.), World Glacier Monitoring Service, VIII, Paris.

Whiteman, D., 2000. Mountain Meteorology, Oxford University Press, pp. 355.

Wigley, T.M.L. and Raper, S.C.B., 2001. Interpretation of high projections for global-mean warming. Science, 293: 451 – 454.

Wigley, T.M.L., Jones, P.D., Briffa, K.R., Smith, G., 1990. Obtaining sub-grid scale information from coarse resolution general circulation model output. J. Geophys. Res., 95: 1943 – 1953.

Wilby, R.L. and Wigley, T.M.L., 1997. Downscaling general circulation model output: a review of methods and limitations. Progress Phys. Geogr., 21: 530 – 548.

Wilby, R.L. and Wigley, T.M.L., 2000. Precipitation predictors for downscaling: observed and general circulation model relationships. Int. J. Climatol., 20: 641 – 661.

Wilhelmi, O.V. and Brunskill, J.C., 2003. Geographic information system in weather, climate and impacts. Bull. Amer. Meteorol. Soc., 84(10): 1409 – 1414.

Wilhelmi, O.V. and Betancourt, T.L., 2005. Evolution of NCAR GIS initiative: Demonstration of GIS interoperability. Bull. Amer. Meteorol. Soc., 86(2): 176 – 178.

Wilks, D.S. and Wilby, R.L. 1999. The weather generator game: A review of stochastic weather models: Progress Phys. Geogr., 23: 329 – 357.

Williams, P.J. and Smith, M.W., 1989. The Frozen Earth: Fundamentals of Geocryology. Cambridge University Press. 306p.

Winkler, J.A., Palutikof, J.P., Andresen, J.A., Goodess, C.M., 1997. The simulation of daily time series from GCM output. Part 2: A sensitivity analysis of empirical transfer functions for downscaling GCM simulations. J. Clim., 10: 2497 – 2513.

Wood, A.W., Leung, L.R., Sridhar, V., Lettenmair, D.P., 2004. Hydrological implications of dynamical and statistical downscaling approach to downscale climate model outputs. Clim. Change, 62: 189 – 216.

Yang, Z. and Arritt, R.W., 2002. Tests of a perturbed physics ensemble approach for regional climate modeling. J. Clim., 15: 2881 – 2896.

Zemp, M., Haeberli, W., Hoelzle, M., Paul, F., 2006. Alpine glaciers to disappear within decades? Geophys. Res. Lett., 33: L13504, doi:10.1029/2006GL026319.

Zhang, T., 2005. Influence of the seasonal snow cover on the ground thermal regime: an overview. Rev. Geophys., 43, RG4002, doi:10.1029/2004RG000157.

Zhang, T., Osterkamp, T.E., Stamnes, K., 1996. Influence of the depth hoar layer of the seasonal snow cover on the ground thermal regime. Water Resour. Res., 32: 2075 – 2086.

Zhang, T., Barry, R.G., Haeberli, W., 2001. Numerical simulation of the influence of the seasonal snow cover on the occurrence of permafrost at high altitudes, Norw. J. Geogr., 55: 261 – 266.

Zhang, T., Barry, R.G., Knowles, K. Ling, F., Armstrong, R.L., 2003. Distribution of seasonally and perennially frozen ground in the Northern Hemisphere. In: Proceedings of 8th International Conference on Permafrost, Proceedings, Swets & Zeitlinger, Lisse, Zürich, 2, 1289 – 1294.

Zimmermann, M. and Haeberli, W., 1992. Climatic change and debris flow activity in high-mountain areas: a case study in the Swiss Alps. Cat. Suppl., 22: 59 – 72.

Zimmermann M., Mani P., Gamma P., Gsteiger P., Heiniger O., Hunziker G., 1997. Murganggefahr und Klimaänderung – ein GIS-basierter Ansatz. Schlussbericht NFP 31. Zürich: vdf, Hochschulverlag an der ETH.

Zorita, E. and von Storch, H., 1999. The analog method as a simple statistical downscaling technique: Comparison with more complicated methods. J. Clim., 12: 2474 – 2489.

Zorita, E. and Gonzalez-Ruoco, F., 2002. Are temperature-sensitive proxies adequate for North Atlantic reconstructions? Geophys. Res. Lett., 29(14): 1703, doi:10.1029/2002GL015404.

Personal Bibliography

Peer-reviewed journal publications

Salzmann, N., Frei, C., Vidale, P.L., Hoelzle, M., 2006. The application of Regional Climate Model output for the simulation of high-mountain permafrost scenarios. *Global and Planetary Change*, doi: 10.1016/j.gloplacha.2006.07.006.

Salzmann, N., Gruber, S., Hugentobler, M., Hoelzle, M., 2006. The Influence of different Digital Terrain Models (DTMs) on alpine permafrost modeling. *Journal of Environmental Modeling and Assessment,* DOI 10.1007/s1066-006-9065-3.

Salzmann, N., Kääb, A., Huggel, C., Allgöwer, B., Haeberli, W., 2004. Assessment of the hazard potential of ice avalanches using remote sensing and GIS-modelling. *Norwegian Journal of Geography* 58, 74 – 84.

Salzmann, N., Noetzli, J., Hauck, C., Gruber, S., Hoelzle, M., Haeberli, W., (in press). Ground-surface temperature scenarios for complex high-mountain topographies based on Regional Climate Model results. *Journal of Geophysical Research – Earth Surface.*

Noetzli, J., Gruber, S., Kohl, T., **Salzmann, N.**, Haeberli, W., (submitted). Three-dimensional distribution and evolution of permafrost temperatures in idealized high-mountain topography. *Journal of Geophysical Research – Earth Surface.*

Paul, F., Machguth, H., Hoelzle, M., **Salzmann, N.**, Haeberli, W., 2006. Alpine-wide distributed glacier mass balance modeling: a tool for assessing future glacier change? In: Orlove, B., and Luckman, B. (eds.): The Darkening Peak: Glacial retreat in scientific and social context. University of California Press (in press).

Huggel, C., Kääb, A., **Salzmann, N.**, 2006. Evaluation of QuickBird and IKONOS imagery for assessment of high-mountain hazards. *EARSeL eProceedings* 5(1), 51 – 62.

Kääb A., Huggel C., Guex S., Paul F., **Salzmann N.**, Schmutz K., Schneider D., Weidmann Y., 2005. Glacier hazard assessment in mountains using satellite optical data. *EARSeL eProceedings* 4(1), 79 – 93.

Kääb, A., Huggel, C., Fischer, L., Guex, S., Paul, F., Roer, I., **Salzmann, N.**, Schlaefli, S., Schmutz, K., Schneider, D., Strozzi, T., Weidmann, Y., 2005. Remote sensing of glacier- and permafrost-related hazards in high mountains: an overview. *Natural Hazards and Earth System Science* 5, 527-554. SRef-ID:1684-9981/nhess/2005-5-527.

Huggel, C., Kääb, A., **Salzmann, N.**, 2004. GIS-based modeling of glacial hazards and their interactions using Landsat-TM and IKONOS imagery. *Norwegian Journal of Geography* 58, 61-73.

Other reports and contributions

Salzmann, N. & Tveito, O.E., 2005. Daily temperature maps for the Swiss Alps. Report of the COST-STSM in Oslo, Norway.

Salzmann, N. & Seidel, K., 2001. Evaluation of different software packages to orthorectify IKONOS imageries. Report for the ETH Zurich, Switzerland.

Permafrost in Switzerland (2004). Vonder Mühll, D., Nötzli, J., Makowski, K., Delaloye, R. (eds). Glaciological Report (Permafrost) No. 2/3; pp. 86.

Huggel, C., Kääb, A., Zgraggen-Oswald, S., **Salzmann, N.**, Schmutz, K., Haeberli, W., 2004. Satellite remote sensing for assessment of high-mountain hazards: experiences from the SDC High-Mountain Hazard Prevention Project, North Ossetia. Report for the Swiss Agency for Development and Cooperation (SDC), Humanitarian Aid, Department of Geography, University of Zurich.

Acknowledgement

Even for geographers it would be impossible to find the right coordinates on the PhD track without the support, tips and equipment provided by colleagues and friends. In this spirit, I would like to thank all those who supported and helped me in various ways during my PhD adventure:

- Wilfried Haeberli gave me the opportunity and the confidence to start this expedition to a foreign land under the flag of the mountain cryosphere. He was the person to contact for any question at any time and he transformed many high mountains into small hills.
- Martin Hoelzle was a very collegial supervisor during my expedition. He supported all my plans and gave me considerable freedom to experience and explore the scientific world.
- The most important contacts established in the foreign land were the people from the IAC-ETHZ.
    - Christoph Frei (now at MeteoSchweiz) gave me valuable and constructive advices concerning RCMs, SDS and alpine climatology. From the discussions with and the feedbacks of him I have learnt many fundamentals about the topics.
    - Pier Luigi Vidale (now at NCAS CGAM, University of Reading, UK) introduced me into handling RCM data and provided me his CHRM outputs. Furthermore, he gave me important and critical feedbacks on my proceeding.
    - Christoph Schär was very cooperative with accessing their CHRM results, was interested in my work and gave me valuable advices and feedbacks.
- Ole Einar Tveito (chair of WG2, COST 719) invited me for an interesting and beneficial stay at the Norwegian Meteorological Institute in Oslo (Norway) and introduced me into Geostatistics for alpine climatology.
- The 3G is a great group of people, not only for science but also as friends for various indoor and outdoor activities and events, and once even for an emergency action at the Corvatsch – Perscheng Assef, Luzia Fischer, Regula Frauenfelder Kääb, Stephan Gruber, Wilfried Haeberli, Susanne Hanson, Martin Hoelzle, Christian Huggel, Andi Kääb, Horst Machguth, Max Maisch, Jeannette Nötzli, Frank Paul, Michi Zemp, Sonja Zgraggen-Oswald.
- There are some people I would like to thank especially for their interest in my PhD and/or other valuable support – Pamela Alean, Regula Frauenfelder Kääb, Christian Hauck, Andi Kääb, Ross Purves, Simon Scherrer and the women of FrauSchafftWissen (e.g. Caplan, 1993).
- Susan Braun-Clarke, Karen Hammes and Ivan Woodhatch did excellent proofreading of my adventure reports, sometimes under quite uncomfortable time frame conditions….thanks a lot!
- Dani Wirz helped me to complete the enormous task of installing all the necessary software, libraries, links, etc., needed to gain access to the RCM data from my computer.

- George Ahlbäumer and his team at the Clinic Gut, St. Moritz, made it possible for me to continue my journey on my own feet, after the ‘extreme event’ at Corvatsch. I am deeply thankful every day for the excellent job he did.
- All my long-lived friends outside the ivory tower for their interest in my studies and, even more important for being a major part for many non-scientific adventures.
- My family never ceased to be interested in my work and always supported me on my way. Thanks very much!
- My deepest gratitude is offered to Roman. With such a wonderful person at my side the frosty days during my PhD expedition seemed to be much warmer and the gladness felt at reaching the mountain peaks was multiplied manifold.

This PhD thesis was made possible thanks to the financial grant of the State Secretariat for Education and Research (SER) within the frame of the COST-Action 719 – The use of GIS in climatology and meteorology.

Curriculum Vitae

Nadine Salzmann, born on May 1, 1975, in Luzern (Switzerland), Swiss citizen.

Education

1995	Graduation: Matura Typus E, Kantonsschule Alpenquai Luzern (Switzerland)
1996 – 2002	Studies in Geography, Environmental Science, Mathematics, Geology and Economics at the University of Zurich (Switzerland) Graduation: MSc Geography Master thesis: Modelling the hazard potentials through ice avalanches using remote sensing and GIS.
2002 – now	Research Assistant at the Institute of Geography, Glaciology and Geomorphodynamics Group, University of Zurich (Switzerland)

Graduate scientific training

08.2003	ICOP field excursion, Svalbard Glacial and periglacial processes in Svalbard
10.2003	PRUDENCE workshop, Wengen (Switzerland) Regional climate change in Europe: Processes and impacts
08.2004	International NCCR-Climate Summerschool 2004, Monte Verita (Switzerland) Climate variability: From observation to prediction
03.2005	Short Term Scientific Mission at Department of Norwegian Meteorological Institute, Oslo (Norway) Geostatistics in alpine climatology
05.2005	ENSEMBLES workshop, Evora (Portugal) Impacts studies and climate model outputs: Synergies and challenges
09.2005	NCCR-Climate workshop, Zurich (Switzerland) Climate change scenarios
06.2006	ICTP workshop, Trieste (Italy) Theory and use of Regional Climate Models

Work experience

06.1999 – 01.2000	Practical training at Defensa Civil, Arequipa (Peru) Setup of a GIS for the hazard assessment of seasonal flooding
02.2000 – 06.2000	Practical training at the Federal Office for Environmental Projection, Luzern (Switzerland) Revitalization of rivers, GIS database and visualization
03.2001 – 06.2001	Project assistant at the Computer Vision Laboratory, ETH Zurich (Switzerland) Evaluation of different software to orthorectify IKONOS satellite images
01.2001 – 06.2002	Part-time employment at Swiss Re (Swiss Reinsurance Company), in the Natural Hazard Research Group, GIS Division, Zurich (Switzerland)
02.2004 – 06.2004	Project employment for the Swiss Agency for Development and Cooperation (SDC), Zurich (Switzerland) Orthorectification of QuickBird satellite images from North Ossetia

International Conferences

04.2003	EGS-AGU-EUG Joint Assembly, Nice, France (Poster)
07.2003	ICOP (International Permafrost Conference), Zurich, Switzerland
02.2004	AGM (Alpine Glaciology Meeting), Innsbruck, Austria (Talk)
04.2004	COST-Meeting, Krakow, Poland (Talk)
04.2004	EGU General Assembly, Nice, France (Poster)
09.2004	EURAC (Interdisciplinary Mountain Research), Stelvio, Italy (Poster)
04.2005	EGU General Assembly, Vienna, Austria (Talk)
06.2005	EUCOP (Europ. Conf. on Permafrost), Potsdam, Germany (Poster)
04.2006	EGU General Assembly, Vienna, Austria (Talk)

PART B

Paper 1

Available online at www.sciencedirect.com

ScienceDirect

ELSEVIER

Global and Planetary Change xx (2006) xxx–xxx

GLOBAL AND PLANETARY CHANGE

www.elsevier.com/locate/gloplacha

The application of Regional Climate Model output for the simulation of high-mountain permafrost scenarios

Nadine Salzmann [a,*], Christoph Frei [b,1], Pier-Luigi Vidale [b,2], Martin Hoelzle [a]

[a] *Department of Geography, Glaciology and Geomorphodynamics Group, University of Zurich, Switzerland*
[b] *Institute for Atmospheric and Climate Science, ETH Zurich, Switzerland*

Received 13 August 2005; accepted 21 July 2006

Abstract

This study investigates the possibilities and limitations of using Regional Climate Model (RCM) output for the simulation of alpine permafrost scenarios. It focuses on the general problem of scale mismatch between RCMs and impact models and, in particular, the special challenges that arise when driving an impact model in topographically complex high-mountain environments with the output of an RCM. Two approaches are introduced that take into account the special difficulties in such areas, and thus enable the use of RCM for alpine permafrost scenario modelling. Intended as an initial example, they are applied at the area of Corvatsch (Upper Engadine, Switzerland) in order to demonstrate and discuss the application of the two approaches, rather than to provide an assessment of future changes in permafrost occurrence.

There are still many uncertainties and inaccuracies inherent in climate and impact models, which increase when driving one model with the output of the other. Nevertheless, our study shows that the use of RCMs offers new and promising perspectives for the simulation of high-mountain permafrost scenarios.

Keywords: alpine permafrost; RCM; climate scenario; high-mountain area; complex topography

1. Introduction

High-mountain environments in general, and the alpine cryosphere in particular, are affected most seriously by climate change (Haeberli and Beniston, 1998; Smith and Riseborough, 2002; Diaz et al., 2003; Harris et al., 2003; Kääb et al., 2005). The thawing of alpine permafrost can have a severe impact on the stability of rock walls and debris slopes and on engineered structures (Haeberli, 1992; Haeberli et al., 1997; Davies et al., 2001; Harris et al., 2001; Kääb et al., 2005). The extremely hot and dry summer of 2003 in the European Alps led to higher incidence of rockfall events, probably from warm permafrost (Schiermeier, 2003; Gruber et al., 2004a). This might be indicative of the aforementioned permafrost sensitivity. At the same time, human settlements, infrastructural development and tourism in high-mountain areas such as the Alps are expanding, which intensifies the permafrost-related hazard potential.

In order to simulate the distribution and evolution of permafrost in topographically complex high-mountain areas, the process-based model TEBAL (Topography

* Corresponding author. Fax: +41 44 635 68 48.
E-mail address: nsalzman@geo.unizh.ch (N. Salzmann).
[1] Now: Federal Office of Meteorology and Climatology, Zurich, Switzerland.
[2] Now: NCAS CGAM, University of Reading, UK.

0921-8181/$ - see front matter © 2006 Elsevier B.V. All rights reserved.
doi:10.1016/j.gloplacha.2006.07.006

Please cite this article as: Nadine Salzmann et al., The application of Regional Climate Model output for the simulation of high-mountain permafrost scenarios, Global and Planetary Change (2006), doi:10.1016/j.gloplacha.2006.07.006.

and Energy Balance) has been developed (Stocker-Mittaz et al., 2002; Gruber et al., 2004b). TEBAL simulates the energy fluxes between the atmosphere and the ground surface based on daily meteorological input data. It is well-suited for modelling the impact of climate change on mountain permafrost (Stocker-Mittaz et al., 2002). However, to date, alpine energy balance models such as TEBAL have only been driven with past or current climate data sets. Scenario simulations have been carried out only in the form of ad hoc scenarios with a very general use of climate model output (Stocker-Mittaz et al., 2002). The use of scenario time series from climate model output has been neglected so far for alpine permafrost modelling. Nevertheless, General Circulation Models (GCMs) have been used for impact studies of lowland permafrost (Anisimov et al., 1997; Stendel and Christensen, 2002). However, the horizontal resolution of a GCM (in the order of 300 km) is not able to describe explicitly the spatial distribution of the climate variables for a local site in areas of complex topography such as the Alps. Therefore, the technique of regional climate modelling (RCM) is required in such regions (Christensen et al., 1998; Giorgi et al., 2001; Frei et al., 2003; Vidale et al., 2003). This technique uses output from GCMs or re-analysis data (global analysis of the state of the atmosphere such as ERA-40 (Kallberg et al., 2004); Re-Analysis from the European Centre for Medium-Range Weather Forecasts (ECMWF)) to provide initial conditions and time-dependent lateral meteorological boundary conditions to drive high-resolution RCM simulations for selected time-slices of the global model run (e.g. Dickinson et al., 1989; Giorgi, 1990; Giorgi and Mearns, 1991). Giorgi et al. (2001) and Denis et al. (2002) showed that the simulation of the spatial patterns of precipitation and temperature over complex terrain is generally improved with the increasing resolution obtained using such regionalisation techniques. The added value of RCMs is also particularly evident for precipitation in the Alps (Frei et al., 2006).

In order to deal with the impact of changing atmospheric conditions on alpine permafrost and to assess the potential of permafrost related hazards, it is essential to establish a link between the latest developments in cryospheric and atmospheric science. Studies dealing with the use of regional climate models to drive impact models have already been carried out in other scientific disciplines, mainly in hydrology (e.g. Arnell et al., 2003; Wood et al., 2004; Kleinn et al., 2005) and agriculture science (e.g. Mearns et al., 1999, 2001). A problem that occurs primarily when driving an impact model with climate model output is the spatial scale mismatch between the two model types (RCM 50 km, alpine permafrost model 25 m). However, the use of RCM output in topographically complex high-mountain environments presents additional challenges. These include:

(1) the low vertical resolution of an RCM that cannot represent high-mountain ranges adequately;
(2) the horizontal shifts of precipitation pattern (at grid boxes scale) that are observed along mountain ranges (Kleinn, 2002);
(3) the high spatial variability of the climate variables, and
(4) the reduced availability of observation data in remote mountain areas.

An additional problem from an impact modeller's point of view is the technical handling of climate model output data (data format, rotated grids, etc.), a topic not discussed in this paper.

This study aims at investigating the possibilities and limitations of the application of RCM output for local high-mountain permafrost scenario simulations, and presents two possible approaches which take into account the special challenges mentioned above. The approaches are applied in the Corvatsch region (Upper Engadine, Switzerland) in order to illustrate and discuss their potential, rather than to make an assessment of the potential future changes in the permafrost occurrence for this region.

The RCM Climate High Resolution Model (CHRM), the permafrost model TEBAL (Topographical Energy Balance), the observation data and the study site are presented in Section 2 of this paper. Section 3 introduces the two approaches. The example of the application at the Corvatsch test site is given in Section 4, followed by a discussion in Section 5, and conclusions and perspectives in Section 6.

2. Models and data

2.1. Climate High Resolution Model (CHRM)

The CHRM limited area model developed at the Institute for Atmospheric and Climate Science, ETH Zurich (IAC-ETHZ), derives from the former numerical weather prediction model, HRM, of the German and Swiss meteorological service (Majewski, 1991). The HRM model has been modified by Lüthi et al. (1996) and Vidale et al. (2003) to provide an RCM. The computational grid of the model is a regular latitude/longitude grid with a rotated pole, a spatial resolution of

Please cite this article as: Nadine Salzmann et al., The application of Regional Climate Model output for the simulation of high-mountain permafrost scenarios, Global and Planetary Change (2006), doi:10.1016/j.gloplacha.2006.07.006.

0.5° (about 56 km) and 20 vertical levels in hybrid coordinates. It includes a full package of physical parameterizations (for details see Vidale et al., 2003).

For this study, we used three different CHRM experiments, each driven with different boundary conditions. In all three simulations, the region of the European Alps is located close to the centre of the domain. A good separation of the investigation site from the models' lateral boundary zones is preferable, since it minimizes the influence of possible spurious boundary effects (McGregor, 1997).

In the following, the three simulations used in this study are briefly described:

i) ERA-40 CHRM: This run is driven at its lateral boundaries with the re-analysis data set ERA-40 for the 1960–2000 time-slice. An RCM simulation that is driven from reanalysis has so-called 'perfect boundary conditions' and hence generates simulations with the best possible quality (Christensen et al., 1997). Such runs allow the identification of model errors caused mainly by model configuration and internal physics, and can thus be used to validate the RCM for the region of interest by comparing the simulation outputs with observations for the same period (Pan et al., 2001).

RCM simulations for climate change studies are driven by a GCM. The second and third simulations that are used in this study are, thus, CHRM experiments driven at their lateral boundaries by the HadAM3H atmospheric GCM (Hadley Centre, UK). These two runs were performed as part of the European project 'PRUDENCE' (Prediction of Regional scenarios and Uncertainties for Defining EuropeaN Climate change risks and Effects; Christensen et al., 2002).

ii) CHRM CTRL: The errors of an RCM driven by GCM fields consist of RCM model errors as well as of GCM errors. In order to assess the performance of such an RCM, the RCM can be driven for present climate conditions ('control' experiment CTRL) and then compared with the observation climatology. The control run was thus driven by the HadAM3H GCM for the 1961–1990 time-slice.

iii) CHRM SCEN: This run represents the scenario experiment for the 2071–2100 time-slice. Here, the CHRM is driven at its lateral boundaries by the HadAM3H atmospheric GCM (Hadley Centre, UK), as forced by the A2 SRES scenario (Special Report on Emission Scenarios; Nakicenovic and Swart, 2000), transient greenhouse gas scenario as specified by the Intergovernmental Panel of Climate Change (IPCC, 2001).

The CHRM was validated for the region of the European Alps by Vidale et al. (2003) and Frei et al. (2003). Vidale et al. (2003) showed that the interannual variations in temperature are generally well represented and that precipitation is modelled better in relatively dry years, especially in summer. Frei et al. (2003, 2006) evaluated the CHRM in view of the statistics of daily precipitation in an intercomparison of four RCMs and one variable-resolution global climate model (all developed and operated at various climate modelling centres across Europe) referring to a daily observational analysis. They did not identify one best model in particular. Each model showed reasonable performance for some statistics but substantial deviations for others. For mean precipitation, the models followed qualitatively the main characteristics of the observed annual cycle and the spatial pattern. However, all models underestimated precipitation intensity and the frequency of heavy precipitation events was too low. The CHRM mainly underestimated summer mean precipitation (August and September) primarily due to too few rainy days, however, with much smaller underestimation from late autumn to early summer. It depicts realistic values of wet-day frequency. The summer dryness is a persistent problem of climate models in the Alpine and Mediterranean regions and in south-eastern Europe (Frei et al., 2003), found in analysis-driven RCMs (Frei et al., 2003), in GCM-driven RCMs (e.g. Machenhauer et al., 1998) and in global high-resolution models (e.g. Wild et al., 1997).

2.2. Topography and Energy BALance model (TEBAL)

The TEBAL energy balance model simulates the main energy exchange processes between the atmosphere and the surface. Different versions have been implemented for different applications (Mittaz et al., 2002; Stocker-Mittaz et al., 2002; Gruber et al., 2004a,b). In this study, we used a grid-based version of TEBAL. The required input data include (i) atmospheric variables (daily values for air temperature, vapour pressure, air pressure, wind speed, radiation at the top of the atmosphere, precipitation and global radiation), (ii) ground surface characteristics (albedo, surface roughness, emissivity), and (iii) topography (elevation, slope, aspect from the DHM25 digital terrain model obtained from the Swiss Federal Office of Topography 'swisstopo'). With this set of input data, the applied TEBAL version is able to simulate the distribution and evolution of daily ground surface temperatures (GST)

Please cite this article as: Nadine Salzmann et al., The application of Regional Climate Model output for the simulation of high-mountain permafrost scenarios, Global and Planetary Change (2006), doi:10.1016/j.gloplacha.2006.07.006.

in complex high-mountain topography at a local to regional scale. The model was validated at a variety of test sites in the Alps (Gruber et al., 2004b). The GST was simulated at 14 locations in the Swiss Alps, where 21 data loggers measured 1-year time series (October 2001 to October 2002) at elevations between 2000 and 4500 m a.s.l. (Gruber et al., 2003). The model results agreed well with the mean annual temperature and the daily temperature fluctuations measured.

The coupling between the mean annual ground surface temperature (MAGST) and the mean annual ground temperature (MAGT) still presents problems. These are related to (a) the limited knowledge of the influence of non-conductive heat transfer processes within the active layer when the subjacent ground is not bedrock or fine-grained material. In alpine environments, the lower limit of discontinuous permafrost is often found along areas with very coarse-grained or blocky surface cover. A coarse surface cover will enhance cooling of the subjacent ground by non-conductive processes (Goering and Kumar, 1996; Harris and Pedersen, 1998; Humlum, 1998; Hoelzle et al., 1999; Hanson and Hoelzle, 2005) and will undergo a variety of complex heat transfer processes and feedback mechanisms that influence the thermal regime of the active layer and thereby the permafrost temperature. These processes within the active layer cannot be simplified so as to be controlled only by differences in conductivity of thawed and frozen materials as in lowland permafrost, for example, as defined by Smith and Riseborough (1996). There are also problems related to the fact that (b) permafrost is a thermal system with slow response to climate forcing. Therefore, the present state of permafrost is influenced by former climatic conditions and affects future developments. The response time of permafrost depends on the thermal conductivity, the ice content and the thickness of the frozen ground (Osterkamp, 1983). These parameters in space are normally not known and can only be estimated by conducting extensive geophysical measurements (e.g. Hauck, 2001). Even relatively warm and thin discontinuous mountain permafrost has a response time which is typically measured in decades to centuries (Haeberli, 1990). In fact, the thickness and some marginal occurrences of alpine permafrost most probably still reflect maximum Holocene cooling during the Little Ice Age, which culminated in the 19th century. Temperature profiles observed in boreholes (Vonder Mühll et al., 1998; Isaksen et al., 2000, 2001; Harris et al., 2003) prove permafrost thicknesses in excess of values expected from present-day mean annual ground temperature (MAGT). In consequence, realistic modelling of permafrost temperatures must actually include such non-stationary conditions at depth and the 3D effects of mountain topography (Gruber et al., 2004b). When facing the problem of possible changes in permafrost conditions, in a first step towards permafrost scenario simulations, it is sufficient to consider the potential changes in the GST of bedrock. Such a surface is the direct connecting layer between the atmosphere and the ground and thus the layer which receives the climate signal and conducts it into the ground. Beside the atmospheric conditions, the GST in mountainous systems is an important element also determined by the topography. TEBAL takes this effect into account by the use of a DTM (see above). Furthermore, the time and duration of the snow cover has a strong impact on the seasonal thermal regime of the ground due to the isolation properties of snow (e.g. Zhang et al., 2001). However, in order to keep the model simple, this effect has been neglected here.

2.3. Observed climatology and study site

The observed meteorological data (OBS) were used as site-specific references in order to evaluate the performance of the CHRM simulation at the study site, and as the basis for the daily scenario time series for the delta approach (see next section).

The meteorological data have been provided by MeteoSwiss (Federal Office of Meteorology and Climatology) from the standard Swiss observational network. We used the daily and monthly means and cumulative amounts from several high-altitude stations in Switzerland for the 1961–1990 period (or to 1997 for some variables). If available, we used the homogenized data (monthly data only) that were produced as part of the projects KLIMA90 (Aschwanden et al., 1996) and NORM90 (Begert et al., 2003, 2005). Otherwise, we reverted to use the measured data.

The test area at Corvatsch-Furtschellas, Upper Engadine, Switzerland (cf. Figs. 1 and 4a) is approximately 4 km^2 in size. The Corvatsch is one of the most frequently investigated mountain permafrost sites in the Swiss Alps (Hoelzle et al., 2002). The climate station in place was set in operation in 1981 and thus the time period covered is shorter than would ideally be required for our approaches. However, it is the only high-elevation station (i.e. well above 3000 m a.s.l.), which provides all the required variables. The Upper Engadine is situated in the Central Alps and due to the protected location the climate is slightly continental. Due to the influence of the south-westerly air masses caused by the flat and broad Malojapass, the climate of this region is classified as south-alpine (Schüpp, 1954). Climate

Please cite this article as: Nadine Salzmann et al., The application of Regional Climate Model output for the simulation of high-mountain permafrost scenarios, Global and Planetary Change (2006), doi:10.1016/j.gloplacha.2006.07.006.

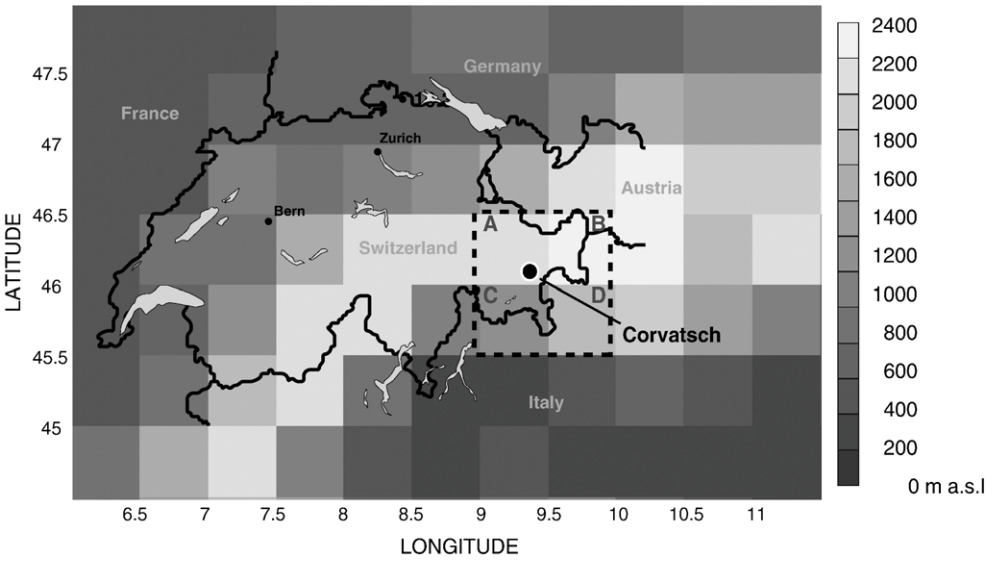

Fig. 1. Switzerland and the Corvatsch research site within the grid system of the CHRM, showing the CHRM topography.

records show high daily and annual amplitudes, low mean annual precipitation of about 1000–2000 mm in the periglacial area (Schwarb et al., 2000) and thus relatively little snowfall. The mean annual 0° isotherm lies at around 2200 m a.s.l.

3. Methods

3.1. Factors to consider

Currently, the horizontal resolution of a multi-decadal RCM simulation, as must be used for climate change studies, is limited to about 1/6° to 1/2° (approx. 20–50 km), due to limited current computational resources (e.g. Räisänen et al., 2004). However, the spatial resolution required to obtain information about alpine permafrost is a few decametres (25 m with the DHM25 digital terrain model). This is necessary, since elevation, slope and aspect change within very short distances in the complex topography of mountain areas, and therefore climate variables and thus ground surface temperatures do so as well. The relatively low horizontal resolution of the RCM is also associated with a coarse representation of the topography (Fig. 1). The high-mountain areas of the Alps reach elevations of up to 4800 m a.s.l, but the maximum altitude of the CHRM in the Alps is 2382 m a.s.l. The grid boxes with the highest elevation are not found where the highest peaks are located, but where the Alps are relatively high in combination with a large north–south elongation. Beyond that, the maximum CHRM altitude of about 2400 m a.s.l. corresponds approximately to the lower limit of discontinuous permafrost occurrence. That means that, based on the altitude represented by the RCM, no permafrost conditions can be simulated in an RCM within the Alps and thus a further regionalization of the variables from RCM output is required.

A further point to consider is that each model grid box represents an area mean. The extent to which this may be expected to truly represent climate variables over this area is not clear. As a reasonable assumption, the representative area for simulated climate variables is somewhere between one and four grid boxes (Frei et al., 2003). Moreover, a shift of the simulated precipitation in regions of significant elevation is often observed in the order of one grid cell (Kleinn, 2002).

For climate change studies, the RCM is normally driven by the output of a GCM. The uncertainties of GCMs are associated mainly with imperfect knowledge and/or representation of physical processes, limitations due to the numerical approximation of the model's equations, simplifications and assumptions made in the model parameterization (e.g. Visser et al., 2000; Mearns et al., 2001; Antic et al., 2004; Räisänen et al., 2004). These inaccuracies are passed on to the RCM and are thus an additional source of error in RCMs apart from those of the RCM itself.

There are mainly two consequences arising of the stated inaccuracies and uncertainties for the use of RCM output in impact models with complex high mountain topography. First, the direct use of RCM output is not recommended. Instead, impact model specific strategies must be found as a way of deriving the local climate information. Second, the grid box, which represents

Please cite this article as: Nadine Salzmann et al., The application of Regional Climate Model output for the simulation of high-mountain permafrost scenarios, Global and Planetary Change (2006), doi:10.1016/j.gloplacha.2006.07.006.

the climate condition of the location of interest, is not necessarily the grid box in which the site of interest is situated in terms of latitude and longitude. Therefore, a choice must be made between the average of the surrounding grid boxes and the grid box that fits best with the climatology of the specific site. The decision whether to use one grid box or the average of several grid boxes depends on the applied approach and also on the specific application and sensitivity of selecting just one, or the average of several grid boxes (see Section 4.3). The 'best' grid box can be chosen from the grid boxes closest to the meteorological station by comparing the model output of the ERA-40 CHRM grid boxes with the OBS on a monthly mean basis by using various skill measures. Different measures quantify different aspects of correspondence skills. Therefore, the application of several different skill measures is indicated to measure the quality of model output (Damrath, 2002). In this study, the selection of the grid box is based on the two skill measures — correlation and root mean square error (RMSE). These two measures also provide information about the ability of the RCM to reproduce the regional characteristics of the present-day climate for a single location.

3.2. Delta approach

The idea of the delta approach is to obtain a scenario time series by adjusting the local baseline observation by the difference (for variables like temperature) or the ratio (for variables like precipitation) between the SCEN and the CTRL time-slice (Fig. 2). Here, the delta value is based on a monthly 30-year average while the adjusting is done to the observed daily time series corresponding to the respective month of the year.

The approach uses only the 30-year average monthly mean changes of the RCM simulations. Consequently, on the one hand, the confidence in the climate model can be moderate in terms of the ability of the model to simulate the daily variability but on the other hand, the assumption must be made that there is no change in interannual and daily variability between the baseline and the future climate. For example, for precipitation, the wet day variability will not change, since only wet days of the baseline change and all observed dry days will also be dry in the scenario time series. Therefore, regarding permafrost, a possible change in the time and duration of the snow cover is caused by temperature and precipitation amount only, and not by the changed variability of precipitation.

For the delta approach, the use of the average of several grid boxes might lead to more robust results than the use of only one grid box.

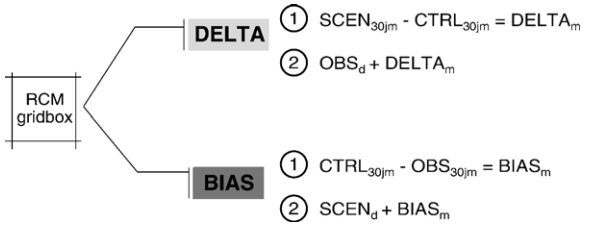

Fig. 2. Schematic diagram of the two approaches.

3.3. Bias approach

The bias approach uses the debiased daily time series output of the SCEN simulation (Fig. 2). The biases, here 30-year monthly means, are calculated by subtracting the monthly 30-year averages of CTRL from the OBS. The daily SCEN output is then debiased by the monthly bias corresponding to the respective month.

The advantage of this approach as opposed to the delta approach is that a possible change in the variability is included since the daily values modelled by the climate model are used. As shown by Schär et al. (2004), the current climate change scenarios do not simulate an increase in temperature alone, but also an increase in the year-to-year variability. In contrast to the delta approach the bias approach is capable of reproducing those higher order changes. However, our application of the bias approach filters out only the systematic errors of the RCM/GCM in mean monthly quantities but not in daily statistics. As an example, the monthly 30-year average of precipitation might be simulated correctly by the model but the frequency of wet days is wrong. In our approach, the frequency bias is not considered. Thus, the bias approach as it is implemented here assumes that the climate model is able to simulate accurate high-order frequency statistics at the daily time scale. This may not necessarily be the case. Procedures for handling selected higher order biases have been proposed (Schmidli et al., 2005) but a comprehensive treatment would require complex statistical modelling.

The bias approach requires the use of individual RCM grid boxes, since there is a chance that the grid box average approach would fail to take regional extreme events into account.

4. A first example of an application for the Corvatsch regions (eastern Swiss Alps)

In order to illustrate the proposed approaches, we provide in the following an application intended as a

Please cite this article as: Nadine Salzmann et al., The application of Regional Climate Model output for the simulation of high-mountain permafrost scenarios, Global and Planetary Change (2006), doi:10.1016/j.gloplacha.2006.07.006.

first example for the test region Corvatsch in the Swiss Alps (see Fig. 1).

4.1. Treatment of the observational data

The observed time series in the form of monthly means and monthly sums is required for the determination of the "best" grid box, for the performance test of the RCM in the region of interest and for the application of the bias approach. Ideally, these should extend back to 1961. Because the climate station of Corvatsch provides data only since 1981, we extended the time series of Corvatsch with simple linear regression using the neighbouring high elevation stations that, on the one hand, go back to 1961 and, on the other hand, show a high correlation with the Corvatsch time series.

In this manner, the time series of the Corvatsch station were extended, using the homogenized monthly means and sums from the following stations: temperature at the Weissfluhjoch station ($r^2=0.98$); precipitation at the Buffalora station ($r^2=0.79$); air pressure at the Jungfraujoch station ($r^2=0.98$); vapour pressure at the Weissfluhjoch station ($r^2=0.96$) and wind speed at the Weissfluhjoch station ($r^2=0.49$). For wind speed, no homogenized time series were available before 1981 and the direct measurements were only available back to 1970. For the variable global radiation no measurements exist at all for the time period from 1961 to 1980, so, we used only the available (short) time period.

4.2. Application of the two approaches

Due to the missing data, the different variables require individual adaptation of the delta and bias approaches. Also, in order to allow for a comparison between the two approaches, in the following investigations we use only the output of one grid box for each. This is reasonable since the tested sensitivity is low (cf. Section 4.3).

4.2.1. Temperature

The 'best' model grid box was determined by calculating the correlation and RMSE between the time series of the four ERA-40 CHRM grid boxes that are located closest to the Corvatsch climate station, and the homogenized time series of Corvatsch for the time period of 1961 to 1997 (Fig. 1, Table 1). These calculations were made for the monthly mean temperature, the monthly minimum and the monthly maximum temperature. Based on the results of these calculations (Table 1), we selected grid box B as the representative one for the Corvatsch area, with $r^2_{tmean}=0.93$ and $RMSE_{tmean}=3.8°$, $r^2_{tmin}=0.84$ and $r^2_{tmax}=0.81$.

In order to assess the performance of the CHRM for our study site, we compared the monthly 30-year average (1961 to 1990) of ERA-40 CHRM with the OBS. The correlation between both data sets is very high ($r^2=0.98$), but modelled mean temperatures are overestimated (3.2 K on average, Fig. 3a), with large seasonal variations. In the winter months (DJF), the deviation is lower, on average 0.8 K. The highest deviation is found in summer (JJA), on average 5.3 K. However, assuming a lapse rate of 0.6 K/100 m and considering an elevation difference of about 1000 m between the RCM grid box elevation and the true elevation, the summer deviation decreases to a difference of 0.7 K between ERA-40 CHRM and OBS, whereas the winter deviation increases to 5.2 K. Thus, a lapse rate correction alone would not improve the results, showing that other inaccuracies and uncertainties that cannot be assigned specifically are jointly responsible for the high seasonal variations and the corresponding deviation between RCM output and OBS.

The 17-year monthly average of the minimum temperature (based on the time period 1980 to 1997, since no OBS data before 1980 are available) shows no important seasonal variation, but the modelled t_{max} are too high all year round, on average 9.5 K (or about 3.5 K including a lapse rate correction of 0.6 K/100 m). The

Table 1
The performance of the grid boxes (ERA-40 CHRM compared to OBS) closest to the Corvatsch site (cf. Fig. 1)

	Grid box A (2053 m a.s.l.)			Grid box B (2382 m a.s.l.)		
	Temperature	Precipitation	Air pressure	Temperature	Precipitation	Air pressure
r^2	0.9	0.4	0.82	0.93	0.37	0.81
RMSE	5.1	1.8	1.84	3.8	1.15	1.9
	Grid box C (1044 m a.s.l.)			Grid box D (1626 m a.s.l.)		
	Temperature	Precipitation	Air pressure	Temperature	Precipitation	Air pressure
r^2	0.9	0.18	0.84	0.92	0.3	0.83
RMSE	8.1	2.8	1.8	5.1	2.3	1.9

Please cite this article as: Nadine Salzmann et al., The application of Regional Climate Model output for the simulation of high-mountain permafrost scenarios, Global and Planetary Change (2006), doi:10.1016/j.gloplacha.2006.07.006.

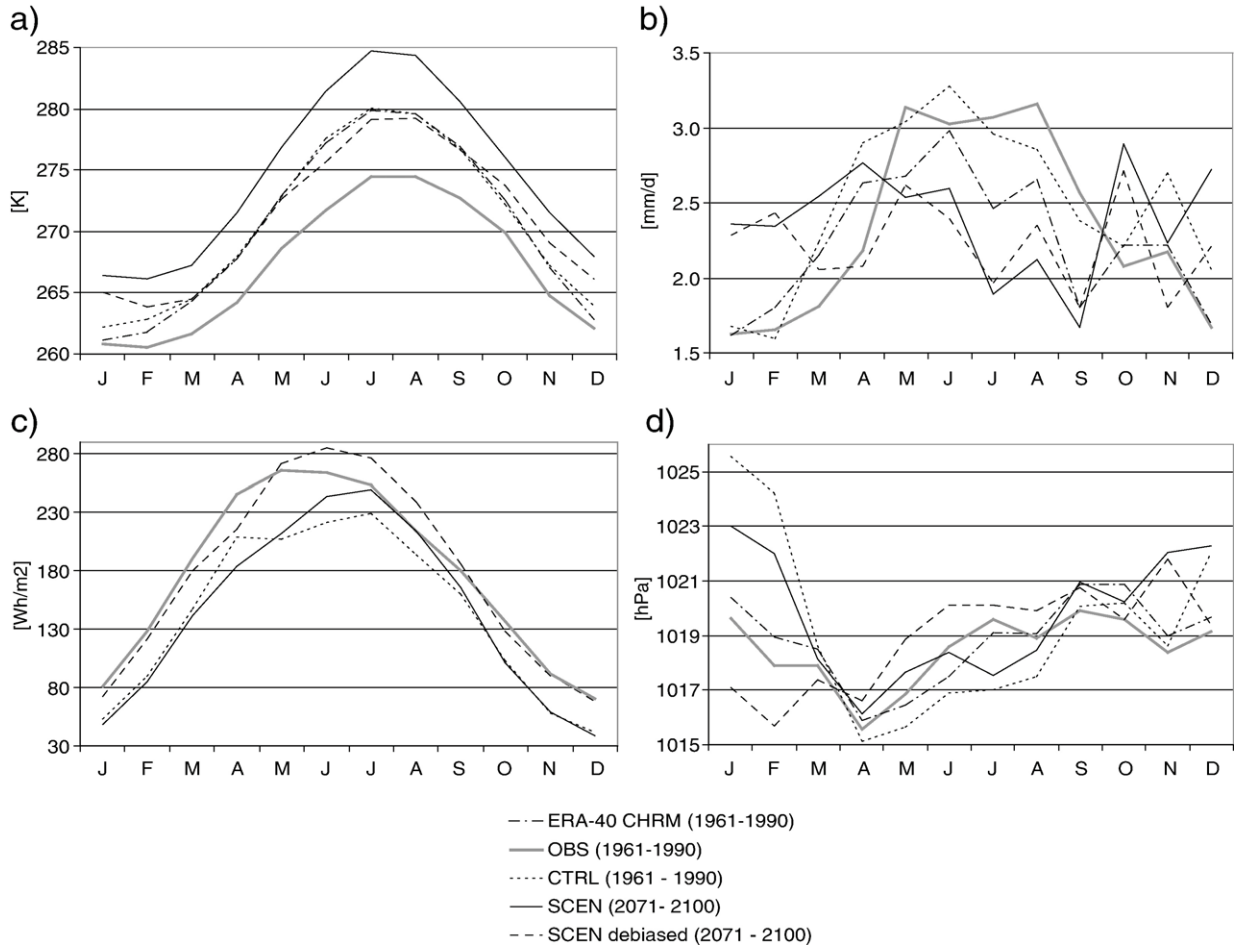

Fig. 3. The 30-year averages (1961–1990) for a) 2m temperature, b) precipitation, c) global radiation, d) air pressure.

17-year monthly average of the maximum temperature deviates seasonally. The t_{max} of the ERA40 CHRM is too low in winter (DJF), on average 6.4 K (0.4 K with lapse rate correction), and too high in summer (JJA) (3.7 K, or 2.3 K too low with lapse rate correction).

For the bias approach, the monthly biases are calculated in order to correct the daily SCEN time series output. For that purpose, we compared the monthly 30-year average (1961–1990) of OBS and CTRL of the grid box B (CTRL without any lapse rate corrections). The monthly bias values are listed in Table 2. In order to create the daily scenario time series for the Corvatsch site, we debiased the daily scenario time series of grid box B based on the monthly biases from Table 2. Since a CHRM model year consists of only 360 days, but the TEBAL model requires 'real' years, we added the missing days by a simple interpolation technique.

For the delta approach, the monthly 30-year average of CTRL (grid box B) is subtracted from SCEN (grid box B). The delta values are listed in Table 2. The monthly delta values are then added to the daily OBS time series in order to create the local scenario daily time series.

4.2.2. Precipitation

For mean precipitation, we found the highest correlation between the monthly time series of ERA-40 CHRM and OBS for the period 1961–1997 for grid box A ($r^2=0.4$) but the best RMSE for grid box B (1.15) (Table 1). Because the difference in correlation is comparatively small, we decided to choose grid box B for consistency with the choice for temperature.

A correlation analysis of the monthly 30-year average between ERA-40 CHRM and OBS yielded a correlation of $r^2=0.61$ (Fig. 3b). Mean precipitation is underestimated by the CHRM for 5 months in summer (MJJAS), on average about 21%. This summer dryness is a known phenomenon and also described by Frei et al. (2003; see also Section 2). During winter, the mean precipitation is overestimated, on average about 8%.

Please cite this article as: Nadine Salzmann et al., The application of Regional Climate Model output for the simulation of high-mountain permafrost scenarios, Global and Planetary Change (2006), doi:10.1016/j.gloplacha.2006.07.006.

Table 2
Calculated monthly biases and monthly delta values for grid box B

	m-BIAS (OBS-CTRL)				m-DELTA (SCEN-CTRL)			
	Temperature (K)	Precipitation (factor)	Global radiation (factor)	Air pressure sl (hPa)	Temperature (K)	Precipitation (factor)	Global radiation (factor)	Air pressure sl (hPa)
Jan	−1.4	0.97	1.52	−5.9	4.2	1.40	0.91	−2.5
Feb	−2.3	1.04	1.43	−6.3	3.3	1.47	0.95	−2.2
Mar	−2.8	0.81	1.29	−0.7	2.8	1.14	0.96	−0.5
Apr	−3.7	0.75	1.17	0.5	3.6	0.95	0.88	1.0
May	−4.3	1.03	1.28	1.2	4.0	0.84	1.03	2.0
Jun	−5.8	0.92	1.19	1.7	3.9	0.79	1.10	1.5
Jul	−5.6	1.04	1.11	2.6	4.7	0.64	1.09	0.5
Aug	−5.1	1.11	1.10	1.4	4.7	0.74	1.10	1.0
Sep	−4.0	1.08	1.13	−0.2	3.9	0.70	1.04	0.9
Oct	−2.3	0.94	1.32	−0.6	3.8	1.31	0.98	0.0
Nov	−2.5	0.80	1.58	−0.3	4.3	0.83	1.01	3.4
Dec	−1.8	0.81	1.69	−2.9	4.0	1.32	0.94	0.3

Calculations of the monthly biases for precipitation have been made by comparing OBS with CTRL based on a monthly 30-year average (1961–1990). The bias values are listed in Table 2 and show an average bias of about 11%. Based on the monthly biases (Table 2) of the mean precipitation, we created the scenario daily time series of the grid box B for the Corvatsch area (cf. section 'Temperature'). The delta values were determined in a similar way as for temperature and are listed in Table 2.

4.2.3. Global radiation

For global radiation we also selected grid box B, since this was the grid box of choice for the variables temperature and precipitation and because no reliable ERA-40 CHRM data of global radiation were available. As there are no observed data of global radiation available before 1980, the monthly biases were calculated from a 10-year climatology (1981–1990). Based on this time period, the comparison between OBS and CTRL showed high correlation ($r^2=0.88$) and a correlation of $r^2=0.98$ for the monthly 10-year average. As shown in Fig. 3c and Table 2, the CTRL run underestimates global radiation values all year (on average only 77% of the OBS), with a sharp downward bend from April to May.

The bias daily scenario time series was calculated from the SCEN daily time series and debiased in relation to the calculated monthly bias (cf. section 'Temperature').

The values for the monthly delta values are listed in Table 2.

4.2.4. Air pressure

The CHRM provides mean sea level pressure only. In order to compare the CHRM outputs with OBS, the measured air pressure values from Corvatsch were reduced to sea level first, based on the barometric formula (e.g. Heyer, 1993):

$$p_{\mathrm{sl}} = p(z)\left(\exp\left\{-\frac{gz}{RT_{\mathrm{m}}}\right\}-1\right) \quad (1)$$

where p_{sl}=air pressure at sea level; $p(z)$=measured air pressure at Corvatsch station; z=elevation of Corvatsch station=3315 m; g (acceleration due to gravity)=9.81 m/s^2; R (gas constant)=287.05 J kg^{-1} K^{-1}; T_{m} (mean vertical temperature)=$T_1+0.00325z$, where T_1=measured temperature at Corvatsch station.

Differences relating to correlation and RMSE between the four grid boxes are moderate (Table 1). For this reason, we again selected grid box B as the representative one, as done for all other variables previously. Fig. 3d shows good agreement between CHRM air pressure values and observations throughout the year.

The monthly biases are calculated by comparing the monthly 30-year average from CTRL and $\mathrm{OBS_{sl}}$ and are listed in Table 2. In addition to the debiasing, the daily scenario air pressure values have to be adjusted to the Corvatsch elevation in order to use them for the TEBAL model. For that purpose, Eq. (1) was applied using the synthetic scenario daily temperatures calculated above for T_{m}.

4.2.5. Vapour pressure

The CHRM provides dew point temperature, which can be transformed into vapour pressure. However, here, we just applied a simple regression model based on the OBS daily vapour pressure time series and the calculated synthetic scenario time series of air temperature, in order to create a scenario of daily vapour pressure time series.

Please cite this article as: Nadine Salzmann et al., The application of Regional Climate Model output for the simulation of high-mountain permafrost scenarios, Global and Planetary Change (2006), doi:10.1016/j.gloplacha.2006.07.006.

4.2.6. Wind speed

For the variable wind speed we also used the daily OBS values for the SCEN run. The CHRM provides only maximum wind speed (no direction) in addition to mean zonal and meridional wind components. We decided that the additional effort to create a scenario time series from these CHRM data was not worth the effort. Nevertheless, we analyzed the change in the wind speed maximum between the CTRL and SCEN experiment. CTRL calculates much lower wind speed maxima in the grid box B for the months April to November, but much higher values for the winter months December to March. Regarding permafrost, this implies in particular that snow transfer is enhanced and thus influences the spatial pattern of permafrost temperatures by the isolation capacity of the snow cover.

4.3. Sensitivity of using one or the average of several grid boxes

We have analysed the sensitivity for the use of one single grid box compared to the use of an average of several grid boxes for monthly delta values of temperature and precipitation. We have not analysed it for the monthly bias values, since we do not recommend an averaging procedure for this approach, as explained above. Two different average combinations have been chosen to calculate the monthly delta values. The first combination (AV4) averages the four grid boxes that are closest to the Corvatsch site (grid box A, B, C, D; cf. Fig. 1; Table 1) and the second combination (AV2) averages the two grid boxes with the highest elevation (grid box A and B). The resulting monthly delta values were then compared with the monthly delta values of the 'best' grid box. Table 3 shows the differences. They are low for both variables and especially for AV2, which represent the average of the two high elevation grid boxes. For this example and the two variables at least, we can conclude that the calculated monthly delta values and thus also the final results do not have a high sensitivity regarding the number of grid boxes (one 'best' or average) included.

Table 3
Differences between the monthly delta values resulting when using the 'best' grid box, 4 averaged grid boxes (AV4), or 2 averaged grid boxes (AV2) for temperature and precipitation

	Temperature difference AV4	Temperature difference AV2	Precipitation difference AV4	Precipitation difference AV2
Jan	0.5	0.0	−0.12	0.01
Feb	0.3	0.1	0.05	0.00
Mar	0.0	0.1	0.06	0.01
Apr	0.3	0.1	−0.06	0.02
May	0.3	0.2	0.02	0.00
Jun	−0.2	−0.1	0.15	−0.01
Jul	−0.1	0.1	0.18	0.06
Aug	−0.4	−0.1	0.18	0.02
Sep	−0.2	−0.2	0.04	0.02
Oct	0.2	0.0	−0.08	0.06
Nov	0.9	0.1	−0.03	0.03
Dec	0.6	0.1	−0.12	−0.04

4.4. Modelling the change of ground surface temperature

We performed several 20-year runs with TEBAL under local current climate conditions (1981–2001) and under local scenario climate conditions (2071–2091), using the bias and the delta approach. In addition to the climate input, TEBAL requires information about ground surface characteristics (albedo, surface roughness, emissivity) and topographical attributes (elevation, slope, aspect, sky-view fraction). The ground surface information for the Corvatsch area was derived from a surface cover classification based on aerial photographs including the surface categories glacier and bedrock/fine-grained debris. The surface cover characteristics were assigned as was done by Stocker-Mittaz et al. (2002) based on Oke (1987) and Stull (1988). The surface cover map was adapted for the scenario calculation based on a study by Hoelzle and Haeberli (1995), where they estimated an almost complete disappearance of the Corvatsch glacier by the year 2025 and the total disappearance by the year 2100. Therefore, we assumed by a simple trend analysis of the glacier extent of 1990 after Maisch (1992) and the two scenarios 2025 and 2100 after Hoelzle and Haeberli (1995) that the Corvatsch glacier will have disappeared already in 2071 when the time period of our analysis starts. Thus, we reclassified the category 'glacier' into the category 'bedrock/fine-grained debris' for the scenario run. The topographical attributes were derived from the digital terrain model DHM25 L2 from 'swisstopo'.

A selection of the modelling results is presented in Fig. 4. Fig. 4a shows a photograph of the Corvatsch test area. Fig. 4b shows the simulated changes in the averaged ground surface temperature between the time-slice 1981–2001 and 2071–2091. Here, the bias approach was applied with a glacier-free surface for the scenario run. Fig. 4c shows the same as Fig. 4b, but with identical surface characteristics for both time-slices (no glacier disappearance). The most distinctive changes in Fig. 4b are found in areas where the surface cover changed from 'glacier' to 'bedrock/fine-grained debris' within the two time-slices. Clearly, the proposed approaches are not required to achieve this result. However, this finding points to two topics that have to be addressed when dealing with climate impacts in high-mountain areas. First, the capability of

Please cite this article as: Nadine Salzmann et al., The application of Regional Climate Model output for the simulation of high-mountain permafrost scenarios, Global and Planetary Change (2006), doi:10.1016/j.gloplacha.2006.07.006.

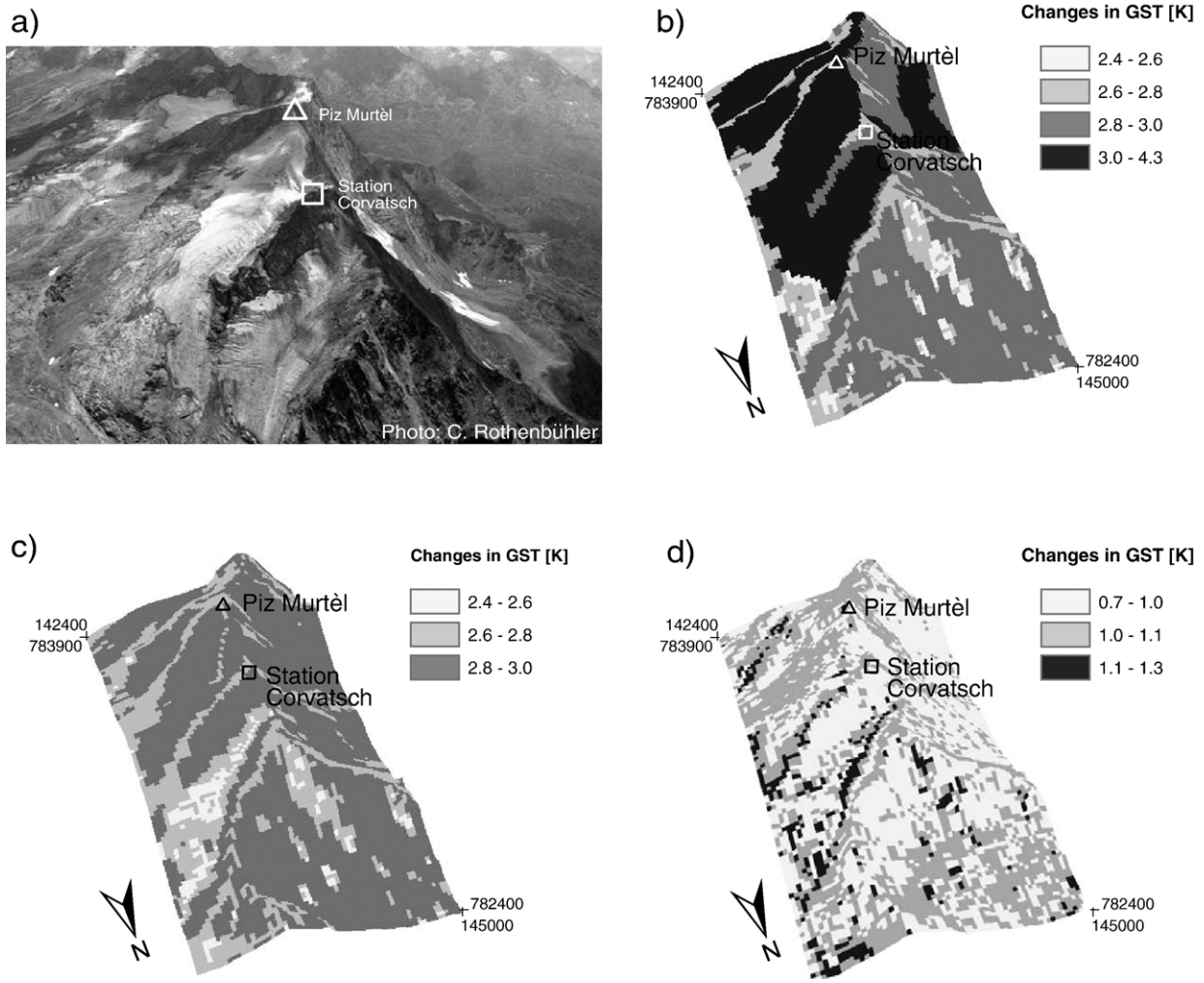

Fig. 4. Three results from the sample study (b–d) and the Corvatsch study site (a). For the localisation of the Corvatsch area, see Fig. 1. (b) The changes in ground surface temperature (GST) between the time-slices 1981–2001 and 2071–2091, using the bias approach and a glacier-free surface for the scenario run. (c) The changes in ground surface temperature (GST) between the time-slices 1981–2001 and 2071–2091, using the bias approach and the same glacier cover for the scenario run as for the present run. (d) The difference in the changes of the ground surface temperature (GST) in [K] between the time-slices 1981–2001 and 2071–2091 when using either the delta or the bias approach.

indirect impacts of climatic changes, in this case glacier disappearance, can have positive feedbacks on another system, in this case permafrost and in this manner even intensify the impacts. Second, this situation can cause a hazard potential such as possible initial zones of debris flows. In 1987, more than 50% of the severe and repeated debris flows in the Swiss Alps (volume > 1000 m^3) were initiated in periglacial areas which were still covered by a glacier 150 years before, but no longer in 1987 (Haeberli et al., 1991; Zimmermann and Haeberli, 1992). Finally, Fig. 4d shows the difference between the model results for the two approaches. The difference between a local scenario time series calculated with the bias or the delta approach is expressed only by the different daily variability of the time series. The resulting difference in the averaged GST is about one Kelvin for the entire test area (Fig. 4d).

Further interpretations are not presented here, since this would require many additional model runs (cf. Discussion), and the aim of this example application is to show how output data of an RCM can be used to drive an alpine permafrost model, rather than to assess the development of the GST for the area of Corvatsch in future.

5. Discussion

In this paper we have introduced two strategies that enable the use of output from regional climate models over topographically complex high-mountain environments.

Please cite this article as: Nadine Salzmann et al., The application of Regional Climate Model output for the simulation of high-mountain permafrost scenarios, Global and Planetary Change (2006), doi:10.1016/j.gloplacha.2006.07.006.

Of the two approaches proposed, the delta approach is the simpler and faster one. It can include only a quantitative change (e.g. increase of temperature) but not a qualitative one (e.g. increase of variability). If a change in the variability ought to be considered the bias approach must be applied. Nevertheless, the calculation of a bias (instead of a direct use of RCM output) is considered essential since the monthly biases calculated in the example application were quite high (cf. Table 2). This applies in particular to complex high-mountain regions where the output of an RCM generally contains more uncertainties than over landscapes with low spatial variability, since such environments are also a challenging territory for RCMs. However, it is also in such areas that the need for RCMs is most obvious (Frei et al., 2003).

The high monthly variation in the temperature bias has also shown that a lapse rate correction of the CHRM output would not automatically reduce the model bias, due to the weak representation of the topography in RCMs. There are too many other uncertainties and errors that influence each other and cannot be identified individually. We thus recommend the calculation and the use of an overall bias, which includes the lapse rate.

In this study, the grid box selection (and also the estimation of the RCM performance for the region of interest) was based on a comparison of the monthly means between the OBS and the CHRM driven from ERA-40 re-analyses. If such a 'perfect boundary run' is not obtainable, the grid box selection is more difficult because it can only be based on systematic error measures not on correlation. Moreover, when using a CTRL run for selecting the 'best' RCM grid box, we have no real indication of the performance of the RCM independently of the GCM. In addition to the missing information about the model error, the result of the determination of the 'best' grid box can be different when using the CTRL rather than the 'perfect boundary run'. In our sample study, the use of CTRL would have resulted in grid box A being the 'best' one for the representation of precipitation at Corvatsch.

The determination of a 'best' grid box is more important for the bias than for the delta approach. For the delta approach the average of the grid box values that are closest to the meteorological station on site can be considered appropriate and may be even more robust than the use of one single grid box. The sensitivity analyses showed that in our example the monthly delta values are not very sensitive in terms of the number of grid boxes (one 'best' or average) included. However, for the bias approach such a 'grid box average approach' is not suitable, since the daily time series of a specific grid box from the SCEN simulation is used as input for the impact model. Any simulated regional extremes, probably represented by only one grid box, would be cut when averaging several grid boxes. Nevertheless, in this study we used one and the same grid box for both approaches in order to allow a better comparison between the two approaches.

The bias approach only uses the monthly biases calculated from the 30-year average change in order to adapt the RCM output to a local site. There are, however, additional ratios and variables that could be calculated, analysed and afterwards used to debias the SCEN output. Additional variables such as T_{min} or T_{max} were analysed to provide a rough assessment of the performance of the CHRM, but not to be used in the calculation of the monthly biases. Additional skill measures are for instance, the frequency or the intensity of precipitation or wind speed, the standard deviation or the comparison of amplitudes. A change in the intensity and the frequency of precipitation would, for example, influence the duration and thickness of the seasonal snow cover, which in turn has a strong impact on the thermal regime in the ground (Zhang et al., 2001; Ishikawa, 2003). However, on the one hand the aim of this study is to present an approach for the use of RCM output for impact modelling rather than to accurately evaluate the performance of the CHRM for the region of the Upper Engadine. On the other hand, debiasing the daily scenario time series with the use of ratios such as the intensity or the frequency, would add substantial complexity. The additional benefit of the extra effort for a 'new' ratio bias should therefore be evaluated first by sensitivity studies of the TEBAL model and the natural system it represents. Depending on the influence of a single variable it needs to be decided whether an intensified effort for some variables is required.

The proposed approaches, in particular the bias approach, require data from long periods of observations. However, for many remote mountain areas, observational data at the required spatial and temporal resolution are lacking and/or difficult to obtain, which reduces the applicability of the proposed approaches. Nevertheless, the data provided by climate models provide global climate change scenarios by feeding the impact models with CTRL and SCEN output. Furthermore, dynamically downscaled re-analysis data sets will be increasingly available in the future and can thus partly replace time series from meteorological stations.

Regarding the example application at the Corvatsch it has to be stressed that this study examines only one single scenario. Scenarios are commonly regarded as being plausible, however they have no future probability

Please cite this article as: Nadine Salzmann et al., The application of Regional Climate Model output for the simulation of high-mountain permafrost scenarios, Global and Planetary Change (2006), doi:10.1016/j.gloplacha.2006.07.006.

attached (Jones, 2000). In addition, there are many errors and uncertainties in the models and the data, which increase when model output is used to drive a second model. Therefore, such results must not be treated as a prediction of the future, since 'the possibility that any single emissions path will occur as described in scenarios is highly uncertain' (Nakicenovic and Swart, 2000). The benefit of such studies is the possibility to assess the sensitivity of ground surface temperature to changes in the atmospheric conditions based on climate models. However, in order to determine a range of possible changes, an impact study must be carried out using a couple of different RCMs with different scenarios and also with several different impact models.

Finally, we must consider whether the application of daily data from an RCM output grid box with a horizontal resolution of about 50 km is appropriate to apply for a small area in complex high-mountain topography. Since we do not apply the RCM output directly to the impact model, but adjust the RCM output using observation data from a 30-year time period, we judge the approach to be reasonable. Furthermore, we applied models and knowledge from the latest research results. At present, these are probably the best instruments available for assessing at least a possible range of the climate change impact. In addition, climate models with higher resolution, which nevertheless on their own do not necessarily guarantee a superior model performance, will be available in near future, for example developed within the framework of the recently launched European project ENSEMBLES (Hewitt and Griggs, 2004). This study aims to act as a catalyst for future investigations of climate change impacts on the cryosphere in high-mountain environments.

6. Conclusion and perspectives

Impact modelling by using output from climate models is an interdisciplinary research field full of promise. Due to the high complexity of climate models and the specialized knowledge needed to handle these data, good collaboration between impact modellers and climate modellers is of critical importance.

As discussed, the amount of information gained from the application of one single RCM run to one single impact model is minimal. Many inherent uncertainties and errors of the models and scenarios even increase in complex terrain and when model output of one model is used to drive a second model. For this reason, this study needs to be repeated with output from different RCMs and scenarios, and more than one permafrost model should be applied.

Furthermore, the most sensitive and thus most important variables for the investigated processes must be determined by performing sensitivity studies with the RCMs and the permafrost impact models. Related to the results of such studies, a smaller amount of effort can be invested in case of less sensitive variables, and more for very sensitive ones. In this way, we can simulate the specific variable for a scenario application by applying a varying degree of effort to the variables related to (i) their importance to the impact process, (ii) the performance of the impact model, and (iii) the RCM.

Acknowledgements

This study was made possible thanks to the European Cooperation in the field of Scientific and Technical Research (COST-Action 719). We are deeply grateful to Christoph Schär for allowing access to CHRM output, and for a very fruitful and friendly collaboration. Further thanks are extended to Stephan Gruber who allowed us to use TEBAL, and to Frank Paul and Wilfried Haeberli for their useful comments. We gratefully acknowledge the constructive remarks of the two reviewers (Ch. Hauck, and anonymous) and the guest editor, which greatly enhanced the manuscript. We are very grateful to Susan Braun-Clarke and Karen Hammes for the English revision of the manuscript.

References

Anisimov, O.A., Shiklomanov, N.I., Nelson, F.E., 1997. Effects of global warming on permafrost and active layer thickness: results from transient general circulation models. Glob. Planet. Change 15, 61–77.

Antic, S., Laprise, R., Denis, B., de Elia, R., 2004. Testing the downscaling ability of a one-way nested regional climate model in regions of complex topography. Clim. Dyn. 23, 473–493.

Arnell, N.W., Hudson, D.A., Jones, R.G., 2003. Climate change scenarios from a regional climate model: estimating change in runoff in southern Africa. J. Geophys. Res. 108 (D16), 4519–4528.

Aschwanden, A., Beck, M., Häberli, Ch., Haller, G., Kiene, M., Roesch, A., Sie, R., Stutz, M., 1996. Bereinigte Zeitreihen - Die Ergebnisse des Projekts Klima90, Bd.1: Auswertungen. Klimatologie der Schweiz, SMA-Zürich, p. 136.

Begert, M., Seiz, G., Schlegel, T., Musa, M., Baudraz, G., Moesch, M., 2003. Homogenisierung von Klimamessreihen der Schweiz und Bestimmung der Normwerte 1961–1990. Schlussbericht des Projektes NORM90, p. 170.

Begert, M., Schlegel, T., Kirchhofer, W., 2005. Homogeneous temperature and precipitation series of Switzerland from 1864 to 2000. Int. J. Climatol. 25, 65–80.

Christensen, J.H., Machenhauer, B., Jones, R.G., Schär, C., Ruti, P.M., Castro, M., Visconti, G., 1997. Validation of present-day climate simulations over Europe: LAM simulations with observed boundary conditions. Clim. Dyn. 13, 489–506.

Christensen, O.B., Christensen, J.H., Machenhauer, B., Botzet, M., 1998. Very high-resolution regional climate simulations over Scandinavia — present climate. J. Clim. 11, 3204–3229.

Please cite this article as: Nadine Salzmann et al., The application of Regional Climate Model output for the simulation of high-mountain permafrost scenarios, Global and Planetary Change (2006), doi:10.1016/j.gloplacha.2006.07.006.

Christensen, J.H., Carter, T.R., Giorgi, F., 2002. PRUDENCE employs new methods to assess European climate change. Eos, Trans. 83, 147.

Damrath, U., 2002. Verifikation von Wettervorhersagen. Promet 28 (1/2), 8–16.

Davies, M.C.R., Hamza, O., Harris, C., 2001. The effect of rise in mean annual temperature on the stability of rock slopes containing ice-filled discontinuities. Permafr. Periglac. Process. 12 (1), 137–144.

Denis, B., Laprise, R., Caya, D., Côté, J., 2002. Downscaling ability of one-way nested regional climate models: the Big-Brother experiment. Clim. Dyn. 18, 627–646.

Diaz, H.F., Grosjean, M., Graumlich, L., 2003. Climate variability and change in high elevation regions: past, present and future. Clim. Change 59, 1–4.

Dickinson, R.E., Enrico, R.M., Giorgi, F., Bates, G.T., 1989. A regional climate model for western United States. Clim. Change 15, 383–422.

Frei, C., Christensen, J.H., Deque, M., Jacob, D., Jones, R.G., Vidale, P.L., 2003. Daily precipitation statistics in Regional Climate Models: evaluation and intercomparison for the European Alps. J. Geophys. Res. 108 (D3), 4124. doi:10.1029/2002JD002287.

Frei, C., Schöll, R., Fukutome, S., Schmidli, J., Vidale, P.L., 2006. Future change of precipitation extremes in Europe: An intercomparison of scenarios from regional climate models. J. Geophys. Res. 111, D06105. doi:10.1029/2005JD005965.

Giorgi, F., 1990. Simulation of regional climate using a limited area model nested in a general circulation model. J. Clim. 3, 941–963.

Giorgi, F., Mearns, L.O., 1991. Approaches to the simulation of regional climate change: a review. Rev. Geophys. 29, 191–216.

Giorgi, F., Hewitson, B., Christensen, J., Hulme, M., Von Stroch, H., Whetton, P., Jones, R., Mearns, L., Fu, C., 2001. Regional Climate Information - Evaluation and Projections. Chapter 10, Climate Change - Third Assessment Report of the Intergovernmental Panel on Climate Change (IPCC). World Meteorological Organization/ United Nations Environment Programme. Cambridge University Press.

Goering, D.J., Kumar, P., 1996. Winter-time convection in open-graded embankments. Cold Reg. Sci. Technol. 24 (1), 57–74.

Gruber, M., Peter, M., Hoelzle, M., Woodhatch, I., Haeberli, W., 2003. Surface temperatures in steep alpine rock faces - a strategy for regional-scale measurement and modelling. Final Int. Conf. Permafrost, Zurich, Switzerland, p. 325–330.

Gruber, S., Hoelzle, M., Haeberli, W., 2004a. Permafrost thaw and destabilization of alpine rock walls in the hot summer of 2003. Geophys. Res. Lett. 31 (13), L13504.

Gruber, S., Hoelzle, M., Haeberli, W., 2004b. Rock-wall temperatures in the Alps: modelling their topographic distribution and regional differences. Permafr. Periglac. Process. 15 (3), 299–307.

Haeberli, W., 1990. Glacier and permafrost signals of 20th-century warming. Ann. Glaciol. 14, 99–101.

Haeberli, W., 1992. Construction, environmental problems and natural hazards in periglacial mountain belts. Permafr. Periglac. Process. 3 (2), 111–124.

Haeberli, W., Beniston, M., 1998. Climate change and its impact on glaciers and permafrost in the Alps. Ambio 27 (4), 258–265.

Haeberli, W., Rickenmann, D., Zimmermann, M., 1991. Murgänge. Ursachenanalyse der Hochwasser 1987, Ergebnisse der Untersuchungen. Mitteilungen des Bundesamtes für Wasserwirtschaft (Bern), p. 4.

Haeberli, W., Wegmann, M., Vonder Mühll, D., 1997. Slope stability problems related to glacier shrinkage and permafrost degradation in the Alps. Eclogae Geol. Helv. 90, 407–414.

Hanson, S., Hoelzle, M., 2005. Installation of a shallow borehole network and monitoring of the ground thermal regime of a high alpine discontinuous permafrost environment, Eastern Swiss Alps. Norw. J. Geogr. 59 (2), 84–93.

Harris, S.A., Pedersen, D.E., 1998. Thermal regimes beneath coarse blocky materials. Permafr. Periglac. Process. 9, 107–120.

Harris, C., Rea, B., Davies, M., 2001. Scaled physical modelling of mass movements on thawing slopes. Permafr. Periglac. Process. 12, 125–135.

Harris, C., Vonder Muehll, D., Isaksen, K., Haeberli, W., Sollid, J.L., King, L., Holmlund, P., Dramis, F., Guglielmin, M., Palacios, D., 2003. Warming permafrost in European mountains. Glob. Planet. Change 39, 215–225.

Hauck, C., 2001. Geophysical methods for detecting permafrost in high mountains. PhD thesis, VAW-ETH Zurich. Mitteilungen Nr. 171, p. 204.

Hewitt, C.D., Griggs, D.J., 2004. Ensembles-based Predictions of climate changes and their impacts. Eos, Trans. 85, 566.

Heyer, E., 1993. Witterung und Klima. Teubner Verlagsgesellschaft, Stuttgart, Leipzig, p. 344.

Humlum, O., 1998. Active layer thermal regime 1991–1996 at Qeqertarsuaq, Disko Island, Central West Greenland. Arc. Alp. Res. 30 (3), 295–305.

Hoelzle, M., Haeberli, W., 1995. Simulating the effects of mean annual air temperature changes on permafrost distribution and glacier size. An example from the Upper Engadin, Swiss Alps. Ann. Glaciol. 21, 400–405.

Hoelzle, M., Wegmann, M., Krummenacher, B., 1999. Miniature temperature dataloggers for mapping and monitoring of permafrost in high mountain areas: First experience from the Swiss Alps. Permafr. Periglac. Process. 10 (2), 113–124.

Hoelzle, M., Vonder Mühll, D., Haeberli, W., 2002. Thirty years of permafrost research in the Corvatsch-Furtschellas area, Eastern Swiss Alps: a review. Norw. J. Geogr. 56, 137–145.

IPCC, 2001. Climate Change 2001: the scientific basis. Contribution of working group 1 to the Third Assessment Report of the Intergovernmental Panel on Climate Change. Cambrige University Press, Cambrige, UK, p. 881.

Isaksen, K., Vonder Mühll, D., Gubler, H., Kohl, T., Sollid, J.L., 2000. Ground surface temperature reconstruction based on data from a deep borehole in permafrost at Janssonhaugen, Svalbard. Ann. Glaciol. 31, 287–294.

Isaksen, K., Holmlund, P., Sollid, J.L., Harris, C., 2001. Three deep alpine-permafrost boreholes in Svalbard and Scandinavia. Permafr. Periglac. Process. 12 (1), 13–25.

Ishikawa, M., 2003. Thermal regimes at the snow–ground interface and their implications for permafrost investigation. Geomorphology 52 (1–2), 105–120.

Jones, R.N., 2000. Managing uncertainty in climate change projections issues for impact assessment. Clim. Change 45 (3/4), 403–419.

Kääb, A., Reynolds, J.M., Haeberli, W., 2005. Glacier and permafrost hazards in high mountains. In: Huber, U.M., Bugmann, H.K.M., Reasoner, M.A. (Eds.), Global Change and Mountain Regions (A State of Knowledge Overview). Springer, Dordrecht, p. 225–234.

Kallberg, P., Simmons, A., Uppala, S., Fuentes, M., 2004. The ERA-40 archive. ERA-40 Project Report, vol. 17, p. 35.

Please cite this article as: Nadine Salzmann et al., The application of Regional Climate Model output for the simulation of high-mountain permafrost scenarios, Global and Planetary Change (2006), doi:10.1016/j.gloplacha.2006.07.006.

Kleinn, J., 2002. Climate change and runoff statistics in the Rhine basin. PhD Thesis, Naturwissenschaften ETH Zürich, Nr. 14663, 2003, p. 114.

Kleinn, J., Frei, C., Gurtz, J., Lüthi, D., Vidale, P.L., Schär, C., 2005. Hydrologic simulations in the Rhine basin driven by a regional climate model. J. Geophys. Res. 110, D04102. doi:10.1029/2004JD005143.

Lüthi, D., Cress, A., Frei, C., Schär, C., 1996. Interannual variability and regional simulations. Theor. Appl. Climatol. 53, 185–209.

Machenhauer, B., Windelband, M., Botzet, M., Hesselbjerg, J., Déqué, M., Jones, G.R., Ruti, M., Visconti, G., 1998. Validation and analysis of regional present-day climate and climate change simulations over Europe. Rep., vol. 275. Max-Planck Inst. of Meteorol., Hamburg, p. 87.

Maisch, M., 1992. Die Gletscher Graubündens: Rekonstruktion und Auswertung der Gletscher und deren Veränderungen seit dem Hochstand von 1850 im Gebiet der östlichen Schweiz. Teil A: Grundlagen - Analysen - Ergebnisse. Zürcher Geographisches Institut der Universität Zürich.

Majewski, D., 1991. The Europa Modell of the Deutscher Wetterdienst. Proceedings of the ECMWF Seminar on Numerical Methods in Atmospheric Models, vol. 2, p. 147–191.

McGregor, J.L., 1997. Regional Climate Modelling. Meteorol. Atmos. Phys. 63, 105–117.

Mearns, L.O., Mavromatis, T., Tsvetsinskaya, E., Hays, C., Easterling, W., 1999. Comparative responses of EPIC and CERES crop models to high and low resolution climate change scenarios. J. Geophys. Res. 104 (D6), 6623–6646.

Mearns, L.O., Easterling, W., Hays, C., Marx, D., 2001. Comparison of agricultural impacts of climate change calculated from high and low resolution climate model scenarios: Part I. The uncertainty due to spatial scale. Clim. Change 51, 131–172.

Mittaz, C., Imhof, M., Hoelzle, M., Haeberli, W., 2002. Snowmelt evolution mapping using an energy balance approach over an alpine terrain. Arc. Alp. Res. 34 (3), 274–281.

Nakicenovic, N., Swart, R. (Eds.), 2000. Emissions Scenarios 2000. Special Report of the Intergovernmental Panel on Climate Change. Cambridge University Press, UK, p. 570.

Oke, T.R., 1987. Boundary Layer Climates, 2nd edn. Routledge, London/New York, p. 435.

Osterkamp, T.E., 1983. Response of Alaskan permafrost to climate. Final Int. Conf. Permafrost, Fairbanks, Alaska. NAS, Washington, pp. 145–152.

Pan, Z., Christensen, J.H., Arritt, R.W., Gutowski Jr., W.J., Takle, E.S., Otenio, F., 2001. Evaluation of uncertainties in regional climate change simulations. J. Geophys. Res. 106 (D16), 17735–17752.

Räisänen, J., Hansson, U., Ullersteig, A., Döscher, R., Graham, L.P., Jones, C., Meier, H.E.M., Samuelson, P., Willen, U., 2004. European climate in the late twenty-first century: regional simulations with two driving global models and two forcing scenarios. Clim. Dyn. 22, 13–31.

Schär, C., Vidale, P.L., Lüthi, D., Frei, C., Häberli, M., Liniger, M.A., Appenzeller, C., 2004. The role of increasing temperature variability for European summer heat waves. Nature 427, 332–336.

Schiermeier, Q., 2003. Alpine thaw breaks ice over permafrost's role. Nature 424, 712.

Schmidli, J., Frei, C., Vidale, P.L., 2005. Downscaling from GCM precipitation: A benchmark for dynamical and statistical downscaling methods. Int. J. Climatol. 26 (5), 679–689.

Schüpp, M., 1954. Witterungsklimatologie der Schweiz. In: Flohn, H. (Ed.), Witterung und Klimatologie in Mitteleuropa.-2. Aufl., Forschungen zur deutschen Landeskunde, vol. 78, pp. 159–167.

Schwarb, M., Frei, C., Schär, C., Daly, C., 2000. Mean annual precipitation throughout the European alps 1971–1990. Hydrological Atlas of Switzerland, Zurich.

Smith, M.W., Riseborough, D.W., 1996. Ground temperature monitoring and detection of climate change. Permafr. Periglac. Process. 16, 313–335.

Smith, M.W., Riseborough, D.W., 2002. Climate and the limits of permafrost: A zonal analysis. Permafr. Periglac. Process. 13 (1), 1–15.

Stendel, M., Christensen, J.H., 2002. Impact of global warming on permafrost conditions in a coupled GCM. Geophys. Res. Lett. 29 (13), GL014345.

Stocker-Mittaz, C., Hoelzle, M., Haeberli, W., 2002. Modelling alpine permafrost distribution based on energy-balance data: a first step. Permafr. Periglac. Process. 13, 271–282.

Stull, R., 1988. An Introduction to Boundary Layer Meteorology. Kluwer Academic Publishers, Amsterdam, p. 666.

Vidale, P.L., Lüthi, D., Frei, C., Seneviratne, S.I., Schär, C., 2003. Predictability and uncertainty in a regional climate model. J. Geophys. Res., [Atmos.] 108 (D18), 4586. doi:10.1029/2002JD002810.

Visser, H., Folkert, R.J.M., Hoekstra, J., de Wolff, J.J., 2000. Identifying key sources of uncertainty in climate change projections. Clim. Dyn. 45, 421–457.

Vonder Mühll, D., Stucki, T., Haeberli, W., 1998. Borehole temperatures in Alpine permafrost: a ten years series. 7th International Conference on Permafrost (Yellowknife. 23–27 June 1998). Collection Nordicana, vol. 57. Centre d'études nordiques, Université Lavai, Québec, p. 1089–1095.

Wild, M., Ohmura, A., Cubasch, U., 1997. GCM simulated surface energy fluxes in climate change experiments. J. Climate 10, 3093–3110.

Wood, A.W., Leung, L.R., Sridhar, V., Lettenmair, D.P., 2004. Hydrological implications of dynamical and statistical downscaling approach to downscale climate model outputs. Clim. Change 62, 189–216.

Zhang, T., Barry, R.G., Haeberli, W., 2001. Numerical simulation of the influence of the seasonal snow cover on the occurrence of permafrost at high altitudes. Norw. J. Geogr. 55, 261–266.

Zimmermann, M., Haeberli, W., 1992. Climatic change and debris flow activity in high-mountain areas: a case study in the Swiss Alps. Cat. Suppl. - Stat. Can. 22, 59–72.

Please cite this article as: Nadine Salzmann et al., The application of Regional Climate Model output for the simulation of high-mountain permafrost scenarios, Global and Planetary Change (2006), doi:10.1016/j.gloplacha.2006.07.006.

Paper 2

Ground-surface temperature scenarios for complex high-mountain topographies based on Regional Climate Model results

Nadine Salzmann[1], Jeannette Nötzli[1], Christian Hauck[2], Stephan Gruber[3,1], Martin Hoelzle[1], Wilfried Haeberli[1]

[1] *Glaciology and Geomorphodynamics Group, Department of Geography, University of Zurich, Winterthurerstrasse 190, 8057 Zurich, Switzerland*

[2] *Institute for Meteorology and Climate Research, University of Karlsruhe/Forschungszentrum Karlsruhe, 76021 Karlsruhe, Germany*

[3] *Laboratoire EDYTEM, CISM Université de Savoie, 73 376 Le Bourget-du-Lac Cedex, France*

in press, Journal of Geophysical Research – Earth Surface

Abstract

Climate change can have a severe impact on the high-mountain cryosphere, such as rockwall instabilities induced by thawing permafrost. However, relating climate change scenarios as produced from global and regional climate models (GCM, RCM) to complex high-mountain environments is a challenging task. In particular, the qualitative and quantitative impact of changes in the climatic conditions on the local to micro scale ground-surface temperature (GST) and thus the ground thermal regime is not entirely known. This study assesses a possible range of changes in the GST (ΔGST) in complex mountain topography. In order to account for the uncertainties associated with RCM output, a set of 12 different scenario climate time series (including ten RCM-based and two incremental scenarios) was applied to the energy-balance model TEBAL to simulate the average ΔGST for 36 different topographical situations. The variability of the simulated ΔGST is mainly related to the emission scenarios, the RCM and the approach used to apply the RCM results to the impact model. In terms of topography, a significant influence on the GST simulation was shown by aspect, because it modifies the received amount of solar radiation at the surface. In addition, N-faces showed a higher sensitivity to the applied climate scenarios, while the uncertainties are higher for S-faces. Based on the results of this study, the use of RCM-based scenarios recommended for mountain permafrost impact studies, as opposed to the use of incremental scenarios.

Keyword: RCM, scenario, high-mountain, complex topography, modeling, permafrost

1. Introduction

The ground thermal regime in high-mountain areas is primarily determined by regional atmospheric processes, the local surface and subsurface characteristics, the topography and the heat flux from the earth's interior. Climatic changes cause changes in the ground surface temperature (ΔGST), which are determined by the energy balance at the surface. The ΔGST will be propagated in the subsurface via heat conduction. In mountain areas with widespread permafrost occurrence such changes can have a severe impact, for example on the stability of rockwalls, of debris slopes and infrastructure [*Haeberli et al.*, 1997; *Diaz et al.*, 2003; *Schiermeier*, 2003; *Kääb et al.*, 2005]. *Davies et al.* [2001] demonstrated that rising temperature influences the stability of frozen rock joints with a minimal stability reached slightly below 0°C.

The assessment of climate impacts on mountain permafrost is, however, challenging. The simulation of climate scenarios on a regional to local scale, as required for regional climate impact studies, is generally difficult and associated with many uncertainties [e.g. *Noguer et al.,* 1998; *Visser et al*., 2000; *Giorgi et al.*, 2001]. Thereby, mountain regions are among the most ambitious areas for simulating future climate conditions [*Denis et al*., 2002; *Frei et al*., 2005], mainly due to their spatially highly heterogeneous environment and the regional to local climatic subsystems that are chiefly caused by topography. In terms of climate impacts on mountain regions, the high-mountain cryosphere constitutes a particularly sensitive system due to its proximity to melting conditions [*Haeberli and Beniston,* 1998]. It is not clear in detail, how climatic changes will affect the GST in complex mountain topography.

Currently, the only physically plausible tools to simulate regional climate change scenarios are Regional Climate Models (RCMs) [e.g. *Giorgi and Mearns*, 1999; *IPCC,* 2001]. The possibilities of applying RCM results to an energy balance model for the simulation of GST in complex high-mountain topography has so far been illustrated and discussed in detail by *Salzmann et al.* [2006a]. However, the use of one single RCM scenario is not sufficient for assessing the possible range of changes in the GST, because of the uncertainties associated with the modeling of scenario climate conditions. These uncertainties mainly arise from the uncertainties of the forcing emission scenarios [*Nakicenovic et al.*, 2000] and of the GCMs/RCMs [e.g. *Visser et al*., 2000; *Pan et al*., 2001; *Noguer et al*., 2003; *Vidale et al.,* 2003] and from possible future changes in the climate variability [*Schär et al*., 2003]. When applying the RCM results to an impact model, the impact model itself is another source of uncertainties for the final outcome. As a consequence, the assessment of a possible range of changes in the GST requires the application of a multi-model approach that includes various emission scenarios, RCMs, and application procedures.

The present study aims at assessing possible ranges of changes in GST in complex high-mountain topography. For that purpose, changes in the GST are simulated with the energy-balance model TEBAL for 36 different topographic situations, based on 12 different scenario climate time series (including ten RCM-based and two incremental scenario time series). As a first step, the study focuses on steep rockwalls (>50°) because factors such as variable seasonal snow cover [e.g. *Zhang et al*., 2001; *Ishikawa,* 2003; *Zhang,* 2005] and strongly heterogeneous surface layers [e.g., *Gorbunov et al*., 2004; *Hanson and Hoelzle*, 2004], both of which significantly modify the GST, can be neglected. Hence, the ΔGST of steep rockwalls is a direct and unfiltered impact of changed atmospheric conditions. The

influence of changed thermal surface conditions to greater depths is not treated in the present study.

2. Data, Models and Methods

2.1 Locally observed climate time series

The observational data (OBS) are taken from the climate station at Corvatsch (3315 m a.s.l. [46.25/9.49], Upper Engadine, Switzerland) and were provided by MeteoSwiss (Swiss Federal Office of Meteorology and Climatology). The area of Corvatsch is among the most intensely investigated permafrost sites in the European Alps [*Hoelzle et al.,* 2002]. The climate station at Corvatsch was set in operation in 1981. In order to generate an observational time series of Corvatsch that covers the same time period as the time slices of the RCM control runs (CTRL; 1961-1990), the time series of Corvatsch were extended with linear regression by using the neighboring high-elevation climate stations that on the one hand reach back to 1961, and on the other hand show a high correlation with the Corvatsch climate time series [for details see *Salzmann et al*., 2006a].

2.2 Scenario climate time series

A set of 12 daily scenario climate time series was constructed (Fig. 1) to be used with the TEBAL model, described below, which simulates local GST for given topographical situations. The set includes ten RCM-based and two incremental scenario time series.

The RCM-based daily scenario climate time series were created from the results of five RCM simulations that were performed within the European project PRUDENCE (Prediction of Regional scenarios and Uncertainties for Defining EuropeaN Climate change risks and Effects) [see *Christensen et al.*, 2002]. The results of the control (CTRL 1961-1990) and scenario (SCEN 2071-2100) simulations of the following three RCMs were taken:

i) Climate High Resolution Model (CHRM; see [*Lüthi et al*., 1996; *Vidale et al.,* 2003]) from the ETH-Z (Switzerland),
ii) Regional Climate Model (RegCM; see [*Giorgi et al*., 1999; *Pal et al.,* 2000]) from the ICTP (Italy) and
iii) Regional atmospheric climate model (HIRHAM see [*Christensen et al.,* 1996]) from the DMI (Denmark).

As illustrated in Fig. 1, each of these RCMs has been driven by the HadAM3H GCM from the Hadley Centre (UK) as forced by the SRES emission scenarios A2 and B2 (CHRM only by A2). The A2 and B2 emission scenarios [*Nakicenovic et al*., 2000] assume different developments of the amount of greenhouse gas (GHG) emissions for the future. The A2 scenario projects high GHG emissions by assuming high population and energy-growth combined with medium gross domestic production. For the B2 scenario, the driving forces are assumed to be more moderate compared to the A2 scenario and thus a lower level of GHG emission is projected. A GCM forced with the A2 emission scenario simulates higher air temperatures than the same GCM forced with the B2 emission scenario. However, different GCMs simulate a range of possible air temperatures due to model internal limitations [e.g. *Visser et al*., 2000; *Räisänen et al*., 2004]. As a consequence, the lower and upper bounds of the uncertainty ranges of the air temperatures

simulated by different GCMs and the two emission scenarios produce a slight overlap [*IPCC*, 2001].

The outputs of the RCMs were adapted for the high-mountain impact analysis using the so-called '*delta'* and '*bias'* approaches, which are discussed in detail by *Salzmann et al*. [2006a]. Both approaches use the output of the single grid box of the RCM out of the four that are closest to the location of interest (here, Corvatsch), whose monthly data of the CTRL run statistically fit best with the monthly observational time series of Corvatsch. The local daily scenario climate time series (d-SCEN, b-SCEN) are calculated from the single RCM grid box results as follows:

$$\text{Delta: } \text{d-SCEN}_d = \text{OBS}_d + (\text{SCEN}_{30y,m} - \text{CTRL}_{30y,m}) \quad (1)$$

$$\text{Bias: } \text{b-SCEN}_d = \text{SCEN}_d + (\text{CTRL}_{30y,m} - \text{OBS}_{30y,m}) \quad (2)$$

where the subscripts *d* stands for 'daily', *30y* for '30-year mean' and *m* for 'monthly', respectively. For solar radiation and precipitation, ratios are used instead of differences.
The main difference between the two approaches is that the bias approach considers, whereas the delta approach ignores, a possible change in variability.

In this study, the following variables from the RCM results were used: 2 m temperature, precipitation, global radiation and air pressure. Since we neglected the snow cover in our study (due to the rockwall steepness) the most important variables for the calculation of the GST are air temperature and global radiation [*Lewkowicz*, 2001, *Gruber et al.*, 2004]. The monthly 30-year averages of these two variables are shown in Figure 2a and b, for OBS and for the constructed and adapted SCENs for the location of Corvatsch. The 2 m temperature (Fig. 2a) shows largest changes during the summer months for all RCMs and emission scenarios. For the global radiation (Fig. 2b), the largest changes are simulated for the (early) summer months.

In addition to the RCM-based scenario climate time series, two incremental scenario time series were created (cf. Fig. 1). For these time series the observed air temperature was increased by arbitrary amounts of 2°C and 3°C, constantly throughout the 20-year time period. The other climate variables were not modified for these scenarios. Incremental scenario approaches are physically not plausible and thus do not present a credible future scenario [*IPCC, 1994*]. However, such climate scenarios are commonly used in climate (cryosphere) impact studies [e.g. *Hoelzle and Haeberli*, 1995; *Stocker-Mittaz et al*., 2002; *Zemp et al.,* 2006)], albeit actually more to explore system sensitivities than scenarios in an intrinsic manner.

2.3 Modeling the Energy balance in complex topography

The energy-balance model TEBAL (Fig. 3) simulates time series of surface energy fluxes and subsurface temperatures in complex topography, based on observed climate time series (usually taken from a climate station), topographic, and surface and subsurface information (cf. earlier applications: [*Gruber et al.,* 2004a,b]). TEBAL has been developed based on PERMEBAL [*Stocker-Mittaz, 2002; Stocker-Mittaz et al*., 2002]. Clear-sky short-wave incident radiation is modeled taking into account sun-terrain geometry based on *Corripio* [2003], as well as atmospheric attenuation based on a standard atmosphere. Measured global radiation is partitioned into direct and diffuse components [*Erbs et al*., 1982].

Diffuse radiation from the sky and surrounding terrain is calculated in a lumped approach, using sky and terrain view factors and ground albedo [*Stocker-Mittaz et al*., 2002]. Long-wave radiation from the sky [*Konzelmann et al*., 1994] and surface temperatures are used to calculate long-wave irradiance in complex topography using terrain and sky view factors [*Plüss and Ohmura*, 1997]. For steep rockwalls, the turbulent latent heat flux was reduced by a factor of 100 due to the assumed lack of snow cover and surface water. Vapor pressure is parameterized according methods described by *Flatau et al*. [1992] and *Plüss* [1997]. Both latent and sensible turbulent fluxes were calculated using the bulk method [*Oke ,*1987, cf. *Suter et a.,l* 2004]. The residuals of the surface energy balance are assigned to the ground heat flux and used as boundary condition for a 1D Crank-Nicholson subsurface heat-conduction scheme. The resulting temperature for the surface node is converged with the initial guess of surface temperature using a secant iteration procedure. Effects of latent heat during freeze or thaw of water in the rock is included as apparent heat capacity based on an exponential representation of unfrozen water content.

We have validated the version of TEBAL used in this study by simulating 14 logger-measured rockwall temperature time series in the Swiss Alps during the hydrological year 2001/2002 by only adjusting slope, elevation and aspect to each logger site as described by *Gruber et al*. [2004]. The driving daily time series were taken from the climate stations Corvatsch (3315 m a.s.l.) and Jungfraujoch (3580 m a.s.l.). The atmospheric lapse rate was taken as 0.006 Km-1, the volumetric heat capacity was set to 1.8 x 106 Jm-3K-1 and the thermal conductivity to 2.2 WK-1m-1, based on *Cermák and Rybach* [1982] and *Wegmann, et al*. [1998]. Horizons (e.g., local shadow effects) of the logger sites were not included in the validation runs. The overall simulation of the rockwall daily mean temperatures resulted in a mean coefficient of determination of $r^2 = 0.85$, an RMS of 3.31 and in a mean absolute difference in MAGST (mean annual ground-surface temperature) of 1.05 °C.

2.4 Applied approach design

The 20-year observed daily climate time series (OBS: 1982-2002) from Corvatsch and the 12 constructed scenario climate time series (2071-2091) were applied to TEBAL in order to calculate the averaged 20-year mean daily GST for 36 specific topographic situations, including three elevation levels (2500, 3500, 4500 m a.s.l.), four slope angles (50°, 60°, 70°, 80°) and three aspect slopes (N, E/W, S). East and west are not differed because daily mean values were used. For the initialization of the temperature profile in TEBAL, a two-year spin-up time in each TEBAL run was included. Equal surface characteristics were used for each run. According to an 'idealized' high-mountain rockwall, the following values were taken: roughness length = 0.0001 m, emissivity = 0.96 and albedo = 0.2.

The change in GST (ΔGST) for each of the 36 topographical situations were calculated by subtracting the 20-year average GST based on the OBS climate time series from each of the 20-year average GST based on the constructed scenario climate time series.

3. Overview of the simulated results

An overview of the simulated changes in the average GSTs and their complex distribution is given in Figure 4, which is summarized with the Figures 5, 6, 7. In the following, the

main findings, denoted by the letters (a) – (f) are mentioned shortly, before the results are discussed in more detail in the subsequent chapter.

(a) The range of simulated ΔGST is quite high, on average about 3.5 °C in this study. This high result variability is mainly caused by the use of different emission scenarios, of different RCMs and of the two approaches (delta and bias) applied. The relative distribution of the individually calculated ΔGST points within the calculated ranges is relatively constant throughout all topographic situations.
(b) Of the three topographic parameters, only aspect has a significant influence on the ΔGST.
(c) Notable in this context is the distinction between the incremental scenarios (crosses) and the RCM-based scenarios (all other symbols). While the latter (except rea2d) lead to significantly higher ΔGST for N-facing slopes than for S-facing slopes, the incremental scenarios are not sensitive to aspect.
(d) The highest ΔGSTs are achieved by applying the A2 emission scenario (filled markers).
(e) If variability is allowed to change between OBS and SCEN (bias approach), the increase in ΔGST is reduced in our study (squares).
(f) The approach used can reverse the result that A2-forced scenario simulations generally yield higher ΔGST than B2-forced scenarios. Here, the same RCM forced once with the B2 and once with the A2 emission scenario can result in higher ΔGST with B2, depending on the approach applied (see also Section 4.4).

4. Discussion

4.1 Higher sensitivity of N-faces

A summary based on the median of all RCM-simulation runs is given in Figure 5. The median is assumed to represent the 'best guess' of all modeled ΔGST. This median is shown for different aspects (x-axis), elevation-levels (color) and slopes (vertical extent). A prominent feature in Fig. 5 is the difference between the RCM-based scenarios and the incremental scenarios. While the RCM-based scenarios show a difference in ΔGST between N-faces and S-faces of about 1°C, sensitivity of the incremental scenarios to aspect is not evident. This is caused by the differences in the solar radiation received at the surface. For the incremental scenarios air temperature was modified but not the variable global radiation. This is in contrast to the RCM-based scenarios, where both variables were modified. The higher sensitivity of N-faces compared to S-faces simulated by the RCM-based scenarios is probably caused by the different solar radiation received at the surface of N- and S-faces. While the average GST of S-faces is mainly a function of the air temperature and the incoming solar radiation throughout the entire year, the average GST of N-faces in winter is to a larger extent dependent on air temperature, because no direct solar radiation is received at the surface during that time of the year. Since the projected change of global radiation is highest during the summer months (see Fig. 2b), the relative change of global radiation is higher for N-faces than for S-faces. As a consequence, N-faces are more sensitive to the climate scenarios applied in this study.

A further prominent result from Fig. 5 is that aspect is the only topographic parameter with a significant influence on ΔGST. The effects of elevation and slope are very small and probably within the internal noise level of the models. This result reflects the relatively

high sensitivity of GST to the received solar radiation at the surface, which is in turn a function of aspect.

4.2 Higher variability in S-faces

Figure 6 shows the 'range of ΔGST' (*R*ΔGST). In contrast to the ΔGST, which decreases from N to S (see Fig. 5), the *R*ΔGST increases from N to S by about 1°C. The variability and thus the uncertainty about the ΔGST are therefore higher in S-faces than in N-faces. Again, this is caused by the higher influence of solar radiation on S-faces, which receive solar radiation during the entire year, while N-faces only receive solar radiation during the summer months.

A similar, but less pronounced effect is theoretically possible by the effect of slope on receipts of solar radiation, since steeper slopes theoretically receive less solar radiation during the annual cycle [e.g. *Oke,* 1987]. However, the value of this effect depends on the related latitude and aspect. In this study, the effects of slope (and also of elevation) are weak.

4.3 Changes in N-S differences

Under current climate conditions in the Swiss Alps, there is a measured difference in mean annual GST of about 6-8°C between N-exposed and S-exposed rockwalls [*Gruber et al*., 2004]. Assuming that the results of the Section 4.1, i.e., a higher sensitivity of N-faces, is valid for the entire Swiss Alps, the observed differences in rockwall GST would decrease under future scenario climate condition as the GST in N-faces would increase to a larger amount than in S-faces. Such aspect-dependent warming of the surface will also affect the qualitative changes of the ground thermal regime [Noetzli et al. subm.] and can lead for example to enhanced rock fall activities in northern slopes as already observed in the European Alps during the hot and dry summer of 2003.

Large decreases (up to about 2°C) of the N-S temperature differences result for HIRHAM and RegCM applied with the bias approach, independent of the forced emission scenario (Fig. 7). Small decreases result with the delta approach, independent of the RCM type and emission scenario. The change in climate variability is thus a dominant factor for the differential warming of N- and S-faces in the applied climate scenarios.

4.4 Combined influences of emission scenario, RCM, changed variability and topography

Generally, the largest ΔGST is achieved by applying the A2 and the lowest by applying the B2 emission scenario, in both cases independent of the RCM type. This tendency can, however, be reversed by the type of RCM used (Fig. 4), which is consistent with the known uncertainties of GCMs/RCMs due to model internal limitations, as mentioned in Section 2.2. Remarkable in this context is that a change in the climate variability (in our case forced by the use of the bias approach), together with a potentially higher amount of received solar radiation (e.g. due to south slope), can result in a higher ΔGST with the B2 than with the A2 emission scenario, although the same RCM is used. This can be seen in Fig. 4 (f), where HIRHAM simulates higher ΔGST with the B2 emission scenario when the delta approach is applied than with the A2 emission scenario and the bias approach. This HIRHAM specific behavior is likely to be caused by the higher global radiation of

HIRHAM B2 compared to HIRHAM A2 during summer (Fig. 2b) and/or by the change in variability associated with the use of the bias approach.

The lowest values of the *R*ΔGST in S-faces are modeled by the HIRHAM B2 used with the bias approach (see Fig. 4 and 6). In N-faces, the RegCM B2 used with the delta approach yields the lowest values of the range of GST change. The highest values are obtained by HIRHAM A2 scenario used with the delta approach for almost all topographical situations (Fig. 4). This is very likely caused by highest simulated annual air temperature of HIRHAM A2, during almost the entire year (see Fig. 2a).

However, a detailed explanation of the model behavior requires an extended analysis of the daily time series instead of the analysis of averages, as presented here.

4.5 Significance of the results

The results of this study are only valid for the specific and theoretical high-mountain situation assumed here. For other regions of the Alps the results must be justified at least for each of the different climatic regions of the Alps e.g. after *Schuepp* [1954] separately by one representative location. For less steep rockwalls than assumed in this study and larger areas, the important influence of a seasonal isolating snow cover and its changes in the timing and the duration must be taken into account. Furthermore, different results would achieve for differences in surface properties and the effects of a surface layer such as debris cover must be taken into consideration, too. Moreover, only three RCMs and two emission scenarios forced from only one GCM were used in this study. The use of different driving GCMs would increase the uncertainty range additionally. When intending to simulate ΔGST over a larger area requiring use of a Digital Terrain Model (DTM), the uncertainties due to the DTM must also be considered [*Salzmann et al*., 2006b].

In this study, the importance of global radiation was emphasized. However, global radiation in high-mountain areas is influenced significantly by cloud convection during summer. RCMs with horizontal resolution of 50 km (as has been used here), cannot resolve these sub-grid processes. Therefore, the RCM results for global radiation are associated with high uncertainty, particularly in mountain areas and during summer. However, this uncertainty was damped in this study by adjusting the direct output of the RCMs to a specific location (Corvatsch) using the delta and bias approach.

5. Conclusion and Perspectives

In this study, we have calculated and analysed the ΔGST and the *R*ΔGST for 36 topographical high-mountain situations derived from an input matrix of ten RCM-based scenario time series (including three RCMs, two SRES emission scenarios, two approaches) and of two incremental scenario climate time series. The main conclusions are:

- The use of RCM-based scenarios instead of incremental scenarios for impact studies is to be preferred in complex mountain topography, when a study aims at assessing the possible impact of climate change scenarios as opposed to studying sensitivities of a process or a model.

- The use of multimodel approaches such as inclusion of different emission scenarios and GCMs/RCMs is required to assess possible ranges of future ground surface temperature changes ($R\Delta$GST) and to cover the uncertainty range associated with the models.
- In terms of topography, aspect is more important than slope and elevation for the GST.
- The influence of topography on ΔGST is generally weaker than the influence of the different emission scenarios, RCMs, and application-approaches (delta/bias).
- Changes in the duration and thickness of a seasonal snow cover will probably be the most important factor for changes in the ground thermal regime. Nevertheless, we show in this study that also relatively simple systems like steep rockwalls require detailed investigations about potential changes in GST.

Based on the strong variability of RCM output, there appear to be many uncertainties associated with possible impacts of climate change on GST in the complex topography of high-mountain environments. The range of uncertainties can only be assessed by using physically plausible RCM-based scenarios, which take into consideration qualitative (e.g. increase of variability) and quantitative (e.g. increase of air temperature) changes of different atmospheric variables (e.g. global radiation).

However, if we assume that the general trend of our results is valid for the entire Alpine region, the changes in GST and the subsequence changes in the ground thermal regime can lead to serious rock fall and landslide events that exceed the frequency and magnitude of related empirical knowledge.

The next steps towards assessing scenarios of the ground thermal regime in complex high-mountain topography include the link to the subsurface [e.g. *Noetzli et al*., subm.]. Furthermore, a thorough analysis of the climate input time series from the RCMs and the time series of the GST as well as the single fluxes of the surface energy balance instead of averages are required. The input data set to drive the local energy-balance model TEBAL should be enlarged by including RCMs driven by different GCMs. Finally, the use of probabilistic scenarios could further enhance the expressiveness of the model results [e.g. *Wigley and Raper,* 2001; *Tebaldi et al*., 2005].

Acknowledgements:
This study was made possible thanks to the European Cooperation in the field of Scientific and Technical Research (COST-Action 719) and Swiss National Science Foundation (NF-20-10796./1). The RCM data have been provided through the PRUDENCE data archive, funded by the EU through contract EVK2-CT2001-00132. We acknowledge the comments and suggestions of the editor, the associated editor and the two anonymous reviewers.

References:

Christensen, J. H., O. B. Christensen, P. Lopez, E. Van Meijgaard and M. Botzet (1996), The HIRHAM4 Regional Atmospheric Climate Model, *Scientific Report 96-4*, 51 pp., DMI, Copenhagen.

Christensen, J. H., T. R. Carter and F. Giorgi (2002), PRUDENCE employs new methods to assess European climate change, *EoS Trans., 83*, 147.

Cermák, V. and L. Rybach (1982), Thermal conductivity and specific heat of minerals and rocks, in *Landolt-Börnstein Zahlenwerte und Funktionen aus Naturwissenschaften und Technik*, Neue Serie, Physikalische Eigenschaften der Gesteine (V/1a), edited by G. Angeneister, pp. 305-343, Springer, Berlin.

Corripio, J. G. (2003), Vectorial algebra algorithms for calculating terrain parameters from DEMs and solar radiation modelling in mountainous terrain, *Int. J. Geogr. Inf. Sci., 17*, 1-23.

Davies, M. C. R., O. Hamza and C. Harris (2001), The effect of rise in mean annual temperature on the stability of rock slopes containing ice-filled discontinuities, *Permafrost Periglac. Process., 12*(1), 137-144.

Denis, B., R. Laprise, D. Caya and J. Côté (2002), Downscaling ability of one-way nested regional climate models: the Big-Brother experiment, *Clim. Dyn., 18*, 627-646.

Diaz, H. F., M. Grosjean and L. Graumlich (2003), Climate variability and change in high elevation regions: past, present and future, *Clim. Change, 59*, 1-4.

Erbs, D. G., S. A. Klein and J. A. Duffie (1982), Estimation of the diffuse radiation fraction for hourly, daily and monthly average global radiation, *Sol. Energy, 28*, 293-304.

Flatau, P. J., R. L. Walko and W. R. Cotton (1992), Polynomial fits to saturation vapor-pressure, *J. Appl. Meteorol., 31*, 1507-1513.

Frei, C., J. H. Christensen, M. Deque, D. Jacob, R. G. Jones, P.L. Vidale (2003), Daily precipitation statistics in Regional Climate Models: Evalution and intercomparison for the European Alps, *J. Geophys. Res. 108*(D3), ACL 9-1 – 9-19.

Frei, C., R. Schöll, S. Fukutome, J. Schmidli, P.L. Vidale (2006), Future change of precipitation extremes in Europe: An intercomparison of scenarios from regional climate models, *J. Geophys. Res.*, 111, D06105, doi:101029/2005JD005965.

Giorgi, F. and L. O. Mearns (1999), Introduction to special section: Regional climate modeling revisited, *J. Geophys. Res.-Atm., 104*(D6), 6335-6352.

Giorgi, F., Y. Huang, K. Nishizawa and C. Fu (1999), A seasonal cycle simulation over eastern Asia and its sensitivity to radiative transfer and surface processes, *J. Geophys. Res., 104*, 6403-6423.

Giorgi, F., B. Hewitson, J. Christensen, M. Hulme, H. Von Stroch, P. Whetton, R. Jones, L. Mearns and C. Fu (2001), Regional Climate Information – Evaluation and Projections. Chapter 10, Climate Change – Third Assessment Report of the Intergovernmental Panel on Climate Change (IPCC). World Meteorological Organization / United Nations Environment Programme. Cambridge University Press.

Gorbunov, A.P., S. S. Marchenko and E. Seversky (2004). The thermal environment of blocky materials in the mountain of central asia, *Permafrost and Periglac. Process*., 15: 95-98.

Gruber, S., M. Hoelzle, W. Haeberli (2004a), Rock-wall temperatures in the Alps: modelling their topographic distribution and regional differences, *Permafrost Periglac. Process., 15*(3), 299-307.

Gruber, S., M. Hoelzle, and W. Haeberli (2004b), Permafrost thaw and destabilization of Alpine rock walls in the hot summer of 2003, Geophys. Res. Lett., 31, doi:10.1029/2004GL0250051.

Haeberli, W., M. Wegmann and D. Vonder Mühll (1997), Slope stability problems related to glacier shrinkage and permafrost degradation in the Alps. *Eclogae Geol. Helv., 90*, 407-414.

Haeberli, W. and M. Beniston (1998), Climate change and its impact on glaciers and permafrost in the Alps, *Ambio, 27*(4), 258-265.

Hanson, S. and M. Hoelzle (2004), The thermal regime of the active layer at the Murtel rock glacier based on data from 2002, *Permafrost Periglac. Process*., 15: 273-282.

Hoelzle, M. and W. Haeberli (1995), Simulating the effects of mean annual air temperature changes on permafrost distribution and glacier size. An example from the Upper Engadin, Swiss Alps, *Ann. Glaciol., 21*, 400-405.

Hoelzle, M., D. Vonder Mühll and W.Haeberli (2002), Thirty years of permafrost research in the Corvatsch-Furtschellas area, Eastern Swiss Alps: a review, *Norwegian J. Geography, 56,* 137-145.

IPCC (1994), Climate Change 1994: Radiative forcing of climate change and evaluation of the IPCC IS92 emission scenarios. Cambrige University Press, Cambrige, UK

IPCC (2001), Climate Change 2001: The scientific basis. Report of the Intergovernmental Panel on Climate Change. Cambrige University Press, Cambrige, UK.

Ishikawa, M. (2003), Thermal regimes at the snow–ground interface and their implications for permafrost investigation, *Geomorphology, 52*(1-2), 105-120.

Kääb, A., J.M. Reynolds and W. Haeberli (2005), Glacier and permafrost hazards in high mountains. In: Huber, U.M., Bugmann, H.K.M., Reasoner, M.A. (eds.), Global Change and Mountain Regions (A State of Knowledge Overview). Springer, Dordrecht, pp. 225-234.

Konzelmann, T., R. S. W. Van de Wal, W. Greuell, R. Binanja, E. A. C. Henneken and A. Abe-Ouchi (1994), Parameterization of global and longwave incoming radiation for the Greenland Ice Sheet, *Global Planet. Change, 9*, 143-164.

Lewkowicz, A. G. (2001), Temperature regime of a small sandstone tor, latitude 80 degrees N, Ellesmere Island, Nunavut, Canada, *Permafrost Periglac. Process., 12* (4), 351_366.

Lüthi, D., A. Cress, C. Frei and C. Schär (1996), Interannual variability and regional simulations, *Theor. Appl. Climatol., 53,* 185-209.

Nakicenovic, N. and co-authors (Eds.) (2000), Emissions Scenarios 2000. Special Report of the Intergovernmental Panel on Climate Change Cambridge University Press, UK. pp. 570.

Noetzli, J., S. Gruber, T. Kohl, N. Salzmann and W. Haeberli, Three-dimensional distribution and evolution of permafrost temperatures in idealized high-mountain topography, *J. Geophys. Res.,* (subm.).

Noguer, M., R. G. Jones and J. M. Murphy (1998), Sources of systematic errors in the climatology of a regional climate model over Europe, *Clim. Dyn.,* 14, 691-712.

Oke, T. R. (1987), Boundary layer climates. Routledge, London/New York, 2nd edition. 435p.

Pal, J. S., E. E. Small and E. A. B. Eltahir (2000), Simulation of regional-scale water and energy budgets: Representation of subgrid cloud and precipitation processes within RegCM, *J. Geophys. Res., 105*, 29579-29594.

Pan, Z., J. H. Christensen, R. W. Arritt, W. J. Gutowski, Jr., E. S. Takle, and F. Otieno (2001), Evaluation of uncertainties in regional climate change simulations. *J. Geophys. Res., 106,* 17735-17752.

Plüss, C. (1997), The energy balance over an alpine snowcover, point measurements and areal distribution, 115 pp., Department of Geography, University of Zürich, Zürich.

Plüss, C. and A. Ohmura (1997), Longwave radiation on snow-covered mountainous surfaces, *J. Appl. Meteorol., 36*, 818-824.

Räisänen, J., U. Hansson, A. Ullersteig, R. Döscher, L. P. Graham, C. Jones, H. E. M. Meier, P. Samuelson and U. Willen (2004), European climate in the late twenty-first century: regional simulations with two driving global models and two forcing scenarios, *Clim. Dyn.,* 22, 13-31.

Salzmann, N., C. Frei, P. L. Vidale and M. Hoelzle (2006a), The application of Regional Climate Model output for the simulation of high-mountain permafrost scenarios. *Global Planet. Change*, doi:10.1016/j.gloplcha.2006.07.006.

Salzmann, N., S. Gruber, M. Hugentobler, M. Hoelzle (2006b), The influence of different Digital Terrain Models (DTMs) on alpine permafrost modeling. *J. Environ. Modeling Assessment*, DOI 10.1007/s10666-006-9065-3.

Schär, C., P.L. Vidale, D. Lüthi, C. Frei, M. Häberli, M. A. Liniger and C. Appenzeller (2004), The role of increasing temperature variability for European summer heat waves, *Nature, 427*, 332-336.

Schiermeier, Q. (2003), Alpine thaw breaks ice over permafrost's role, *Nature, 424,* 712.

Schüpp, M., 1954, Witterungsklimatologie der Schweiz. In: Flohn, H.: Witterung und Klimatologie in Mitteleuropa.- 2. Aufl., Forschungen zur deutschen Landeskunde 78, 159-167.

Stocker-Mittaz, C. (2002), Permafrost distribution modeling based on energy balance data. PhD. University of Zurich, Zurich.

Stocker-Mittaz, C., M. Hoelzle and W. Haeberli (2002), Modelling alpine permafrost distribution based on energy-balance data: a first step, *Permafrost Periglac. Process., 13*, 271-282.

Suter S., M. Hoelzle and A. Ohmura (2004). Energy balance at a cold, alpine firn saddle, Seserjoch, Monte Rosa. *Int. J. Clim., 24*, 1423-1442.

Tebaldi, C., R. Smith, D. Nychka and L. O. Mearns (2005), Quantifying uncertainty in projections of regional climate change: a Bayesian approach to the analysis of Multimodel Ensembles, *J. Clim., 18*(10), 1524-1540.

Vidale, P. L., D. Lüthi, C. Frei, S. I. Seneviratne and C. Schär (2003), Predictability and uncertainty in a regional climate model, *J. Geophys. Res. Atmos., 108* (D18), 4586, doi: 10.1029/2002JD002810.

Visser, H., R. J. M. Folkert, J. Hoekstra, J. J. de Wolff (2000), Identifying key sources of uncertainty in climate change projections, *Clim. Dyn., 45*, 421-457.

Wegmann, M., G. H. Gudmundsson and W. Haeberli (1998), Permafrost changes in rock walls and the retreat of Alpine glaciers: a thermal modelling approach, *Permafrost Periglac. Process., 9*, 23-33.

Wigley, T. M. L. and S. C. B. Raper (2001), Interpretation of high projections for global-mean warming, *Science,* 293, 451-454.

Zemp, M., W. Haeberli, M. Hoelzle, F. Paul (2006), Alpine glaciers to disappear within decades? Geophys. Res. Lett., *33*, L13504, doi:10.1029/2006GL026319.

Zhang, T., R.G. Barry and W. Haeberli (2001), Numerical simulation of the influence of the seasonal snow cover on the occurrence of permafrost at high altitudes, *Norwegian Journal of Geography, 55*, 261-266.

Zhang, T. (2005), Influence of the seasonal snow cover on the ground thermal regime: an overview. *Rev. Geophys., 43*, RG4002, doi:10.1029/2004RG000157.

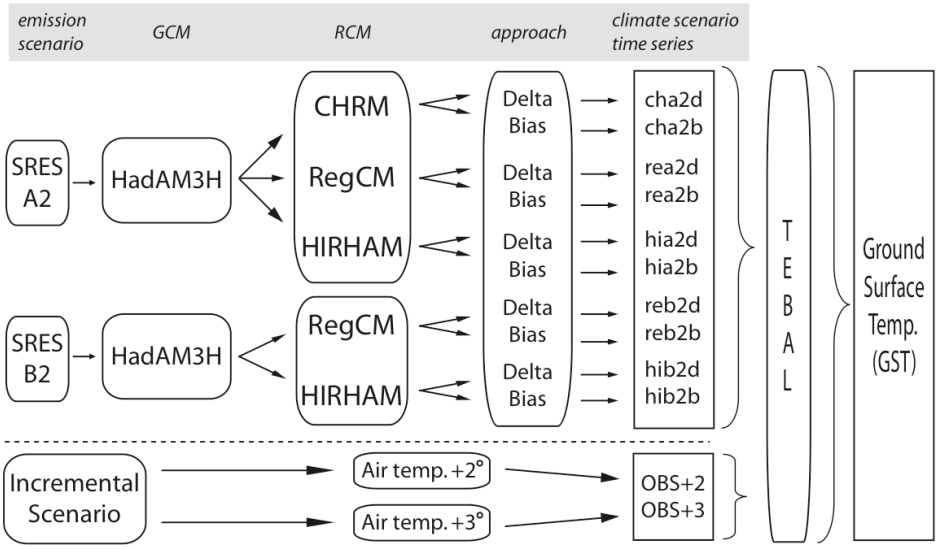

Figure 1
Matrix of the 12 constructed scenario climate time series that are applied to the energy-balance model TEBAL for the simulation of GST.

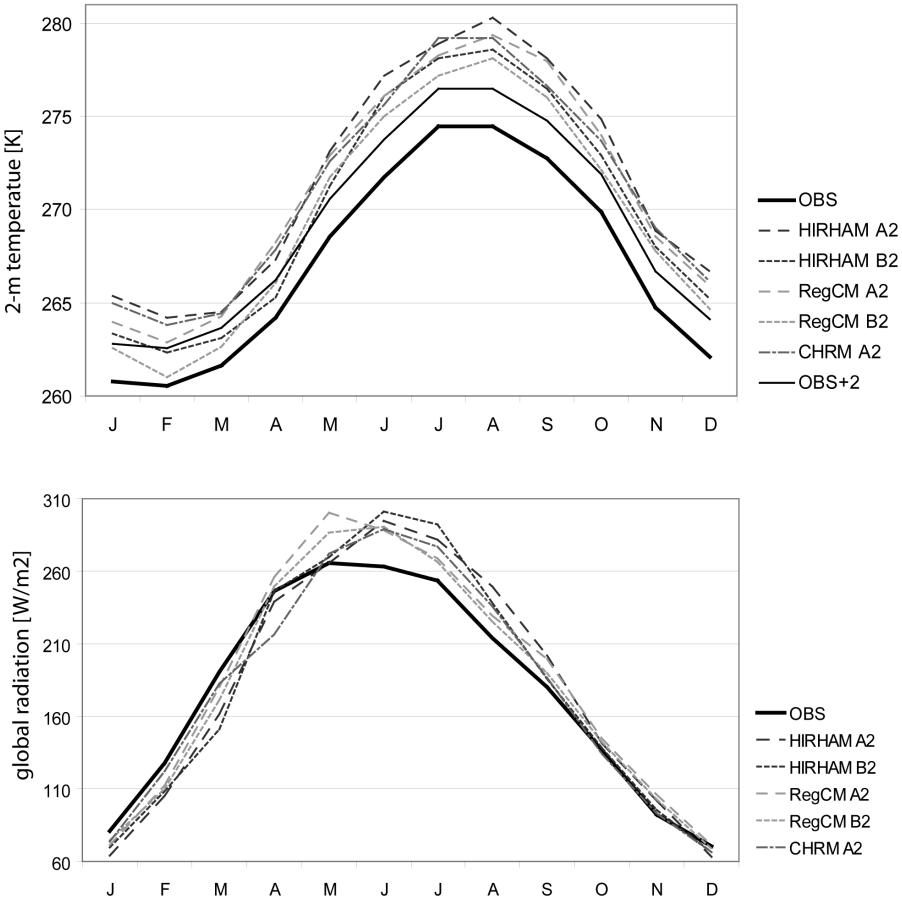

Figure 2a,b
The monthly 30-year averages for (a) 2 m-temperature and (b) global radiation of the OBS (Corvatsch) climate time series and the constructed RCM-based scenario climate time series (adapted for Corvatsch).

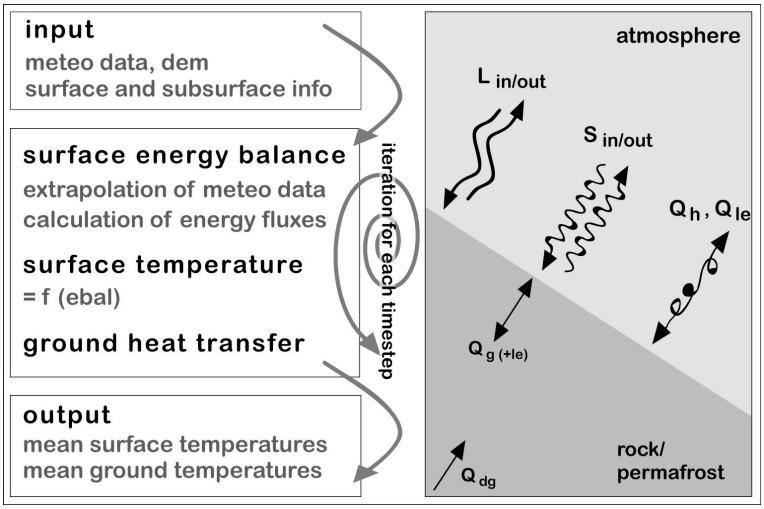

Figure 3
Scheme of the energy-balance model TEBAL.

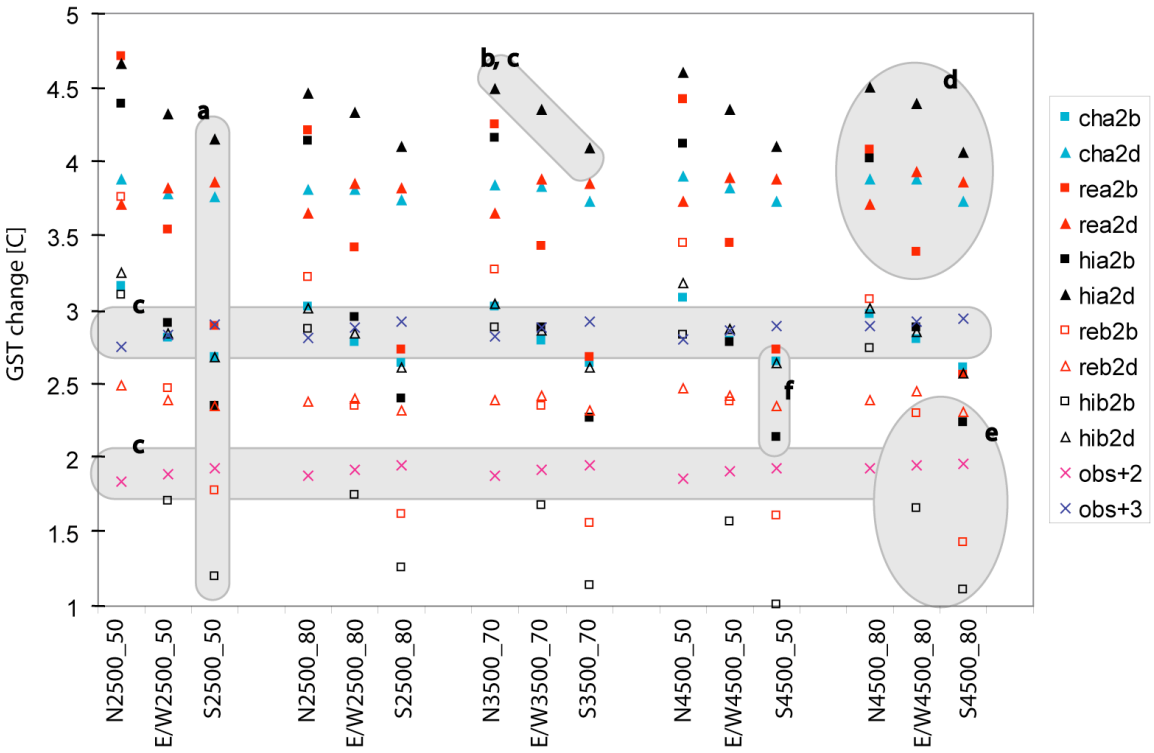

Figure 4
Plot of the 12 simulated changes of GST (ΔGST = SCEN – OBS) for a selection of chosen topographical situations. Each of the triplets (on the x-axis) represents an elevation level with a specific slope that is allocated to the three different aspects (N, E/W, S); N2500_50 stands for: North exposition, 2500 m a.s.l., 50° slope.
Due to the use of daily climate values (i.e. no afternoon convection), east and west are equal. Each RCM is represented by a different marker color. Simulations with the delta approach are represented by a triangle, simulations with the bias approach by a square. Filled markers represent ΔGST based on A2 emission scenarios, unfilled marker represent ΔGST based on B2 emission scenarios. Crosses represent results for the incremental scenarios.
The highlighted subsets of GST results which are marked with letters, are related to the summary in chapter 3.

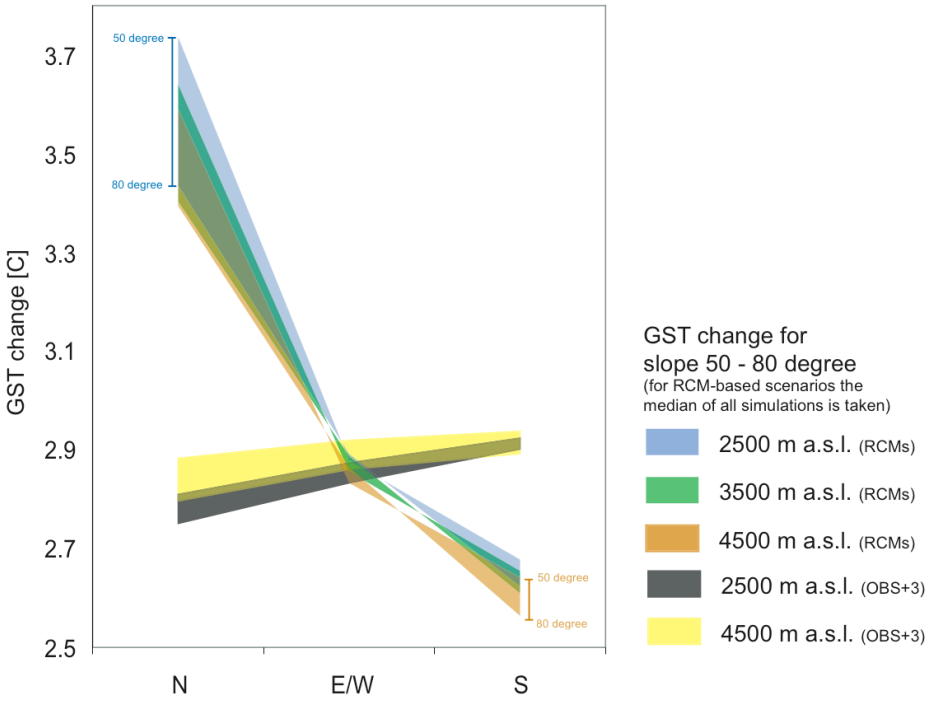

Figure 5
Median of ΔGST for all scenario climate simulations, with separation between RCM-based and incremental scenarios (only OBS+3 is shown) and as a function of aspect (x-axis), elevation (color) and slope (vertical extent).

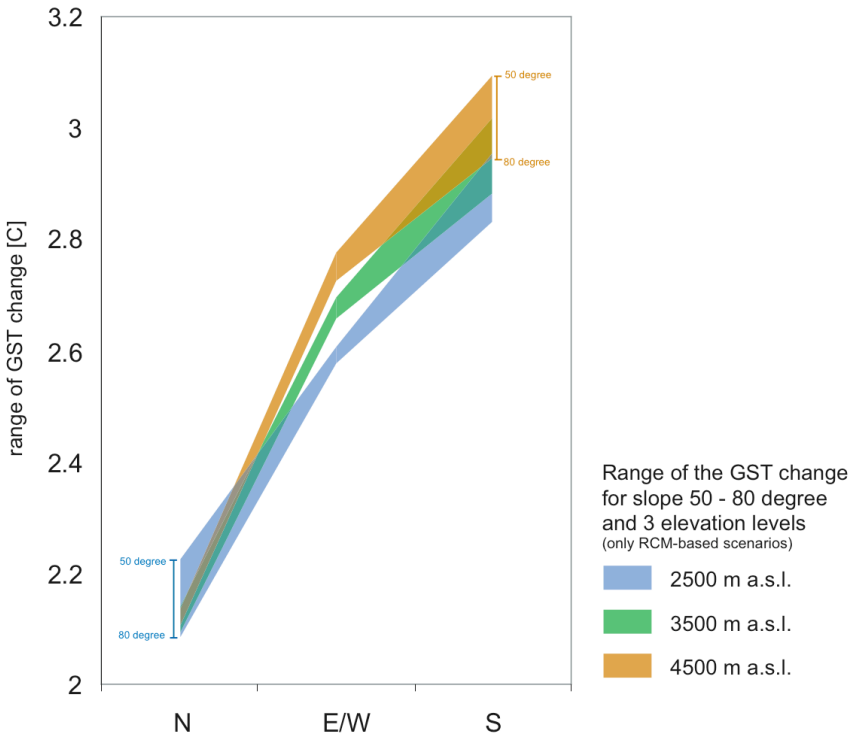

Figure 6
Range of ΔGST (*R*ΔGST) including all scenario climate simulations (except the incremental scenarios) as a function of aspect (x-axis), elevation (color) and slope (vertical extent).

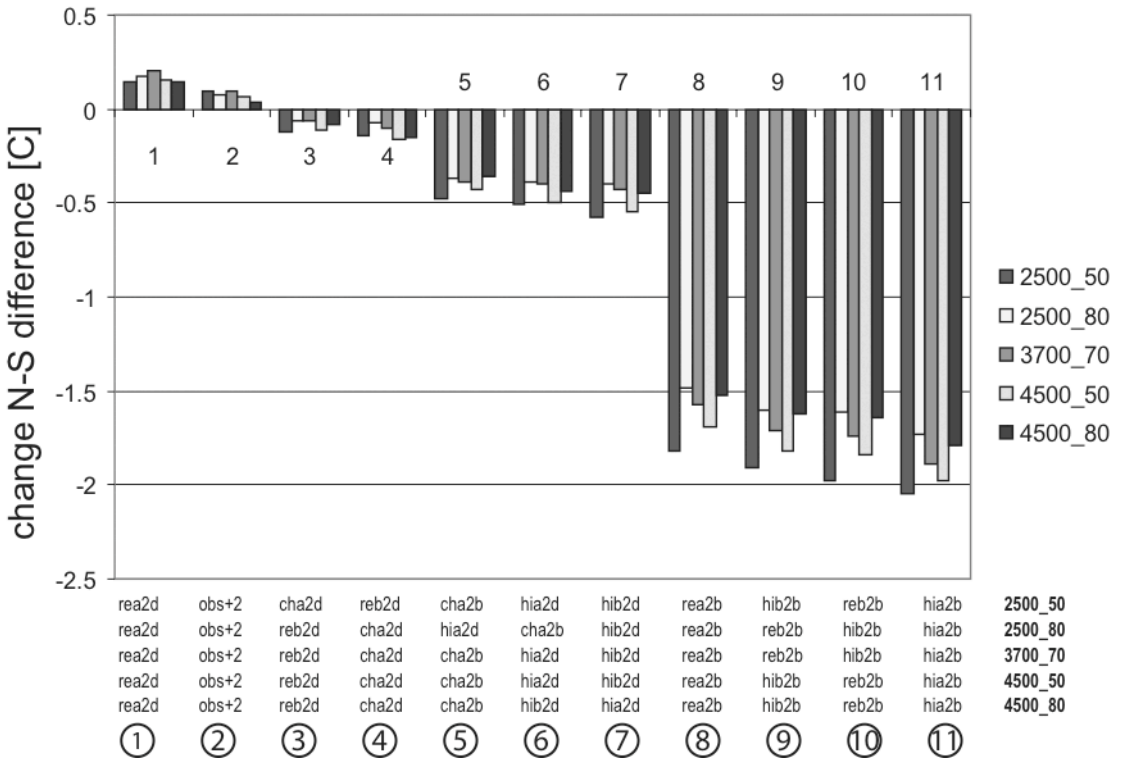

Figure 7
Change in the N-S difference for calculated GST for the scenario climate simulation (except OBS+3) shown as difference to the observed climate time series.

Paper 3

Three-dimensional distribution and evolution of permafrost temperatures in idealized high-mountain topography

Jeannette Noetzli[1], Stephan Gruber[1,2], Thomas Kohl[3], Nadine Salzmann[1] and Wilfried Haeberli[1]

[1]*Glaciology and Geomorphodynamics Group, Department of Geography, University of Zurich, Switzerland*

[2]*EDYTEM Lab, UMR 5204 CNRS – Université de Savoie, France*

[3]*Geowatt AG, Zurich-Oerlikon*

submitted, Journal of Geophysical Research – Earth Surface

Abstract

Permafrost degradation is regarded as a crucial factor influencing the stability of steep rockwalls in alpine areas. Discernment of zones of fast temperature changes requires knowledge about the temperature distribution and evolution at and below the surface of steep rock. In complex high-mountain topography, strong lateral heat fluxes result from topography and variable surface temperatures and profoundly influence the subsurface thermal field. To investigate such 3-dimensional effects, numerical experimentation was conducted using typical idealized geometries of high mountain topography, such as ridges, peaks or spurs. The approach combines a surface energy-balance model with a 3-dimensional ground heat conduction scheme to investigate below ground temperature distribution and permafrost occurrence in high mountain topography. Time-dependent simulations are based on scenario data gained from Regional Climate Models. Results indicate complex 3-dimensional patterns of temperature distribution and heat flow density below mountainous topography for equilibrium conditions, which are additionally perturbed by transient effects. Permafrost occurs at many locations where temperatures at the surface do not indicate it, e.g., on the south face of ridges or below the edges of a peak. The modeling tools applied bear potential for a number of studies in high-mountains addressing questions related to permafrost distribution and evolution at depth in real topographies, as for instance the re-analysis of temperature-related instabilities.

Keywords: permafrost degradation, subsurface temperature distribution, complex topography, temperature evolution.

1. Introduction

Permafrost in European mountains has warmed by 0.5 to 0.8 °C in the upper tens of meters during the past century [Harris*, et al.*, 2003]. This effect is connected to changes in atmospheric conditions and, in view of projected climatic change [*IPCC*, 2001; *Knutti et al.*, 2002; *Stott and Kettleborough*, 2002; *Zwiers*, 2002], is likely to intensify in the future. Permafrost degradation is regarded as one of the crucial factors influencing the stability of steep rock faces in high mountains and a temperature-dependent reduction in rockwall stability has recently been demonstrated both in theory and laboratory experiments [*Davies et al.*, 2001; *Haeberli et al.*, 1997; *Harris et al.*, 2001a]. The exceptional rockfall activity during the hot summer of 2003 in the European Alps [e.g., *Keller*, 2003] provided additional strong evidence for a relation between rockfall and climate change via permafrost degradation and pointed to the serious and fast response of perennially frozen steep rock to increasing air temperatures [*Gruber et al.*, 2004a; *Schiermeier*, 2003]. Frozen rock-joints were shown to reach minimal stability little below 0 °C, i.e., a jointed rock slope may become unstable as the ice warms [*Davies et al.*, 2001]. Thus, instabilities are expected to originate mainly in warm permafrost areas [*Deline,* 2001; *Dramis et al.*, 1995; *Haeberli et al.*, 1997], where the detachment zones of many rockfalls that occurred in the Alpine periglacial areas during the past century are located [*Noetzli et al.*, 2003]. We therefore consider both warming and thawing of permafrost as degradation.

To discern zones of fast permafrost degradation detailed knowledge about the ground temperature distribution and evolution is required, both at and below the surface. In alpine environments most topographic features such as mountain peaks or steep ridges are 3-dimensional in nature and 3-dimensional thermal effects exist in the underground: Variable topography influences the distribution of the heat flow density [*Kohl*, 1999; *Sergueev et al*., 2003] and 2-dimensional variations in surface temperatures lead to 3 dimensional effects in the underground, such as strong lateral heat fluxes [*Gruber et al.*, 2004b]. These effects profoundly affect the temperature distribution at depth, violating the common assumption of predominantly one-dimensional vertical heat transport. Little is known, however, about how these effects influence permafrost occurrence in high mountains. Widely established permafrost distribution models are typically based on proxy variables of selected factors of the surface energy balance without considering the thermal conditions at depth [*Etzelmüller et al*., 2001; *Gruber and Hoelzle*, 2001; *Haeberli*, 1975; *Hoelzle and Haeberli,* 1995; *Hoelzle et al.*, 2001; *Keller*, 1992]. Also newly developed physics-based approaches to determine near-surface temperatures, such as TEBAL [*Gruber*, 2005; *Stocker-Mittaz et al*., 2002], the CoupModel [*Jansen and Karlberg*, 2004] or SNOWPACK [*Bartelt and Lehning*, 2002; *Lehning et al.*, 2002; *Luetschg* 2004], do not take into account a 3-dimensional character of the subsurface heat flow.

This study explores the influence of 3-dimensional high-mountain topography on the subsurface thermal field in steady state, and its evolution over time given changing surface temperatures. We investigate whether there are typical locations exposed to significantly faster permafrost degradation related to topography effects. For this purpose, we developed a modeling chain that considers the processes in the atmosphere (climate), at the surface (energy balance) and in the deeper subsurface (heat conduction): We combined a surface energy balance model with a 3-dimensional heat conduction scheme and for time-dependent calculations we obtained scenario climate time series from Regional Climate Models (RCMs). Owing to the complex and highly variable conditions found in nature, our study is based on numerical experimentation with idealized test cases of typical

topographic features in high-mountains. The results obtained are thus more easy to interpret and a step towards assessing natural and more complex situations.

2. Background

A wealth of studies exists about the influence of inhomogeneous surface conditions (e.g., lakes, buildings) on ground temperatures [for a review see *Gold and Lachenbruch* [1973]) and about the perturbation of a vertical steady state heat flow field induced by topography leading to increased heat fluxes below valleys and lower values below mountain ridges (for a review see *Kohl* [1999]). A few recent studies report on the subsurface thermal regime below complex mountain topography involving transient effects [e.g., *Kohl*, 1999; 2001; *Sergueev*, 2003]. In most studies surface temperatures were held constant or related to air temperatures and their changes alone. Yet in rugged topography the aspect-dependent variation of the radiation balance is a major factor influencing the distribution of surface temperatures [*Mittaz et al.*, 2000]. *Blackwell* [1980] and *Safanda* [1999] calculated surface temperatures subject to variable slope orientation and found that it perturbs the subsurface temperature field and heat flow density significantly. This effect was also discussed by *Kukkonen and Safanda* [2001], but only 1-dimensional vertical heat transfer was considered. First approaches taking into account aspect-dependent surface temperatures as well as 2-dimensional heat fluxes that originate from mountain sides having different temperatures were presented in case studies in the Swiss Alps [*Gruber et al.*, 2004b; *Wegmann et al.*, 1998] and substantial influence of lateral heat fluxes on the ground temperatures was demonstrated. So far, however, the 2- and 3-dimensional influence of both topography and variable surface temperatures on the ground thermal regime in high mountains has not been systematically investigated, and little is known about subsurface permafrost below complex alpine topography.

3. Numerical modeling of ground temperatures in idealized geometries

3.1 Modeling approach

We perform model simulations for idealized test-cases in order to assess natural and more complex situations. We identified ridges and mountain peaks as the main forms typically comprising alpine topography and simplified them to triangular prisms and pyramid geometries (Figure 1). In addition, in many rockwalls spurs can be found that modify the surface. To model thermal surface and subsurface conditions of these geometries we generated corresponding artificial digital elevation models (DEMs) of triangular prisms, pyramids and surfaces with spurs and varied their topographic attributes: elevations were set between 2000 and 4500 m a.s.l., representing the common elevation range of permafrost in the Alps, slope values were set between 50° and 70°, corresponding to the typical slope range for steep rockwalls in high mountains, and the four main slope orientations were considered. The spatial resolution of the DEMs was set to 20 m, a resolution often used in regional-scale permafrost modeling [Salzmann et al., 2006a]. However, for the regular geometric forms considered here the spatial resolution is not significant.

Ground temperatures for geometries were modeled by coupling an energy balance model and a heat-conduction scheme (Figure 2). The energy balance model TEBAL [*Gruber,* 2005; *Stocker-Mittaz et al.*, 2002] is driven by climate time series and calculates mean

annual ground surface temperatures (MAGST). These are imposed as upper boundary condition in the numerical heat conduction scheme FRACTure [*Kohl and Hopkirk*, 1995], which computes a 3-dimensional subsurface temperature field. In the first step, model simulations were performed for equilibrium conditions to describe the thermal regime of the subsurface under the influence of topography and spatial variability of the surface temperatures alone. In a second step, time-dependent experiments were conducted, allowing for changing surface temperatures induced by climate change. Time-dependent calculations were based on model runs of the energy balance model, driven by scenario climate time series generated based on output from RCMs. RCM output was downscaled to local mountain situations using different application procedures [*Salzmann et al.*, 2006b, in press]. Transient calculations were performed with pure heat conduction and, additionally, taking into account the effect of pore ice and latent heat.

3.2 Modeling of rock surface temperatures

The surface temperature distribution has been identified to be one of the most sensitive parameters when estimating below ground temperatures [e.g., *Rybach and Pfister,* 1994]. Surface temperatures are controlled by the energy balance at the surface and mainly depend on climatologic variables, on topographic factors and on surface characteristics [*Hoelzle et al.,* 2001; *Mittaz et al.,* 2000]. In complex high mountain topography a realistic calculation of surface temperatures is particularly important as they are highly variable in space and time and are the main cause for lateral ground heat fluxes. As thick snow cover and coarse blocky active layers [*Harris and Pederson,* 1998] are largely absent in steep rock, the surface temperatures of a rockwall change primarily with aspect (shortwave radiation), altitude (sensible heat and longwave incoming radiation) and lithology [*Gruber,* 2004c; *Lewkowicz,* 2001; *Wegmann,* 1998].

3.2.1 The TEBAL model

The energy-balance model TEBAL simulates time series of surface energy fluxes and near-surface temperatures in complex topography, based on input of observed climate time series and topographic information (i.e., a single point with known values of elevation, slope and aspect or an input surface grid such as a DEM). Climate time series are usually taken from operational climate stations and include air temperature, air pressure, relative humidity, wind speed and direction, precipitation as well as global radiation in daily or hourly resolution. Surface (albedo, emissivity and surface roughness) and subsurface characteristics (thermal conductivity, heat capacity and pore volume) have to be supplied for each point.

The surface energy balance and resulting temperatures are calculated based on the following steps: Clear-sky short-wave incident radiation is modeled taking into account sun-terrain geometry based on *Corripio* [2003], as well as atmospheric attenuation based on a standard atmosphere. Measured global radiation is partitioned into direct and diffuse components [*Erbs et al*., 1982]. Diffuse radiation from the sky and surrounding terrain is calculated in a lumped approach, using sky and terrain view factors and ground albedo [*Stocker-Mittaz et al*., 2002]. Long-wave radiation from the sky [*Konzelmann et al*., 1994] and surface temperatures are used to calculate long-wave irradiance in complex topography using terrain and sky view factors [*Plüss and Ohmura*, 1997]. For steep rockwalls, the turbulent latent heat flux was reduced by a factor of 100 due to the assumed lack of snow cover and surface water. Vapor pressure is parameterized according methods described by *Flatau et al*. [1992] and *Plüss* [1997]. Both latent and sensible turbulent

fluxes are calculated using the bulk method [*Oke*,1987, cf. *Suter et al,.* 2004]. The residuals of the surface energy balance are assigned to the ground heat flux and used as boundary condition for a 1-dimensional Crank-Nicholson heat-conduction scheme. The resulting temperature for the surface node is converged with the initial guess of surface temperature using a secant iteration procedure. Effects of latent heat during freeze or thaw of water in the rock is included as apparent heat capacity based on saturated conditions and an exponential representation of unfrozen water content.

In the context of this paper, we used the version of the TEBAL model with hourly time steps which allows for the investigation of effects caused by diurnal fluctuations (e.g., convective clouding) that result in differing surface temperatures of east- and west-facing slopes. For daily time steps the TEBAL model has been validated earlier by *Gruber and co-workers* [2004c]. We re-validated the model for hourly time steps in an analogous manner using the same data and parameters: 14 logger-measured rockwall temperature time series in the Swiss Alps for the hydrological year 2001/2002 were simulated and only topographic factors (slope, elevation and aspect) were adjusted to each logger site (Figure 3). Locations of the data loggers are distributed over the elevation range 2000 to 4500 m a.s.l. and all aspects [*Gruber et al.,* 2004c]. The driving time series were taken from the climate stations Corvatsch (3315 m a.s.l.) and Jungfraujoch (3580 m a.s.l., Data source: MeteoSwiss). Surface characteristics were set to albedo=0.2, emissivity=0.96 and roughness length=0.0001 m and an atmospheric lapse of 0.006 Km-1 is assumed. Volumetric heat capacity was set to 2.0 x 106 Jm-3K-1 and thermal conductivity to 2.5 WK-1m-1 based on published values [*Cermák and Rybach*, 1982; *Safanda*, 1999; *Wegmann et al.*, 1998]. The lower boundary of the heat-conduction scheme is set at a depth of 15 m. Due to transient and 3-dimensional effects it is not known whether the heat flux here is positive or negative and it is therefore assumed to be zero.

The overall simulation of daily mean rock temperatures resulted in a mean coefficient of determination (r2) of 0.78 and in a mean absolute difference in MAGST of 1.7 °C which lies within the accuracy range of the previous validation with daily time steps and is considered encouraging. It should be kept in mind that calculated surface temperatures accumulate all errors in the input data, extrapolations (over large horizontal and vertical distances in extreme terrain geometries) and parameterizations of all other variables and fluxes. Convective clouds, for instance, reduce surface temperatures through shading of direct radiation and are spatially and temporally highly variable. The difficulties to model such phenomena may also be the main reason for a small seasonal bias in the differences between modeled and measured temperatures (Figure 3) as cloud effects are mainly important during summer. Furthermore, visibility horizons (e.g., for local shadow effects) or any site specific information other than topographic were not included in the validation runs.

In mountainous topography surface temperatures at a given elevation vary strongly between aspects due to the different amount of direct short-wave solar radiation received. This is the primary factor leading to lateral heat fluxes in the subsurface. It is therefore important for this study to correctly model differences in surface temperature as related to slope exposition. For a check, we compared the temperature offset for modeled and measured data: Modeled temperature differences for a location at an elevation of 3000 m a.s.l. and with a 60° slope are approximately 7 °C between north and south exposition and 2.5 °C between east and west, respectively. These values correspond well to the measured data of rock temperatures [*Gruber et al.*, 2003; *Gruber et al.,* 2004c].

3.2.2 Model TEBAL runs

MAGST was calculated for a ten-year period (1990-1999) using hourly time series from the high elevation site at Corvatsch (3315 m a.s.l.), Upper Engadine (Data source: MeteoSwiss) for the DEMs described above. Surface and subsurface characteristics as well as the lower boundary condition were set according to the validation runs and a spin-up of one year was added before the start of the actual model run to initialize the temperature profile. As only the surface temperatures were used for coupling with the heat conduction scheme a spin-up time of one year is considered sufficient. The resulting MAGST grid was used for coupling with the heat conduction scheme.

3.3 Modeling of subsurface temperatures in bedrock

3.3.1 Thermal processes in bedrock solved by the numerical tool FRACTure

Below ground temperatures in bedrock are generally controlled by the spatial and temporal variations of surface temperatures and the upward flow of heat from the interior of the earth. They are further modified by topography as well as by material properties and advection processes. The effects of fluid flow can be neglected in bedrock permafrost as a first approximation [*Kukkonen and Safanda*, 2001]. Further processes such as radiogenetic heat production are not considered as they only become important at great depth (i.e., >1000 m). In our approach, a conductive transient thermal field under highly variable topography is considered in an isotropic and homogeneous medium [*Carslaw and Jaeger*, 1959]:

$$\frac{\delta T}{\delta t} = \kappa \nabla^2 T \qquad (1)$$

where T[K] is the temperature at times t [s] and k_[m2s-1] is thermal diffusivity, defined as the ratio of thermal conductivity l [Wm-1K-1] to volumetric heat capacity rcp [Jm-3K-1]. This parameter describes the pace at which the signal propagates into the subsurface. Water contained in the pore space and crevices of rock delays the response to surface warming by the uptake of latent heat and can influence the time and depth scales of permafrost degradation by an order of magnitude [*Kukkonen and Safanda*, 2001; *Romanovsky and Osterkamp*, 2000; *Wegmann*, 1998]. The latent heat effect can be handled by substituting an apparent heat capacity rca for the volumetric heat capacity rcp of unfrozen soil in the heat transfer equation [e.g. *Mottaghy and Rath*, 2006], based on an approximately exponential representation of unfrozen water content [*Dash et al.*, 1995; *Williams and Smith*, 1989]:

$$\rho c_a = \rho c_p + \rho_i L_f \frac{d\theta_u}{dT} \qquad (2)$$

where ri is the density of ice, Lf is the specific latent heat of fusion for ice and qu is the volumetric unfrozen water content.

The finite element code FRACTure (Flow, Rock And Coupled Temperature effects) [*Kohl and Hopkirk*, 1995] was broadly applied in the past for temperature calculations below complex topography [*Kohl*, 1998]. Herein the simulator was used for the calculation of the above-described processes of subsurface temperatures in a forward modeling scheme. FRACTure allows for the calculation of heat transfer processes in a full 3-dimensional

formulation. Recent developments enable an easy integration of topography and locally varying surface conditions into a robust and well-tested calculation scheme.

For the definition of the boundary conditions and transient effects the following assumptions were taken: Temporal variations of the near-surface temperatures have diurnal to millennial timescales and lead to thermal disturbances with variable penetration depths and amplitudes [*Lunardini*, 1996; *Kohl*, 1998]. In this study, we ignore annual temperature variations that may penetrate up to about 12 m in bedrock (*Gruber et al.*, 2004b) and only consider long-term variations as related to climate change (time scales of decades to centuries). However, long-term surface temperature variability still occurs on much shorter timescales than the geological processes that determine the geothermal heat flow. Therefore, the climatologic perturbations are treated as transient effects defined for the upper boundaries. The transient thermal field is then superimposed on a steady state temperature regime defined from the lower basal heat flow boundary condition. This corresponds to the approach used by *Pollak and Huang* [2000]. For time-dependent calculations so-called load-time functions were defined that describe the evolution of the upper boundary condition (see below).

3.3.2 Model runs

Structural data such as topography and subsurface material properties were assigned to a discretization scheme with the generation of the finite element (FE) mesh. The FE-mesh was created for different geometries. Vertical refinement was increased from 250 m at depth to 10 m for elements closest to the surface. Laterally, the element size was set to 20 m corresponding to the DEM resolution. Below the geometry, a roughly discretisized rectangle box with a height of 1000 m and no heat transfer across its sides was added. In total, the mesh consisted of around 35'000 nodes. A uniform lower boundary condition heat flux of 70 mWm-2 (*Medici and Rybach*, 1995) was set and as upper boundary condition the modeled MAGST (see above) was imposed.

In the purely diffusive and stationary state, the thermal conductivity is the only petrophysical parameter of importance. It was set to 2.5 WK-1m-1 based on published values [*Cermák and Rybach*, 1982; *Safanda*, 1999; *Wegmann et al.*, 1998]. In transient simulations, the temperature change experienced additionally depends upon the volumetric heat capacity, set to 2.0 x 106 Jm-3K-1 [*Cermák and Rybach*, 1982], and on the ice/water content. The porosity for rock was set to 3% [*Cermák and Rybach*, 1982]. For sensitivity studies thermal conductivity, geothermal heat flux and porosity were varied in the simulations. Transient calculations were conducted with yearly time-steps. Time steps were increased from 10 seconds to 1 year within roughly 100 steps during spin-up. Sensitivity runs with higher refinement of the FE-mesh or changing to smaller time-steps did not significantly change any of the results and a maximum difference in modeled temperatures was assessed to be below 0.1 °C.

3.3.3 Time-dependent calculations

The transient calculations were started from the steady-state conditions of the above-described runs. In FRACTure so called load-time functions are used to calculate time-dependent boundary conditions:

$$T_{n+1} = T_n + \Delta t(1-\gamma)\frac{dT}{dt} \qquad (3)$$

where Tn is the initial boundary condition, Tn+1 is the boundary condition at time tn, Dt is the length of the time step, dT/dt is the time derivative of the local temperature and g is a time integration parameter (i.e., g=0.5 corresponds to the often used Crank-Nicholson scheme).

To define a boundary condition Tn and corresponding load time functions, we calculate future surface temperatures based on TEBAL-runs with scenario climate time series driving the model. The scenario climate time series were generated from output of RCM simulations in the scope of a study by *Salzmann et al.* [accepted]. In their study a matrix of different emission scenarios, RCMs and application procedures was used to assess possible changes in surface temperatures in steep high-mountain rockwalls: A set of 12 RCM-based daily climate time series was created from the results of five RCM simulations that were performed within the European project PRUDENCE [see *Christensen et al.*, 2002]. Three RCMs (CHRM from the ETH-Z in Switzerland [see *Lüthi et al.,* 1996], RegCM from the ICTP in Italy [see *Giorgi et al.*, 1999], and HIRHAM from the DMI in Denmark [see *Christensen et al*., 1996]) were driven by the HadAM3H GCM from the Hadley Center (UK) as forced by the SRES emission scenarios A2 and B2 (CHRM only by A2). The results of the RCM control (1961-1990) and scenario runs (2071-2100) were adapted for high-mountain situations using the so-called delta and bias approaches that are discussed in detail by *Salzmann et al.* [2006b, in press]. The constructed scenario climate time series were applied to TEBAL and the average change in surface temperature was calculated for 36 specific topographical situations. Results showed an approximately 1 °C stronger warming on north-facing rockwalls compared to south-facing rockwalls within the next 100 years and the climate conditions at Corvatsch (3315 m a.s.l.), Upper Engadine, that can mainly be attributed to differing amounts of direct solar radiation received. As the RCM results used do not provide diurnal fluctuations, no difference between the warming in east- and west-facing slopes could be modeled. The exact modeling procedure and detailed results of this study are described by *Salzmann et al.* [accepted].
Based on the results from these scenario runs, three types of linear load-time functions were defined to distinguish warming on north-, south- and east/west-oriented slopes. Possible changes in MAGST between the time periods 1982-2002 and 2071-2091 were simulated for a 60° slope at an elevation of 3500 m a.s.l. Because all scenarios are equally valid, the median of all runs was calculated to derive a best guess of the possible temperature change: for north-oriented slopes we assumed a linear temperature change over the next 100 years of +3.5 °C, for south- and east/west-oriented slopes the change was set to 2.5 °C and 3 °C, respectively.

4. Subsurface temperatures in mountainous topography

4.1 Steady state conditions

Due to the difficulties in illustrating 3-dimensional situations in 2-dimensional graphics the main results are first visualized for cross-sections of ridges. In Figure 4 the ground temperature fields of six idealized ridges with altitudes between 2000 and 4000 m a.s.l., north-south and east-west aspects and a slope of 60° are shown. The permafrost base corresponds to the 0 °C-isotherm and is highlighted by a black line. The temperature distribution is governed by the difference in surface temperatures between the two flanks of the ridges, which leads to near-vertical isotherms in the top part of the ridge. Isotherms are curved as a result of the geometry. The main heat flux is directed horizontally from the warmer to the colder side in the top part and diagonally upwards in the middle part of the

ridge and vertical heat fluxes only exist at the base of the geometry (Figure 5a). The heat flux density is largest at the top due to the largest temperature difference on the shortest distance. In addition, a zone of increased temperature gradients and heat flux can be found at the foot of the colder side. A corresponding zone of lower heat flux density is located in the middle of the warmer side.

A larger difference in MAGST between the two sides of a mountain, i.e. north-south vs. east-west ridges (cf. Figure 4a-c vs. d-f), leads to larger horizontal temperature gradients, to more vertical isotherms and, hence, to a stronger horizontal heat flux. This effect also increases with the steepness of the topography. Changes in elevation have no major effect on the relative temperature distribution pattern. However, as the isotherms are inclined, the shape of the permafrost body changes significantly with elevation (Figure 4). At elevations up to 4000 m a.s.l. thick permafrost exists on both sides. Permafrost thickness (which we consider here in the direction of heat conduction into the subsurface, i.e., vertical to the surface) decreases with increasing height mainly on the warmer side. At elevations lower than ca. 3500 m a.s.l. surface temperatures are above 0 °C on the southern side of our model. But at these heights permafrost may exist right below the surface, induced by the opposite colder mountain flank (e.g., Figure 4b, c, f).

To demonstrate the influence of the geothermal heat flux on the temperature distribution in steep topography, we re-calculated the thermal field of a ridge with a zero heat flux lower boundary condition. The result was then subtracted from the thermal field modeled with the constant lower boundary condition used in the model runs (Figure 6). The influence of the geothermal heat flux decreases exponentially towards the top and becomes negligible in the upper half of the geometry (Figure 6a): the top part of the ridge is virtually decoupled from the half-space below the geometry under consideration. A lower thermal conductivity slightly increases the influence of the geothermal heat flux (Figure 6b), whereas steeper and more extreme topography decreases it.

In a pyramid geometry similar effects can be observed but with four sides having different surface temperatures. With slices taken along the x-, y-, and z-axis the 3-dimensional nature of the permafrost body in alpine topography becomes visible (Figure 7) and effects not present in 2-dimensional ridge situations can be shown. For instance, permafrost can be found only meters to decameters below the surface of the edges of the pyramid: In Figure 8 this is visualized in cross sections along the edges. Additionally, irregularities on rockwall surfaces such as spurs with sides exposed to different aspects may modify the subsurface temperature field. In Figure 9 an example of a spur on a south-facing rockwall is shown. Due to the lower temperatures on the western side of the spur, lower subsurface temperatures are induced inside and even below the spur. This leads, for instance, to local permafrost occurrence in a south-facing rockwall that generally does not contain permafrost.

4.2 Transient ground temperatures

In a simple experiment, time and depth scales of the influence of a climatic signal on ground temperatures can be demonstrated with a 1-dimensinal solution for the vertical temperature distribution and a step-like increase in surface temperature [*Carslaw and Jaeger*, 1959]:

$$T = T_0 \times erfc\left(\frac{z}{2\sqrt{\kappa \times t_i}}\right) \qquad (4)$$

where T0 [K] is the change in MAGST, z [m] is the depth, k [m2s-1] is the thermal diffusivity and ti [s] is the duration after the change. Thus, taking k=1.25 x 10-6 m2s-1, 50% of the amplitude of the temperature step has reached a depth of approximately 60 m after a time period of 100 years and 25% has reached around 100 m. Considering a time period of 200 years the respective values amount to 80 m for 50% and 150 m for 25% of the signal. This means that within only one or two centuries of after a temperature increase permafrost occurrence several hundred meters below the surface is not substantially affected. This corresponds to the results obtained in our simulations: In the 3 dimensional situations modeled, a change in MAGST propagates into the ground perpendicularly to the surface from two or more sides (Figure 10), leading to an increase in the pace at which permafrost degrades. For more exposed 3-dimensional situations such as a pyramid, the warming even takes place from 4 different sides (Figure 11). With raising surface temperatures the permafrost base changes until it is situated parallel to the surface. In the examples shown in Figure 11, it can be seen that the permafrost base mainly changes on the warmer side because of the curved form of the isotherms. After a period of 100 or 200 years the parts deeper than ca. 200 m are still not reached by the climate signal (Figures 10 and 11). A permafrost body can remain unaffected by changes at the surface over centuries to millennia where temperatures little below the surface have changed significantly and many parts of the surface have become free of permafrost.

The main heat flux is directed horizontally from the warmer to the colder side (Figure 5b,c) as shown for equilibrium conditions, but strongest heat fluxes exist in the upper part on the warmer side. Temperature gradients and heat fluxes near the surface increase strongly due to the larger temperature difference between the warming surface and the temperatures at depth that still remain unchanged. On the colder side a reversal of the direction of heat fluxes takes place and, hence, at the depth reached by the temperature signal a zone exists where heat flows towards it from both sides.

Where the temperature raises towards 0 °C, energy is needed to melt ice contained in pore spaces. This effect leads to a delay in the propagation of the temperature signal into the subsurface and increases the time lag between changes in surface conditions and temperatures at depth. The difference between model runs with and without latent heat is illustrated in Figure 12. Locations where a difference can be observed show the areas where temperature changes take place just below 0 °C and, hence, where permafrost is actually degrading. The influence, as calculated with a porosity of 3% and homogeneous material properties, amounts to a maximum of about 0.5 °C within 100 years. Considering the low porosity of rock this difference can be referred to as substantial, and latent heat effects additionally modify the distribution of the underground thermal field at the degrading permafrost boundaries.

5. Discussion

With the experiments conducted in this study we demonstrated the strong 3-dimensional effects on the subsurface thermal field and the occurrence of permafrost in high mountain topography. In the upper parts of the geometries under consideration the influence of the

geothermal heat flux is negligible and ground temperatures and heat fluxes are governed almost solely by variable temperatures at the surface of the mountain sides: temperatures change with position between the mountain sides and heat fluxes are mainly horizontal. Due to the 3-dimensional effect of mountainous topography, permafrost occurs inside mountains only a few meters to decameters below the surface where MAGST is clearly above 0 °C. These effects were shown for simplified geometries even in steady state conditions. In terms of temperature-related instabilities, a thawing and migrating permafrost base in such a situation may, for instance, lead to rockfall occurring on the warm or 'permafrost-free' side of a ridge or peak. In fact, several detachment zones exist, where slope failure occurred in similar situations as, for instance, the event at Punta Thurwieser on 18 September 2004 in the Italian Val Zebrù [*Cola*, 2005]. The rockfall detached at an elevation of approximately 3600 m a.s.l. from a 70° steep and south-exposed rockwall that is part of a mainly east-west-trending ridge. This situation is comparable to the one shown in Figure 4b. The starting zone of the rockfall event on 15 July 2003 at the Hörnligrat, the NE-ridge of the Matterhorn, Switzerland, is located in a situation where permafrost occurs only below the surface (cf. Figure 8b). Consequently, it is important to consider the effects of complex topography and variable surface temperatures when assessing below ground temperatures and permafrost occurrence in high-mountains. Traditional 2-dimensional permafrost maps can serve as indicators of potential permafrost occurrence in an area, but they do not provide sufficient information on the conditions at depth. However, it has to be emphasized that the steady state conditions shown do not describe a situation as found today in nature and that transient perturbations to the steady state temperature field exist as described below. Nevertheless, they are a step towards understanding the temperature distribution at depth in high-mountain terrain.

3-dimensional mountain topography also plays a decisive role for temperature changes entering into the ground. In the time-dependent simulations it can be seen that the warming signal that intrudes into the underground perpendicularly to the surface reaches the permafrost body from more than one side, i.e. from 2 sides in the case of a ridge, from even 4 sides in a pyramid-like situation. Together with the above described decoupling from the geothermal heat flux this describes a basic difference to permafrost degradation in high latitudes or in more gentle terrain and increases the pace of deeper permafrost degradation.

The transient effects caused by changing surface temperatures additionally complicate the temperature distribution below the surface. Changes at the surface and the upper hundred meters are substantial as modeled for the next 100 years and the conditions assumed in test-cases. For instance, in Figure 9 the lower limit of permafrost distribution at the surface rises to nearly 4000 m a.s.l. on south-facing rockwalls, which is higher than most peaks in the European Alps. However, a substantial permafrost body remains in the underground but surface conditions no longer indicate it. For a realistic assessment of today's thermal state and permafrost distribution at grater depth in high mountains it is therefore necessary to consider transient effects in addition to 3-dimensional effects. For example, an assumed 10 °C cooler surface temperature during the last Pleistocene Ice Age 70,000-10,000 years b.p. still causes a temperature difference of more than -4 °C at a depth of 1000 m compared to steady state conditions [*Kohl et al.*, 2001; cf. also *Safanda and Rajver*, 2001]. The recent much smaller 20th century warming [*Beniston et al.*, 1997; *Diaz and Bradley*, 1997; *Haeberli and Beniston*, 1998] has not yet penetrated to greater depth but affects temperatures in the upper decameters. When additionally considering the retarding

influence of pore ice on temperature evolution, even in low-porosity rockwalls, temperatures may be much colder than in the example above and substantial permafrost may remain today inside high mountains.

The direction of heat fluxes is important, for instance, for the direction of unfrozen water migrating in pore spaces. As seen in Figure 5, with rising temperatures at the surface, a zone develops on the colder side of a mountain where heat flows towards it from two sides. This can influence the movement of unfrozen water in the pore space and the distribution of ice content in the subsurface [cf. also *Gruber and Haeberli*, submitted].

In the highly variable topography found in natural environments the subsurface temperature field is a complex result of many interrelated influences and may differ substantially from the simplified test cases presented. The calculation of surface temperatures using TEBAL is validated for near-vertical situations of bare rock and we assumed average values for and a homogeneous distribution of surface and subsurface characteristics. Modifications are likely to be caused by various factors, such as snow remaining in less steep parts, heavy fracturing of the rock due to weathering or geological discontinuities [*Gruber and Haeberli*, submitted]. Knowledge about the water and ice content of rockwalls, its freezing characteristics and its spatial and temporal variability is absent or rare. Massive ice in jointed rock (as found in many rockfall scarps in 2003, e.g., the Matterhorn south face) can lead to a highly complex thermal field and strongly retard degradation at depth. The hydrology of rockwalls and water possibly percolating therein, which may lead to non-conductive heat transfer within the subsurface, are poorly understood so far. Such effects may counter the retarding effect caused by the uptake of latent heat. First results from the application of geophysical monitoring in the Turtmann Valley, Swiss Alps, point to their importance in connection with permafrost occurrence in solid rockwalls [*Krautblatter et al.*, submitted].

We accomplished the combination of RCMs, energy balance and heat conduction models by passing output from one model as input to the next. The model chain represents processes initiated by changes in atmospheric conditions that lead to changes in the surface energy balance and below-ground temperatures. However, the models are not yet fully coupled and output from a first model serves as input to the next without accounting for possible feedback. This first approach using such a model chain bears potential for a number of studies and may provide a basis for numerical experimentation in order to investigate thermal processes in frozen rockwalls and for case studies of real topography. It may also be beneficial for the re-analysis of rockfall events that occurred in periglacial areas, for support of engineering studies (e.g. cable cars) or interpretation of geothermal profiles. The perturbation of the ground thermal field also constitutes a major obstacle for the interpretation of transient signals contained in T(z)-profiles measured in boreholes located in high mountains [*Gruber et al.*, 2004b; *Kohl and Gruber,* 2003]. Its separation from topographic effects is crucial for the quantification of the warming signal. Only then, conclusions on the temperature history at the surface may be drawn correctly from the inversion of these profiles, e.g. for monitoring programs such as PACE [*Harris et al.*, 2001b] or PERMOS [*Vonder Mühll et al.*, 2004].

6. Conclusions and perspectives

The experiments conducted in this study and the results described above lead to the following conclusions:

- The steady state temperature field below high mountain topography is mainly controlled by spatially varying surface temperatures between different mountain sides and is little influenced by the geothermal heat flux in the higher parts. Isotherms are nearly vertical and a strong heat flux is directed from the warmer to the colder side of the mountain.
- Permafrost may occur underground at locations where surface temperatures do not indicate it, even in steady state conditions. Traditional 2D-maps do not provide sufficient information to assess permafrost distribution at depth in complex high-mountain topography.
- Irregularities on the surface, such as spurs, may modify ground temperatures and induce local permafrost occurrence.
- Permafrost degradation in steep topography takes places from different sides, affecting both the permafrost table and the permafrost base. This leads to an increase in the pace of deeper permafrost degradation as compared to permafrost in flat terrain, where warming typically penetrates vertically into the ground.
- Owing to the long time needed for a temperature signal to penetrate to greater depth, permafrost can remain inside mountains over centuries. At some locations where surface temperatures rise above 0 °C substantial permafrost occurrence can be found. Time scales involved in deep permafrost degradation are on the order of millennia, even without the retarding effect of latent heat. The influence from past cold periods such as the last ice-age is likely to still be found in the interior of mountain peaks.
- With rising surface temperatures, heat fluxes strongly increase near the surface.
- For the assessment of permafrost occurrence in complex topography, the 3-dimensional situation as well as transient effects should be taken into account. Preferably, physically based 3-dimensional models are used.
- An energy balance model has been successfully combined with a numerical 3D heat conduction scheme to model ground temperatures and permafrost distribution at depth in complex topography. In addition, output from RCMs was downscaled to local climate conditions and used for time-dependent model runs.

Permafrost in steep bedrock slopes is still a very young field of research and many factors influencing the ground thermal regime in steep rock are poorly understood today. Examples include the influence of snow cover, ice contained in pore spaces, percolating water or local inhomogeneities [Gruber and Haeberli, submitted]. The focus of future activities is on realistic process understanding and quantitative and numeric modeling of the processes involved in permafrost degradation in steep high mountain rock walls. For the understanding and quantification of present-day or future temperature conditions the time scales needed in model spin up to account for transient effects of past cold periods are investigated. The model chain applied in this study may be established for future studies on the subsurface distribution and evolution of mountain permafrost, such as the re-analysis of recent periglacial rockfall events or the study of the present transient state of thermal fields in real topographies. A validation study combining the models presented with measured temperature data and geophysical soundings for a test site in Switzerland is planned for the near future.

Acknowledgements
This study was supported by the Swiss National Science Foundation, as part of the NF 20-10796./1 project 'Frozen rock walls and climate change: transient 3-dimensional investigation of permafrost degradation' and by the European Cooperation in the field of Scientific and Technical Research (COST-Action 719). The authors appreciate their financial support. Careful comments by two anonymous reviewers and the editors are greatly acknowledged.

References

Bartelt, P. B., and M. Lehning (2002), A physical SNOWPACK model for avalanche warning services, *Climatic Change*, 36, 233-251.

Beniston, M., H. F. Diaz, and R. S. Bradley (1997), Climatic change at high elevation sites: An overview, *Climatic Change*, 36, 233-251.

Blackwell, D.D., J.L Steele, Ch.A. Brott, (1980), The terrain effect on terrestrial heat flow, *J. Geophys. Res*., 9 (B85), 4757-4772.

Carslaw, H. S., and J. C. Jaeger (1959), *Conduction of heat in solids*, 510pp., Clarendon Press, Oxford.

Cermák, V., and L. Rybach (1982), Thermal conductivity and specific heat of minerals and rocks, in Landolt-Börnstein Zahlenwerte und Funktionen aus Naturwissenschaften und Technik, Physikalische Eigenschaften der Gesteine (V/1a), edited by G. Angeneister, Springer, Berlin.

Christensen, J. H., O. B. Christensen, P. Lopez, E. Van Meijgaard and M. Botzet (1996), The HIRHAM4 Regional Atmospheric Climate Model, Scientific Report 96-4, 51 pp., DMI, Copenhagen.

Christensen, J. H., T. R. Carter and F. Giorgi (2002), PRUDENCE employs new methods to assess European climate change, *EoS Trans.,* 83, 147.

Cola, G. (2005), La grande frana della cresta Sud-Est della Punta Thurwieser (Thurwieser-spitze) 3658 m, (Alta Valtellina, Italia), *Terra Glacialis*, 8, 38-45.

Corripio, J. G. (2003), Vectorial algebra algorithms for calculating terrain parameters from DEMs and solar radiation modelling in mountainous terrain, *Int J. Geogr. Inf. Sc*., 17, 1-23.

Dash, J. G., H. Fu, and J. S. Wettlaufer (1995), The premelting of ice and its environmental consequences, *Rep. Prog. Phys*., 58.

Davies, M. C. R., O. Hamza, and C. Harris (2001), The effect of rise in mean annual temperature on the stability of rock slopes containing ice-filled discontinuities, *Permafrost Periglac*., 12, 137-144.

Deline, P. (2001), Recent Brenva rock avalanches (Valley of Aosta): new chapter in an old story? *Geogr. Fis. Din. Quarter*., 55-63.

Diaz, H. F., and R. S. Bradley (1997), Temperature variations during the last century at high elevation sites, *Climatic Change*, 36, 253-279.

Dramis, F., M. Govi, M. Guglielmin, and G. Mortara (1995), Mountain permafrost and slope instability in the Italian Alps: the Val Pola landslide, *Permafrost Periglac*., 6, 73-82.

Erbs, D. G., S. A. Klein, and J. A. Duffie (1982), Estimation of the diffuse radiation fraction for hourly, daily and monthly average global radiation, *Sol. Energy*, 28, 293-304.

Etzelmüller, B., M. Hoelzle, E. S. F. Heggem, K. Isaksen, C. Mittaz, D. Vonder Mühll, R. S. Ødegård, W. Haeberli, and J. L. Sollid (2001), Mapping and modelling the occurrence and distribution of mountain permafrost, *Norsk. Geol. Tidsskr*., 55, 186-194.

Flatau, P. J., R. L. Walko and W.R. Cotton (1992), Polynomial fits to saturation vapor-pressure, *J. Appl. Meteorol.*, 31, 1507-1513.

Giorgi, F., Y. Huang, K. Nishizawa and C. Fu (1999), A seasonal cycle simulation over eastern Asia and its sensitivity to radiative transfer and surface processes, *J. Geophys. Res.,* 104, 6403-6423.

Gold, L. W., and A. H. Lachenbruch (1973), Thermal conditions in permafrost – a review of North American literature, 2nd International Conference on Permafrost. Proceedings, National Academy of Sciences, Washington D.C., 3-25.

Gruber, S. (2005), Mountain permafrost: Transient spatial modelling, model verfication and the use of remote sensing, Ph.D. thesis, 121pp. University of Zurich, Zurich.

Gruber, S., and M. Hoelzle (2001), Statistical modelling of mountain permafrost distribution: local calibration and incorporation of remotely sensed data, *Permafrost Periglac*., 12, 69-77.

Gruber, S. and W. Haeberli (in review), Permafrost in steep bedrock slopes and its temperature-related destabilization following climate change, *J. Geophys. Res*.

Gruber, S., M. Peter, M. Hoelzle, I. Woodhatch, and W. Haeberli (2003), Surface temperatures in steep alpine rock faces – A strategy for regional-scale measurement and modelling, 8th International Conference on Permafrost, Proceedings, Swets & Zeitlinger, Lisse, Zurich.

Gruber, S., M. Hoelzle, and W. Haeberli (2004a), Permafrost thaw and destabilization of Alpine rock walls in the hot summer of 2003, *Geophys. Res. Let*., 31, doi:10.1029/2004GL0250051.

Gruber, S., L. King, T. Kohl, T. Herz, W. Haeberli, and M. Hoelzle (2004b), Interpretation of geothermal profiles perturbed by topography: The Alpine permafrost boreholes at Stockhorn Plateau, Switzerland, *Permafrost Periglac*., 15, 349-357.

Gruber, S., M. Hoelzle, and W. Haeberli (2004c), Rock wall temperatures in the Alps: Modelling their topographic distribution and regional differences, *Permafrost Periglac*., 15, 299-307.

Haeberli, W. (1975), Untersuchungen zur Verbreitung von Permafrost zwischen Flüelapass und Piz Grialetsch (Graubünden), Mitteilungen der VAW-ETH Zürich, 221 pp., ETH Zürich, Zürich.

Haeberli, W., and M. Beniston (1998), Climate change and its impacts on glaciers and permafrost in the Alps, in *AMBIO – A Journal of the Human Environment*, edited by A. Rapp and E. Kessler, pp. 258-265, The Royal Swedish Academy of Sciences.

Haeberli, W., M. Wegmann, and D. Vonder Mühll (1997), Slope stability problems related to glacier shrinkage and permafrost degradation in the Alps, *Eclogae Geol. Helv*., 90, 407-414.

Harris, C., M. C. R. Davies, and B. Etzelmüller (2001a), The assessment of potential geotechnical hazards associated with mountain permafrost in a warming global climate, *Permafrost Periglac*., 12, 145-156.

Harris, C., W. Haeberli, D. Vonder Mühll, and L. King (2001b), Permafrost monitoring in the high mountains of Europe: the PACE project in its global context, *Permafrost Periglac*., 12, 3-11.

Harris, C., D. Vonder Mühll, K. Isaksen, W. Haeberli, J. L. Sollid, L. King, P. Holmlund, F. Dramis, M. Guglielmin, and D. Palacios (2003), Warming permafrost in European mountains, *Global Planet. Change*, 39, 215-225.

Harris, S.A., and D.E. Pedersen (1998), Thermal regimes beneath coarse blocky material, *Permafrost Periglac*., 9, 107-120.

Hoelzle, M., and W. Haeberli (1995), Simulating the effects of mean annual air temperature changes on permafrost distribution and glacier size. An example from the Upper Engadin, Swiss Alps, *Ann. Glaciol.*, 21, 400-405.

Hoelzle, M., C. Mittaz, B. Etzelmüller, and W. Haeberli (2001), Surface energy fluxes and distribution models of permafrost in European mountain areas: an overview of current developments, *Permafrost Periglac*., 12, 53-68.

IPCC (2001), *Third assessment report*, Working Group 1, Cambridge University Press, Cambridge.

Jansson, P.E., and L. Karlberg, 2004, *Coupled heat and mass transfer model for soil-plant-atmosphere systems*, Royal Institute of Technology, Dept of Civl and Environmental Engineering, Stockholm, 435 pp.

Keller, F. (1992), Automated mapping of mountain permafrost using the program PERMAKART within the Geographical Information System ARC/INFO, *Permafrost Periglac*., 3, 133-138.

Keller, F. (2003), Kurzbericht über die Steinschlagereignisse im heissen Sommer 2003 im Bergell(Project report on rockfall 2003 to the Kanton Graubuenden), report, Institut für Turismus und Landschaft Academia Engiadina, Samedan, Switzerland.

Knutti, R., T. F. Stocker, F. Joos, and G. K. Plattner (2002), Constraints on radiative forcing and future climate change from observations and climate model ensembles, Nature, 416, 719-723.

Kohl, T. (1998), Paleclimatic signals – can they be washed out?, *Tectonophysics*, 291, 225-234.

Kohl, T. (1999), Transient thermal effects at complex topographies, *Tectonophysics*, 306, 311-324.

Kohl, T., and R. J. Hopkirk (1995), ‚FRACTure' a simulation code for forced fluid flow and transport in fractured porous rock, *Geothermics*, 24, 345-359.

Kohl, T., and S. Gruber (2003), Evidence of paleaotemperature signals in mountain permafrost areas, 8th International Conference on Permafrost, Extended Abstracts, University of Zurich, Zurich.

Kohl, T., S. Signorelli, and L. Rybach (2001), Three-dimensional (3-D) thermal investigation below high Alpine topography, *Phys. Earth Planet. In*., 126, 195-210.

Konzelmann, T., R. S. W. Van de Wal, W. Greuell, R. Binanja, E. A. C. Henneken, and A. Abe-Ouchi (1994), Parameterization of global and longwave incoming radiation for the Greenland Ice Sheet, *Global Planet. Change*, 9, 143-164.

Krautblatter, M., C. Hauck, and R. Dickau (submitted), First DC resitivity monitoring of permafrost in solid rockwalls, *J. Geophys. Res*.

Kukkonen, I. T., and J. Safanda (2001), Numerical modelling of permafrost in bedrock in northern Fennoscandia during the Holocene, *Global Planet. Change*, 29, 259-273.

Lehning, M., P. B. Bartelt, R. L. Brown, C. Fierz, and P. Satyawali (2002), A physical SNOWPACK model for the Swiss Avalanche warning services. Part III: Meteorological boundary conditions, thin layer formation and evaluation, *Cold Reg. Sci. Technol*., 35, 169-184.

Lewkowicz, A. G. (2001), Temperature regime of a small sandstone tor, latitude 80°N, Ellesmere Island, Nunavut, Canada, *Permafrost Periglac*., 12, 351-366.

Luetschg, M. (2004), A model and field analysis of the interaction between snow cover and Alpine permafrost, Ph.D. thesis, 258 pp., University of Zurich, Zurich.

Lunardini, V.J. (1996), Climatic warming and the degradation of warm permafrost, *Permafrost Periglac.,* 7, 311-320.

Lüthi, D., A. Cress, C. Frei and C. Schär (1996), Interannual variability and regional simulations, *Theor. Appl. Climatolo*. 53, 185-209.

Medici, F., and L. Rybach, (1995), *Geothermal Map of Switzerland 1995 (Heat Flow Density),* Matériaux pour la Géologie de la Suisse, Géophysique 30. Schweizerische Geophysikalische Kommission.

Mittaz, C., M. Hoelzle, and W. Haeberli (2000), First results and interpretation of energy-flux measurements of Alpine permafrost, *Ann Glaciol*., 31, 275-280.

Mottaghy, D. and V. Rath (2006), Latent heat effects in subsurface heat transport modeling and their impact on paleotemperature reconstructions, *Geophys. J. Int.,* 164, 236-245.

Noetzli, J., M. Hoelzle, and W. Haeberli (2003), Mountain permafrost and recent Alpine rock-fall events: a GIS-based approach to determine critical factors, 8th International Conference on Permafrost, Proceedings, Swets & Zeitlinger, Lisse, Zürich.

Oke, T. R. (1987), Boundary Layer Climates, 2nd ed., Routledge.

Plüss, C. (1997), The Energy Balance Over an Alpine Snowcover, Point Measurements and Areal Distribution, Ph.D. thesis, 115 pp., University of Zurich, Zurich.

Plüss, C., and A. Ohmura (1997), Longwave radiation on snow-covered mountainous surfaces, *J. Appl. Meteorol*., 36, 818-824.

Pollak, H. N., and J. Huang (2000), Climate reconstruction from subsurface temperatures, *Ann Rev. Earth Pl. Sc*., 28, 339-365.

Romanovsky, V. E., and T. E. Osterkamp (2000), Effects of unfrozen water on heat and mass transport processes in the active layer and permafrost, *Permafrost Periglac*., 11, 219-239.

Rybach, L., and M. Pfister (1994), How to predict rock temperatures for deep Alpine tunnels, *J. Appl. Geophys*., 31, 261-270.

Safanda, J. (1999), Ground surface temperature as a function of slope angle and slope orientation and its effect on the subsurface temperature field, *Tectonophysics*, 306, 367-375.

Safanda, J., and D. Rajver (2001), Signature of the last ice age in the present subsurface temperatures in the Czech Republic and Slovenia, *Global Planet. Change*, 29, 241-257.

Salzmann, N., S. Gruber, M. Hugentobler, and M. Hoelzle, 2006a, The influence of different Digital Terrain Models (DTMs) on alpine permafrost modeling, *Environ Model Assess,* doi 10.1007/s10666-006-9065-3.

Salzmann, N., C. Frei, P. L. Vidale, and M. Hoelzle (2006b), The Application of Regional Climate Model output for the simulation of high-mountain permafrost scenarios, *Global Planet. Change*, doi:10.1016/j.gloplcha.2006.07.006.

Salzmann, N., J. Noetzli, C. Hauck, S. Gruber, and W. Haeberli (accepted), RCM-based ground temperature scenarios in high-mountain topography and their uncertainty ranges, *J. Geophys. Res*.

Schiermeier, Q., (2003), Alpine thaw breaks ice over permafrost's role, *Nature*, 424, 712.

Sergueev, D., G. Tipenko, V. Romanovsky, and N. Romanovskii (2003), Mountain permafrost thickness evolution under influence of long-term climate fluctuations (results of numerical simulation), 8th International Conference on Permafrost, Swets & Zeitlinger, Lisse, Zurich.

Stocker-Mittaz, C., M. Hoelzle, and W. Haeberli (2002), Permafrost distribution modeling based on energy-balance data: a first step, *Permafrost Periglac*., 13, 271-282.

Stott, P. A., and J. A. Kettleborough (2002), Origins and estimates of uncertainty in predictions of twenty-first century temperature rise, *Nature*, 416, 723-726.

Suter S., M. Hoelzle and A. Ohmura (2004), Energy balance at a cold, alpine firn saddle, Seserjoch, Monte Rosa. *International Journal of Climatology*, 24, 1423-1442.

Vonder Mühll, D., J. Noetzli, K. Makowski, and R. Delaloye (2004), Permafrost in Switzerland 2000/2001 and 2001/2002. Glaciological Report (Permafrost) No. 4/5 of the Glaciological Commission (GC) of the Swiss Academy of Sciences (SAS) and Institute of Geography, Universitiy of Zurich, 80 pp.

Wegmann, M. (1998), Frost dynamics in high-alpine rock walls at the example of the Jungfraujoch-Aletsch Region, CH (Frostdynamik in hochalpinen Felswänden am Beispiel der Region Jungfraujoch-Aletsch), Ph.D. thesis, 143 pp., ETH Zurich, Zurich.

Wegmann, M., G. H. Gudmundsson, and W. Haeberli (1998), Permafrost changes in rock walls and the retreat of Alpine glaciers: a thermal modelling approach, *Permafrost Periglac.*, 9, 23-33.

Williams, P. J., and M. W. Smith (1989), *The Frozen Earth*, Cambridge University Press, Cambridge, 306 pp.

Zwiers, F. W. (2002), The 20-year forecast, *Nature*, 416, 690-691.

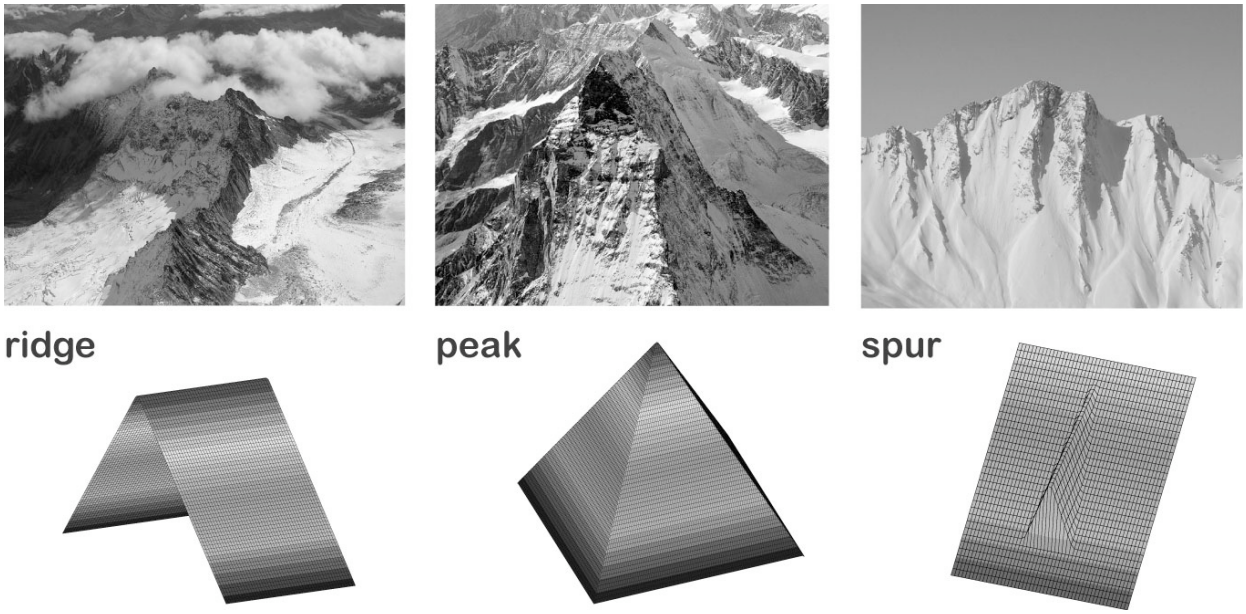

Figure 1
Examples of the most prevalent topographical forms of high mountain topography: ridges (left, e.g. Dammastock, CH) and peaks (middle, e.g. Matterhorn, CH) are simplified as triangle and pyramid geometries. Additionally, rockwalls are often modified by spurs (right, e.g. Piz Terri, CH). Photos left and middle taken by Ch. Rothenbühler.

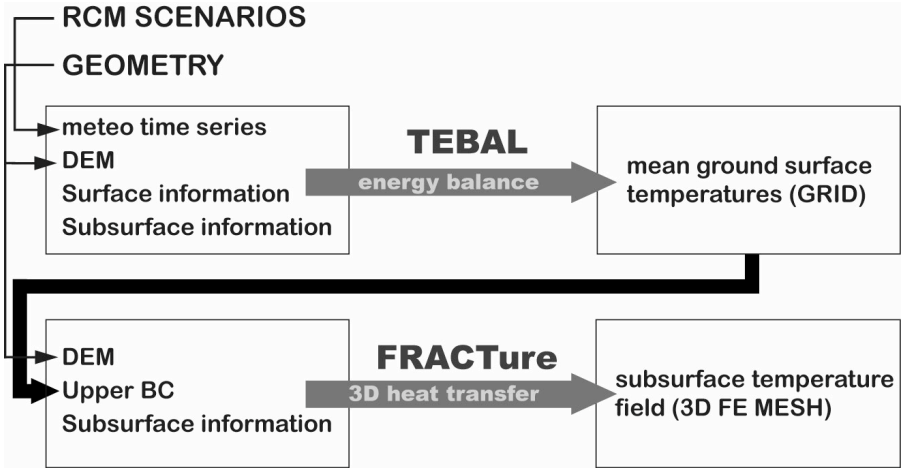

Figure 2
To compute below ground temperature fields different models were combined in a model chain: Ground surface temperatures are calculated by the energy balance model TEBAL (*Gruber*, 2005; *Stocker-Mittaz et al.,* 2002) and used as upper boundary condition in the FE heat conduction code FRACTure (*Kohl and Hopkirk,* 1995) that determines a 3-dimensional subsurface temperature field. For time-dependent calculations, the energy-balance model was driven by climate time series generated based on output from Regional Climate Models (RCMs).

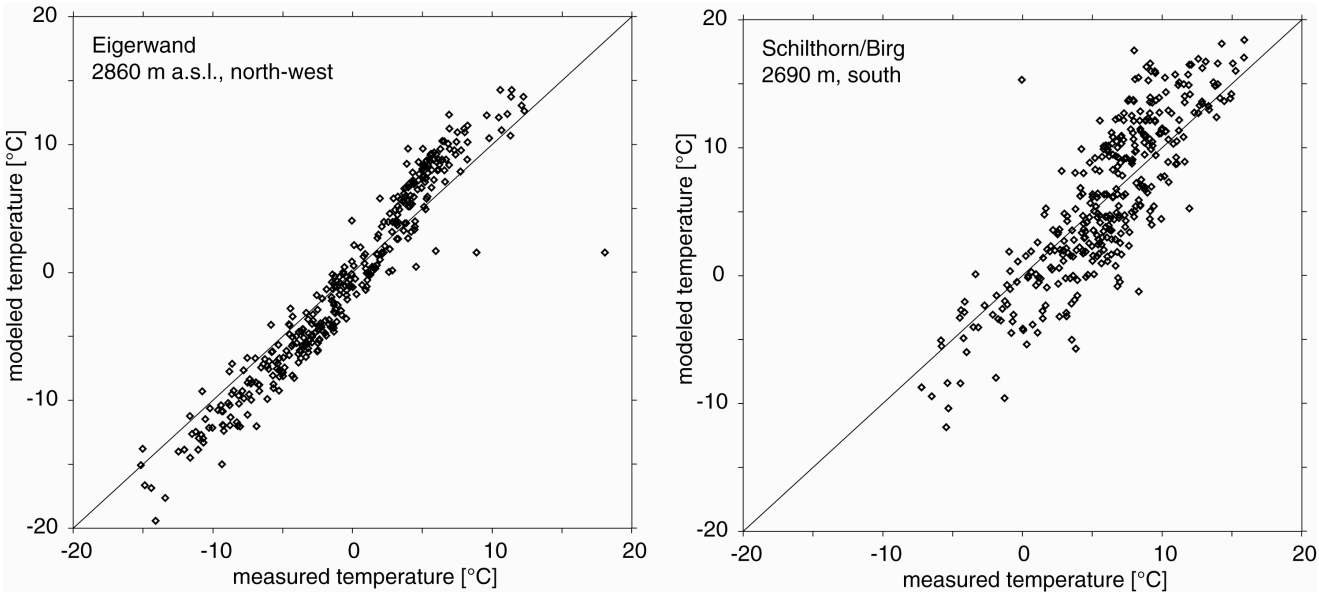

Figure 3
Measured versus modeled daily means of near-surface temperatures [°C] at two logger sites for the hydrological year 2001/2002. Modeled temperatures were calculated with the energy balance model TEBAL and hourly time steps.

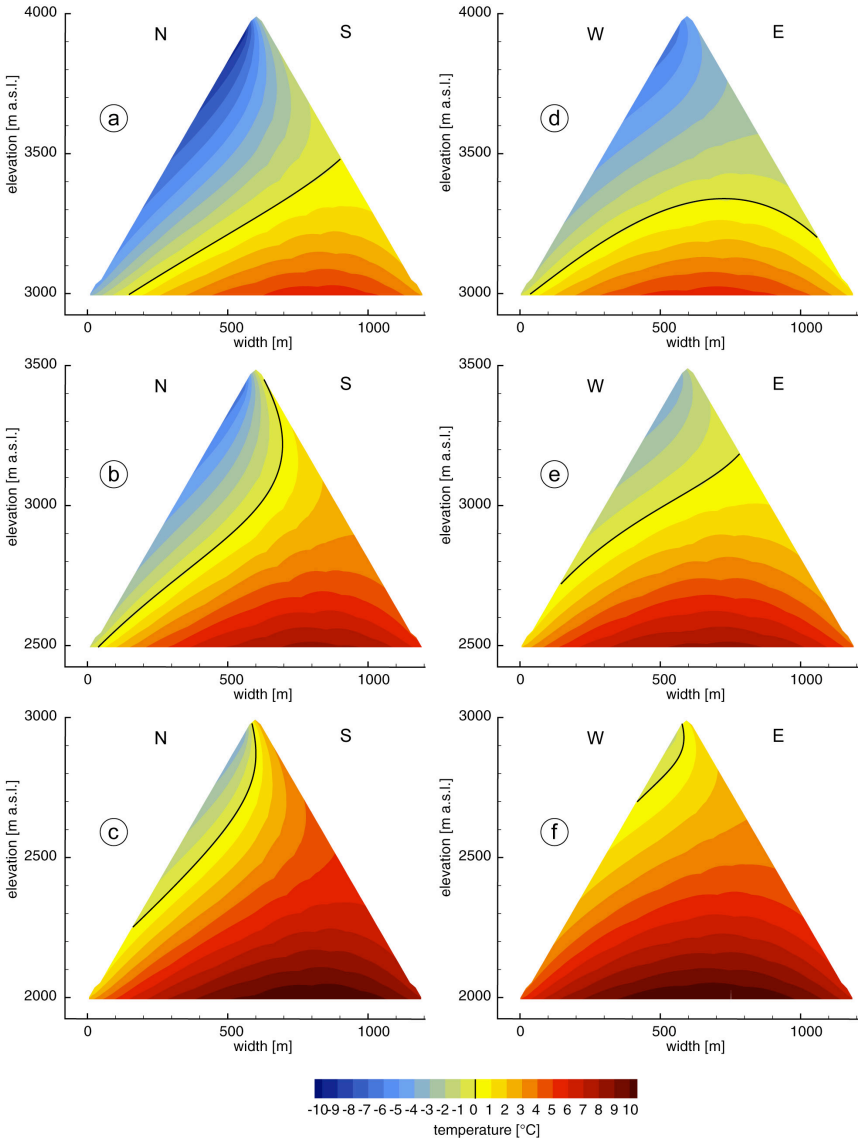

Figure 4
Steady state subsurface temperature fields in six idealized ridges with a slope steepness of 60°. The black line corresponds to the 0 °C-isotherm and represents the permafrost boundary. Ridges a)-c) have north and south-facing slopes, ridges d)-f) west- and east-facing slopes, respectively. Three different elevation ranges are shown.

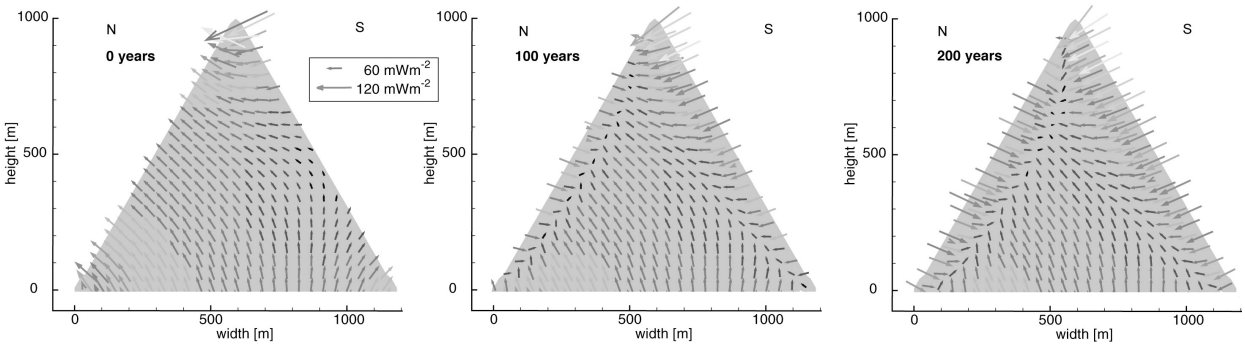

Figure 5
Distribution of heat fluxes in an idealized ridge with south- and north-facing slopes for steady state conditions (0 y), the situation after 100 y and after 200 y, considering a rise in ground surface temperatures of 3.5 °C on the northern and 2.5 °C in the southern flank, respectively.

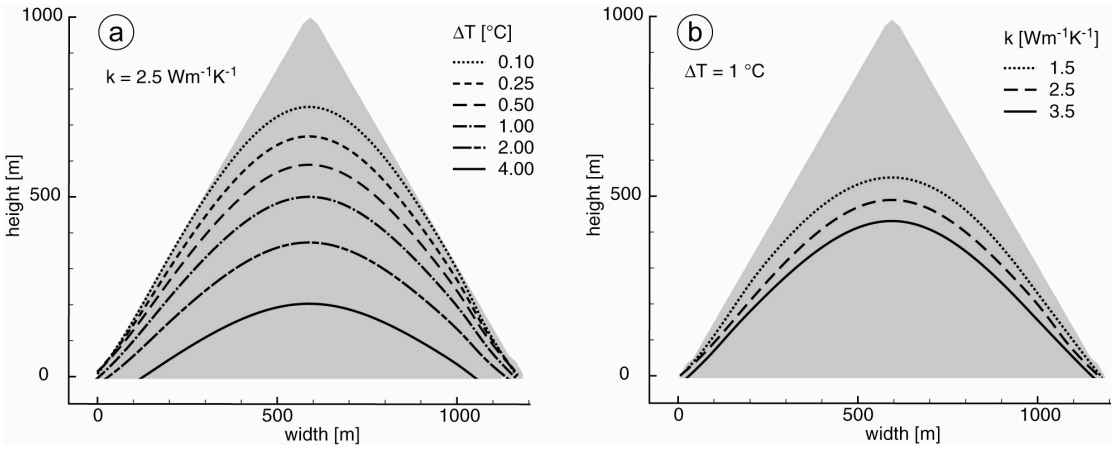

Figure 6
The influence of the geothermal heat flux exponentially decreases towards the top of the geometry. On the left (a), the temperature difference between model runs with a constant geothermal heat flux und such calculated with a zero heat flux lower boundary condition is shown. On the right (b), the line above which this difference amounts to less than 1 °C is drawn for different thermal conductivities.

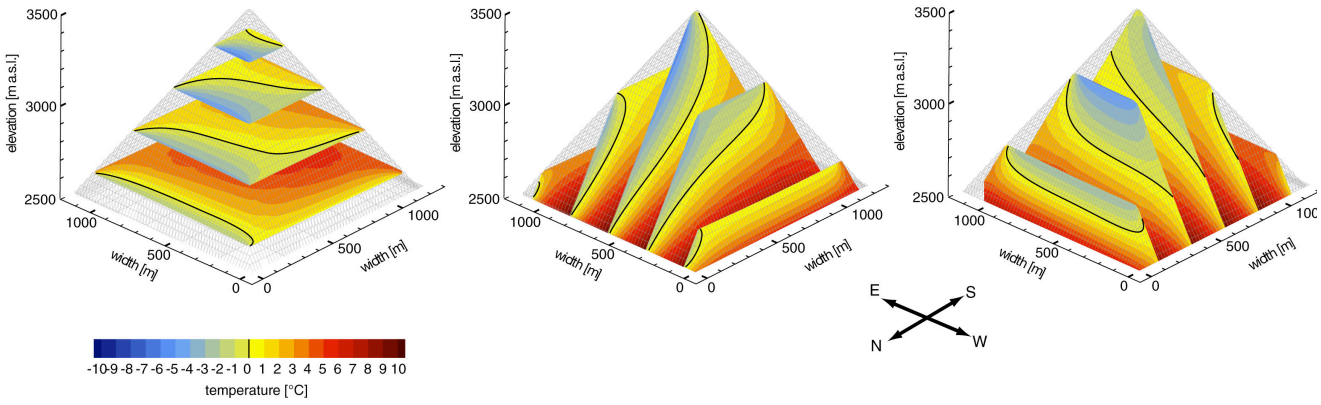

Figure *7*
The temperature distribution in a pyramid that represents a simplified peak is visualized with x-, y- and z-slices. The black line corresponds to the 0 °C-isotherm and represents the permafrost boundary. The three-dimensional character of the permafrost body becomes evident.

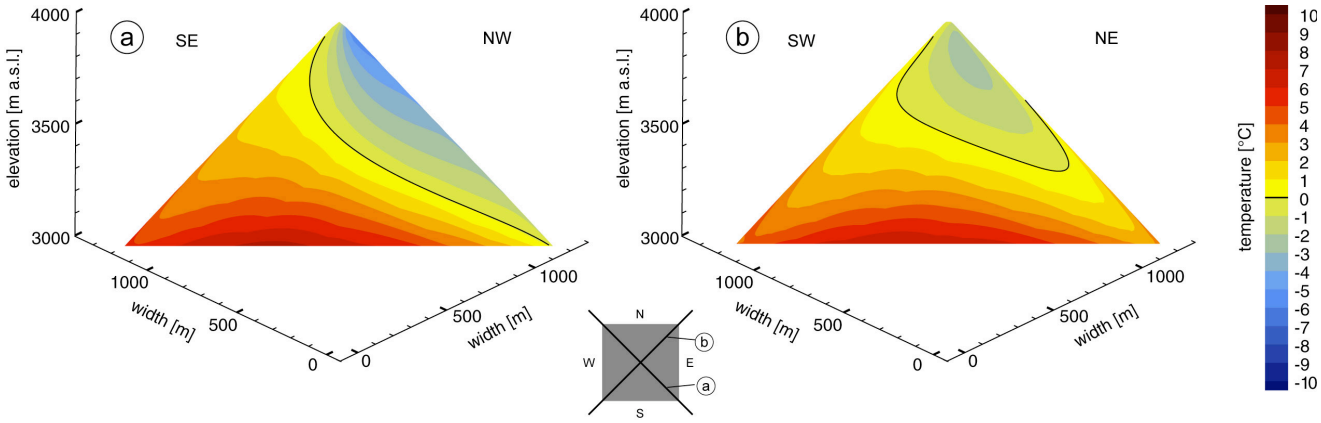

Figure 8
Steady state temperature distribution shown in two slices taken along the edges of a pyramid geometry. The temperatures a few decameters below the edges strongly differ from the thermal conditions at the surface as a result of 3-dimensional effects.

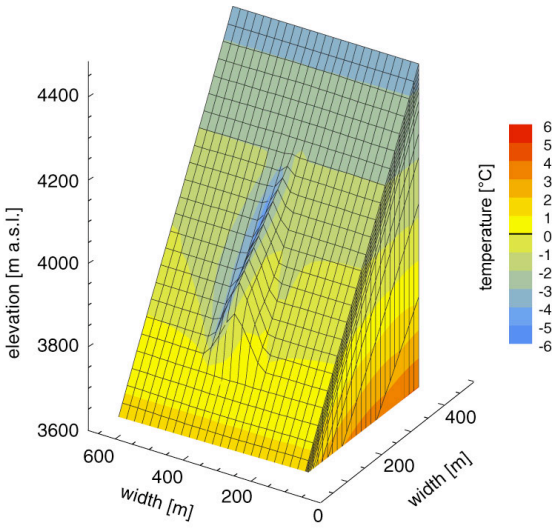

Figure 9
Situation of a spur on a south-facing rockwall. The spur modifies the surface temperatures and therewith the temperatures in the underground. This may lead to local permafrost occurrence in a rockwall that generally does not contain permafrost.

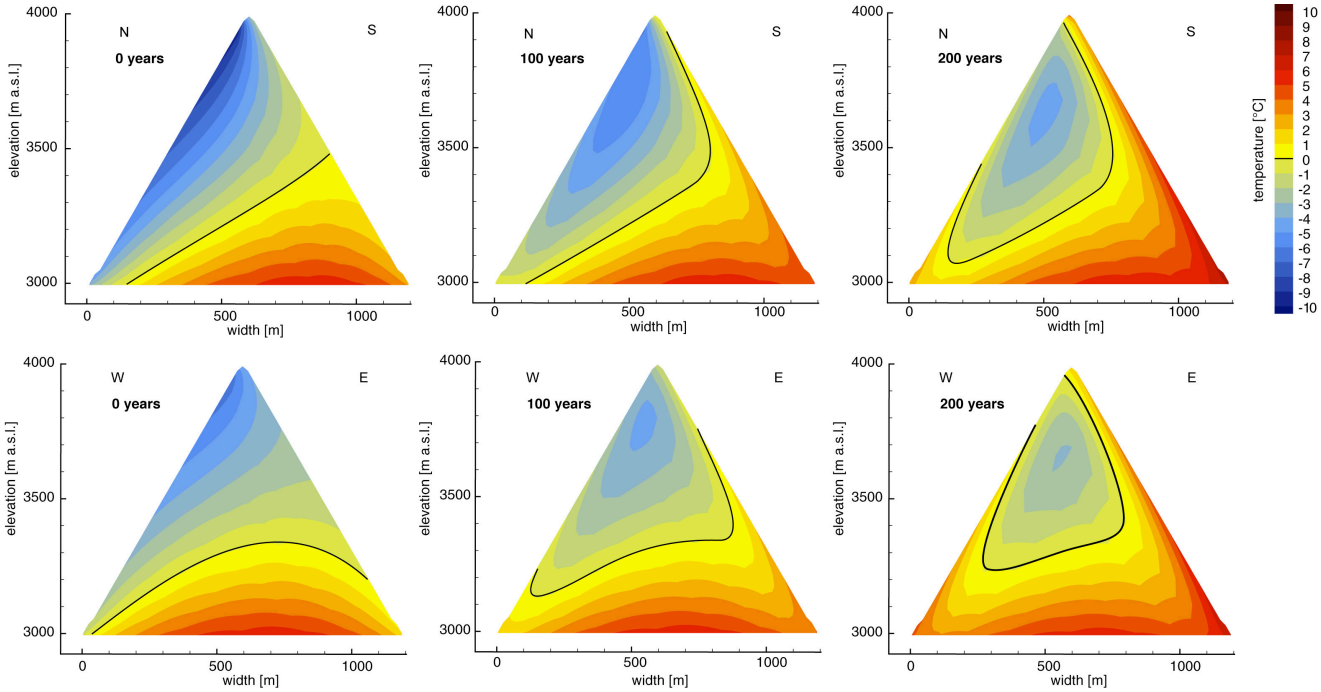

Figure 10
Evolution of subsurface temperatures in a ridge with a south and a north slope (top) and an east and a west slope (bottom), respectively, for steady state and after a time period of 100 and 200 years. The warming at the surface was set to +3.5 °C for north slopes, +2.5 °C for south slopes and +3 °C for east and west slopes over a time period of 100 years The black line corresponds to the 0 °C-isotherm and represents the permafrost boundary.

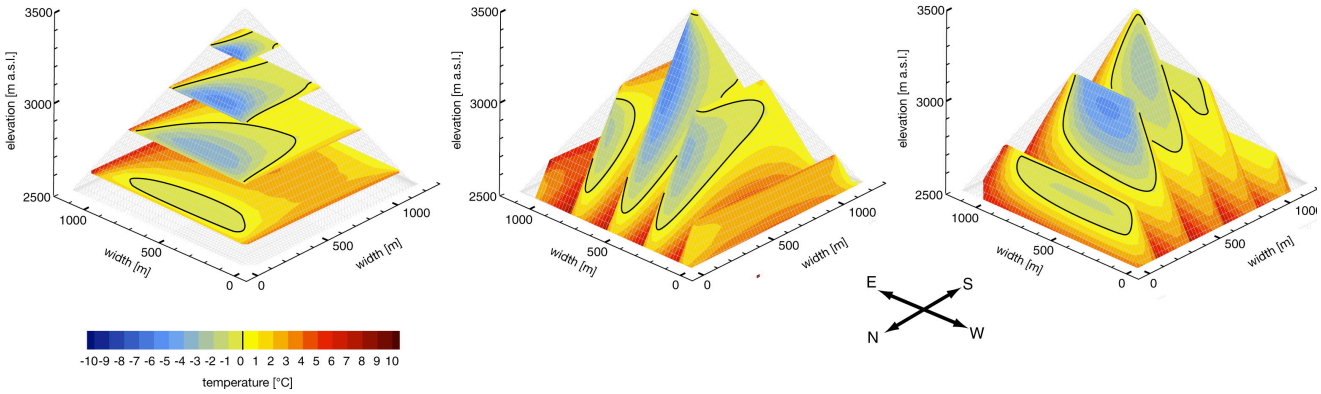

Figure 11
Temperature evolution of the pyramid situation shown in Figure 6, considering a warming at the surface of +3.5 °C for north slopes, +2.5 °C for south slopes and +3 °C for east and west slopes over a time period of 100 years. The black line corresponds to the 0 °C-isotherm and represents the permafrost boundary.

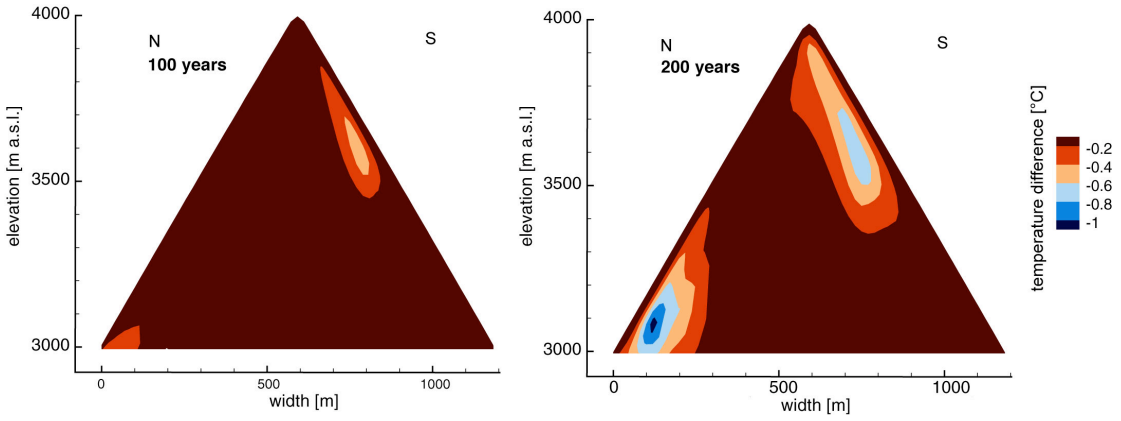

Figure 12
Difference between model runs with no heat source and such taking into account latent heat effects as modeled for a porosity of 3% and a time period of 100 (left) and 200 years (right). At locations that show differences between the model runs phase changes take place and, hence, these locations designate areas where permafrost is actually degrading.

Paper 4

The Influence of Different Digital Terrain Models (DTMs) on Alpine Permafrost Modeling

Nadine Salzmann[1], Stephan Gruber[1], Marco Hugentobler[2], Martin Hoelzle[1]

[1] *Physical Geography Division, Glaciology and Geomorphodynamics Group*

[2]*Geographic Information Systems Division*

both at: Department of Geography, Winterthurerstrasse 190, University of Zurich, CH-8057 Zurich, Switzerland

in press, Journal of Environmental Modeling and Assessment

Abstract

The thawing of alpine permafrost due to changes in atmospheric conditions can have a severe impact, e.g. on the stability of rock walls. The energy balance model PERMEBAL was developed in order to simulate the changes and distribution of ground surface temperature (GST) in complex high mountain topography. In such environments, the occurrence of permafrost depends greatly on the topography, and thus, the digital terrain model (DTM) is an important input of PERMEBAL. This study investigates the influence of the DTM on the modeling of the GST. For this purpose, PERMEBAL was run with six different DTMs. Five of the six DTMs are based on the same base data, but were generated using different interpolators. To ensure that only the topographic effect on the GST is calculated, the snow module was turned off and uniform conditions were assumed for the whole test area. The analyses showed that the majority of the deviations between the different model outputs related to a reference DTM had only small differences of up to 1 Kelvin, and only a few pixels deviated more than 1 Kelvin. However, we also observed that the use of different interpolators for the generation of a DTM can result in large deviations of the model output. These deviations were mainly found at topographically complex locations such as ridges and foot of slopes.

Keywords: complex topography, digital terrain model (DTM), high mountain permafrost, modeling, sensitivity

1. Introduction

Permafrost is a widespread phenomenon in high-mountain environments such as the European Alps [1]. It is defined as lithospheric material that remains at or below a temperature of 0°C for at least one year [2]. In complex mountain topography, permafrost can stabilize infrastructure, rock walls and debris-covered slopes [3,4,5]. The close link between permafrost and the atmosphere together with permafrost temperatures that in the European Alps are often close to melting conditions, make permafrost especially sensitive to climatic changes. As a result, some permafrost is thawing [6,7,8], resulting in severe slope stability problems and other adverse ecological consequences [4,7,5,9]. In high-mountain regions with intense human activities such as in the Alps, permafrost degradation has increased the risk of permafrost-related hazards [10,11,12,13]. Therefore, knowledge of the distribution and dynamics of permafrost is important in order to develop mitigation strategies.

To simulate the distribution and changes of alpine permafrost the process-based energy balance model PERMEBAL was developed [14,15,16]. PERMEBAL is able to calculate the average ground surface temperature (GST), which is an indicator for the presence or absence of permafrost. In complex high-mountain topography, the microclimate, and thus the permafrost distribution, is strongly dependent on topoclimatic factors [17]. Therefore, the digital terrain model (DTM) is a key input variable of PERMEBAL [15]. The study of Hoelze [18], for example, showed that the horizontal resolution of the DTM has a significant influence on the calculation of the solar radiation in mountain environments, and thus, on the modeled permafrost distribution. Hence, we assume that the DTM significantly affects the calculation of the average GST. Latest research in the field of digital terrain modeling offers a range of sophisticated triangle-based terrain models [19], which can be used as input for PERMEBAL.

This study evaluates the sensitivity of simulated ground surface temperatures on the use of various DTM inputs. To date, only the DTM 'DHM25' (see below) has been used for alpine permafrost modeling on the decameter scale. Therefore, in this study, the uncertainties of the modeled GST outputs caused by the application of six different high-resolution DTMs are analyzed and discussed.

2. Data and Models

2.1 Study site

The sensitivity study was carried out within the Corvatsch area (Upper Engadine) of Switzerland, one of the most frequently investigated mountain permafrost sites in the Alps [20]. The climate in this part of the Alps is slightly continental and mainly influenced by SW air masses. The mean annual precipitation in the periglacial area is about 1000-2000 mm [21] and the mean annual 0°-isotherm lies at around 2200 m a.s.l.. The test area (782400/142400 and 783900/145000) covers the station Corvatsch, Piz Murtèl and the rock glacier Murtèl (Fig. 1).

2.2 The digital terrain models (DTMs)

The DTMs applied in this study have a horizontal resolution of 10 m. To allow accurate comparison, the same spatial resolution was used for each DTM. Furthermore, except for

the *ph* (for details, see below), base data are provide by the DHM25 for all the other DTMs; these data are owned and supplied by the swisstopo (Swiss Federal Office of Topography, Berne). Therefore, these five DTMs differ only through their interpolators. In the following, a short introduction is given about the basis for and interpolation methods used for the raster calculation of the DTMs.

d10 is the resampled DHM25. The original DHM25 has a horizontal resolution of 25 m. The base data for the DHM25 are digitized contours, peaks, breaklines and lake borders. The calculation of a 25 m raster from these data has been performed using a search-ray-based approach. From every raster point, a number of search rays pointing in different directions are used to locate intersections with contours. Spline curves were then fitted to the rays and their elevations averaged at the raster point [22]. These data were resampled to a 10 m resolution by applying bilinear interpolation in order to produce *d10*.

ph is a photogrammetrically-derived DTM. It is based on two scanned infrared aerial photographs and was automatically derived using the digital photogrammetrical software SOCET SET from the Leica-Helava system [23]. This technique is based on studying the differences in the optical contrasts of the aerial photographs. The two aerial photographs delivered by swisstopo were taken at the end of the hydrological year (7 September 1988) in order to ensure a maximum snow-free state. However, the glaciers in the area are still snow-covered. The DTM was computed by A. Kääb, University of Oslo.

For the following triangle-based interpolators (*li*, *co*, *ct*, *sc*), the DHM25 base data have been tessellated with a constrained Delaunay triangulation. This ensures that no triangle edge crosses a contour or a breakline.

li - the triangles have been interpolated linearly, and thus gradient and aspect are constant within one facet.

co - a cubic Coons interpolator was applied over triangular patches. The resulting surface is one time continuously differentiable. To better represent sharp features in high-mountain areas, a breakline extension was used [19]. As a result, the surface is continuous across breaklines, but not continuously differentiable.

ct - a cubic interpolator based upon Clough-Tocher triangles [24]. The surface is also one time continuously differentiable and a breakline extension similar to the Coons patch was used. The derivatives orthogonal to the triangle boundary curves are linearly interpolated.

sc - a smoothed version of the Clough-Tocher interpolant. The derivatives orthogonal to the triangle boundary curves were interpolated in a way that the curvature change at the border of the triangles is slower than with linearly interpolated cross-derivatives [19].

The DTMs *d10* and *ph* only provided the surface parameter elevation. The calculations of 'slope' and 'aspect' were performed using the commands *slope* and *aspect* within the software package ArcINFO (ESRI). The surface parameters slope and aspect of the TIN-(Triangulated Irregular Network) based DTMs were calculated directly from the surface.

2.3 The energy-balance model PERMEBAL

The energy-balance model PERMEBAL simulates the main energy-exchange processes between the atmosphere and the surface, and includes calculations for shortwave net radiation, longwave incoming and emitted radiation, turbulent fluxes and snow distribution [14,15,16]. In addition to the data from the DTM, the model is driven with meteorological time series and ground surface characteristics (Fig. 2). After providing this set of input data, the 2D version of PERMEBAL, which we use in this study, is able to simulate the distribution and changes of daily ground surface temperatures (GST) in complex high-mountain topography at a local to regional scale.

2.4 The PERMEBAL runs

The six model runs were all performed with the same settings. For this study, a 5 yr simulation (according to the hydrological year) was conducted and initiated in 1998. The meteorological input data were provided by MeteoSwiss (Swiss Federal Office of Meteorology and Climatology, Zurich) from their meteorological station at Piz Corvatsch (3315 m a.s.l., 783160/143525).

Snow has a strong impact on the seasonal thermal regime [17] due to its low thermal conductivity, which makes it a good insulator [25,26,27,28]. Hence, seasonal snow cover modifies the topographic feedback signal. This study assesses the influence of the topographic input only. Therefore, the snow module was turned off to ensure that only the topographic effect on surface temperature is calculated, and thus PERMEBAL does not take snow cover into account.

Similar to the snow cover, local surface conditions, such as vegetation and subsurface layers like organic matter, coarse blocks or glaciers, act as a buffer between the atmosphere and the ground [29,30]. Therefore, the potential effects of these factors were also eliminated and a rock surface was assumed for the entire test region.

By ignoring the snow cover and by using uniform surface characteristics, comparable conditions for all parameters over the entire test region are given. Hence, no other signals are included than those of the various DTMs, thereby allowing us to assess the sensitivity of PERMEBAL to these inputs.

3. Results

The results are divided into three sections and presented as follows: First, elevation (3.1.1), slope (3.1.2) and aspect (3.1.3) of the different DTMs are compared, as well as the modeled average GST (3.1.4). Second, the locations of the differences in the model outputs using image subtractions are reported. Finally, transect analyses are performed on two areas selected on the basis of the findings reported in the first two sections.

3.1 Comparison of the DTM surface parameters and the resulting modeling outputs (value ranges and frequency values)

A first, general impression as well as a comparison of the applied DTMs and the model output (average GST) is given by the analyses of their value ranges (see Table 1) and frequency values (see Fig. 3) over the entire test area.

3.1.1 Elevation

The range of the mean elevation values and the standard deviations for the entire test area are summarized in Table 1. The differences between the ranges are small. The mean elevations and standard deviations vary within only 1 m and 9 m respectively. The frequency curves for the elevation (Fig. 3a) also show only small variations between the six DTMs. Therefore, as these marginal differences in elevation do not significantly influence the resulting GST, they will not be a major focus in this paper.

3.1.2 Slope

The differences between the slope samples are far greater than those for the elevations. The differences in slope maxima vary by up to 23° (Table 1) and the frequency curves also show considerable variations (Fig. 3b). The majority and also the highest differences occur between about 20° and 45° (Fig. 3b). The image plots of slope (Fig. 4a) also reveal

significant differences and notable slope patterns appear in *d10*, *ph* and *li*. The pattern of *d10* is very smoothed and is caused by the spatial resampling applied. In contrast, the pattern of *ph* displays large differences between neighboring pixels in the snow-covered areas. This is probably caused by the snow cover (see above and the discussion). Finally, the *li* has quite a patchy pattern.

3.1.3 Aspect

The distributions of the aspect frequency (Fig. 3c) are quite similar apart from *co* and especially the *li*, where some single data values are either very frequent or rare in comparison to the others. These very high frequency values are all N-exposed. Most similarities between the frequency curves are found between about 150° and 250° (south sector). At the same time, the south exposition is least represented in our test area. The image plots of aspect (Fig. 4b) show similar distinctive feature as the slope images (Fig. 4a). *d10* is very smoothed, *ph* shows an unsettled image in the glacier area and *li* has large aspect variations in the westerly part.

3.1.4 Average ground surface temperature

The modeled GSTs show differences for the minima of 1.1 Kelvin (K) and for the maxima of 1.4 K. These values are related to single pixel values, and thus are not so important. The mean values differ within 0.6 K (Table 1). The frequency curves all have quite similar progression; however, note how the curves shift vertically between about 271 K and 273 K, (Fig. 3d).

On the output images (Fig. 4c), the patterns of the surface parameters elevation, slope and aspect are well reflected in the pattern of the modeled average GST and therefore, their relationship to elevation is clear. Moreover, the pattern of slope is reflected in the model output, particularly in the image of *ph*, where the noisy pattern of slope is well recognizable in the pattern of the average GST. Furthermore, the patchy slope pattern of *li* is also reflected in the corresponding image of the average GST. Finally, the pattern of the aspect over the entire test area is also apparent in the modeled results.

3.2 Deviation detection using difference images

For the following analyses, a reference DTM was selected. In respect to choice of the reference DTM, we have taken into account practical aspects, because an objective criterion, such as e.g. accuracy or quality, is lacking. The DHM25 is the only commercial DTM within our sample, and thus probably the most frequently used in Switzerland. Hence, we have chosen the *d10* as the reference DTM since it is the closest derivative of the DHM25. We have assumed that it would be most interesting to know, where and how large the deviations are, if alternative DTMs from the *d10* are used as model input. The locations and absolute values of the deviations that result, when PERMEBAL is run with the different DTM inputs, were detected by subtracting the output images from each other. The basic statistics (min, max, mean, SD) are summarized in Table 2. The pixel by pixel based minimum and maximum deviations are within –3.9 K and 5.4 K and have a mean value between -0.2 K and 0.4 K. The standard deviation is very similar for all subtraction images (about 0.5 K), with only ph showing a higher value of 0.8 K.

The detected areas of deviation are shown in Figure 5 and the absolute values of the percentage deviations are listed in Table 3. The ranges of deviation were classified into three groups: 1) ‘high deviation pixels’ with a deviation of the calculated average GST of more than ± 1 K compared to the output modeled with *d10*; 2) ‘moderate deviation pixels’ with a deviation between -1 – -0.5 K and 1 – 0.5 K respectively; and 3) ‘low deviation

pixels' with a deviation of less than ± 0.5 K.
Comparing the number of 'high deviation pixels' of the different model outputs, we found that the output based on *ph* counts most pixels (20%) in this class (Fig. 5). Only 50% of the pixels are classified as 'low deviation pixels' and 30% are in the class of 'moderate deviation pixels'. The positive deviation pixels are mainly located at the S-exposed sections and the highest deviations tend to be near the ridges. The spatial distribution of the negative deviation pixels is more disperse. However, there is also a tendency that they are located near or at the ridges.
The subtraction images of *co*, *ct* and *sc* show similar, but much less distinct tendencies, in particular for *sc* and *ct*, where the highest negative deviation pixels are not primarily found at the ridges. In these model outputs, the negative-deviation pixels are mainly located at the NE-N slopes and in the lower elevated NW corner of the test area. Most of the positive-deviated pixels are found in the SE-S-SW exposition and at the ridges.
When comparing the simulation run of *li* with that of *d10*, we find that most of the pixels (79%) were classified as 'low-deviation pixels'. In contrast to the other subtraction images, more pixels (13%) were classified as 'moderate- (negative-) deviation pixels'. The negative deviation part of this class is dispersed over the whole test site with the highest negative deviations to be found, as similar with the other subtraction maps, mainly at the ridges and in the NW corner. The positive deviation pixels are found almost only at the ridges.
In general, most of the deviation pixels and in particular those with the highest absolute values are found at topographically complex sites like ridges or foot of slopes.

3.3 Profiles
One profile was extracted in each of the two areas where the main deviations have been located. An E-W one (Fig. 4 and Fig. 6a) through the lower elevated NW corner where some large deviations have been found between the model outputs, and a N-S one (Fig. 4 and Fig. 6b) through the high elevated regions where many ridges exist and the deviations were mainly relatively high.
The two profiles show the causes of the deviations in the modeled average GST. In general, it is recognizable that when the curves of slopes from the different DTMs and also those of aspect are similar, then the differences between the curves of average GST are also low (Fig. 6a,b). The analyses in more details are given below.
In the E-W profile (Fig. 6a) between 25 and 32 on the x-axis, the average GST varies by up to 2 K between the DTMs. This is mainly caused by *li* and *ph*, with other profile curves of slope and aspect not having strong deviations. From about 33 to 40 along the x-axis, the slope curves vary quite strongly and the aspects change frequently between NE and NW. However, as in the section before, in the average GST, only *li* and *ph* deviate significantly. Within about 42 to 50 on the x-axis, the average GST is quite similar for all DTMs and the profiles of slope and aspect also show very low deviations. From the x-axis 55 to about 59, the average GST is again quite similar for all DTMs apart from *d10* and *ph*, which have quite a less steep slope in this section and NE aspect. The *co* in this section is also NE-exposed, but the slope is only moderately steep. Nevertheless, the average GST of *co* is very close to the ones of *ct*, *li* and *sc*. After about 60 along the x-axis until 68, the curve progressions are quite similar apart from that of *ph* and *ct* at around 60 on the x-axis. In the very last section, the aspect of *d10*, *li* and *ph* are NW, while the others change to NE. The slope values are quite similar for all DTMs. With the change form NW to NE, the related curves of the average GST rise about 1 K.
In the N-S profile, which is located in the glacierized area, the most noticeable point is the high variability of all of the *ph* profile curves. Between about 150 and 170 on the y-axis,

the slope curves are quite similar apart from *d10* and *ph*. The aspect curves of *li* and *ph* change in this section between NW and NE. The resulting average GSTs are quite similar apart from *d10*. In the sections, where the curves of slope and aspect have quite a similar form (about 170 to 220 along the y-axis), the curves of the average GST are also quite equal or at least parallel. Between about 230 and 240 on the y-axis, the slopes and aspects are also quite similar. The curves of the resulting average GST in this section however, have a similar progression but are parallel-shifted. The motion of the slope and the aspect curves are reflected in the average GST between 210 and 240 on the y-axis. However, in this section and in general, it seems that aspect has a slightly stronger impact on the average GST than slope.

4. Discussion and Conclusions

The purpose of this study was to assess the sensitivity of the energy balance model PERMEBAL to various DTM inputs. The mean average GST over the entire test area varies only within 0.6 K. The pixel values of the average GST modeled with *d10* as compared with those modeled using the other DTMs, showed in general low deviations. About 75 – 79% of the calculated average GST (except for *ph* with only 50%) were in the class of ± 0.5 K (low-deviation pixels). At the locations of this class, the differences in elevation, slope and aspect between the different DTMs were also low. Only 1 – 5% of the total number of pixels in the test area (except for *ph* where this increased to 18%) deviated more than ± 1 K (class of high-deviation pixels). These pixels were located mainly at the ridges, and thus at locations of most complex topography. These sites were expected to be most critical, since here significant topographical changes occur within very short spatial distance. Furthermore, such areas represent extreme locations also from the geological and (micro-) climatological point of view. Therefore, the uncertainties at such locations will always be the greatest, due to the uncertainties of the topographical input as well as difficulties in modeling the physical processes. Here, deviations of up to 5.4 K for single pixel values resulted between calculations made with *d10* compared to calculations made with the other DTMs.

The differences in aspect, in particular when a change from N to S or from W to E and vice versa is included, have led to quite high deviations. Furthermore, S-exposed areas seem to be slightly more sensitive to topographical variations; this phenomenon can be explained by the higher amount and importance of incoming radiation in the energy-balance of south aspect slopes. The influence of slope seems to play a less dominant role than aspect.

The high-deviation single-pixel values are mainly found at topographically complex sites like ridges or foot of slopes. Such areas represent extreme locations also from a geomorphological and (micro-) climatological point of view. Hence, not only the topographical input data have most uncertainties in these areas, but also the modeling of the energy balance will be most critical at such locations. Therefore, the results of PERMEBAL should be treated especially carefully in such areas.

We have seen that the average GSTs modeled with the photogrammetrically-derived DTM (*ph)* differ significant from those modeled with the other DTMs. This result is to be expected since each DTM, except *ph*, is based on the same base data. Because of the equal base date, the deviations in the PERMEBAL output are only caused by the different interpolation techniques that were used to generate the DTMs. Furthermore, the majority of the deviation pixels of *ph* are located in the glacierized, snow-covered areas. This can be explained by the compilation technique of the *ph* DTM and the specific natural

circumstances at the time of taking the aerial photograph. The technique of photogrammetrically deriving DTM is based on optical contrasts. However, the optical contrasts are generally reduced in infrared photographs and even more reduced or almost non-existent over snow covered areas or glaciated areas [31]. Without strong optical contrast, the calculation of the elevation is difficult and this can lead to miscalculations. Therefore, the major part of the deviation pixels in this area can be explained with the weakness of photogrammetrically-derived DTMs from infrared photographs, especially over snow-covered areas.

5. Perspectives

In this study, six different DTMs have been used to assess the influence of the topographic input on each of these specific DTMs. Further analysis of the sensitivity of PERMEBAL should be carried out. As an example, artificial DTMs should be used with a topography that represents 'mountains' in an idealized geometrical form, e.g. a cone or a cylinder. In this way, the influence of the topography can be analyzed using a more systematic approach.

In a similar manner, sensitivity studies should be conducted that include snow cover and different surface characteristics. Therewith, the effect of these buffers layers on the influence of the topographic input can be assessed.

In the context of climate change and its impact on alpine permafrost, further studies are needed that link PERMEBAL with scenario output from Regional Climate Models (RCMs) [32]. Such model combinations offer promising perspectives; however, they should also include knowledge about the uncertainties caused by the DTM applied.

Acknowledgements

This study was made possible thanks to the European Cooperation in the field of Scientific and Technical Research (COST-Action 719). We gratefully acknowledge the review of the manuscript by I. Woodhatch, the critical comments of W. Haeberli (both at University of Zurich), the support of A. Kääb (University of Oslo) concerning questions in photogrammetry, the very valuable comments of one of the anonymous reviewers and the worthy proof reading by Ruth Willmott.

References

[1] F. Keller, R. Frauenfelder, J.M. Gardaz, M. Hoelzle, C. Kneissel, R. Lugon, M. Philips, E. Reynard and L. Wenker, Permafrost map of Switzerland, in: Proceedings of 7th International Conference on Permafrost, Vol. 57, Yellowknife, Canada, 1998, pp. 557–562.

[2] A.L. Washburn, Geocryology: A survey of periglacial processes and environments, Arnold Ltd., London, 1997.

[3] W. Haeberli, Construction, environmental problems and natural hazards in periglacial mountain belts, Permafrost Periglac. Process. 3(2) (1992) 111–124.

[4] W. Haeberli, M. Wegmann and D. Vonder Muehll, Slope stability problems related to glaciers shrinkage and permafrost degradation in the Alps, Eclogae Geol. Helv. 90 (1997) 407–414.

[5] C. Harris, B. Rea and M. Davies, Scaled physical modelling of mass movement processes on thawing slopes, Permafrost Periglac. Process. 12(1) (2001) 125–135.

[6] W. Haeberli and M. Beniston, Climate change and its impact on glaciers and permafrost in the Alps, Ambio 27(4) (1990) 258–265.

[7] M.C.R. Davies, O. Hamza and C. Harris, The effect of rise in mean annual temperature on the stability of rock slopes containing ice-filled discontinuities, Permafrost Periglac. Process. 12(1) (2001) 137–144.

[8] C. Harris, D. Vonder Muehll, K. Isaksen, W. Haeberli, J.L. Sollid, L. King, P. Holmlund, F. Dramis, M. Guglielmin, M. and D. Palacios, Warming permafrost in European mountains, Global Planet. Change 39 (2003) 215–225.

[9] S. Gruber, M. Hoelzle and W. Haeberli, Permafrost thaw and destabilization of alpine rock walls in the hot summer of 2003, Geophys. Res. Lett. 31 (13) (2004) L13504.

[10] M. Zimmermann and W. Haeberli, Climatic change and debris flow activity in high mountain areas: a case study in the Swiss Alps, in: Greenhouse-Impact on Cold-Climate Ecosystems and Landscapes, eds. M. Boer and E. Koster, Catena Supplement 22 (1992) 59–72.

[11] J. Noetzli, M. Hoelzle and W. Haeberli, Mountain permafrost and recent alpine rock fall events: a GIS-based approach to determine critical factors, in: Proceedings of 8th International Conference on Permafrost, Vol. 1, July 20-25, Zurich, Switzerland, 2003, pp. 827–832.

[12] A. Kääb, J.M. Reynolds and W. Haeberli, Glacier and permafrost hazards in high mountains, in: Global change and mountain regions: a state of knowledge overview. Advances in global change research, eds. U.M. Huber, M.A. Reasoner and B. Gugmann, Kluwer Academic Publishers, Dordrecht, 2005, pp. 225–234.

[13] C. Huggel, W. Haeberli, A. Kääb, D. Bieri and S. Richardson, Assessment procedures for glacial hazards in the Swiss Alps, Can. Geotech. J. 41(6) (2004) 1068–1083.

[14] C. Mittaz, M. Imhof, M. Hoelzle and W. Haeberli, Snowmelt evolution mapping using an energy balance approach over an alpine terrain, Arc. Antarc. Alp. Res. 34(3) (2002) 274–281.

[15] C. Stocker-Mittaz, M. Hoelzle and W. Haeberli, Modelling alpine permafrost distribution based on energy-balance data: a first step, Permafrost Periglac. Process. 13 (2002) 271–282.

[16] S. Gruber, M. Hoelzle and W. Haeberli, Rock-wall temperatures in the Alps: modelling their topographic distribution and regional differences, Permafrost Periglac. Process. 15 (3) (2004) 299–307.

[17] F. Keller and H. Gubler, Interaction between snow cover and high mountain permafrost, Murtèl–Corvatsch, Swiss Alps, in: Proceedings of 6th International Conference on Permafrost, Vol. 1, July 5-9, Beijing, PR China, 1993, pp. 332–337.

[18] M. Hoelzle, Permafrost und Gletscher im Oberengadin, Mitteilungen VAW/ETH Zurich, Switzerland, Vol. 132, 1994.

[19] M. Hugentobler, Terrain modelling with triangle based free-form surfaces, PhD thesis, Department of Geography, University of Zurich, Switzerland, 2004.

[20] M. Hoelzle, D. Vonder Muehll and W. Haeberli, Thirty years of permafrost research in the Corvatsch-Furtschellas area, Eastern Swiss Alps: a review, Norw. J. Geogr. 56 (2002) 137–145.

[21] M. Schwarb, C. Frei, C. Schaer and C. Daly, Mean annual precipitation throughout the European Alps 1971-1990, in: Hydrological Atlas of Switzerland, Landeshydrologie und Geologie, Bern, 2000.

[22] B. Schneider, Geomorphologisch plausible Rekonstruktion der digitalen Repraesentation von Gelaendeoberflaechen aus Hoehenliniendaten, PhD thesis, Department of Geography, University of Zurich, Switzerland, 1998.

[23] A. Kääb and M. Vollmer, Surface geometry, thickness changes and flow fields on creeping mountain permafrost: automatic extraction by digital image analysis, Permafrost Periglac. Process. 11 (2000) 315–326.

[24] G. Farin, Curves and surfaces for CAGD: a practical guide, Morgan Kaufmann Publishers Inc., San Francisco, CA, 1997.

[25] T. Zhang, T.E. Osterkamp and K. Stamnes, Influence of the depth hoar layer of the seasonal snow cover on the ground thermal regime, Water Resour. Res. 32 (1996) 2075–2086.

[26] T. Zhang, R.G. Barry, R.G. and W. Haeberli, Numerical simulation of the influence of the seasonal snow cover on the occurrence of permafrost at high altitudes, Norw. J. Geogr. 55 (2001) 261–266.

[27] F. Ling and T. Zhang, A numerical model for surface energy balance and thermal regime of the active layer and permafrost containing unfrozen water, Cold Reg. Science Technol. 38(1) (2004) 1–15.

[28] M. Ishikawa, Thermal regimes at the snow–ground interface and their implications for permafrost investigation, Geomorphology 52 (1-2) (2003) 105–120.

[29] J. Luthin and G. Guymon, Soil moisture – vegetation – temperature relationships in central Alaska, J. Hydrol. 23 (1974) 233–246.

[30] S. Harris and D. Pedersen, Thermal regimes beneath coarse blocky materials, Permafrost Periglac. Process. 9 (2) (1998) 107–120.

[31] E. Lutz, T. Geist and J. Stoetter, Investigations of airborne laser scanning signal intensity on glacial surfaces – Utilising comprehensive laser geometry modeling and orthophoto surface modeling (A case study: Svartisheibreen, Norway), in: Proceedings, ISPRS Workshop on 3-D reconstruction from airborne laserscanner and INSAR data, Dresden, Germany, 2003.

[32] N. Salzmann, C. Frei, P.L. Vidale, M. Hoelzle, The application of Regional Climate Model output for the simulation of high-mountain permafrost scenarios. Global Planet. Change (2006) doi:10.1016/j.gloplacha.2006.07.006.

Table 1: Value ranges of surface parameters for each DTM over the entire test area.

		d10	ph	co	ct	li	sc
Elevation [m a.s.l.]	mean	2992	2992	2991	2991	2991	2991
	SD	2254	2250	2259	2259	2257	2259
Slope [deg]	min	7	0	0	0	0	0
	max	66	70	73	85	81	89
	mean	31	32	32	32	32	32
	SD	12	13	13	14	14	14
Average GST [K]	min	268.0	267.0	267.8	267.8	267.9	266.9
	max	277.3	276.5	277.0	277.1	277.9	277.4
	mean	272.6	272.2	272.4	272.4	272.8	272.5
	SD	1.5	1.5	1.5	1.5	1.6	1.5

Table 2: The deviations of the image subtraction related to d10

		ph	co	ct	li	sc
Average GST [K]	min	-3.7	-3.5	-3.5	-3.9	-3.7
	max	4.9	4.9	4.6	4.6	5.4
	mean	0.4	0.2	0.2	-0.2	0.1
	SD	0.8	0.5	0.5	0.5	0.5

Table 3: Deviation [%] of average GST [K] from d10

	ph	co	ct	li	sc
< -1	2	1	1	3	2
-1 – -0.5	6	5	6	13	6
-0.5 – 0.5	50	75	77	79	78
0.5 – 1	24	15	11	3	9
> 1	18	4	5	2	5

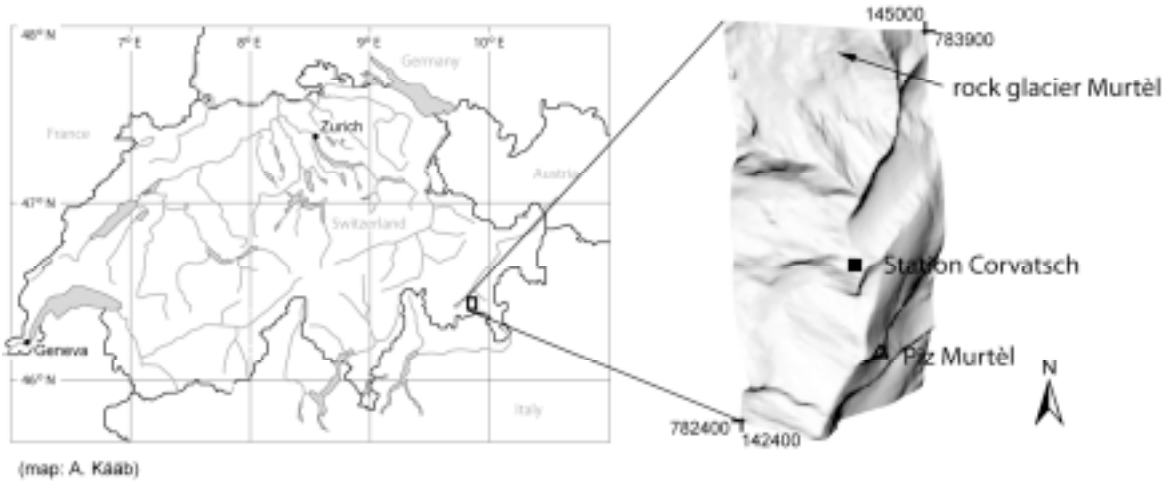

Figure 1
Location of the study site and topography of the test area in a 3D visualization.

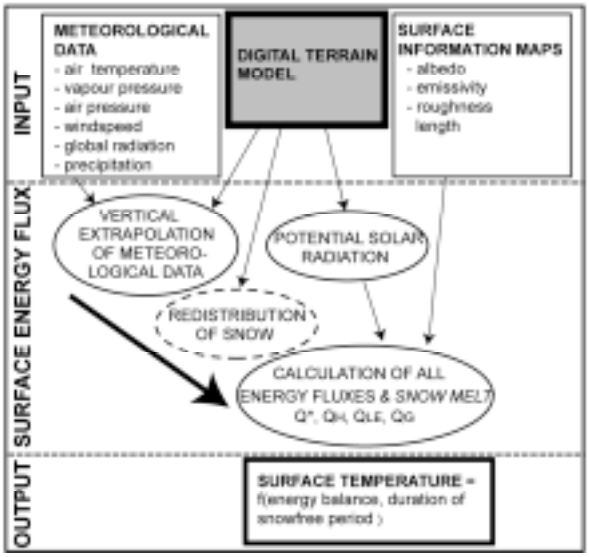

Figure 2
Schematic of PERMEBAL as applied in this study (after Stocker-Mittaz et al. [15]). The input that was varied for this study is bold bordered, and those, which were kept equal during all investigations, are normal bordered. The calculation steps that were omitted, are dash bordered or in italic letters.

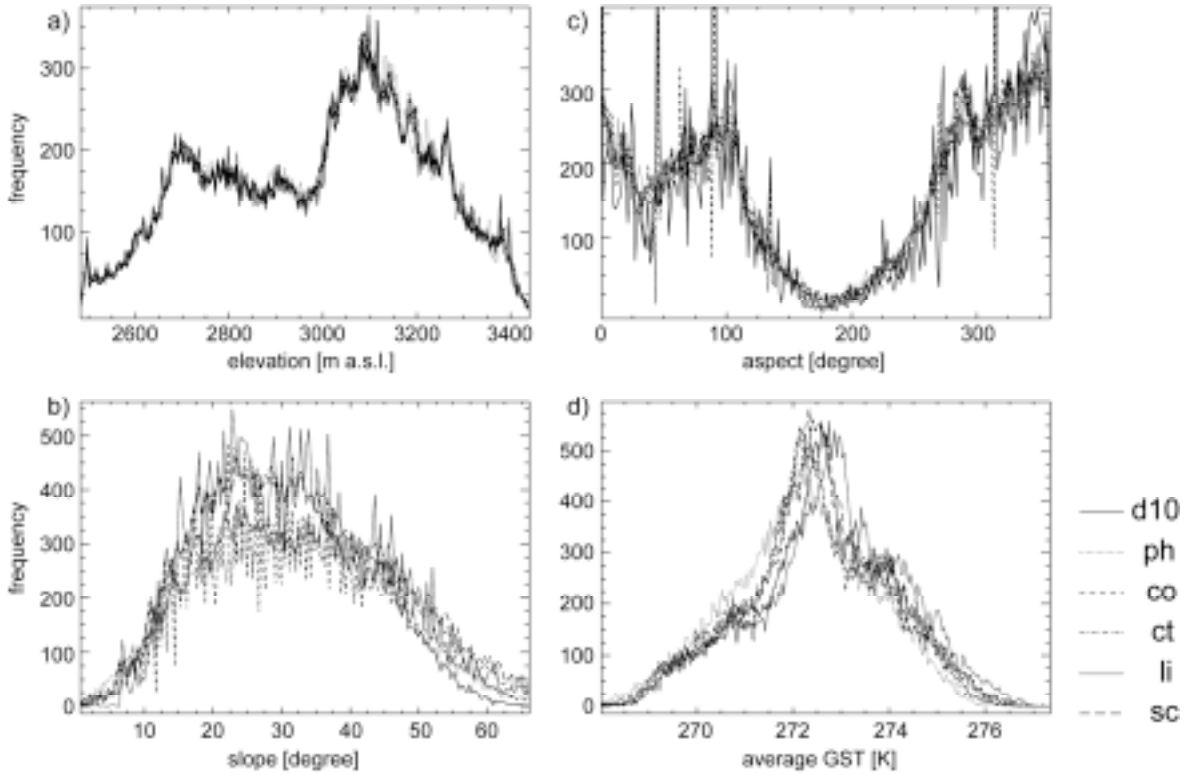

Figure 3
Frequency distribution over the entire test area of elevation (a), slope (b), aspect (c) and the modeled average GST (d).

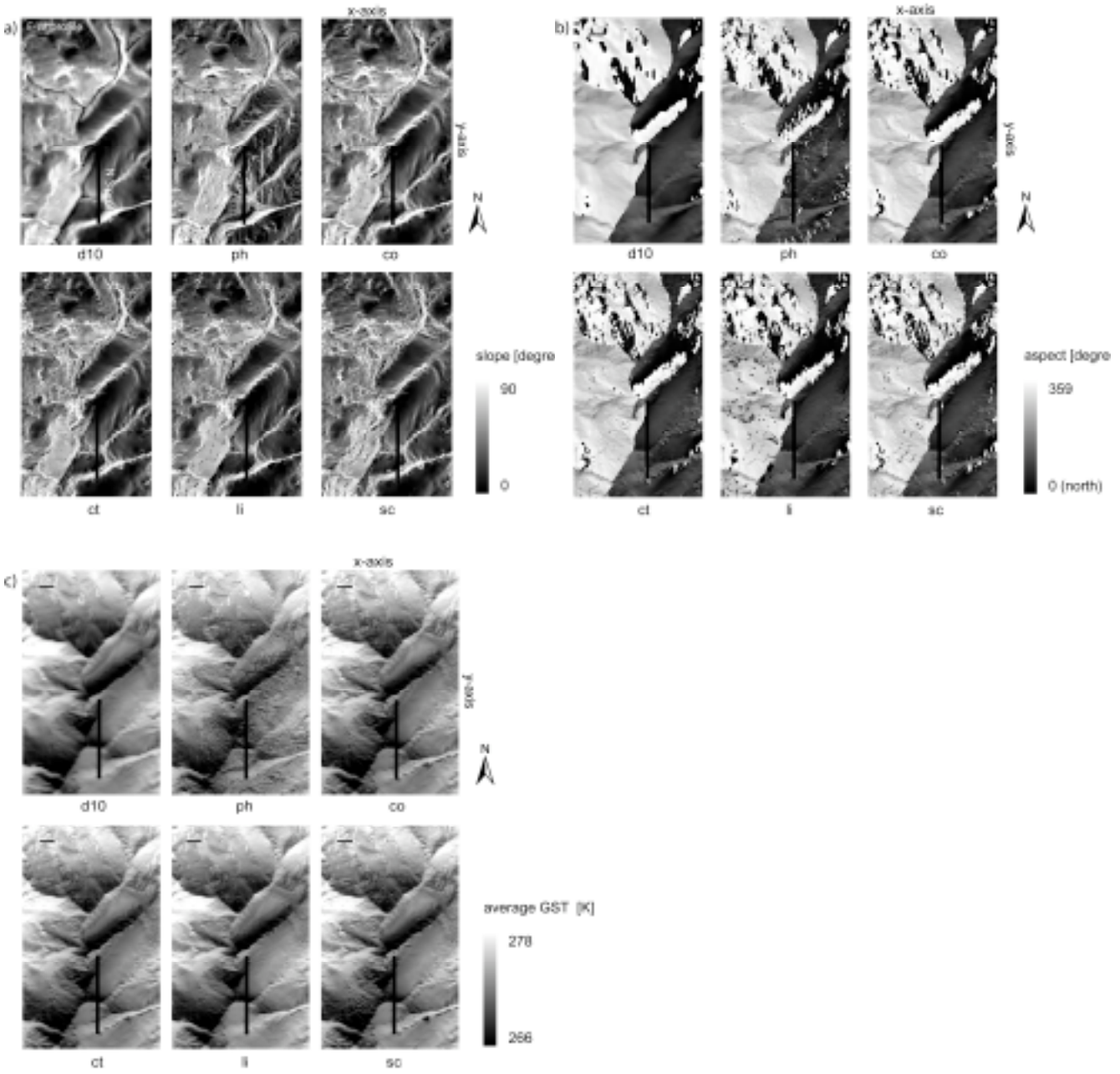

Figure 4a-c
2D image plots of slope (a), aspect (b) and the modeled average GST (c). The black bars show the location of the horizontal and vertical profiles that are investigated in Section 3.3.

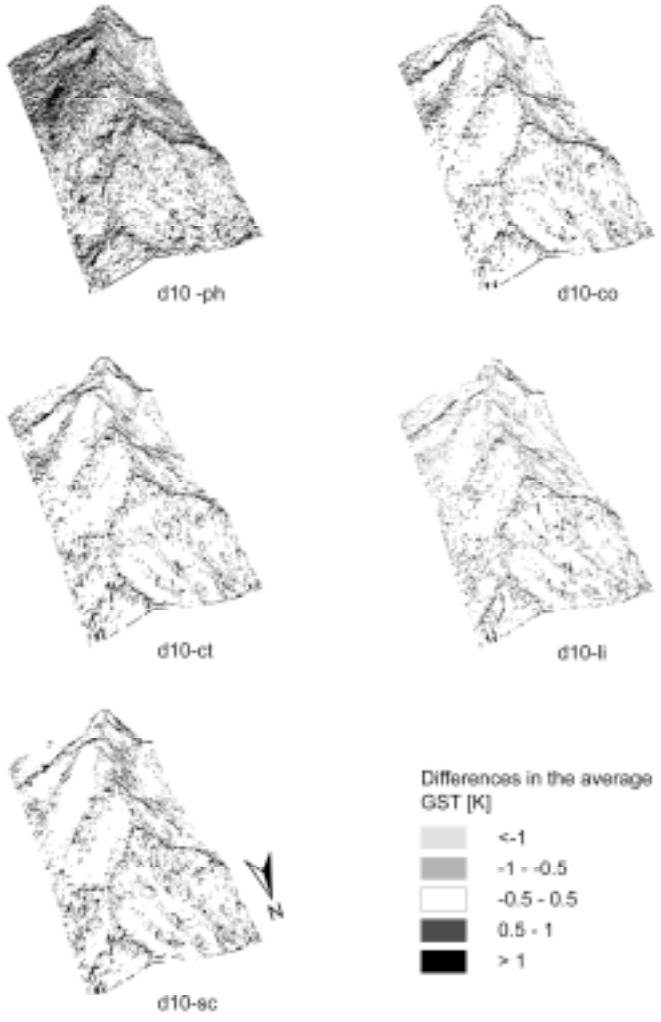

Figure 5
3D plots of the subtraction maps.

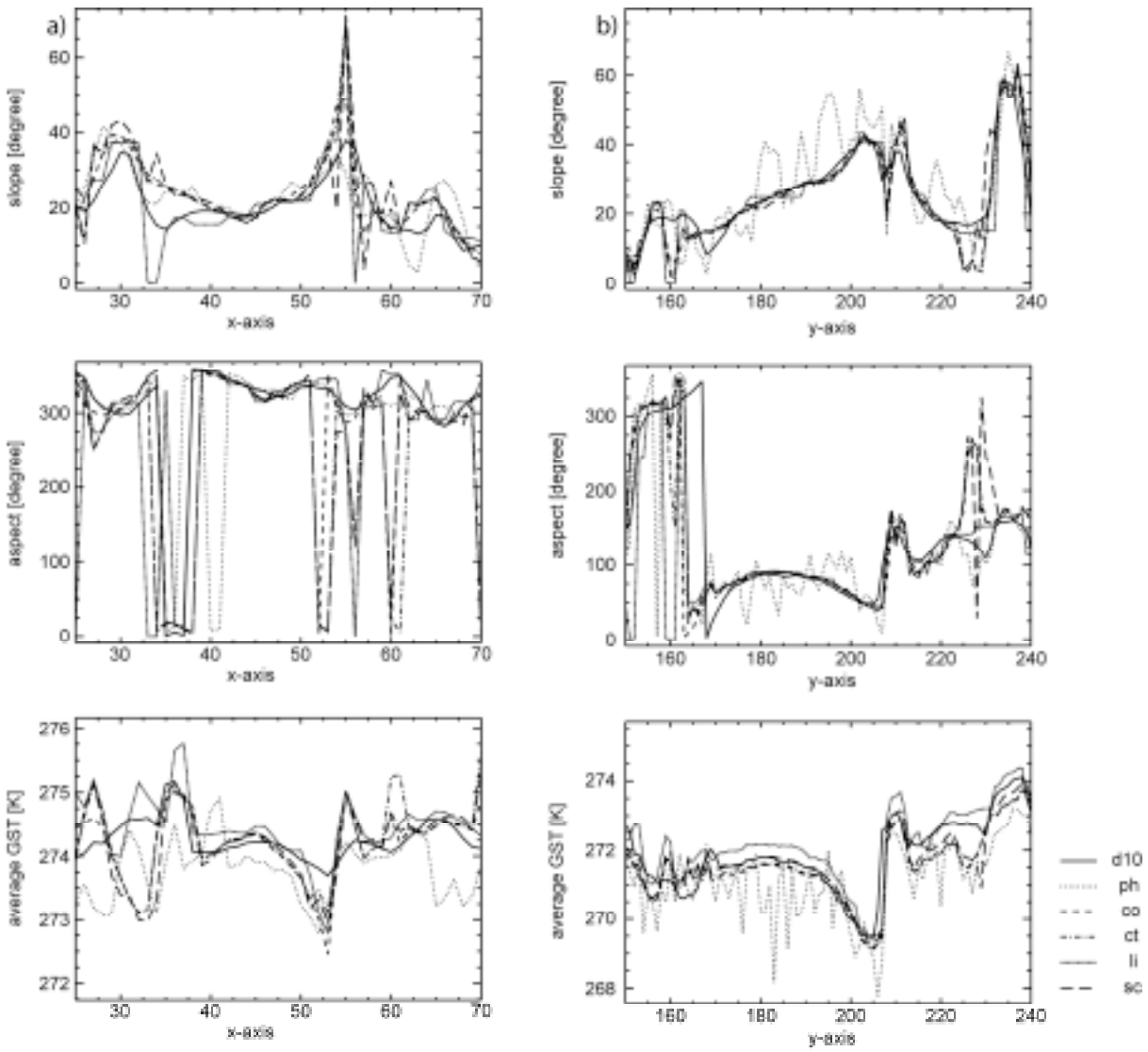

Figure 6
The E-W (a) and N-S (b) profiles of slope, aspect and the modeled average GST. For the location of the profiles, see Figure 4.